

Dynamics of Coarsening in Systems of Non-living and Living Objects

A Thesis

Submitted for the Degree of
DOCTOR OF PHILOSOPHY
in the Faculty of Science

by

Saikat Chakraborty



THEORETICAL SCIENCES UNIT
JAWAHARLAL NEHRU CENTRE FOR ADVANCED SCIENTIFIC
RESEARCH
Bangalore – 560 064

DECEMBER 2016

To my parents

DECLARATION

I hereby declare that the matter embodied in the thesis entitled “**Dynamics of Coarsening in Systems of Non-living and Living Objects**” is the result of investigations carried out by me at the Theoretical Sciences Unit, Jawaharlal Nehru Centre for Advanced Scientific Research, Bangalore, India under the supervision of Prof. Subir K. Das and that it has not been submitted elsewhere for the award of any degree or diploma.

In keeping with the general practice in reporting scientific observations, due acknowledgement has been made whenever the work described is based on the findings of other investigators.

Saikat Chakraborty

CERTIFICATE

I hereby certify that the matter embodied in this thesis entitled “**Dynamics of Coarsening in Systems of Non-living and Living Objects**” has been carried out by Mr. Saikat Chakraborty at the Theoretical Sciences Unit, Jawaharlal Nehru Centre for Advanced Scientific Research, Bangalore, India under my supervision and that it has not been submitted elsewhere for the award of any degree or diploma.

Prof. Subir K. Das
(Research Supervisor)

Acknowledgements

I am immensely grateful to my thesis supervisor Prof. Subir K. Das for being a constant source of motivation, support and help. He introduced me to interesting research problems and guided me through their analyses with utmost care.

I would like to acknowledge other faculty members of Theoretical Sciences Unit (TSU) - Prof. Umesh V. Waghmare, Prof. Shobhana Narasimhan, Prof. Srikanth Sastry, Prof. Swapan K. Pati, Prof. Kavita Jain, Prof. N.S. Vidhyadhiraja and Dr. Meher K. Prakash for their important scientific inputs.

Acknowledgements are due to all the course instructors - Prof. Subir K. Das, Prof. Swapan K. Pati, Prof. N.S. Vidhyadhiraja, Prof. Kavita Jain, Prof. Shobhana Narasimhan, Prof. Umesh V. Waghmare, Prof. Balasubramanian Sundaram and Prof. Rajesh Ganapathy.

I thank all my past and present labmates - Dr. Suman Majumder, Dr. Sutapa Roy, Dr. Shaista Ahmad, Saugata Patra, Sunita, Jiarul, Subhajit, Nalina, Koyel and Arabinda for creating and sustaining a research-friendly atmosphere in the lab.

I am indebted to my school and college teachers. My budding years were

blessed to have their presence.

Apart from the labmates, I found some wonderful friends like Abhijit, Arpan, Somnath, Chandan, Sisir and many others who made my stay at JNCASR a memorable one. Here, I thank my long-standing friend Sabya.

My sincere gratitude goes towards the staffs of Library, Complab, Administration, Academics, Dhanvantary, Dining hall, Hostel mess and House-keeping.

I thank JNCASR for financial support.

I am grateful to my brother and sister-in-law for their love and support. They gifted me an ambience of home away from home. Finally, I express my deepest gratitude to my parents and grandparents for all the sacrifices they made so that I could be here.

Synopsis

In this thesis we undertake studies of few important aspects of kinetics of phase transitions in model magnetic, binary mixture and active matter systems. In the magnetic case we confine ourselves to para- to ferromagnetic transitions. In the **first chapter** we discuss the prerequisites for the works to be presented in the subsequent chapters. Important aspects like pattern formation, growth, persistence and aging are introduced in significant depth. We provide relevant theoretical background and discuss crucial analytical and computational techniques. On the technical side, emphasis has been put on the difficulties related to simulations of phase transitions, e.g. critical slowing down, finite-size effects, etc. State-of-the-art methods, like finite-size scaling analysis, to overcome these problems, are discussed.

In **chapter 2** we have studied the dynamics of ordering in Ising ferromagnets via Monte Carlo simulations. (This simulation method and model are used in the next three chapters as well.) In this chapter, we present results for domain growth and persistence probability in space dimensions $d = 2$ and 3 , for quenches from different initial temperatures (T_i). For the decay (power-law) of persistence probability we make significant new observations: i) The exponent of the power-law for $T_i = T_c$ is different from that for $T_i = \infty$; ii) Intermediate values of T_i carry signatures of both the above values of T_i . These results we understand via appropriate scaling analyses involving the equilibrium correlation length at T_i . The domain growth, on the other hand, appear insensitive to the variation in T_i .

One of the primary objectives in **chapter 3** has been to investigate

the dimensionality (d_f) of the fractal pattern formed by persistent spins. Like in the previous chapter, we study the dependence of this dimensionality on initial temperature, in $d = 2$ and 3 . It is observed that d_f has strong dependence upon T_i , even though the effect is weaker in $d = 3$ than in $d = 2$. In addition, we present results for the global persistence. Furthermore, important observations on the domain growth and persistence probability are reported for quenches from $T_i = \infty$ to the final temperature $T_f = 0$, in $d = 3$. A controversy, related to the value of the exponent of the power-law growth (with time), has been resolved.

In **chapter 4**, we continue with the coarsening dynamics for $T_i = \infty$ to $T_f = 0$ quenches. In addition to providing further discussion on the domain growth and persistence, we present important new results on pattern and aging. For $d = 3$, it has been shown that the pattern at $T_f = 0$ is different from that for temperatures above the roughening transition and is not describable by the well-known Ohta-Jasnow-Kawasaki form for the two-point equal time correlation function. For the above mentioned choices of T_f , we demonstrate important difference in the aging phenomena as well. The temperature dependence observed in $d = 3$ has been compared with that in $d = 2$.

In **chapter 5** we obtain accurate quantitative information on the time-decay of the two-time order-parameter autocorrelation function, relevant for understanding of aging phenomena, for quenches from $T_i = \infty$ to $T_f = 0$, in $d = 2$ and 3 , via finite-size scaling analysis. While the behavior in $d = 2$ is found to be the same as that for $T_f > 0$, in the case of $d = 3$ we show that the late time power-law decay is significantly slower than that for $T_f > T_R$, T_R

being the roughening transition temperature. The corresponding exponent (for $T_f = 0$ in $d = 3$) apparently violates a well-known lower-bound. This we have understood via appropriate analyses of the structure.

In **chapter 6**, we have studied the kinetics of phase separation in a two-dimensional model active matter system, via molecular dynamics simulations. Results are presented on pattern, cluster growth and aging. These are compared with the corresponding results from a relevant passive binary mixture model. Note that the self-propulsion in our active matter model is of Vicsek type where direction of motion of an individual is influenced by its neighbors. Via demonstration of the well-known scaling properties of the correlation function and structure factor, we confirmed the self-similarity of structure during the growth process. The autocorrelation function is also shown to scale in a fashion similar to standard passive phase ordering systems. Though various correlation functions show qualitatively similar behavior in both active and passive cases, it is shown that there exist quantitative discrepancies between the two cases. Furthermore, the exponent for the (power-law) cluster growth in active system is found to be much larger than the conserved passive dynamics.

List of Publications

- “Role of Initial Correlation in Coarsening of a Ferromagnet”, **Saikat Chakraborty** and Subir K. Das, Eur. Phys. J. B **88** 160, (2015).
- “Fractality in Persistence Decay and Domain Growth during Ferromagnetic Ordering: Dependence upon initial correlation”, **Saikat Chakraborty** and Subir K. Das, Phys. Rev. E **93** 032139, (2016).
- “Kinetics of Ferromagnetic Ordering in 3D Ising Model: How far do we understand the case of zero temperature quench?”, Subir K. Das and **Saikat Chakraborty** (to appear in 2017).
- “Aging during Coarsening in Ferromagnetic Ising Model for Zero Temperature Quench”, **Saikat Chakraborty** and Subir K. Das (to be submitted).
- “Pattern Formation, Growth and Aging in a 2D Active Matter Model”, **Saikat Chakraborty** and Subir K. Das (manuscript in preparation).

List of Figures

1.1	Phase diagram of a chemical substance in the P vs. T plane. Various equilibrium phases, critical point (T_c, P_c) and triple point (T_t, P_t) are marked on the figure.	2
1.2	Phase diagram of the chemical substance of Fig. 1.1 in temperature (T) vs. density (ρ) plane, in the vicinity of the vapor-liquid critical point. In real situations the coexistence curve is not perfectly symmetric like the one drawn here.	3
1.3	Phase behavior of a magnetic material in the external magnetic field (h) vs. temperature (T) plane. Above T_c , the system is in paramagnetic phase and below T_c , it is in ferromagnetic phase.	4
1.4	Snapshots during the evolution of an Ising ferromagnet. The dots represent the spins in +1 state or the up direction and the unmarked sites are the locations of down spins. Results are presented from four different times which are mentioned on top of the frames, in units of Monte Carlo steps (MCS).	8

-
- 1.5 Snapshots showing the evolution of a conserved system, obtained via Monte Carlo simulations of Kawasaki exchange Ising model, upon quenching from a high temperature to a temperature $T = 0.6T_c$. The black dots mark the locations of A particles (up spins) and the down spins (location of B particles) are left unmarked. 11
- 1.6 Schematic plots of the autocorrelation function $C_{ag}(t, t_w)$, with the variation of $(t - t_w)$, for three different values of t_w 13
- 1.7 Snapshots of the persistent spins from four different times, during the ferromagnetic ordering. The spins marked with dots represent the persistent spins. 17
- 1.8 Picture of a school of fish. Picture courtesy: S. Paul, K. Das, Nalina V. 18
- 1.9 A schematic diagram showing the equilibrium correlation length ξ in a system of linear size L . Spins inside the shaded regions are correlated. Maximum value of ξ can be equal to L 24
- 2.1 Upper panels show snapshots during the evolution of the Glauber Ising model with $T_i = \infty$, $T_f = 0$ and $L = 512$. The dotted regions represent domains of up spins. The lower panels show the unaffected spins, marked by dots, corresponding to the evolution snapshots above them. These results are from $d = 2$. 34

2.2	Plots of persistence probability, P , vs, time, on a log-log scale, for quenches from $T_i = \infty$, with $L = 512$, in $d = 2$. Four different values of T_f are included. The solid line there has a power-law decay with exponent 0.22.	35
2.3	Log-log plots of P vs t , for quenches from different values of $T_i (\geq T_c)$, to $T_f = 0$, in $d = 2$ with $L = 512$. Continuous lines there correspond to power-law decays with exponents 0.22 and 0.04.	36
2.4	Instantaneous exponents θ_i are plotted vs $1/\ell$, for the quenches in Fig. 2.3, excluding $T_i = T_c$ case. Here we have included only the late time behavior. The dashed lines in this figure are guides to the eyes.	38
2.5	Instantaneous exponents θ_i are plotted vs $1/\ell$ for two of the quenches in Fig. 2.3. Here we have focused on the first step of the decays, exponents for which are obtained from the flat regions. The values of $\theta_1(T_i)$, for different T_i s are extracted from the horizontal lines. The results are for $d = 2$ in a square lattice with $L = 512$	39
2.6	The values of θ_1 , obtained from the exercise in Fig. 2.5, are plotted vs $\epsilon = T_i - T_c$. The continuous line here is a power-law fit (see text).	40
2.7	Log-log plots of P vs t , for two different system sizes, with $T_i = T_c$ and $T_f = 0$. The results correspond to $d = 2$	41

-
- 2.8 Plots of θ_i vs $1/\ell$, for three different values of L , with $T_i = T_c$. The dashed line is a linear extrapolation using data in the small ℓ region. The flat regions, marked by the horizontal solid lines, provide the value of L -dependent instantaneous exponents, $\theta_c(L)$. The results are from simulations in $d = 2$ 42
- 2.9 The L -dependent exponents, $\theta_c(L)$, obtained from flat regions of the plots (see the horizontal solid lines) in Fig. 2.8 are plotted vs $1/L$. The solid line there is a linear fit. 43
- 2.10 Average domain sizes, $\ell(t)$, are plotted vs t , for quenches to $T_f = 0$ from $T_i = \infty$ and T_c , in $d = 2$. The solid line represents $t^{1/2}$ behavior. Results are obtained from simulations in $d = 2$, on a square lattice with $L = 512$ 45
- 2.11 Instantaneous exponents, α_i , corresponding to the plots in Fig. 2.10, vs $1/t$, are shown. Long time limit data, suffering from strong finite-size effects, have been discarded. 46
- 2.12 Scaling plot of persistence probability, P , versus t/t_c where the crossover time (to the asymptotic behavior) t_c has been used as an adjustable parameter to obtain optimum data collapse. All results were obtained using $L = 512$ in $d = 2$ 49
- 2.13 Double log plots of $\ell_c - 1$ versus ϵ . The circles correspond to estimates of ℓ_c from t_c , where we obtain the t_c values from the exercise as in Fig. 2.12. The squares are directly obtained from the scaling plots of P vs ℓ/ℓ_c . The solid line has $d = 2$ Ising critical divergence of correlation length. See the text for further details. 50

-
- 2.14 Plots of $P(t)(\ell/\ell_c)^{2\theta}$, θ being set to 0.225 [see Fig. 2.4], vs the scaled variable ℓ/ℓ_c , for several values of T_i , using linear scale. Results are presented using $L = 512$ in $d = 2$ 51
- 2.15 Same as Fig. 2.14 but on a log-log scale and only for $T_i = 2.35$. The continuous line there is a fit to Eq. (2.13) (see text for details). 52
- 2.16 Log-log plot of P vs t , for quenches from $T_i = \infty$ and $T_i = T_c$, to $T_f = 0$. In each of the cases results from two different system sizes are included. The solid lines have power-law decays with exponents 0.1 and 0.18, as indicated on the figure. All results correspond to $d = 3$ 55
- 2.17 Instantaneous exponents θ_i are plotted vs $1/\ell$, for quenches from $T_i = T_c$ to $T_f = 0$ in $d = 3$. Results from different values of L are included. The horizontal solid lines are related to the estimation of L -dependent θ_c 56
- 2.18 Plot of $\theta_c(L)$ vs $1/\ell$ (see Fig. 2.17). The continuous line there is a linear fitting (see text for details). 57
- 2.19 Plots of θ_i vs $1/\ell$, for two different values of T_i . Estimation of θ_1 corresponding to the first step in decay has been done following the procedure used in Fig. 2.5. Here, $L = 256$ and $d = 3$ 58
- 2.20 Plot of the Exponent θ_1 as a function of ϵ . The continuous line is a non-linear fitting. Further details are provided in the text. Presented results are for $L = 256$ in $d = 3$ 59

2.21	Scaling plot of P , versus ℓ/ℓ_c , for three different T_i values in $d = 3$, for $L = 128$, in log-log scale. The solid line has a power-law decay with exponent 0.54.	60
2.22	Double-log plot of $\ell_c - 1$, in $d = 3$, versus ϵ . The solid line there has $d = 3$ Ising critical divergence of ξ . We have presented results for $L = 128$ (circles) as well as $L = 256$ (squares). . . .	61
2.23	$P(t)(\ell/\ell_c)^{3\theta}$, with $\theta = 0.18$, are plotted vs ℓ/ℓ_c , for quenches from three values of T_i to $T_f = 0$, in $d = 3$, using linear scale.	62
2.24	Log-log plot of $P(t)(\ell/\ell_c)^{3\theta}$ vs ℓ/ℓ_c for $T_i = 4.6$. The continuous line is a fit to the function in Eq. (2.13). Further details are provided in the text.	63
3.1	Log-log plots of local persistence probability, $P(t)$, vs t , for quenches (of the Glauber Ising model) from different values of initial temperature T_i ($\geq T_c$, the critical temperature), to the final value $T_f = 0$. All results correspond to space dimension $d = 2$ and square lattice, with linear dimension of the square box being $L = 2048$, in units of the lattice constant a . The lines represent various power-law decays, values of the exponents being mentioned in appropriate places.	73
3.2	Snapshots of the persistent spins are shown for quenches from $T_i = \infty$ and T_c , to $T_f = 0$. The results correspond to $d = 2$, $L = 2048$ and $t = 10^4$ MCS. In both the cases only parts of the boxes are shown. The persistent spins are marked in dots.	76

3.3	Snapshots of the persistent spins from different times, mentioned on the figure, are shown for $T_i = 2.4$ and $T_f = 0$. Other details are same as Fig. 3.2.	76
3.4	Density correlation functions, $D(r, t)$, related to the persistent spins, are plotted vs r . Results are presented from two different times, for $T_i = 2.4$ and $T_f = 0$. The system dimensionality is $d = 2$ and value of L is 2048.	81
3.5	Scaling analysis of $D(r, t)$ for the $d = 2$ Ising model, with $T_i = T_c$ and $T_f = 0$, where $f(x)$ is plotted vs $x = r/\ell_p$, using data from different times after the quench, on log-log scale. The solid line corresponds to a power-law decay with an exponent 0.09. The value of L is 2048 for all the results.	82
3.6	Same as Fig. 3.5 but for $T_i = \infty$. The solid line here has the power-law decay exponent 0.45.	83
3.7	Log-log plot of persistence length scale, ℓ_p , as a function of t , for $d = 2$ Ising model, following quench from $T_i = \infty$ to $T_f = 0$, with $L = 2048$. The solid line represents a power-law growth with the exponent $1/2$	84
3.8	Same as Fig. 3.7, but here $T_i = T_c$. The solid line corresponds to power-law growth with exponent $1/2$	85
3.9	Instantaneous exponent, z_i , obtained using the data in Fig. 3.7. The horizontal dashed line correspond to our estimate for z , whereas solid line is guide to the eyes.	86
3.10	Same as Fig. 3.9, but here $T_i = T_c$. The dashed and the solid lines have the same meaning as in Fig. 3.9.	87

3.11	Log-log plot of ℓ vs t , in $d = 3$, for $T_i = \infty$. The solid lines correspond to different power laws, exponents for which are mentioned.	88
3.12	Plot of instantaneous exponent α_i , as a function of $1/\ell$. The dashed horizontal lines represent exponent values 0.36 and 0.48. The results are for $T_i = \infty$ and $d = 3$	89
3.13	Log-log plot of $P(t)$ vs t , for $d = 3$ and $T_i = \infty$	90
3.14	Instantaneous exponent θ_i is plotted as a function of $1/\ell$. Horizontal dashed lines are for $\theta = 0.176$ and 0.15 . The results correspond to $T_i = \infty$ and $d = 3$	91
3.15	Log-log plot of ℓ vs t , for $d = 3$, $L = 400$ and $T_i = T_c$. The solid line corresponds to a power-law growth with exponent 0.45.	92
3.16	Plot of P vs t , for $d = 3$, $T_i = T_c$ and $T_f = 0$, on log-log scale. The solid line there represents a power-law decay with exponent 0.105.	93
3.17	Scaling function $f(x)$ is plotted vs x , for $d = 3$, $T_i = \infty$ and $T_f = 0$, using data from few different times. The solid line has a power-law decay with exponent 0.38. The results were obtained for simple cubic lattice with $L = 256$	94
3.18	Same as Fig. 3.17 but for $T_i = T_c$. Here the solid line has a power-law decay exponent 0.24.	95

3.19	Log-log plot of persistence length scale, ℓ_p , as a function of t , for $d = 3$ Ising model, following quench from $T_i = \infty$ to $T_f = 0$, with $L = 512$. The solid lines correspond to power-law growths with exponents mentioned there.	96
3.20	Same as Fig. 3.19, but here $T_i = T_c$ and $L = 256$	97
3.21	Instantaneous exponent, z_i , obtained using the data in Fig. 3.19, is plotted vs. $1/\ell_p$. The horizontal dashed line correspond to our estimates for z and the solid line there is guide to the eyes.	98
3.22	Same as 3.21, with $T_i = T_c$ and $L = 256$	99
3.23	Plots of block persistence probabilities, $P_b(t)$, vs t , from different values of ℓ_b , for $T_i = T_c$, in $d = 2$. We have used $L = 2048$	100
3.24	Scaling plots of the persistence probabilities in Fig. 3.23. The scaling function $h(x)$ is plotted, on a log-log scale, vs $x = t/\ell_b^{1/\alpha}$. Various power-law decays are shown by solid lines with the exponent values being mentioned next to appropriate lines.	101
3.25	Scaling plot similar to Fig. 3.24 is presented for $T_i = \infty$ with $d = 2$ and $L = 2048$. Solid lines in the figure represent various power-laws with exponents mentioned there.	102

-
- 4.1 Log-log plots of the average domain length, $\ell(t)$, vs time, for $T_f = 0$. Results from both $d = 2$ and 3 are presented. In both the cases linear dimension of the system is $L = 200$. The solid lines correspond to two different power-law growths, exponents being mentioned in the figure. 117
- 4.2 Plots of the instantaneous exponent, α_i , vs $1/\ell$, obtained from the data in Fig. 4.1. 118
- 4.3 Finite-size scaling exercise for the $d = 3$ results for $\ell(t)$. Here we have shown the scaling function Y with the variation of the dimensionless quantity y . Y was obtained from the best collapse of data from three different system sizes (mentioned in the figure). The solid line corresponds to a power law decay with exponent 0.35. These results are from $T_f = 0$ 119
- 4.4 Log-log plot of $\ell(t)$ vs t , for $d = 3$ and $T_f = 0$, with $L = 512$. The rest of the results are presented for this particular system size. The solid lines indicate different power-law growths, the exponents being mentioned. 120
- 4.5 Plot of instantaneous exponent α_i as a function of t , the x -axis being in log scale, for the data presented in Fig. 4.4. The horizontal solid lines there correspond to $\alpha = 1/3$ and $1/2$ 121
- 4.6 Same as Fig. 4.4 but for $T_f = 0.6T_c$. The continuous line there corresponds to a power-law growth with exponent 0.48. 122
- 4.7 Log-log plot of the persistence probability, $P(t)$, as a function of t , for $d = 3$, $T_f = 0$ and $L = 512$ 123

-
- 4.8 Instantaneous exponent, θ_i , vs t , x -axis being in a log scale. The horizontal solid lines there correspond to the ordinate values 0.176 and 0.15. 124
- 4.9 Log-log plots of the autocorrelation function, $C_{\text{ag}}(t, t_w)$, vs ℓ/ℓ_w , for $T_f = 0$ and $0.6T_c$. For each value of T_f , results from multiple ages are presented. The solid line corresponds to a power-law decay, exponent for which is mentioned on the figure. 125
- 4.10 Plot of the instantaneous exponent, λ_i , vs $1/x$, for $T_f = 0.6T_c$, with $t_w = 300$ MCS. The solid line is a guide to the eyes. . . 127
- 4.11 Log-log plot of the ratio, R , between the master curves for the autocorrelations at $T_f = 0.6T_c$ and 0, as a function of x 128
- 4.12 Scaling plot of the two-point equal time correlation functions from $T_f = 0$ and $d = 3$. The distance along the abscissa has been scaled by the average domain sizes at different times from which data are presented. The solid curve corresponds to the OJK form (see Eq. (4.8)). 130
- 4.13 Same as Fig. 4.12, but for $T_f = 0.6T_c$. The solid curve there represents the OJK form (see Eq. (4.8)). 131
- 4.14 Scaled correlation functions from different T_f in $d = 2$. The continuous curve is the the OJK function of Eq. (4.8). 132
- 4.15 Plots of the structure factors, from $T_f = 0$ and $0.6T_c$, vs k . The solid line represents the Porod law. For both the temperatures, we have presented results from $t = 5000$. These results are from $d = 3$ 133

-
- 4.16 Log-log plots of ℓ vs t , with (modified) and without (original) subtracting the interface width ($\omega(t)$) from $\ell(t)$. The solid line represents a power-law with $\alpha = 1/2$ 136
- 4.17 Plots of λ_i vs $1/x$ ($x = \ell/\ell_w$) with and without subtracting $\omega(t)$ from ℓ and ℓ_w . The solid lines are guides to the eye. All results correspond to $d = 3$ and $T_f = 0.6T_c$ 137
- 5.1 Plots of the average domain size, ℓ , vs time, on a log-log scale. Results from both $d = 2$ and 3 are included. The solid lines represent power-laws, exponents for which have been mentioned. The horizontal dashed line marks the location of the appearance of finite-size effects. 152
- 5.2 Log-log plots of the correlation function $C_{ag}(t, t_w)$, vs ℓ/ℓ_w , for $d = 2$. Results from a few different values of t_w are shown. The solid line corresponds to a power-law decay with exponent $\lambda = 1.29$ 153
- 5.3 Same as Fig. 5.2, but here it is for $d = 3$. The solid line here has the power-law exponent 1.67. 154
- 5.4 Instantaneous exponent, λ_i , for the $d = 2$ Ising model, is plotted as a function of ℓ_w/ℓ . The values of t_w are mentioned on the figure. The solid line is a guide to the eye. 155
- 5.5 Same as Fig. 5.4, but here it is for $d = 3$ 156
- 5.6 Same as Fig. 5.2, but here we have fixed the value of t_w and presented data from different L in $d = 2$. The value of t_w is mentioned. 157

5.7	Same as Fig. 5.6, but here it is for $d = 3$ and t_w value is different.	158
5.8	Finite-size scaling analysis of the autocorrelation function in $d = 2$. Here we have obtained the scaling function Y from the collapse of data from different system sizes, for a fixed value of t_w , mentioned on the figure.	159
5.9	Same as Fig. 5.8, but here we do the exercise for $d = 3$	160
5.10	Scaling plot of the structure factor in $d = 2$. The solid line represents a power-law, exponent for which is mentioned in the figure.	161
5.11	Same as Fig. 5.10, but here it is in $d = 3$	162
5.12	Plots of the structure factor, vs k , on a double log scale, for $d = 2$ and $d = 3$	162
6.1	Evolution snapshots of the active system from four different times. The locations of the particles are marked by dots.	174
6.2	Upper frames: Evolution snapshots from the Kawasaki exchange Monte Carlo simulations of the Ising model. Lower frames: Same as above but from Glauber kinetics. The times are in units of number of Monte Carlo steps.	175

-
- 6.3 Scaling plot of the two-point equal time correlation function, for the active system. Data from four different times are presented. The symbols in the inset show $C(r, t)$ from the conserved Ising model, simulated by using the Kawasaki exchange Monte Carlo method. The solid curve there is the Ohta-Jasnow-Kawasaki (OJK) function, that matches with the correlation function for the nonconserved order-parameter dynamics of the Ising model. 177
- 6.4 Log-log plot of the scaled structure factor. The solid lines there represent different power laws, the exponents of which are mentioned. 178
- 6.5 Plot of the average domain length, $\ell(t)$, vs t , in a double log scale. The solid lines represent various power-laws, exponents for which are mentioned. 179
- 6.6 Instantaneous exponent for domain growth, α_i , is plotted as a function of $1/\ell$. Solid lines there are guides to the eye. The early time data is consistent with $2/3$. The late time data show convergence towards 1. 180
- 6.7 Plots of the autocorrelation function, C_{ag} , vs translated times $t - t_w$. We have presented data from three different values of t_w 181
- 6.8 The autocorrelation function, C_{ag} , is plotted vs ℓ/ℓ_w . The values for t_w are mentioned on the figure. 182

List of Tables

3.1	List of some nonequilibrium exponents for Ising model.	75
-----	--	----

Contents

Acknowledgements	iii
1 Introduction	1
1.1 Phase Transition	1
1.2 Phase Ordering Dynamics	6
1.2.1 Coarsening mechanisms and growth laws based on order- parameter conservation	8
1.2.2 Aging Dynamics	14
1.2.3 Persistence	16
1.3 Coarsening in Active Matters	18
1.4 Methodologies	19
1.5 Finite-Size Effects in Numerical Simulations and Finite-Size Scaling Analysis	25
Bibliography	27
2 Decay of Persistence Probability during Ordering in Ising Ferromagnet: Role of Initial Correlation	30
2.1 Introduction	30

2.2	Methods	33
2.3	Results	33
2.3.1	$d = 2$	34
2.3.2	$d = 3$	54
2.4	Conclusions	62
	Bibliography	66
3	Fractality in Persistence Decay and Domain Growth during Ferromagnetic Ordering: Dependence upon Initial Correla- tion	70
3.1	Introduction	70
3.2	Model and Method	77
3.3	An Overview of the Background On fractality of persistence pattern	78
3.4	Results	80
3.5	Conclusion	103
	Bibliography	106
4	Kinetics of Ferromagnetic Ordering in 3D Ising Model for Zero Temperature Quench	109
4.1	Introduction	109
4.2	Methods	114
4.3	Results	116
4.4	Conclusion	137

Bibliography	140
5 Aging during Coarsening in Ferromagnetic Ising Model for Zero Temperature Quench	145
5.1 Introduction	145
5.2 Methods	150
5.3 Results	151
5.4 Conclusion	163
Bibliography	165
6 Pattern Formation, Growth and Aging in a 2D Active Matter Model	168
6.1 Introduction	168
6.2 Model and Methods	171
6.3 Results	173
6.4 Conclusion	183
Bibliography	184

Chapter 1

Introduction

1.1 Phase Transition

Materials are found in multiple phases in the nature. A typical example is water, which is commonly seen in solid, liquid and vapor phases. Various equilibrium phases are decided by thermodynamic parameters like temperature (T), pressure (P), magnetic field (h), etc. A *phase transition* [1–4] occurs whenever the system undergoes a change from one equilibrium phase to another with the variation of these parameters. Phase transition is also observed in collective behavior of biological entities [5,6]. Here, unlike inanimate or “passive” objects, system constituents are self propelled. This type of systems are called the “active” matter to distinguish them from the standard “passive” cases. In active matter transitions, usually a steady state is the counterpart of above mentioned equilibrium state. Large portion of this thesis deals with the passive systems. Therefore, unless mentioned explicitly, we will refer to a “passive system” simply as a “system”.

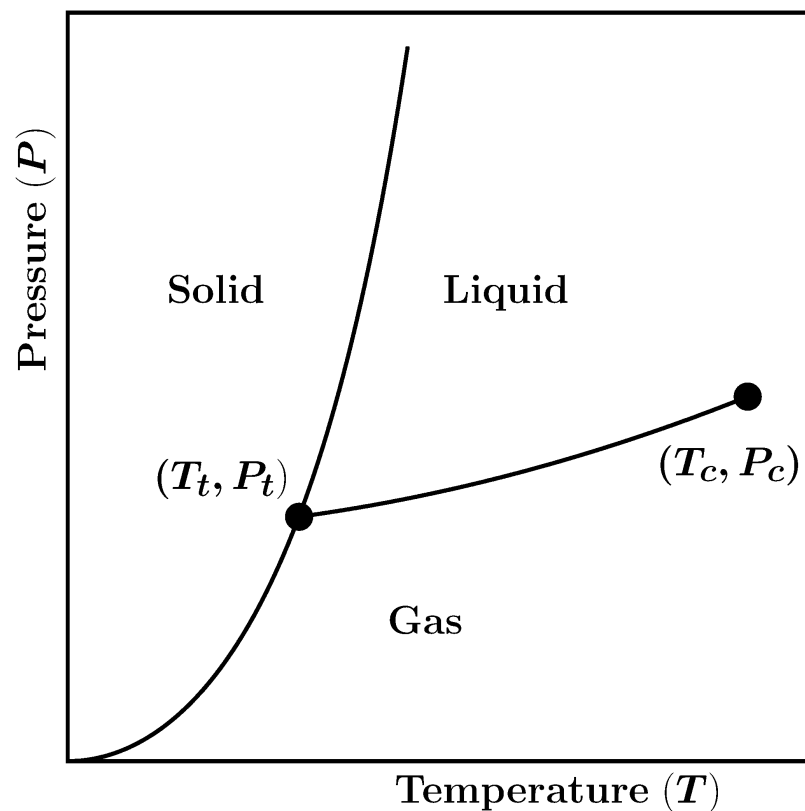


Figure 1.1: Phase diagram of a chemical substance in the P vs. T plane. Various equilibrium phases, critical point (T_c, P_c) and triple point (T_t, P_t) are marked on the figure.

In Fig. 1.1 we show a phase diagram of a standard chemical system in pressure-temperature plane. Solid, liquid and vapor phases are marked. These are separated from each other by the coexistence curves. Along each of these curves two phases coexist. These boundaries are lines of first order phase transitions [7]. The point (T_t, P_t) , where these three lines merge, is called the triple point. At this point all three phases coexist. The solid-liquid line continues forever, whereas the gas-liquid coexistence curve terminates at a point (T_c, P_c) . This point is called the critical point and in the vicinity of this point many static (e.g., specific heat, magnetic susceptibility) and

dynamic (e.g., viscosity, thermal conductivity) quantities show singularity. These facts are referred to as the critical phenomena [1, 4].

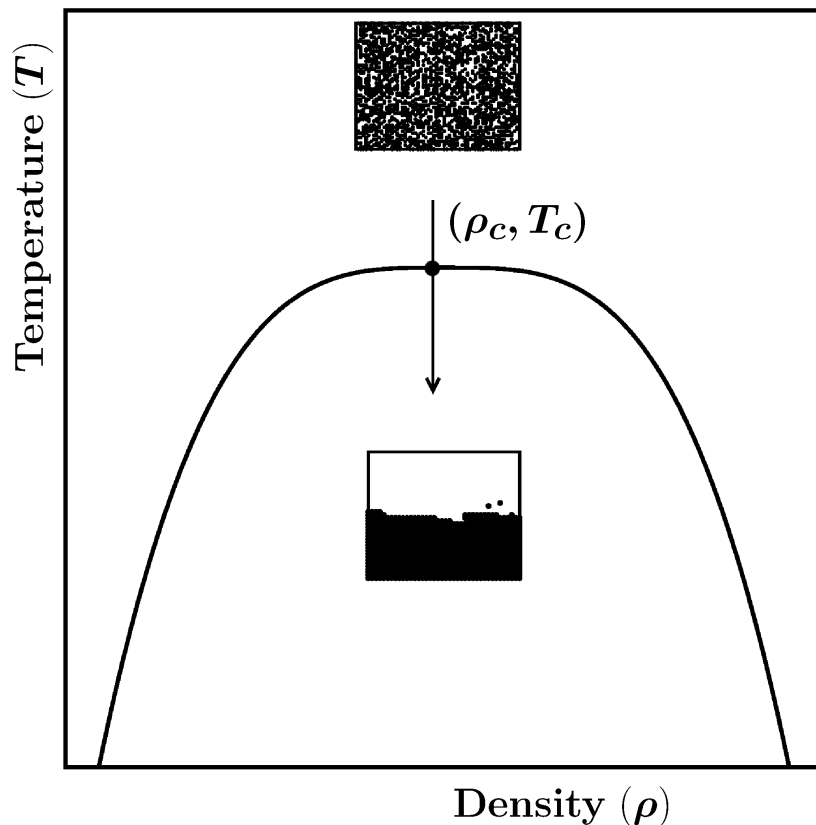


Figure 1.2: Phase diagram of the chemical substance of Fig. 1.1 in temperature (T) vs. density (ρ) plane, in the vicinity of the vapor-liquid critical point. In real situations the coexistence curve is not perfectly symmetric like the one drawn here.

In Fig. 1.2, we show the vapor-liquid coexistence curve in the temperature vs. density (ρ) plane. Outside the coexistence curve, a system is in a homogeneous density phase and inside the coexistence curve, it is in a phase-separated state. The left branch corresponds to the low density vapor phase and the right branch represents the high density liquid phase. In the context of a binary mixture ($A + B$), similar diagram can be drawn to

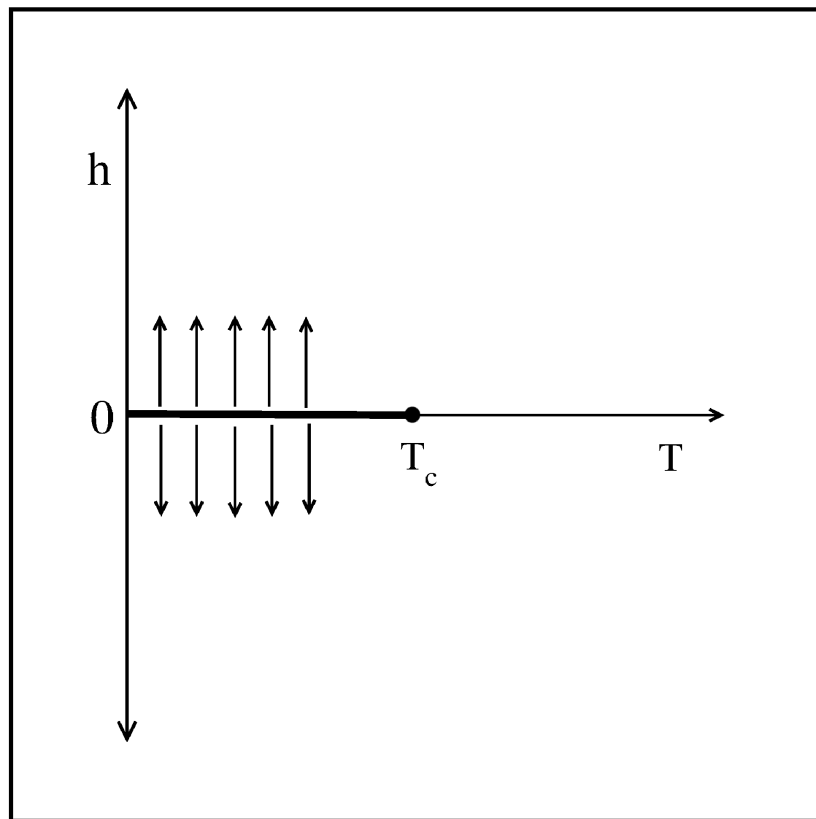


Figure 1.3: Phase behavior of a magnetic material in the external magnetic field (h) vs. temperature (T) plane. Above T_c , the system is in paramagnetic phase and below T_c , it is in ferromagnetic phase.

describe the phase behavior for demixing transitions, if the abscissa is replaced by the concentration, say, x_A , of one of the types of particles, A . Here, $x_A = N_A/(N_A + N_B)$, N_i ($i = A, B$) being the number of the i th kind of particles. Outside the coexistence curve two types of particles are mixed uniformly. Inside it, in equilibrium, the system is separated into A and B particle dominant phases. The left branch of the coexistence curve will then correspond to the B rich phase and right one to the A rich phase.

Similar phase diagram can also be obtained for a magnetic material undergoing paramagnetic to ferromagnetic phase transition, by replacing ρ by magnetization m . In Fig. 1.3, we show the phase diagram for such a transition in a different plane, i.e., in the h vs T plane. At high temperatures ($> T_c$, so called Curie temperature), the system is in a paramagnetic phase, with random alignment of spins (atomic magnetic moments) resulting in zero net magnetization. Below T_c , the spins tend to align in a particular direction. In that case, the system has a nonzero value of m even for $h = 0$, a feature of the ferromagnetic phase. A quantity which varies in this way, to indicate different phases, is referred to as an *order parameter* [2,3]. Order parameter can be constructed for above mentioned other phase transitions too. For example, in the case of gas-liquid phase transition a relevant order parameter is the difference between the densities of the two phases, i.e., $\rho_l - \rho_g$, where ρ_l and ρ_g are the densities of the liquid and gas phases respectively. At a high temperature, the system being in a phase of uniform density (or zero “magnetization”) the value of the order parameter is zero, and below T_c , inside the coexistence curve, it varies as a function of T as $\sim (T - T_c)^\beta$, where β is a critical exponent [4]. Such power-law behavior is observed in other quantities as well. E.g. the correlation length, ξ , diverges as $(T - T_c)^{-\nu}$. In the thesis, we will deal with only scalar order parameter, though it can have any number of components depending upon the system under consideration.

1.2 Phase Ordering Dynamics

Here we discuss various aspects of the kinetics of different kinds of phase transitions. One is interested in the nonequilibrium dynamics related to the evolution of a system to a new equilibrium state, having been quenched from a configuration prepared outside the coexistence curve to inside it. At high temperature the system is in a homogeneous phase. If the temperature of the system is quenched below T_c , the system becomes unstable to fluctuations and tries to attain its new equilibrium state at that temperature. The process is not instantaneous and comprises complex nonlinear dynamics, involving the formation and growth (“coarsening”) of domains. This process is called the *phase ordering* or *domain coarsening* [2,3].

To illustrate, let us retort to the previously stated paramagnetic to ferromagnetic phase transition. As stated above, for $T > T_c$ the system is in the paramagnetic phase and below T_c it is in the ferromagnetic phase. In the paramagnetic phase, the spins are disordered. If the system is now quenched below the Curie temperature, it tries to obtain the ferromagnetic ordering at that temperature. This equilibration process, as stated earlier, takes time and final ordered state is reached via formation and growth of domains of like spins. In the case of a binary mixture ($A + B$), outside the coexistence curve both types of particles are homogeneously mixed. When quenched inside the coexistence curve, the system falls out of the equilibrium and proceeds towards the equilibrium phase-separated state via formation and growth of A - and B -rich domains.

The domain pattern typically shows an interesting “scaling” dynamics [2].

The patterns at later times are statistically similar to those at earlier times, apart from a global change in length scale. As a consequence the two-point equal time correlation function

$$C(r, t) = \langle \psi(\vec{r}, t) \psi(\vec{0}, t) \rangle - \langle \psi(\vec{r}, t) \rangle \langle \psi(\vec{0}, t) \rangle, \quad (1.1)$$

r being the distance between two points, shows the scaling behavior

$$C(r, t) \equiv \tilde{C}(r/\ell(t)), \quad (1.2)$$

where $\ell(t)$ is the average size of domains at time t and \tilde{C} is independent of time. In addition to finding out the functional forms of $C(r, t)$ for various types of transitions, another natural question to ask is to how the characteristic length scale (ℓ) grows with time (t). It is found that in many phase ordering systems [2, 3]

$$\ell(t) \sim t^\alpha, \quad (1.3)$$

where α is the *growth exponent* [2]. The value of α depends on order-parameter conservation, number of components of the order-parameter, transport mechanism, system dimensionality, etc.

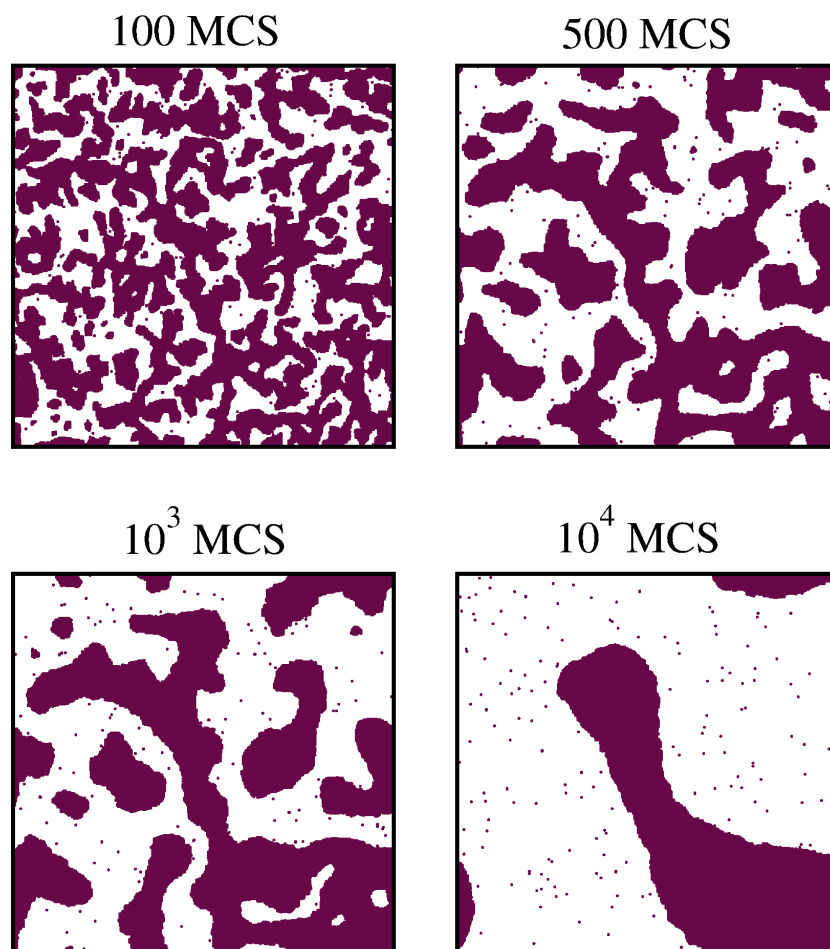


Figure 1.4: Snapshots during the evolution of an Ising ferromagnet. The dots represent the spins in +1 state or the up direction and the unmarked sites are the locations of down spins. Results are presented from four different times which are mentioned on top of the frames, in units of Monte Carlo steps (MCS).

1.2.1 Coarsening mechanisms and growth laws based on order-parameter conservation

1.2.1.1 Nonconserved order-parameter dynamics

The phase ordering dynamics during the paramagnetic to ferromagnetic phase transition is an example of nonconserved order-parameter (NCOP)

dynamics [2,3]. There, one kind of domain grows at the expense of other, so that the total system magnetization does not remain conserved throughout the evolution. Snapshots of such evolution from different times are shown in Fig. 1.4. These were obtained via Monte Carlo simulations of the Ising model. See below for further details.

At the atomistic level, such systems can be studied via Monte Carlo simulations by introducing the Glauber spin flip mechanism [8,9] in spin-1/2 Ising model [9]. The Hamiltonian of the Ising model is given by [9]

$$H = -J \sum_{\langle ij \rangle} S_i S_j, \quad J > 0, \quad S_i = \pm 1, \quad (1.4)$$

where J is the interaction strength, S_i is the spin at the i th site of a regular lattice. The angular brackets there indicate the consideration of only nearest neighbor interaction. Starting from this model, using a master equation involving the probability of a spin configuration in one state to go to another and applying a mean field approximation one can obtain the time dependent Ginzburg-Landau (TDGL) equation [2,3]. In absence of external magnetic field, the TDGL equation is given by [3]

$$\frac{\partial}{\partial t} \psi(\vec{r}, t) = \psi(\vec{r}, t) - \psi(\vec{r}, t)^3 + \nabla^2 \psi(\vec{r}, t), \quad (1.5)$$

where $\psi(\vec{r}, t)$ is a order parameter field, typically obtained by coarse-graining the Ising spins over the equilibrium correlation length. One can study ferromagnetic ordering by numerically solving this equation. Because of the

coarse-grained nature, in this case it is possible to access larger characteristic length scales.

Now, to obtain the growth law, we consider a spherical domain of radius ℓ . Considering the curvature driven nature of the dynamics during the evolution, the velocity of domain boundary can be expressed as

$$v_\ell = \frac{d\ell}{dt} \sim \frac{1}{\ell}, \quad (1.6)$$

so that

$$\ell \sim t^{1/2}. \quad (1.7)$$

This is the Cahn-Allen (CA) growth law [10]. Numerical simulations carried out for the Ising model (and the TDGL equation) confirmed the growth exponent, with some exceptions [11–15].

1.2.1.2 Conserved order-parameter dynamics

In a conserved order-parameter (COP) dynamics [2, 3], the total order parameter remains constant throughout the evolution process. A typical example of COP dynamics is the phase separation in a solid binary mixture when it is subjected to a quench from above T_c to a temperature below it. Evolution snapshots in such a situation are presented in Fig. 1.5. The results are obtained from Monte Carlo simulations of the Ising model with Kawasaki exchange mechanism. Vapor-liquid phase transition and subsequent ordering is also an example of such dynamics.

As stated above, at the microscopic level the kinetics of phase separation in a solid binary mixture is studied via the Kawasaki exchange [2, 3, 9, 16]

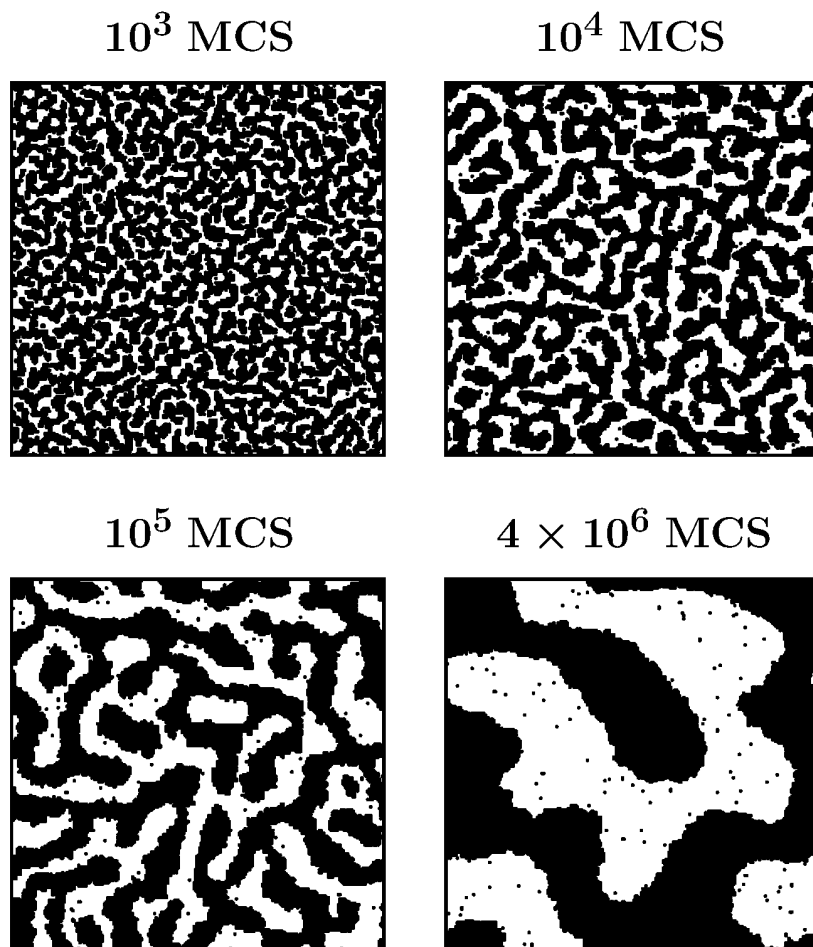


Figure 1.5: Snapshots showing the evolution of a conserved system, obtained via Monte Carlo simulations of Kawasaki exchange Ising model, upon quenching from a high temperature to a temperature $T = 0.6T_c$. The black dots mark the locations of A particles (up spins) and the down spins (location of B particles) are left unmarked.

Monte Carlo simulation of the Ising model. There the up and down spins correspond to the two different types of particles. Again, like NCOP dynamics, via a master equation approach, one can arrive at a coarse-grained

dynamical equation. This is written as

$$\frac{\partial}{\partial t}\psi(\vec{r}, t) = -\nabla^2[\psi(\vec{r}, t) + \nabla^2\psi(\vec{r}, t) - \psi^3(\vec{r}, t)], \quad (1.8)$$

which is referred to as the Cahn-Hilliard (CH) equation [17]. There exists phenomenological derivations as well for the TDGL and CH equations.

To obtain the growth law let us look at the mechanism of the enhancement of length scale. Diffusion is the sole mechanism of transport for domain growth in solids, the driving force coming from the chemical potential gradient. Therefore, the interface velocity and the chemical potential can be interconnected as

$$\frac{d\ell(t)}{dt} \sim |\vec{\nabla}\mu| \sim \frac{\sigma}{\ell(t)^2}, \quad (1.9)$$

where σ is the $A - B$ interfacial tension. Solving Eq. (1.9) one obtains,

$$\ell(t) \sim t^{1/3}. \quad (1.10)$$

This is known as the Lifshitz-Slyozov (LS) growth law [2, 3, 18].

In fluids the growth is much faster due to hydrodynamics. For the sake of completeness, we briefly mention the effect of hydrodynamics [19, 20] in COP dynamics for fluid systems. There exist three distinct regimes of growth. Without getting into the details, below we quote the values of the growth

exponent at different regimes [19, 20] (in order of their appearance):

$$\ell(t) = \begin{cases} t^{1/3} & \text{(Diffusive Growth),} \\ t & \text{(Viscous Hydrodynamic Growth),} \\ t^{2/3} & \text{(Inertial Hydrodynamic Growth).} \end{cases} \quad (1.11)$$

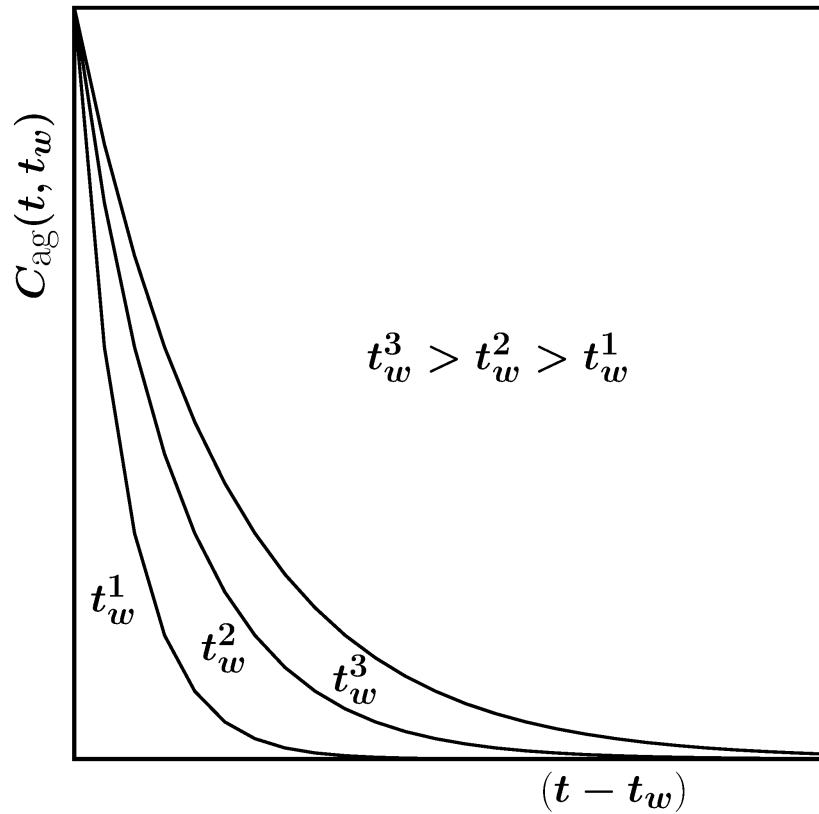


Figure 1.6: Schematic plots of the autocorrelation function $C_{\text{ag}}(t, t_w)$, with the variation of $(t - t_w)$, for three different values of t_w .

1.2.2 Aging Dynamics

Aging dynamics [3, 21–23] holds extreme relevance in the study of a system driven out of equilibrium via external perturbation. When the system tries to approach the equilibrium state at the given values of the thermodynamic parameters, their relaxation time grows with the age of the system. Essentially, a younger system relaxes faster than the older ones. This phenomena is known as aging. As can be judged by the fact, aging is probed via two time quantities such as single point two-time autocorrelation function, $C_{\text{ag}}(t, t_w)$ [3], dynamic susceptibility, $R(t, t_w)$, etc., that provide information on the relaxation of a system with its age. Here, t is the observation time and t_w is the waiting time or the age of the system. $C_{\text{ag}}(t, t_w)$ and $R(t, t_w)$ are defined as [3]

$$C_{\text{ag}}(t, t_w) = \langle \psi(\vec{r}, t) \psi(\vec{r}, t_w) \rangle - \langle \psi(\vec{r}, t) \rangle \langle \psi(\vec{r}, t_w) \rangle, \quad (1.12)$$

$$R(t, t_w) = \frac{\delta \langle \psi(t) \rangle}{\delta \langle h(t_w) \rangle}, \quad (1.13)$$

where $h(t_w)$ is a weak perturbation imparted on the system at $t = t_w$. In the rest of the section and in the thesis we discuss $C_{\text{ag}}(t, t_w)$ only. Fig. 1.6 shows a schematic diagram depicting the behavior of $C_{\text{ag}}(t, t_w)$ as a function of translated time $t - t_w$ for different values of t_w . If the system had been in equilibrium, all the plots would have collapsed on top of each other. This is called the *time translation invariance*. However, in case of a nonequilibrium system, since $C_{\text{ag}}(t, t_w)$ decays slower with the age, this time translational

invariance is violated.

The study of aging is of immense importance in the slowly relaxing systems, covering a wide range of topics such as structural and spin glass systems, phase-separating multicomponent mixtures, ferromagnetic ordering, etc. One is interested in finding out and understanding the scaling properties of $C_{\text{ag}}(t, t_w)$. From the study of spin glass systems, Fisher and Huse (FH) predicted that $C_{\text{ag}}(t, t_w)$ should scale in a power-law fashion [21, 22, 24] as

$$C_{\text{ag}}(t, t_w) \sim \left(\frac{\ell}{\ell_w} \right)^{-\lambda}, \quad (1.14)$$

where λ is an aging exponent, and ℓ and ℓ_w are the domain lengths of the system at t and t_w , respectively. The value of λ depends on the conservation of the order parameter, spatial dimensionality, effect of hydrodynamics, etc. FH also proposed bounds on λ given as [21]

$$\frac{d}{2} \leq \lambda \leq d. \quad (1.15)$$

Later Yeung, Rao and Desai (YRD) improved the bounds (by including both NCOP and COP dynamics) to [24]

$$\lambda \geq \frac{d + \beta}{2}, \quad (1.16)$$

where β is related to the small wave-number (k) behavior of the structure

factor $S(k, t)$, which has the form

$$S \sim k^\beta. \quad (1.17)$$

Note that $S(k, t)$ is the Fourier transform of $C(r, t)$ and has the scaling form

$$S(k, t) \equiv \ell^d \tilde{S}(k\ell), \quad (1.18)$$

\tilde{S} , like \tilde{C} , is a time independent master function.

1.2.3 Persistence

Various correlation functions discussed above probe order parameter fluctuations (in space and time) in both equilibrium and nonequilibrium systems. In this context another important quantity is the persistence probability, $P(t)$ [25–29], which is defined as the probability that a given stochastic variable $\phi(t)$ retains its sign during the time interval $[0 : t]$. In the thesis we are concerned with the persistence in ferromagnetic ordering. In that case, $P(t)$ is defined as the fraction of spins that do not change sign (or flip) until time t . In this case as well as in many other phase transitions, $P(t)$ is observed to exhibit a power-law behavior [25, 30, 31]

$$P(t) = t^{-\theta}. \quad (1.19)$$

The (persistence) exponent θ depends upon the conservation of the order parameter, spatial dimensionality, symmetry of the order parameter, etc.

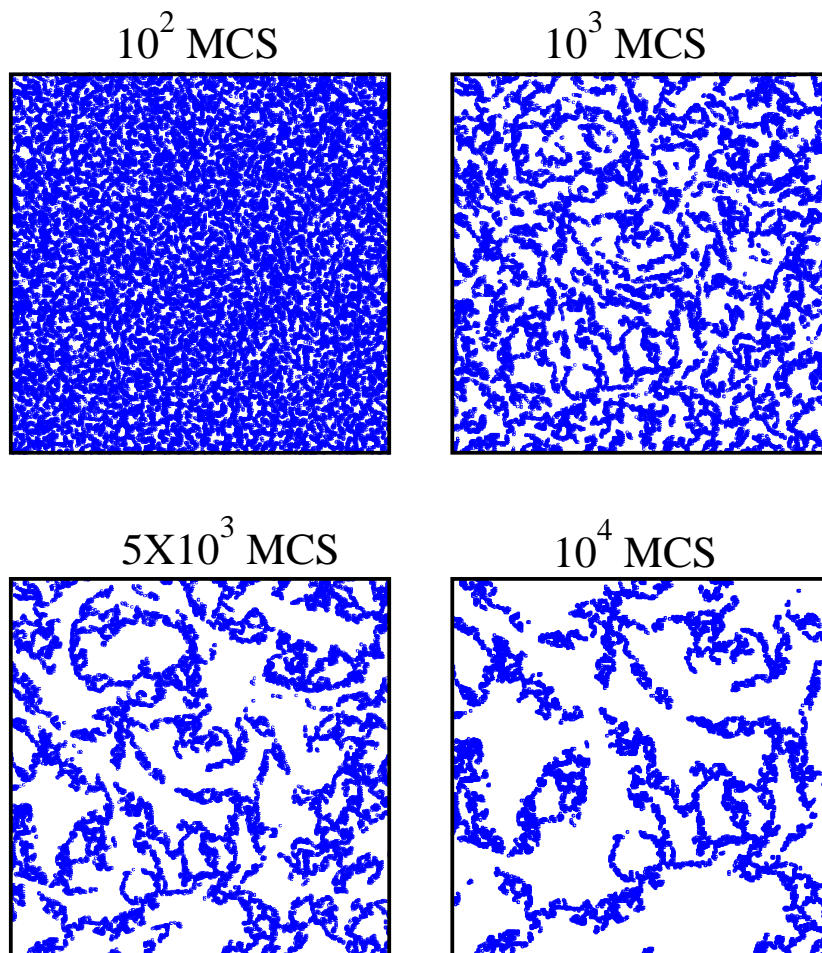


Figure 1.7: Snapshots of the persistent spins from four different times, during the ferromagnetic ordering. The spins marked with dots represent the persistent spins.

In Fig. 1.7 we have shown the snapshots of the persistent spins from four different times during the evolution of nonconserved Ising model. Beautiful fractal patterns [15, 32, 33] are observed. It is then natural to ask questions related to the fractal dimensionality, d_f , of these patterns as well.

Above definition of persistence probability is related to the change of sign of a single spin placed at a lattice site. However, if one is interested in probing the change in sign of order parameter over large length scales,

say over the whole system, the corresponding persistence is called the 'global persistence' [13,29] and the related decay exponent as the global persistence exponent. Both kinds of persistence have been discussed in the thesis.



Figure 1.8: Picture of a school of fish. Picture courtesy: S. Paul, K. Das, Nalina V.

1.3 Coarsening in Active Matters

Collective behavior [5, 6] of the biological systems has received a lot of attention in the recent years. A school of fish, a herd of sheeps or a swarm of bees move in a coherent manner, creating beautiful spatio-temporal patterns. In Fig. 1.8, a school of fish is shown. However, when attacked by some predator the coherence is lost. This can be seen as an order-disorder transition [34]. Though, first observed in living objects, it is not confined in the biological systems only. Various experiments have been set up with

vibrating rods, polymers, etc., that show similar features. The primary interest from physicists' point of view would be to look for universality in this kind of behavior. A good model to capture this sort of phase transition was proposed by Vicsek *et al.* There exist reports in favor of existence of second order transitions in such situations. This, however, still remains a matter of controversy. While the standard literature in this field deals with the emergence of such collective behavior, details of ordering or clustering dynamics started receiving attention only recently. In the thesis we ask the same questions as in the context of phase ordering dynamics in passive systems. We will provide further details on active matter later in this chapter.

1.4 Methodologies

In this thesis we have performed computer simulations of various atomistic models. These or similar models are frequently used in the literature to describe phase transitions in passive and active systems. In the domain of passive phase transitions, we are interested in the para- to ferromagnetic transition. For this purpose we have used the Monte Carlo (MC) simulations. First we discuss methods related to this.

In the first step, the system is prepared at a desired temperature above the critical temperature. The initial temperatures (T_i) of the configurations play a pivotal role since the correlations within the systems are temperature dependent. Close to T_c , the system has a large equilibrium correlation length

ξ . Recall that [35]

$$\xi \sim \epsilon^{-\nu} \quad (1.20)$$

where $\epsilon = |T_i - T_c|$ and ν is a static critical exponent. Between the two kinetic mechanisms touched upon above, viz., the Glauber and Kawasaki, the former is faster. In this method, a spin is randomly chosen and flipped. Nevertheless, it would require long simulation runs for a single spin flip algorithm like Glauber spin flip mechanism to prepare equilibrium configurations close to T_c . To avoid the difficulty, we follow an algorithm proposed by Wolff, in which a single cluster is grown and flipped subsequently.

The Wolff algorithm [36] starts with the random choice of single site on the lattice. All nearest neighbors with the same state are then connected to each other with the probability [9, 36]

$$p = 1 - \exp(-2\beta J). \quad (1.21)$$

This process is continued until no new bond is found. All the spins in the connected cluster is then flipped. This method has its origin in the Fortuin-kasteleyn theorem [9] which states that, it is possible to map ferromagnetic Potts model onto a corresponding percolating model. Now in percolation theory, states are generated by throwing particles or bonds in an uncorrelated manner. Hence, there is no critical slowing down.

Next step of the simulation is the updation of the system with time, after the quench. This we discuss following Ref. [9]. In our MC simulations we use

the standard Metropolis algorithm [9], in which the transition from one state to other depends on the energy difference between the final and the initial states.

Let us introduce the time dependent probability $P_n(t)$ of the system to be at given state n of the system. The time dependent behavior of the states of the system is captured by the master equation

$$\frac{\partial P_n(t)}{\partial t} = - \sum_{n \neq m} [P_n(t)W_{n \rightarrow m} - P_m(t)W_{m \rightarrow n}], \quad (1.22)$$

where $W_{n \rightarrow m}$ is the transition rate for $n \rightarrow m$. In equilibrium, there must not be any current, so that

$$\frac{\partial P_n(t)}{\partial t} = 0. \quad (1.23)$$

Hence,

$$P_n(t)W_{n \rightarrow m} = P_m(t)W_{m \rightarrow n}. \quad (1.24)$$

This expression is referred to as the detailed balance. The probability of a classical system to be in the n th state is given by

$$P_n(t) = \frac{\exp(-E_n/k_B T)}{Z}, \quad (1.25)$$

where Z is the partition function. The probability cannot be exactly calculated because of the lack of knowledge of the partition function. However, if a Markov chain is considered, where a new state m is generated from the preceding state n , then the transition probability depends only on the energy difference between the two states. Now, any transition rate which satisfies

the detailed balance is acceptable. The Metropolis form is given as [9]

$$W_{n \rightarrow m} = \begin{cases} \exp(-\Delta E/k_B T), & \Delta E > 0 \\ 1, & \Delta E \leq 0, \end{cases} \quad (1.26)$$

where $\Delta E (= E_n - E_m)$ is the energy difference between the two states. The algorithm is implemented in computer simulation via the following steps.

- (1) A particle (spin) or a cluster (of particles) i is randomly chosen.
- (2) The energy change ΔE , which results due to the random displacement or flipping, is calculated.
- (3) A random number r is generated such that $0 < r < 1$.
- (4) If $r < \exp(-\Delta E/k_B T)$, the move is accepted.

Note that the kinetics, following the temperature quench, we have studied via the Glauber spin-flip moves with Metropolis acceptance algorithm.

In active matters velocity field plays important role. We intend to study such systems at the atomistic level. Thus, molecular dynamics (MD) simulations [37, 38] are well suited for that. In MD simulations, a smooth potential is used as interparticle interactions and from there one calculates the force on each particle. After computing the force, the Newton's equation of motion is needed to be solved. Various algorithms are proposed for this purpose. In the thesis we have used the velocity Verlet algorithm [37]. In this algorithm, the position update rule is governed by the following equation

$$\vec{r}_i(t + \Delta t) = \vec{r}_i(t) + \vec{v}_i(t)\Delta t + \frac{\vec{f}_i(t)}{2m_i}\Delta t^2, \quad (1.27)$$

where \vec{r}_i , \vec{v}_i , \vec{f}_i are the position, velocity and acceleration of the i -th particle with mass m_i . The velocity update in this formulation is given by

$$\vec{v}_i(t + \Delta t) = \vec{v}_i(t) + \frac{\vec{f}_i(t + \Delta t) + \vec{f}_i(t)}{2m_i} \Delta t. \quad (1.28)$$

These equations can be shown to have the time reversal symmetry, an integral part of the Newton's equation.

In our study of active matter the self propelling activity is introduced by using the Vicsek model [34]. In this model, at each discrete time step (Δt), a particle moving with a constant velocity orients its direction depending on the average direction of the particles within a radius of influence and an external perturbation which is of thermal origin. The position updation rule is given by

$$\vec{r}_i(t + \Delta t) = \vec{r}_i(t) + \vec{v}_i(t) \Delta t. \quad (1.29)$$

The velocity at time $(t + \Delta t)$, $\vec{v}_i(t + \Delta t)$, has an unchanged magnitude v and the direction is given by

$$O(t + \Delta t) = \langle O(t) \rangle_r + \Delta O, \quad (1.30)$$

where $\langle O(t) \rangle_r$ is the average direction of the particles within radius r from the particle and ΔO is the noise, which is chosen from a set of uniform random number. In our active matter study we have combined the Vicsek rule with inter-particle interaction. For the interparticle interaction part, we have performed MD simulations.

To keep the temperature fixed, we performed MD simulations in canonical

ensemble. Here, we use the the Langevin thermostat. There one solves the Langevin equation

$$m_i \ddot{\vec{r}}_i = -\vec{\nabla} u_i - \gamma m_i \dot{\vec{r}}_i + \sqrt{6\gamma k_B T m_i} \vec{R}(t), \quad (1.31)$$

where u_i is the interparticle potential, γ is the damping constant and $\vec{R}(t)$ is a noise which is δ correlated in space and time. There exists other thermostats in the literature. Unlike the Langevin one, some other thermostats satisfy requirements of hydrodynamics.

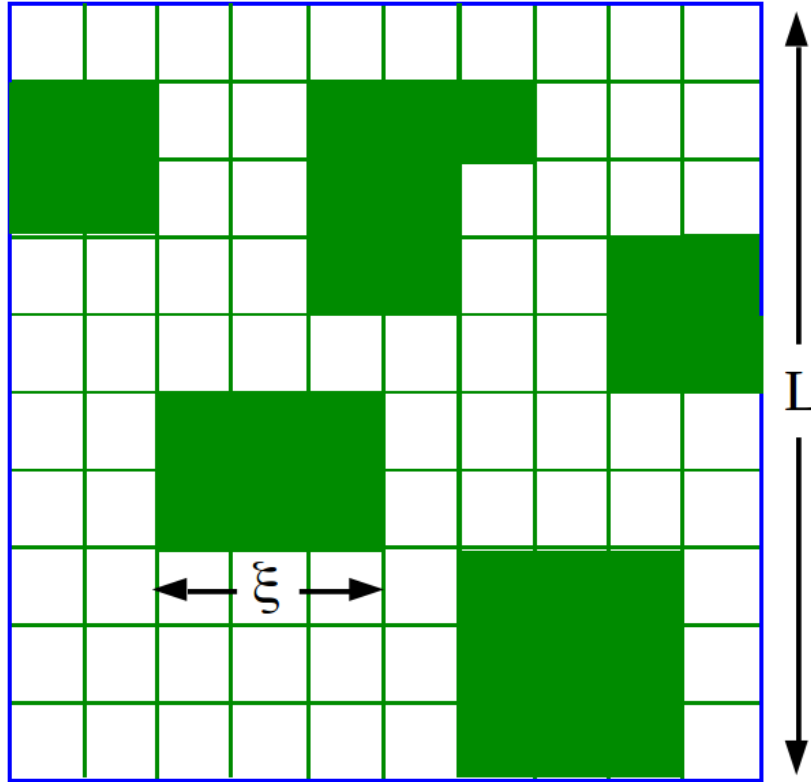


Figure 1.9: A schematic diagram showing the equilibrium correlation length ξ in a system of linear size L . Spins inside the shaded regions are correlated. Maximum value of ξ can be equal to L .

1.5 Finite-Size Effects in Numerical Simulations and Finite-Size Scaling Analysis

The motto of statistical physics is to predict the thermodynamic behavior of a system starting from the microscopic knowledge of the system. The standard procedure is to calculate the partition function

$$PF = \sum_i \exp[-\beta E_i], \quad (1.32)$$

and then calculate the (relevant) free energy,

$$F = -k_B T \ln PF. \quad (1.33)$$

Here, E_i is the energy of the the system in the i th state. Now, the occurrence of second order phase transition demands the nonanalyticity of F at the critical point. Here, we note that, this is only possible in the thermodynamic limit [35]. In computer simulations we deal with finite system sizes with finite number of degrees of freedom. This means that the free energy is analytic everywhere and “true” phase transition is not observed in computer simulations. With smaller system sizes, the (pseudo) critical point for a particular phase transition gets displaced further and further away from its value in the thermodynamic limit. Furthermore, maximum limit of ξ being at most the system size (see the depiction of ξ in Fig. 1.9), the divergence is hindered by the finite-size effects (FSE). Nevertheless, such FSE can be taken care of by the scaling analysis proposed by Fisher [39] in the context

of equilibrium critical phenomena. In fact FSE can be used to our advantage if such analysis is performed.

In critical phenomena the divergence of a quantity Z is expressed as

$$Z \sim \epsilon^{-z}, \quad (1.34)$$

where z is a critical exponent. To account for the size effects in finite systems one introduces the scaling function $Y(y)$ to write

$$Z \approx Y(y)\epsilon^z, \quad (1.35)$$

where $y = L/\xi$ is a dimensionless scaling variable. The function Y is independent of the system size. So data from different system sizes should collapse on top of each other if the exponent is chosen appropriately. This is the working principle of finite-size scaling analysis to quantify thermodynamic limit behavior from systems of small sizes. Such analysis has gained importance in domain coarsening phenomena as well. This we will discuss as we address the relevant problems.

Bibliography

- [1] A. Onuki, *Phase Transitions Dynamics* (Cambridge University Press, Cambridge, UK, 2002).
- [2] A.J. Bray, *Adv. Phys.* **51**, 481 (2002).
- [3] S. Puri and V. Wadhawan (ed.), *Kinetics of Phase Transitions* (Boca Raton: CRC Press, 2009).
- [4] H.E. Stanley, *Introduction to Phase Transitions and Critical Phenomena* (Oxford University Press, Oxford, 1971).
- [5] T. Vicsek and A. Zafeiris, *Phys. Rep.* **517**, 71 (2012).
- [6] M.C. Marchetti, J.F. Joanny, S. Ramaswamy, T.B. Liverpool, J. Prost, M. Rao, and R.A. Simha, *Rev. Mod. Phys.* **85**, 1143 (2013).
- [7] K. Binder, *Rep. Prog. Phys.* **50**, 783 (1987).
- [8] R.J. Glauber, *J. Math. Phys.* **4**, 294 (1963).
- [9] D.P. Landau and K. Binder, *a Guide to Monte Carlo simulations in Statistical Physics* (Cambridge University Press, Cambridge, 2009).
- [10] S.M. Allen and J.W. Cahn, *Acta Metall.* **27**, 1085 (1979).

-
- [11] J.G. Amar and F. Family, Bull. Am. Phys. Soc. **34**, 491 (1989).
- [12] J.D. Shore, M. Holzer, and J.P. Sethna, Phys. Rev. B **46**, 11376 (1992).
- [13] S. Cueille and C. Sire, J. Phys. A **30**, L791 (1997).
- [14] F. Corberi, E. Lippiello, and M. Zannetti, Phys. Rev. E **78**, 011109 (2008).
- [15] S. Chakraborty and S.K. Das, Phys. Rev. E **93**, 032139 (2016).
- [16] K. Kawasaki, Phys. Rev. **145**, 224 (1966).
- [17] P.C. Hohenberg and B.I. Halperin, Rev. Mod. Phys. **49**, 435 (1977).
- [18] I.M. Lifshitz and V.V. Slyozov, J. Phys. Chem. Solids **19**, 35 (1961).
- [19] E.D. Siggia, Phys Rev. A **20**, 595 (1979).
- [20] S.K. Das, S. Roy, and J. Midya, Comptes Rendus Physique, **16**, 303 (2015).
- [21] D.S. Fisher and D.A. Huse, Phys. Rev. B **38**, 373 (1988).
- [22] F. Liu and G.F. Mazenko, Phys. Rev. B **44**, 9185 (1991).
- [23] S. Majumder and S.K. Das, Phys. Rev. Lett. **111**, 055503 (2013).
- [24] C. Yeung, M. Rao, and R.C. Desai, Phys. Rev. E **53**, 3073 (1996).
- [25] A.J. Bray, S.N. Majumdar, and G. Schehr, Adv. Phys. **62**, 225 (2013).
- [26] B. Derrida, A.J. Bray, and C. Godrèche, J. Phys. A **27**, L357 (1994).

-
- [27] D. Stauffer, J. Phys. A **27**, 5029 (1994).
- [28] S.N. Majumdar, C. Sire, A.J. Bray, and S.J. Cornell, Phys. Rev. Lett. **77**, 2867 (1996).
- [29] S.N. Majumdar, A.J. Bray, S.J. Cornell, and C. Sire, Phys. Rev. Lett. **77**, 3704 (1996).
- [30] D. Stauffer, Int. J. Mod. Phys. C **8**, 361 (1997).
- [31] G. Manoj and P. Ray, Phys. Rev. E **62**, 7755 (2000).
- [32] G. Manoj and P. Ray, J. Stat. Phys. A **33**, 5489 (2000).
- [33] S. Jain and H. Flynn, J. Phys. A **33**, 8383 (2000).
- [34] T. Vicsek, A. Czirók, E. Ben-Jacob, I. Cohen, and O. Schochet, Phys. Rev. Lett. **75**, 1226 (1995).
- [35] N. Goldenfeld, *Lectures on Phase Transition and the Renormalization Group* (Perseus Books Publishing, Massachusetts, 1992).
- [36] U. Wolff, Phys. Rev. Lett. **62**, 361 (1989).
- [37] D. Frenkel and B. Smit, *Understanding Molecular Simulations: From algorithms to applications* (Academic Press, San Diego, 2002).
- [38] M.P. Allen and D.J. Tildesley, *Computer Simulations of Liquids* (Clarendon, Oxford, 1987).
- [39] M.E. Fisher, in *Critical Phenomena*, edited by M.S. Green (Academic Press, London, 1971).

Chapter 2

Decay of Persistence

Probability during Ordering in Ising Ferromagnet: Role of Initial Correlation

2.1 Introduction

When a homogeneous system is quenched below the critical point, the system becomes unstable to fluctuations and approaches towards the new equilibrium via the formation and growth of particle rich and particle poor domains [1–4]. In such nonequilibrium evolutions, over several decades, aspects that received significant attention are the domain pattern [3, 5–9], rate of domain growth [5, 10–15], persistence [16–25] and aging [26–31]. Average

size, ℓ , of domains typically grows with time (t) as [5]

$$\ell \sim t^\alpha. \quad (2.1)$$

The value of the exponent α for nonconserved order-parameter dynamics [5, 12], e.g., during ordering in an uniaxial ferromagnet, is $1/2$, in space dimension $d = 2$. In addition to the interesting structures exhibited by the domains of like spins (or atomic magnets) in a ferromagnet, the unaffected or persistent spins also form beautiful fractal patterns [16–19, 21, 22]. Typically, fraction of such spins, henceforth will be referred to as the persistent probability, P , decays as

$$P \sim t^{-\theta}, \quad (2.2)$$

with [20, 21] θ having a value $\simeq 0.22$ for the Ising model in space dimension $d = 2$ and $\simeq 0.18$ in $d = 3$.

The values of the exponents mentioned above are understood to be true for the perfectly random initial configurations, that mimics the paramagnetic phase at temperature $T = \infty$. Another relevant situation is to quench a system from finite initial temperature (T_i) with a large equilibrium correlation length ξ . However, this problem has received only occasional attention [32–35], though experimentally very relevant. In this context, the behavior of the two-time equal point correlation function, relevant in the aging phenomena, was studied [33, 34] in $d = 2$ for $T_i = T_c$, the critical temperature. It was pointed out that such quenches would form a *new universality class* and was shown that the decay of the above correlation was significantly slower for $T_i = T_c$ than $T_i = \infty$. In view of that, a slower decay

of P is also expected [35]. On the other hand, the behavior of P and ℓ are expected to be disconnected [36]. Nevertheless, the rate of growth of ℓ may be different for $T_i = T_c$ and $T_i = \infty$, at least during the transient period. In this chapter, we address the T_i dependence for persistence and domain growth in a ferromagnet, via Monte Carlo (MC) simulations [37] of nearest neighbor Ising model [37]

$$H = -J \sum_{\langle ij \rangle} S_i S_j; \quad S_i = \pm 1, \quad J > 0, \quad (2.3)$$

in $d = 2$ and $d = 3$, on square and simple cubic lattices, respectively.

Starting from a high value, as T_i approaches T_c [37] [$\simeq 2.27J/k_B$ in $d = 2$ or $4.51J/k_B$ in $d = 3$, k_B being the Boltzmann constant], a two-step decay in P becomes prominent, except for $T_i = T_c$. For the latter initial temperature, power-law behavior with exponents much smaller than the ones observed for quenches from $T_i = \infty$ lives forever. In addition to identifying these facts, a primary objective of the chapter is to accurately quantify these decays and find out the influence of dimensionality. For the domain growth, on the other hand, we do not observe a modification to the time dependence with the variation of T_i , *almost* from the very beginning.

The rest of the chapter is organized as follows. In section 2.2 we briefly describe the methods. Results from both the dimensions are presented in section 2.3. Section 2.4 concludes the chapter with a summary and outlook.

2.2 Methods

The nonconserved order-parameter dynamics in the MC simulations have been incorporated via the Glauber spin-flip mechanism [38]. In this method, a randomly chosen spin is tried for a change in sign which is accepted according to the standard Metropolis algorithm [37]. We apply periodic boundary conditions in all directions. Time is expressed in units of MC steps (MCS), each MCS consisting of L^d trials, L being the linear dimension of a square or cubic box. We have computed ℓ from the domain size distribution, $P_d(\ell_d, t)$, as [15]

$$\ell(t) = \int \ell_d P_d(\ell_d, t) d\ell_d, \quad (2.4)$$

where ℓ_d is calculated as the distance between two successive interfaces in any direction. All lengths are expressed in units of the lattice constant a . We present the results after averaging over multiple initial configurations. This number ranges from 20 (for $L = 1024$) to 200 (for $L = 400$) in $d = 2$ and from 10 (for $L = 256$) to 50 (for $L = 64$) in $d = 3$. The initial configurations for T_i close to T_c were carefully prepared via very long runs. At T_c , for $d = 2$, depending upon the system size, length of such runs varied between 5×10^6 to 10^8 MCS.

2.3 Results

In this section we present the MC results and their analyses, first from $d = 2$ (subsection 2.3.1), followed by $d = 3$ (subsection 2.3.2).

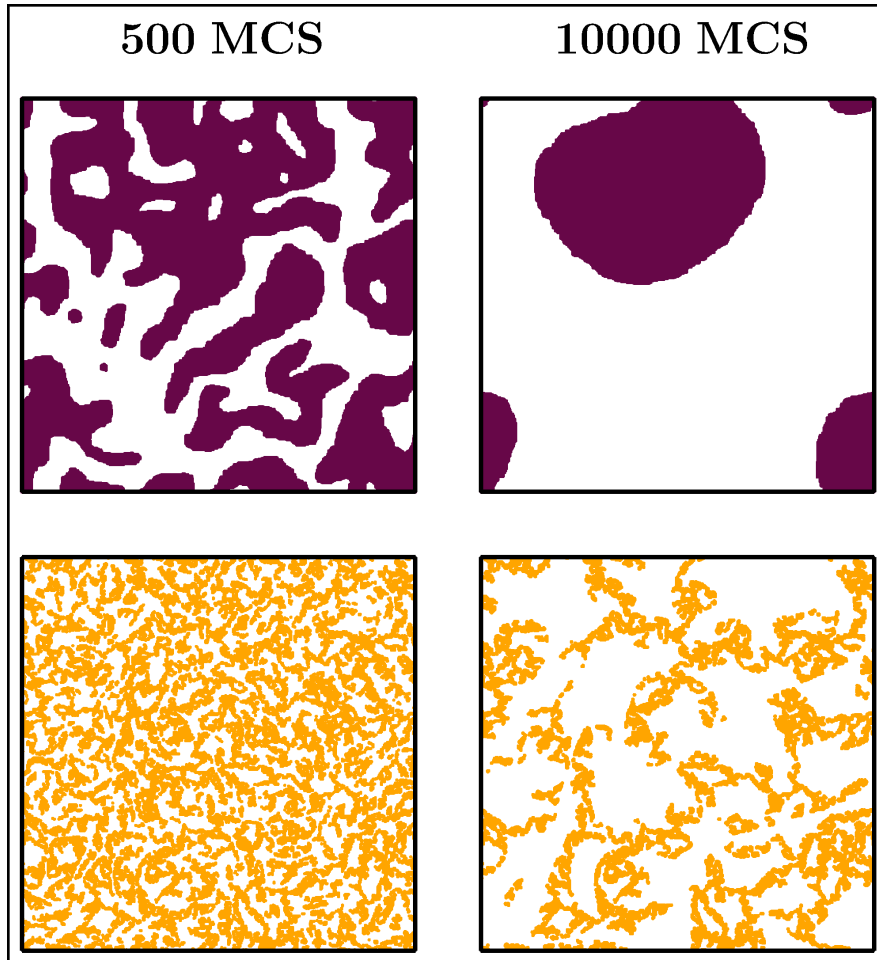


Figure 2.1: Upper panels show snapshots during the evolution of the Glauber Ising model with $T_i = \infty$, $T_f = 0$ and $L = 512$. The dotted regions represent domains of up spins. The lower panels show the unaffected spins, marked by dots, corresponding to the evolution snapshots above them. These results are from $d = 2$.

2.3.1 $d = 2$

Growth of the domains have been demonstrated in the upper frames of Fig. 2.1 for the system size $L = 512$ in $d = 2$. There we show snapshots from two different times during the evolution of the Glauber Ising model. In the lower frames of the figure, we show pictures marking only the persistent

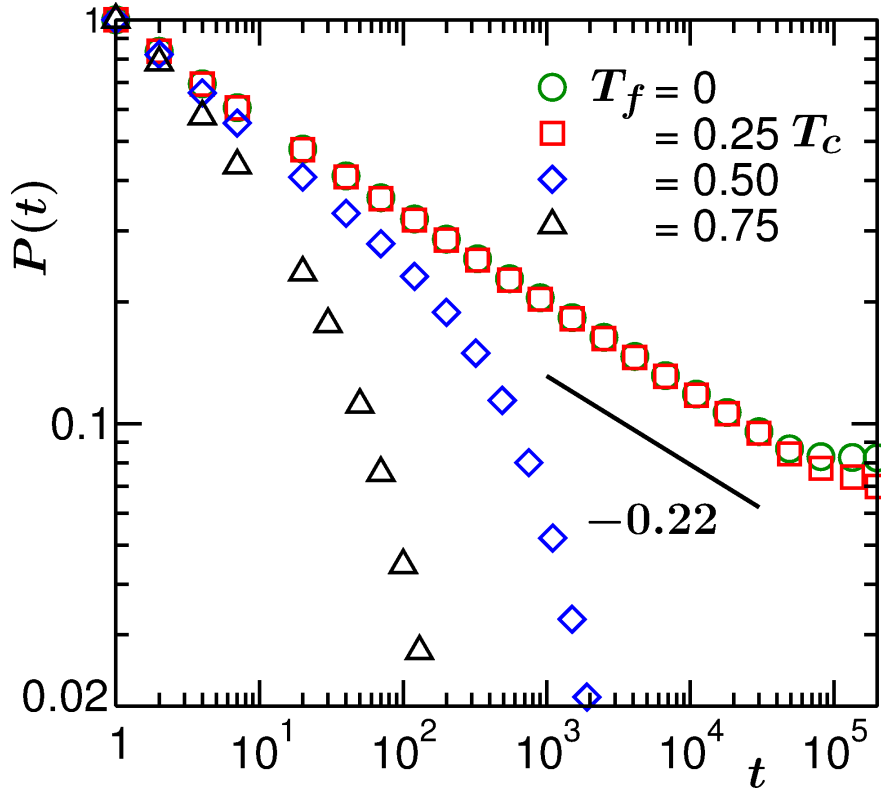


Figure 2.2: Plots of persistence probability, P , vs, time, on a log-log scale, for quenches from $T_i = \infty$, with $L = 512$, in $d = 2$. Four different values of T_f are included. The solid line there has a power-law decay with exponent 0.22.

spins. Beautiful patterns are visible. These results correspond to a quench from $T_i = \infty$ to the final temperature $T_f = 0$.

Plots of P , for $T_i = \infty$ and few different values of T_f , vs t , are shown in Fig. 2.2. The data for $T_f = 0$ and $0.25T_c$ are consistent with each other and follow power-law, the exponent being $\theta \simeq 0.22$. The flat behavior at the end is due to the finite-size effects. This value of θ is consistent with the previous observations [20, 21]. However, for higher values of T_f , as also previously observed [18, 19], the decay is not of power-law type. This is thought to be due to thermal fluctuation. When this fluctuation is taken care of, via the

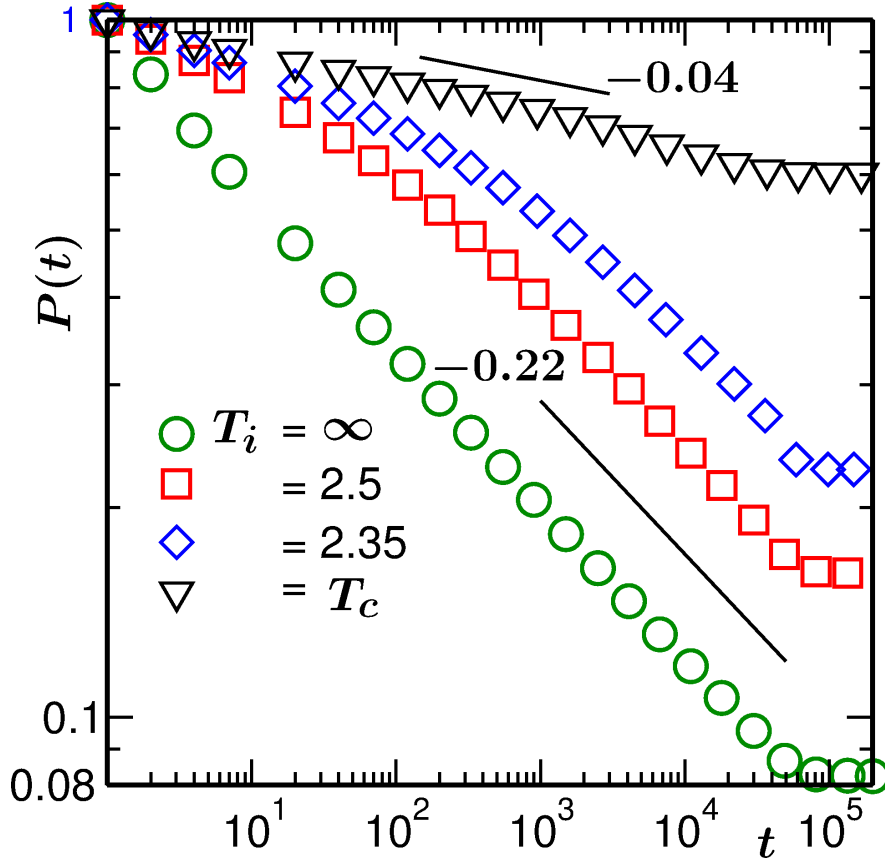


Figure 2.3: Log-log plots of P vs t , for quenches from different values of $T_i (\geq T_c)$, to $T_f = 0$, in $d = 2$ with $L = 512$. Continuous lines there correspond to power-law decays with exponents 0.22 and 0.04.

method described below, we observe $\theta \simeq 0.22$ for all the values of T_f included in Fig. 2.2, in agreement with Ref. [20]. In zero temperature situation spin-flips are related to the motion of the domain boundaries, leading to the growth of ℓ . At nonzero temperature, on the other hand, thermal noise causes flips in the bulk of the domains as well. Following Derrida [19], counting of these bulk spins was discarded by simulating an ordered configuration. In this method, flips common between the original (coarsening) system and the ordered system were identified as part of bulk dynamics and thus were

subtracted from the total number of flips, to stay only with the effects of boundary motion.

It is thought that persistence and domain growth are not strongly connected to each other. Interestingly, different behavior in Fig. 2.2 for $T_f > 0.25T_c$ and $T_f < 0.25T_c$ is strongly reflected in the domain growth also. Essentially a faster early time growth is observed for $T_f \lesssim 0.25T_c$. This we will briefly discuss later.

In Fig. 2.3 we show P vs t plots, on a log-log scale, for quenches to $T_f = 0$, from a few different values of T_i , all for the same system size $L = 512$. It appears that, in the long time limit, for $T_i > T_c$, the decay is power-law, with the same exponent $\theta \simeq 0.22$. Crossover to this exponent gets delayed as T_i approaches T_c . In the pre-crossover regime, another power-law decay, with smaller exponent, to be represented by θ_1 , becomes prominent with the decrease of T_i . Such a slower decay becomes ever-lived for $T_i = T_c$. The exponent for the latter case will be denoted by $\theta_c [= \theta_1(T_i = T_c)]$.

In Fig. 2.4 we present the instantaneous exponent, θ_i , calculated as [14,15]

$$\theta_i = -\frac{d \ln P}{d \ln t}, \quad (2.5)$$

vs $1/\ell$, with the objective of accurate quantification of the second step of the decays for T_i close to, but greater than, T_c . For the abscissa variable we have adopted $1/\ell$, instead of $1/t$, to visualize the long time limit better. This is due to the fact that when plotted vs $1/t$, overall abscissa range increases which makes appreciation of an extrapolation difficult for the data sets corresponding to lower T_i . Within statistical error, for all the presented temperatures,

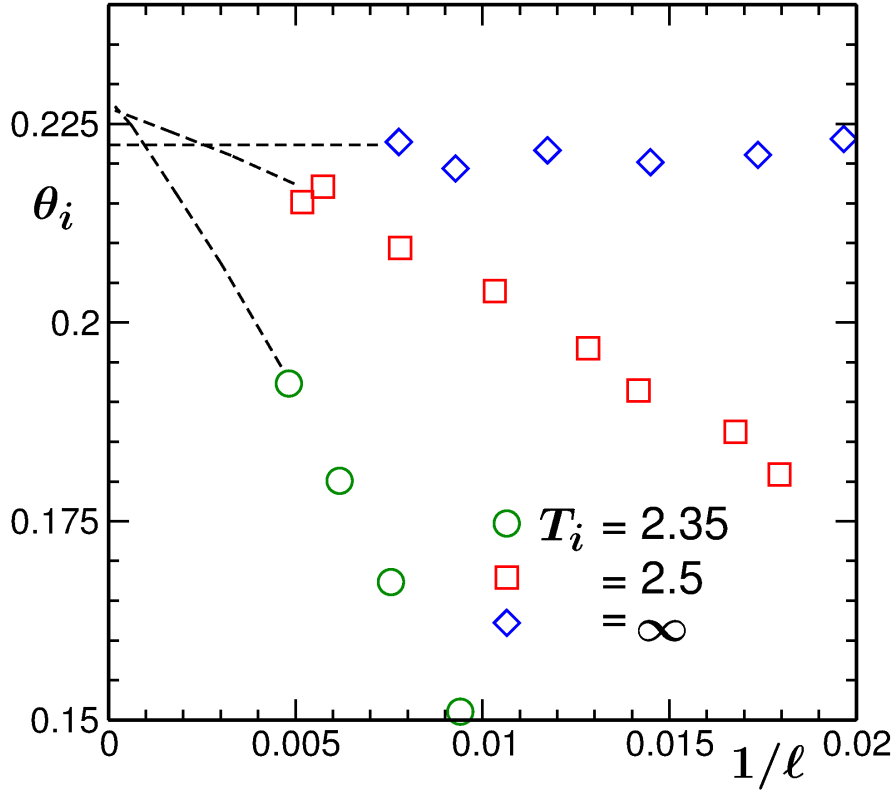


Figure 2.4: Instantaneous exponents θ_i are plotted vs $1/\ell$, for the quenches in Fig. 2.3, excluding $T_i = T_c$ case. Here we have included only the late time behavior. The dashed lines in this figure are guides to the eyes.

it appears that the values of θ are consistent with that for the quench from $T_i = \infty$ to $T_f = 0$. From this exercise we conclude $\theta = 0.225 \pm 0.005$.

Next we move to identify the exponent for $T_i = T_c$ and $T_f = 0$. In Fig. 2.3, it appears that the $T_i = T_c$ data are reasonably consistent with $\theta_c = 0.04$. Nevertheless, before the final finite-size effects appear (showing flat nature at very late time), there is a faster decay, albeit for a brief period. This can well be due to the fact that for a finite system, ξ is not infinite at $T = T_c$, effectively implying that the initial configurations are prepared away from T_c . Thus, in this problem, finite-size effects have two sources.

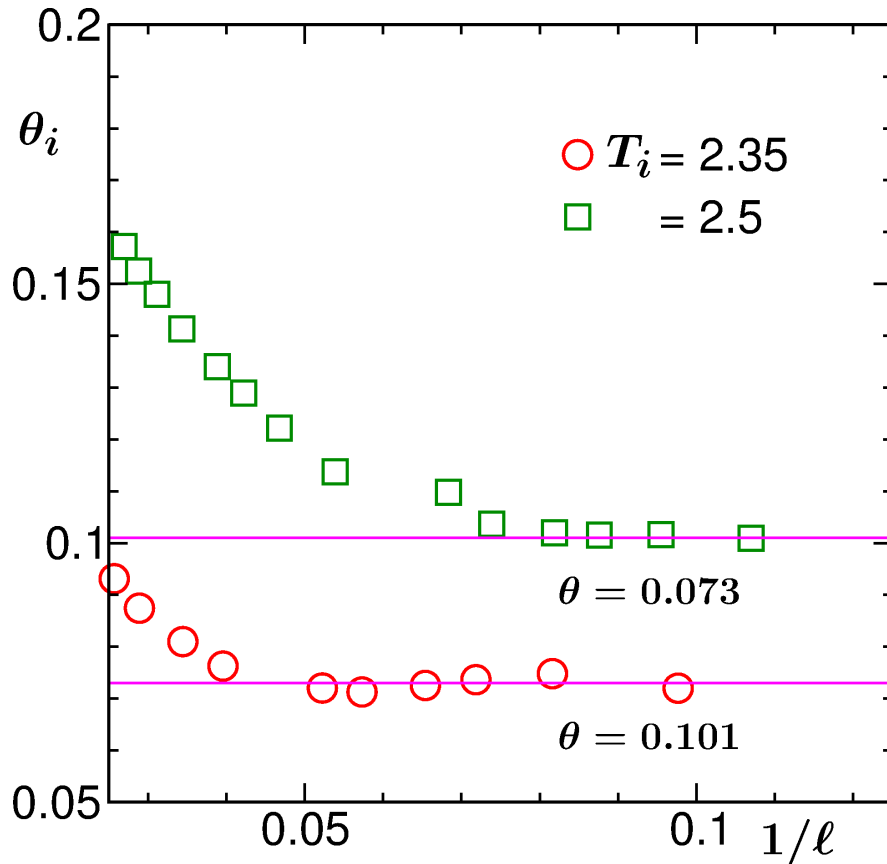


Figure 2.5: Instantaneous exponents θ_i are plotted vs $1/\ell$ for two of the quenches in Fig. 2.3. Here we have focused on the first step of the decays, exponents for which are obtained from the flat regions. The values of $\theta_I(T_i)$, for different T_i s are extracted from the horizontal lines. The results are for $d = 2$ in a square lattice with $L = 512$.

One coming from the finiteness of the equilibrium correlation length, other being faced when the nonequilibrium domain size is close to the system size. Thus, a quantification of the exponent θ_c via finite-size scaling [39] becomes a challenging task. However, we appropriately take care of the shortcoming below, in various different ways which provide results consistent with each other.

In Fig. 2.5 we show the instantaneous exponents θ_i , vs $1/\ell$, with the

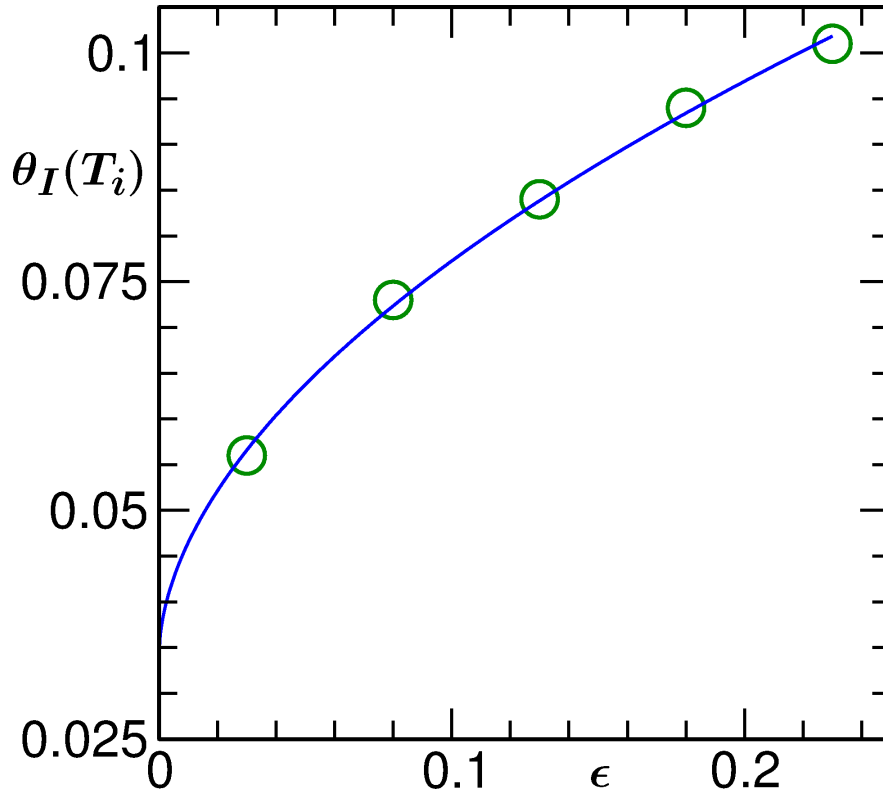


Figure 2.6: The values of θ_I , obtained from the exercise in Fig. 2.5, are plotted vs $\epsilon = T_i - T_c$. The continuous line here is a power-law fit (see text).

objective of quantifying the first step of the decays, for two values of T_i , close enough to T_c . As demonstrated, from the flat regions we identify the exponent θ_I , which exhibits T_i dependence. These numbers are plotted in Fig. 2.6 as a function of $\epsilon = T_i - T_c$. The continuous line there is a fit to the form

$$\theta_I(T_i) = \theta_c + A\epsilon^x, \quad (2.6)$$

providing $\theta_c = 0.034$, $A = 0.15$ and $x = 0.54$. Recall that θ_c is the only decay exponent for $T_i = T_c$.

To verify the above value of θ_c further, in Fig. 2.7 we present an exercise

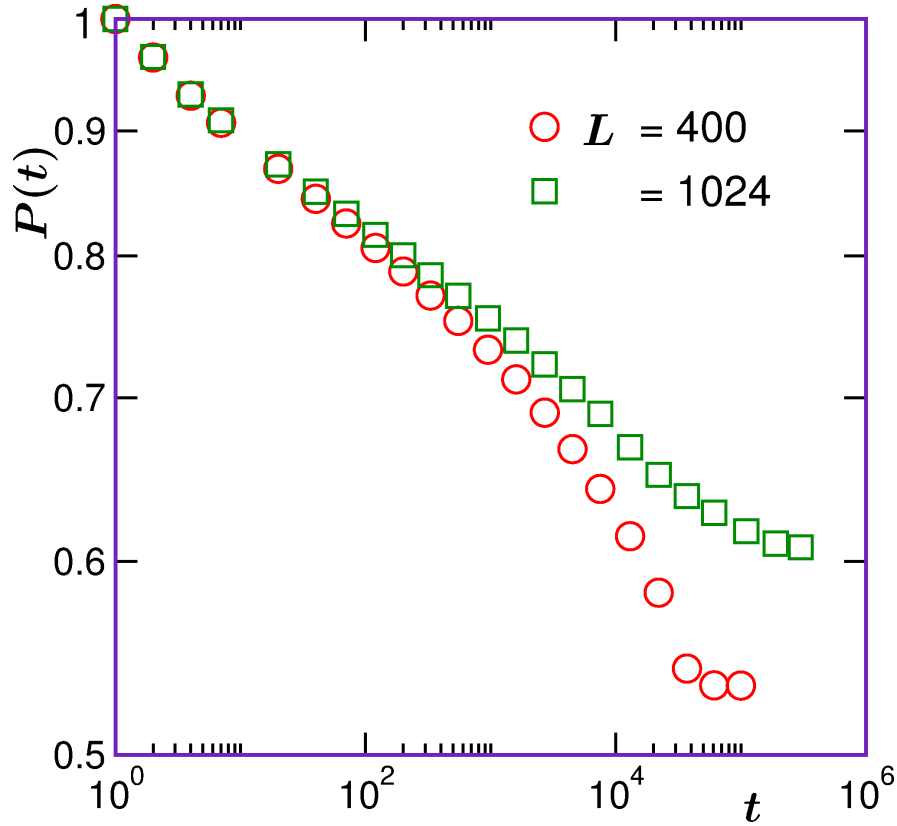


Figure 2.7: Log-log plots of P vs t , for two different system sizes, with $T_i = T_c$ and $T_f = 0$. The results correspond to $d = 2$.

with different system sizes. Here, we present P vs t data, for $T_i = T_c$, from two different values of L . It is seen that with the increase of the system size, there is a tendency of the data to settle down to a power-law for a longer period of time, following a marginally faster decay at very early time. In Fig. 2.8 we show θ_i vs $1/\ell$ for three different system sizes with $T_i = T_c$. The early time behavior appears linear, extrapolation of which leads to $\theta_c \simeq 0.029$. However, if the data in the figure is closely examined, as already mentioned above, this part corresponds to the preasymptotic behavior, thus, should be discarded from the analysis. Actual exponents should be extracted from the

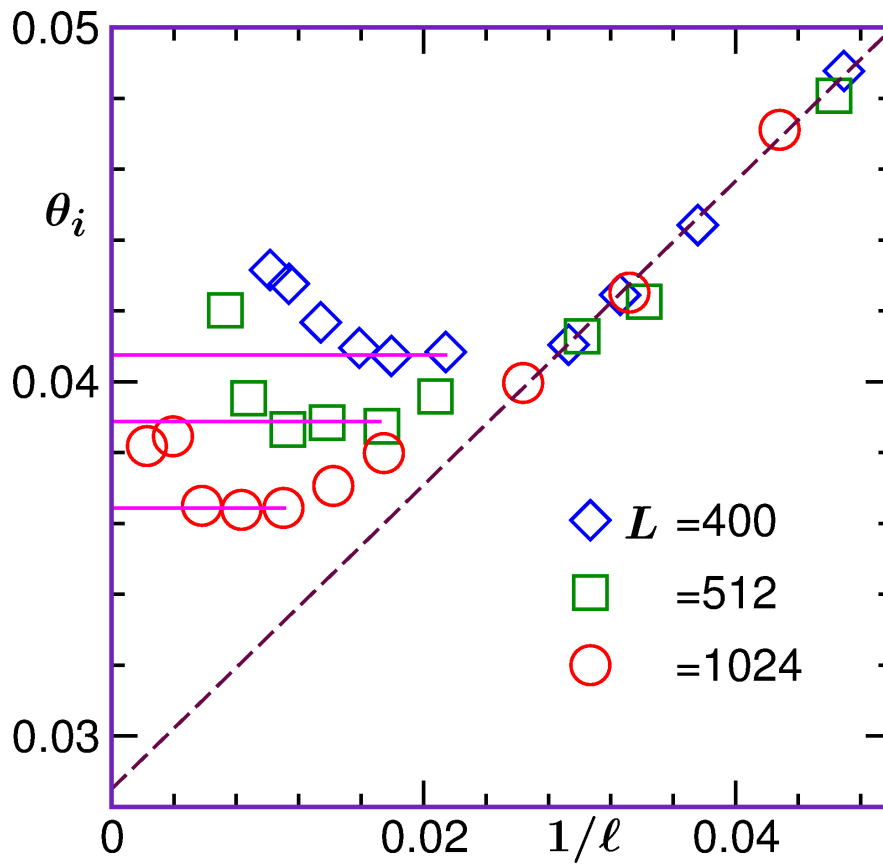


Figure 2.8: Plots of θ_i vs $1/\ell$, for three different values of L , with $T_i = T_c$. The dashed line is a linear extrapolation using data in the small ℓ region. The flat regions, marked by the horizontal solid lines, provide the value of L -dependent instantaneous exponents, $\theta_c(L)$. The results are from simulations in $d = 2$.

flat regions of the plots. In the plots of θ_i vs $1/\ell$, the flat portions appear very short. But the actual time (or length) range over which the flat behavior, before deviating due to finite-size effects, extends, is reasonably long, say, a few hundred MCS for the largest system size. The numbers obtained from these flat parts, as discussed, differs due to the finite-size effects and thus, should be extrapolated to $L = \infty$ appropriately. These L -dependent values, $\theta_c(L)$, are plotted in Fig. 2.9 as a function of $1/L$. A very reasonable linear

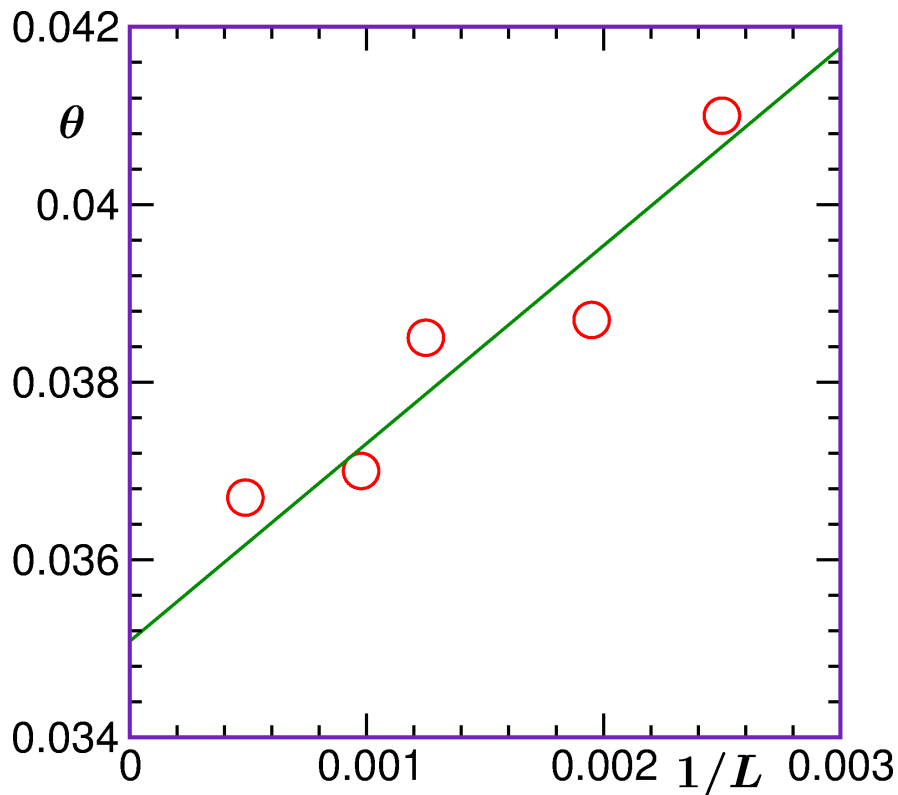


Figure 2.9: The L -dependent exponents, $\theta_c(L)$, obtained from flat regions of the plots (see the horizontal solid lines) in Fig. 2.8 are plotted vs $1/L$. The solid line there is a linear fit.

fit (see the solid line) is obtained, providing $\theta_c = \theta_c(L = \infty) = 0.035$. On the other hand, a nonlinear fit (by adding a quadratic term) provides $\theta_c = 0.037$. From all these exercises we conclude that $\theta_c = 0.035 \pm 0.005$. This picture remains true for quenches from T_c to nonzero values of T_f as well, if thermal fluctuation effects are appropriately taken care of. On this issue of thermal fluctuation, here, as well as for $T_i = \infty$, our conclusions are based on studies with small system sizes.

The decay of the previously mentioned two-time correlation is also of power-law type. For quenches from $T_i = T_c$, the value of the exponent for this

quantity in $d = 2$ gets reduced by a factor $\simeq 10$, compared to $T_i = \infty$. In the present case the reduction factor is $\simeq 6.3$. While there may be connection between the two phenomena, but a search for matching between the two factors may not be justified. As we will see, this reduction factor is much smaller in $d = 3$. This fact, however, is consistent with the corresponding prediction for aging dynamics [34].

It is certainly relevant to ask, if, like the decay of the persistence probability and the two-time correlation [33], the growth of the average domain size also exhibits initial temperature dependence. While it is expected [32–34,36] that the long time behavior will be similar, there may be difference at the transient level. For this quantity we make direct examination only for the cases $T_i = \infty$ and $T_i = T_c$, for quenches to $T_f = 0$. Conclusion drawn from these cases will be indirectly shown to be true for other T_i values later.

In Fig. 2.10 we present the ℓ vs t plots for these two cases, using a log-log scale. Both the data sets appear to grow slower than $t^{1/2}$, even if marginally. This can well be due to the presence of significantly big initial length ℓ_0 , which we examine below. While from this figure it is difficult to identify any difference in the growth exponent between the two cases, there certainly exists visible difference in the finite-size effects, noting that $L = 512$ in both the cases.

To learn better about the exponents, in Fig. 2.11 we present the instantaneous exponents [14,15]

$$\alpha_i = \frac{d \ln \ell}{d \ln t}, \quad (2.7)$$

with the variation of t . Here, while calculating α_i , we have subtracted ℓ_0

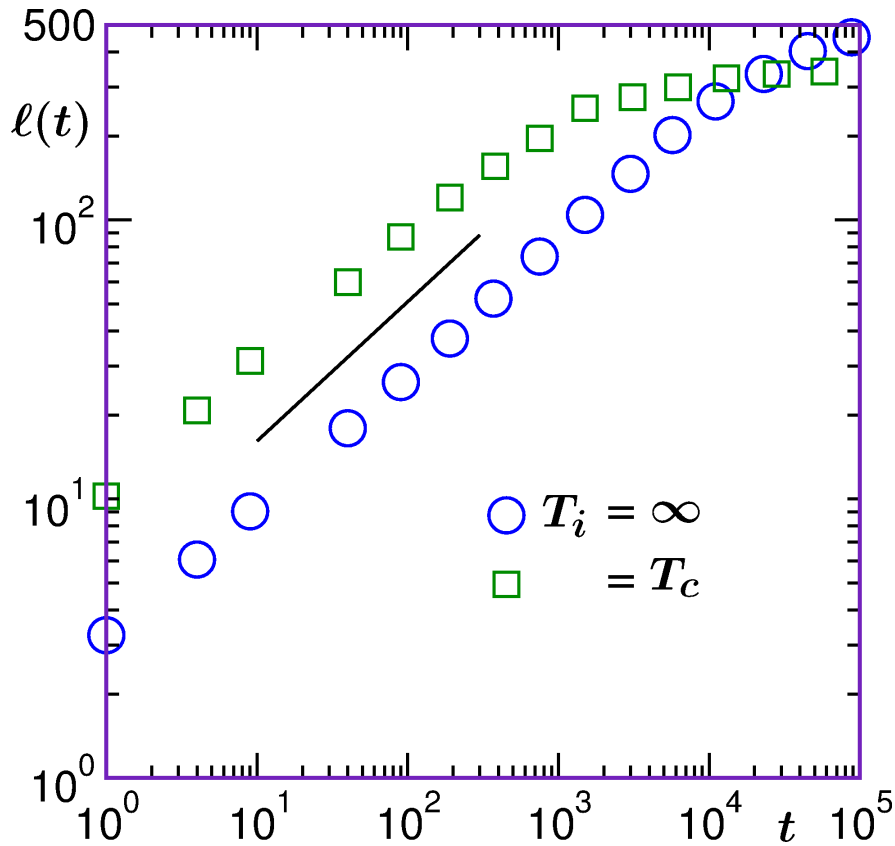


Figure 2.10: Average domain sizes, $\ell(t)$, are plotted vs t , for quenches to $T_f = 0$ from $T_i = \infty$ and T_c , in $d = 2$. The solid line represents $t^{1/2}$ behavior. Results are obtained from simulations in $d = 2$, on a square lattice with $L = 512$.

which are $\simeq 2$ and $\simeq 6.65$, respectively, for $T_i = \infty$ and T_c . This subtraction is meaningful, considering the fact that the pure scaling with respect to time is contained in $\ell - \ell_0$. Calculation of α_i , without such subtraction, provided early time exponents much smaller than the theoretical expectation for the conserved dynamics [14]. This has previously been understood to be due to the curvature dependent correction in small domain size limit. Such confusion has recently been corrected [15]. Note that, there may be a delay time for a system to become unstable following a quench. Thus, for an even more

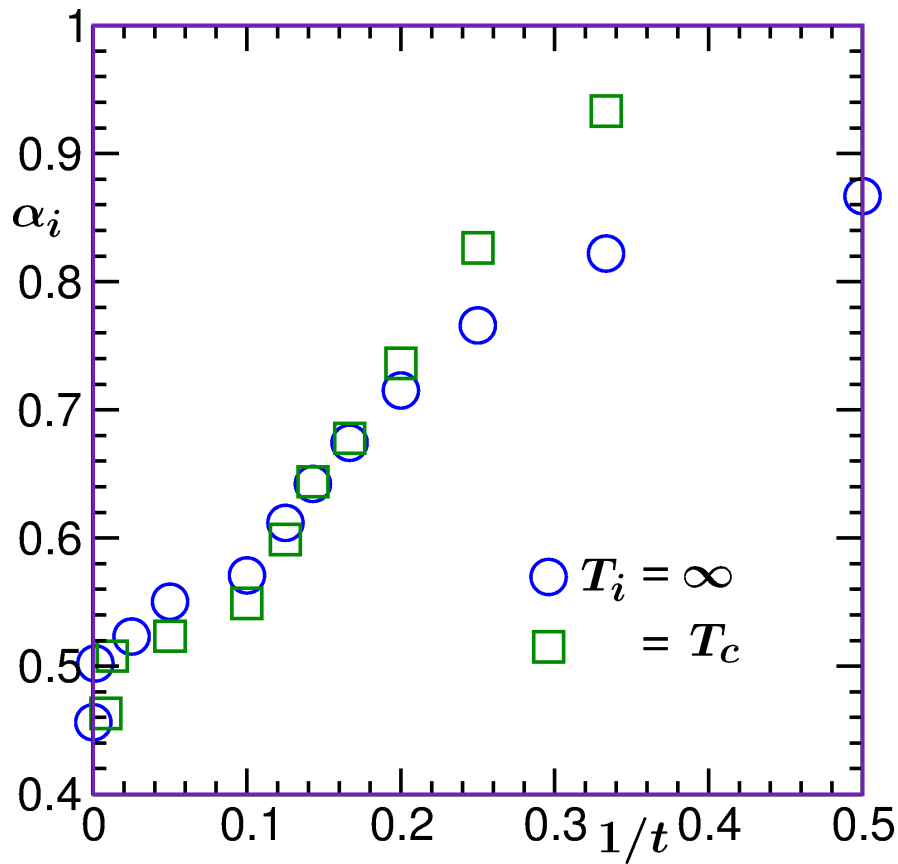


Figure 2.11: Instantaneous exponents, α_i , corresponding to the plots in Fig. 2.10, vs $1/t$, are shown. Long time limit data, suffering from strong finite-size effects, have been discarded.

appropriate understanding of a time dependent exponent, the value of ℓ_0 need not be treated as the length at $t = 0$, rather as the (fluctuating) length at which the system falls unstable. Via finite-size scaling analysis, this was demonstrated in a recent work [15]. Here, however, we do not undertake such a task.

For the analysis related to Fig. 2.11, the value of ℓ_0 , as mentioned above, was taken to be that of ℓ at $t = 0$. Thus, ℓ_0 may be treated as the length proportional to ξ at $T = T_i$. Question, however, may be raised that the

value of ℓ_0 should then match the system size L for $T_i = T_c$, since ξ is of the order of L at T_c . Note here that, at criticality fluctuations exist at all length scales, giving rise to clusters of all possible sizes, the average, ℓ_0 here, being much smaller than L . These estimates, even though obtained as first moments of the cluster size distributions, are also related to the decay of the two-point correlation functions. The latter function, at the critical point, has power-law decay. The exponential part, that contains information on ξ , is unity at criticality due to diverging value of ξ . Our calculation of ℓ_0 cannot thus be directly related to ξ , particularly close to T_c .

First important observation from Fig. 2.11 is that the value of α_i approaches $1/2$ from the upper side. This fact remains true for $T_f \lesssim 0.25T_c$, as previously mentioned. This is in contrast with the corresponding behavior for the conserved order parameter dynamics with T_f very close to zero [40]. In the latter case, the early time dynamics provides a growth exponent much smaller than the expected asymptotic value $1/3$. Second, after $t \simeq 5$, both the data sets practically follow each other, implying no difference in the growth of ℓ almost from the beginning!

From the length (or time) dependence of α_i , one can write

$$\alpha_i = \alpha + f(1/\ell), \quad (2.8)$$

to obtain

$$\int \frac{d\ell}{\alpha \ell [1 + \frac{1}{\alpha} f(1/\ell)]} = \ln t. \quad (2.9)$$

If $f(1/\ell)$ can be quantified accurately from the simulation data, a full time dependence of ℓ is obtainable. E.g., if $f(1/\ell)$ is a power law, A_β/ℓ^β , A_β being

a constant, by taking $\alpha l^\beta > A_\beta$, one finds

$$\ln \frac{\ell^{1/\alpha}}{t} \sim \frac{1}{\alpha^2 \beta \ell^\beta}. \quad (2.10)$$

Assuming that a correction disappears fast, such that $\ell \simeq t^\alpha$, we obtain

$$\ell \sim t^\alpha \exp\left(-\frac{C}{\alpha \beta t^{\alpha \beta}}\right), \quad (2.11)$$

C being a constant. Such full forms are useful for a finite-size scaling analysis to accurately quantify the exponent α . It appears that even for a power-law behavior of $f(1/\ell)$, the asymptotic behavior in the growth law is reached exponentially fast. Of course, from least square fitting exercise of the ℓ vs t data also one can aim to obtain the early time corrections. However, this method is more arbitrary. Often derivatives help guessing the functional forms better. This full form with the exponential correction factor provided a good fitting to the simulation data from which we obtain α within less than 2% deviation from the expected number 0.5.

Before moving on to presenting results in $d = 3$, we discuss the issue of persistence again. The essential feature in the initial configurations prepared at different temperatures is the variation in the equilibrium correlation length ξ . The basic question, prior to the study, one asks, how does the value of ξ affect the decay of persistence probability? For each value of ξ , do we have a unique exponent describing the full decay? The answer, as we have observed, is certainly not in affirmative. Essentially, the decay exponent for $T_i = \infty$ is recovered for all $\xi (< \infty)$ in the long time limit. Only the crossover to this

asymptotic behavior gets delayed with the increase of ξ . It is then relevant to ask if this crossover occurs when ℓ crosses ξ , an expectation naturally occurs from renormalization or coarse-graining point of view. Of course a confirmation on this expectation can be obtained from scaling plots (see below) of $P(t)$ by invoking the critical singularity of ξ . However, without detailed knowledge about the finite-size effects of P and ξ , we take an alternative route, by appropriately estimating the crossover length ℓ_c , from the available simulation data.

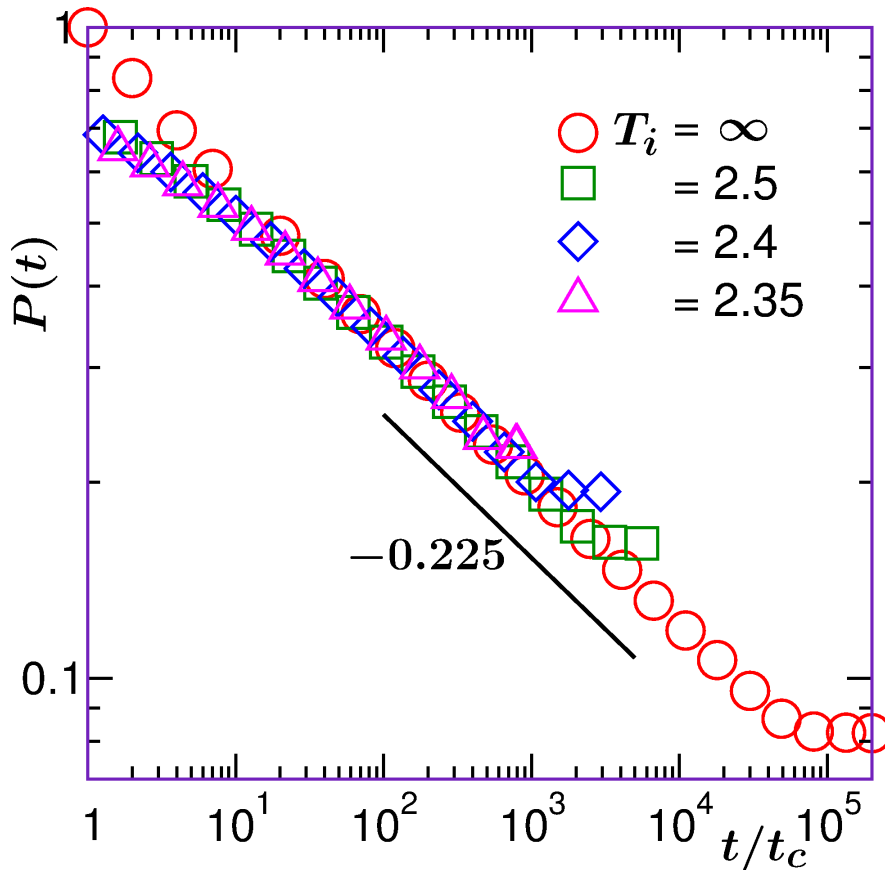


Figure 2.12: Scaling plot of persistence probability, P , versus t/t_c where the crossover time (to the asymptotic behavior) t_c has been used as an adjustable parameter to obtain optimum data collapse. All results were obtained using $L = 512$ in $d = 2$.

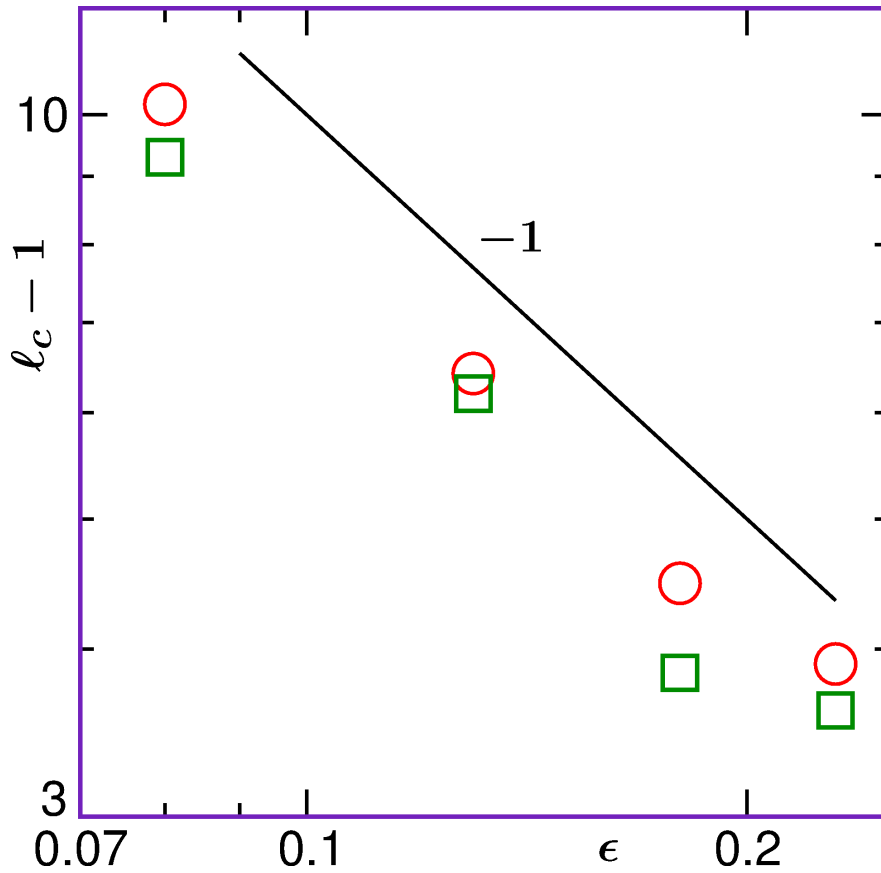


Figure 2.13: Double log plots of $\ell_c - 1$ versus ϵ . The circles correspond to estimates of ℓ_c from t_c , where we obtain the t_c values from the exercise as in Fig. 2.12. The squares are directly obtained from the scaling plots of P vs ℓ/ℓ_c . The solid line has $d = 2$ Ising critical divergence of correlation length. See the text for further details.

In Fig. 2.12 we show plots of persistence from different values of T_i , for quenches to $T_f = 0$. Here the time axis is scaled by appropriate factors (proportional to cross over time t_c) to obtain collapse of data in the asymptotic regime. Quality of collapse, on top of the $T_i = \infty$ data set, again confirms that $\theta \simeq 0.225$ in the $t \rightarrow \infty$ limit for all $T_i (> T_c)$. From the square roots of these T_i dependent scaling factors, one can obtain ℓ_c (within a proportionality

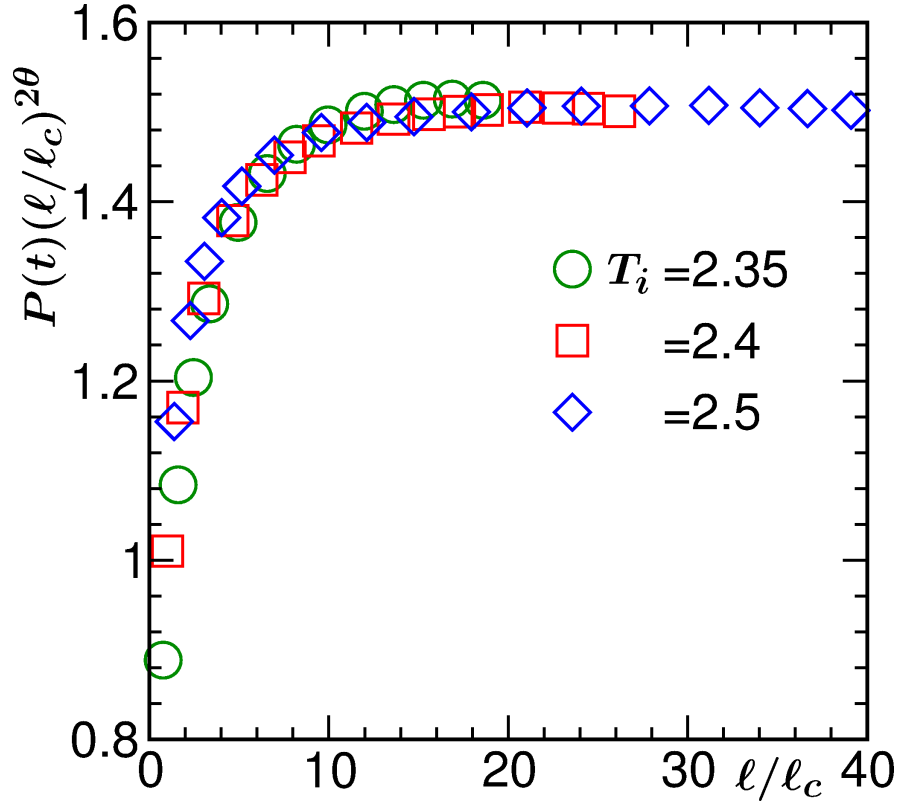


Figure 2.14: Plots of $P(t)(\ell/\ell_c)^{2\theta}$, θ being set to 0.225 [see Fig. 2.4], vs the scaled variable ℓ/ℓ_c , for several values of T_i , using linear scale. Results are presented using $L = 512$ in $d = 2$.

factor) which is expected to scale as

$$\ell_c \sim \xi \sim \epsilon^{-\nu}. \quad (2.12)$$

Note that for the Ising model $\nu = 1$ in $d = 2$ and $\simeq 0.63$ in $d = 3$. Considering that the $T_i = \infty$ data have been used as the reference case, it will be appropriate to fit the data set for ℓ_c to the form $\ell_c - 1 = A_c \epsilon^{-\nu}$, since (for the current method of estimation) $\ell_c \rightarrow 1$ for $T_i = \infty$. Unless we are very close to T_c such additional term cannot be neglected. In Fig. 2.13 we have

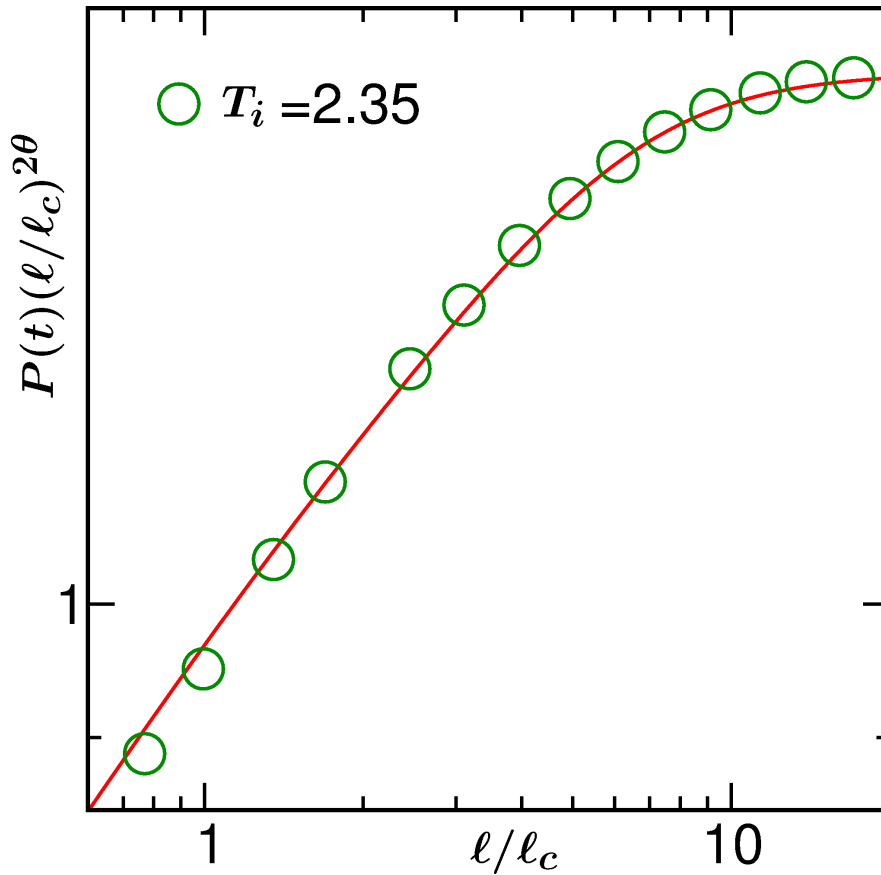


Figure 2.15: Same as Fig. 2.14 but on a log-log scale and only for $T_i = 2.35$. The continuous line there is a fit to Eq. (2.13) (see text for details).

plotted $\ell_c - 1$ as a function of ϵ , on a log-log scale. The data set (circles) appear consistent with $\nu = 1$. When ℓ_c is extracted from t_c , a more careful exercise requires incorporation of ℓ_0 and growth amplitude for each T_i . To avoid this problem, we have also obtained ℓ_c directly from the scaling plots of persistence data vs ℓ/ℓ_c [see this exercise in Fig. 2.14]. These values of ℓ_c are represented by squares. Both data sets appear nicely consistent with each other. Least square fittings of these data sets provide $\nu \simeq 0.95$.

As mentioned above, in Fig. 2.14 we show scaling plots of the persistence

probability as a function of ℓ/ℓ_c , for three values of T_i . There, in the ordinate, $P(t)$ has been multiplied by $(\ell/\ell_c)^{2\theta}$, the factor 2 in the exponent coming from the expectation that $\alpha = 1/2$ for all values of T_i . For θ , we use 0.225, the value we obtained from the analysis in Fig. 2.4. The regions of the data sets that suffer from finite-size effects have been carefully discarded. The nice collapse of the data and flat behavior in the long time limit reconfirms the following facts: $\alpha = 1/2$ for all values of T_i and, for $\ell > \ell_c \sim \xi$, in all cases, $P(t)$ decays as $t^{-\theta}$.

It will be interesting to extract the crossover behavior from the transient (first step) to the asymptotic (second step) decay. For this purpose, in Fig. 2.15 we have plotted the $T_i = 2.35$ data set on a log-log scale, for better visibility of the early time regime. In critical phenomena, in the finite-size scaling analysis of simulation results [41, 42], there have been long-standing interest in obtaining such crossover functions involving thermodynamic and finite-size limit behaviors. There typically one aims to identify if these two limits are bridged by a power-law or by an exponential function. Along the same line we write

$$P(t)x^{2\theta} = A \left(\frac{x}{g(x) + x} \right)^\phi ; x = \ell/\ell_c. \quad (2.13)$$

For an exponential convergence to the asymptotic behavior we write

$$g(x) = \frac{B_0}{1 + B_1 \exp(x)}, \quad (2.14)$$

and for a power-law one

$$g(x) = \frac{C_0}{1 + C_1 x^\psi}. \quad (2.15)$$

In the limit $x \rightarrow 0$, $P(t)x^{2\theta} \sim x^\phi$, for both the forms of $g(x)$. This limiting behavior was set by considering the fact that for $\ell < \xi$, there exist a power-law decay in $P(t)$ with an exponent θ_1 , different from θ . For $T_i = 2.35$, this value is $\theta_1 = 0.073$ [see Fig. 2.5]. In that case $\phi \simeq 0.304$, taking $\theta = 0.225$. The constant A in Eq. (2.13) sets the value of the plateau in the plots of Fig. 2.14, since for $x \rightarrow \infty$, $P(t)x^{2\theta} \rightarrow A$. It appears that fit to the power-law form of $g(x)$ looks better and is best for the integral value $\psi = 2$. Other best fit parameters are $A = 1.52$, $C_0 = 3.52$ and $C_1 = 0.033$. The correctness in the value of A can straightway be checked from the figure. The continuous line in Fig. 2.15 represents the corresponding full function of Eq. (2.13). It will be interesting to see if such empirical full form can be confirmed via first principle analytical calculations.

2.3.2 $d = 3$

In this subsection we explore $d = 3$. All the important facts being discussed in the previous subsection, here we straightway present the results. Noting that nothing remarkable happened for domain growth in the lower dimension, we do not present any direct results for this aspect. However, remarks will be made from indirect analysis.

In Fig. 2.16 we show the P vs t plots for quenches from $T_i = \infty$ and $T_i = T_c$, keeping $T_f = 0$ in both the cases. For each value of T_i , results from two different system sizes are presented. The data for $T_i = \infty$ are consistent

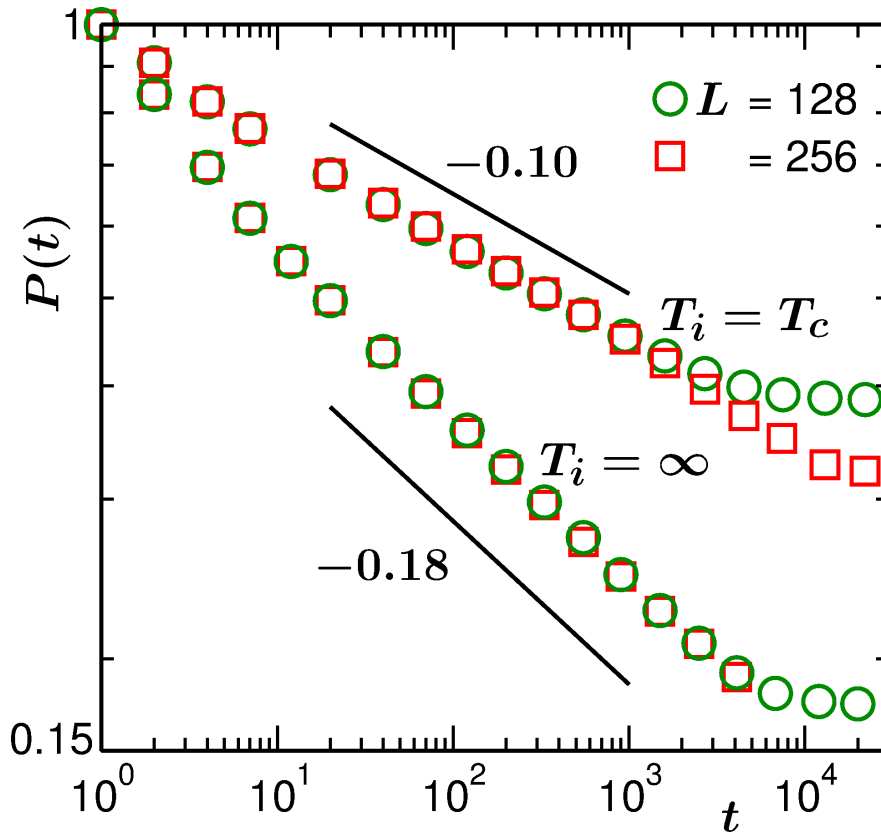


Figure 2.16: Log-log plot of P vs t , for quenches from $T_i = \infty$ and $T_i = T_c$, to $T_f = 0$. In each of the cases results from two different system sizes are included. The solid lines have power-law decays with exponents 0.1 and 0.18, as indicated on the figure. All results correspond to $d = 3$.

with $\theta = 0.18$, reported previously [20]. Thus, here we aim to accurately quantify the value of θ_c only.

Even though, for $T_i = T_c$, data from both the system sizes in Fig. 2.16 look consistent with each other, finite-size effects are detectable from a closer look. In Fig. 2.17 we plot θ_i versus $1/\ell$ for a few different values of L . Like in $d = 2$, from the flat regions we identify system size dependent θ_c , a plot of which is shown in Fig. 2.18. Again, the $\theta_c(L)$ vs $1/L$ data exhibits a reasonable linear trend and an extrapolation to $L = \infty$ provides $\theta_c = \theta_c(L =$

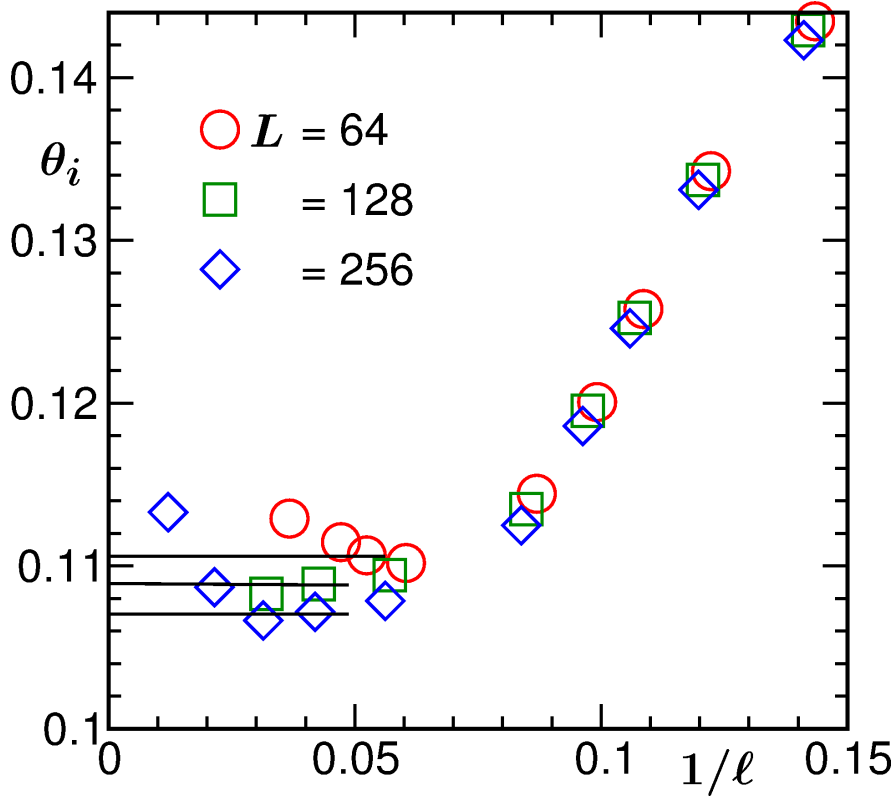


Figure 2.17: Instantaneous exponents θ_i are plotted vs $1/\ell$, for quenches from $T_i = T_c$ to $T_f = 0$ in $d = 3$. Results from different values of L are included. The horizontal solid lines are related to the estimation of L -dependent θ_c .

$\infty) \simeq 0.106$.

Similar to $d = 2$, for $T_c < T_i < \infty$, two step decays exist in $d = 3$ as well. In Fig. 2.19 we have demonstrated the estimation of θ_1 corresponding to the first step, for two representative values of T_i . In Fig. 2.20 we have plotted these exponents as a function of ϵ . A fit of this data set to the form in Eq. (2.6) provides $\theta_1(T_i = T_c) = \theta_c = 0.103$, $A = 0.074$ and $x = 0.47$. Note the similarity in the values of x in $d = 2$ and 3. This value of θ_c is in good agreement with the one obtained from Fig. 2.17. In $d = 3$, we quote $\theta_c = 0.105 \pm 0.005$. Thus, the effect of growing correlation length in the

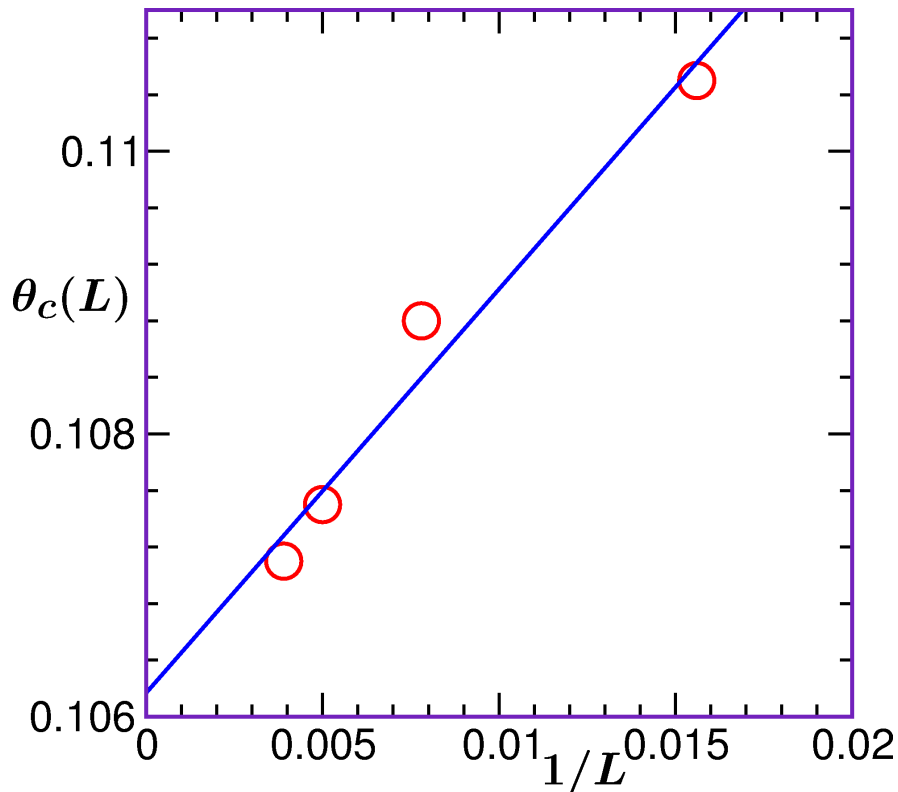


Figure 2.18: Plot of $\theta_c(L)$ vs $1/\ell$ (see Fig. 2.17). The continuous line there is a linear fitting (see text for details).

initial configurations certainly appears weaker in this space dimension. Even though, in both $d = 2$ and 3 , fits to the power-law form in Eq. (2.6) appear good, due to the similarity of the values in different dimensions, x cannot be connected to any of the other exponents ν and α , used in this chapter, in a simple way. In this work, thus, we treat this exercise only as a reasonably accurate numerical analysis whose validity is justified by the fact that the derivatives of the corresponding (original) simulation data sets, with respect to ϵ , in both dimensions, provide linear looks on double-log plots.

In Fig. 2.21 we show scaling plots of P , vs ℓ/ℓ_c , using data from different values of T_i , with $L = 128$. Collapse of data is again good. The late time

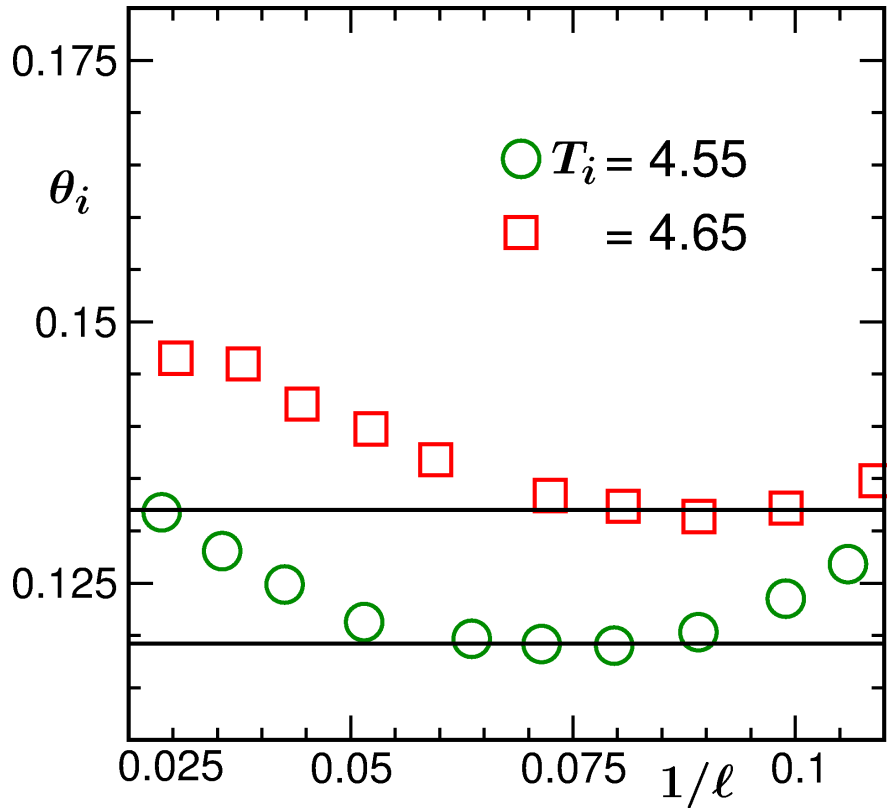


Figure 2.19: Plots of θ_i vs $1/\ell$, for two different values of T_i . Estimation of θ_1 corresponding to the first step in decay has been done following the procedure used in Fig. 2.5. Here, $L = 256$ and $d = 3$.

behavior is power-law and is consistent with a decay exponent 0.54. Considering that $\theta \simeq 0.18$ in $d = 3$, this implies $\alpha = 1/3$ in $d = 3$. The nice collapse of data sets in Fig. 2.21, for all values of T_i , implies the initial configuration independence of this exponent. As stated in Ref. [43], deviation of α , in this dimension, from $1/2$, is not yet understood. To avoid this fact, as well as to get rid of the influence of T_i dependent ℓ_0 and growth amplitude, we have obtained ℓ_c from these plots only and no attempts have been made to extract it from scaling plots vs t/t_c .

As we will see in later chapters, at very late time $\alpha = 1/2$ even for $d = 3$.

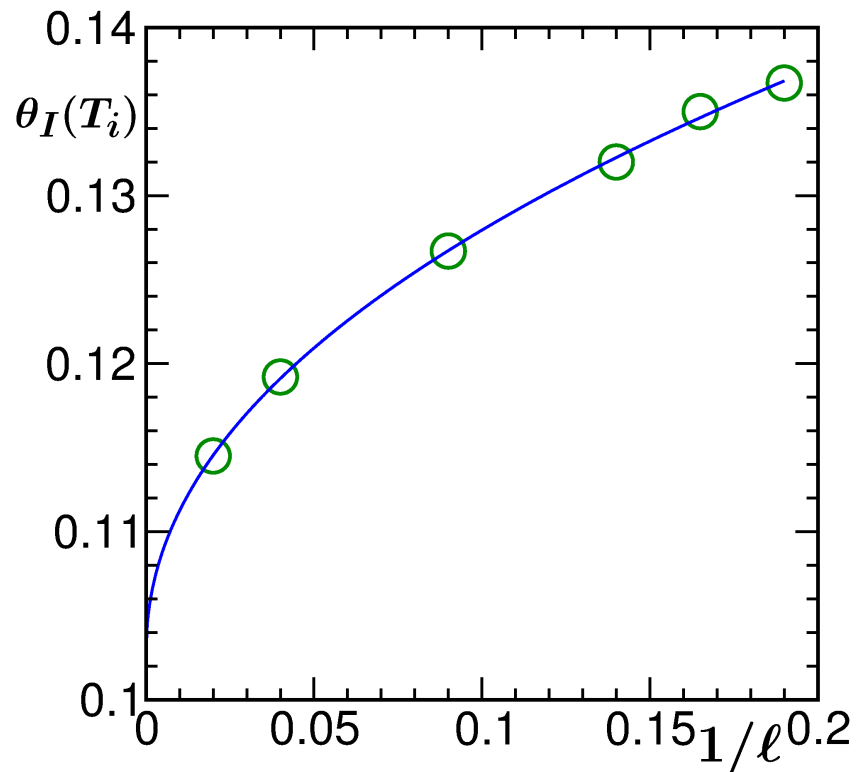


Figure 2.20: Plot of the Exponent θ_I as a function of ϵ . The continuous line is a non-linear fitting. Further details are provided in the text. Presented results are for $L = 256$ in $d = 3$.

Absence of this regime in the analysis of the results here do not alter our conclusions or prescriptions to achieve various scaling properties, including the one involving the equilibrium correlation length.

In Fig. 2.22 we plot $\ell_c - 1$ as a function of ϵ , on a log-log scale, for two different system sizes. The divergence of the length scale is consistent with a power law exponent 0.63 which is the critical exponent for ξ in $d = 3$. The deviation from this exponent at smaller values of ϵ is due to finite-size effects. It is clearly seen that for the bigger system ($L = 256$) the effects are much less pronounced. Note that in $d = 3$ it is extremely time consuming to deal

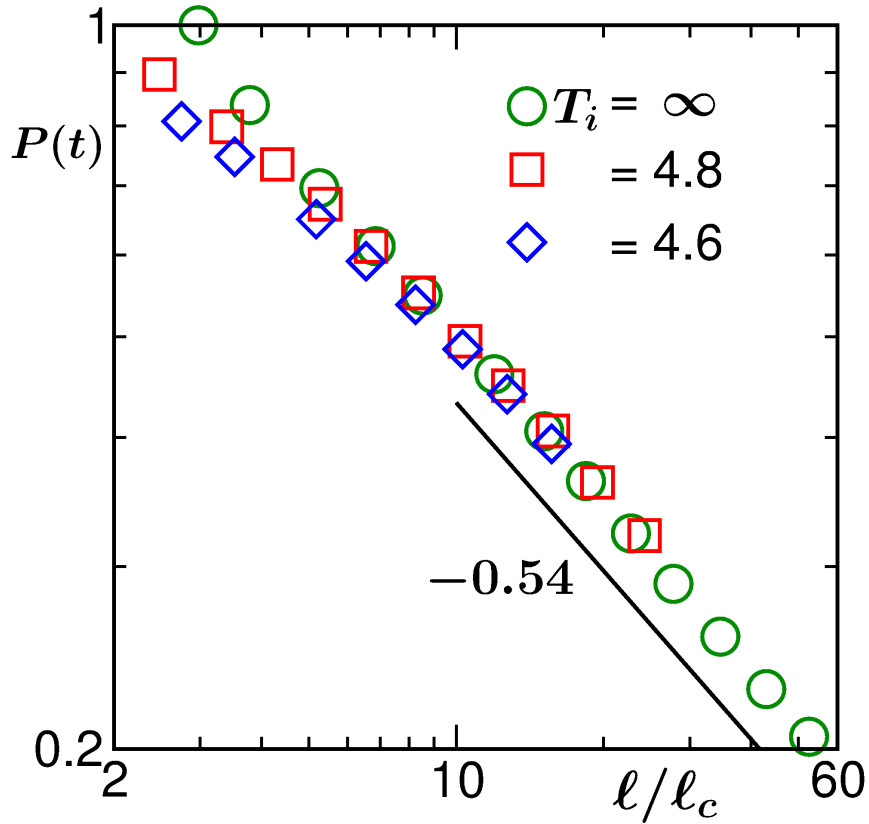


Figure 2.21: Scaling plot of P , versus l/l_c , for three different T_i values in $d = 3$, for $L = 128$, in log-log scale. The solid line has a power-law decay with exponent 0.54.

with bigger systems, including initial configuration preparation at $T_i = T_c$. To save time for the preparation of initial configuration, in this dimension we have used a combination of Wolff algorithm [44] and Glauber kinetics. In both $d = 2$ and 3, behavior of l_c , as a function of ϵ , have been analyzed for T_i values deviating by maximum of 10% from T_c .

An exercise similar to Fig. 2.14 is shown in Fig. 2.23, for $d = 3$. In this case the exponent on the ordinate is 3θ , instead of 2θ . This is due to a different value of α in the present dimension. Here also we see nice collapse

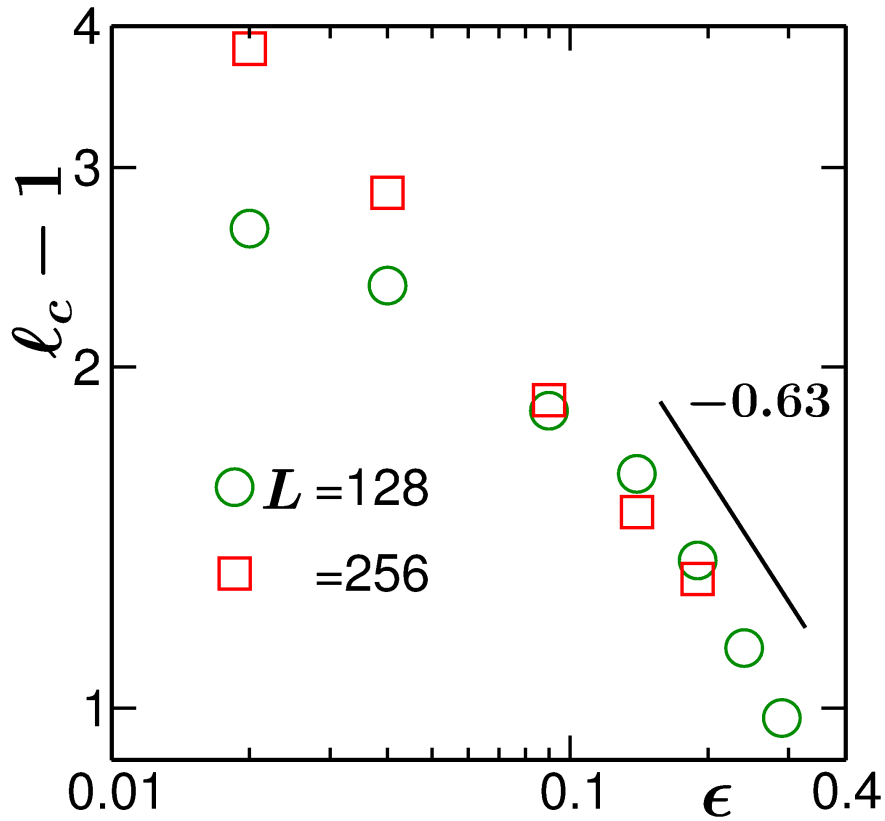


Figure 2.22: Double-log plot of $l_c - 1$, in $d = 3$, versus ϵ . The solid line there has $d = 3$ Ising critical divergence of ξ . We have presented results for $L = 128$ (circles) as well as $L = 256$ (squares).

for all the three sets of data we have presented. In Fig. 2.24 we do the exercise related to the crossover function, using $T_i = 4.6$ data set. Here the value of ϕ was set to 0.17, in accordance with the first step of the decay. Again a power-law form of $g(x)$ with the integral value of $\psi = 2$ provides best fit, with other parameters being $A = 1.76$, $C_0 = 12.46$ and $C_1 = 0.055$. Corresponding full function is represented by the continuous line in the figure.

In both $d = 2$ and 3, expectation from coarse-graining point of view that when ℓ exceeds the value of $\xi(T_i)$, $P(t)$ decays with the exponent θ , has been

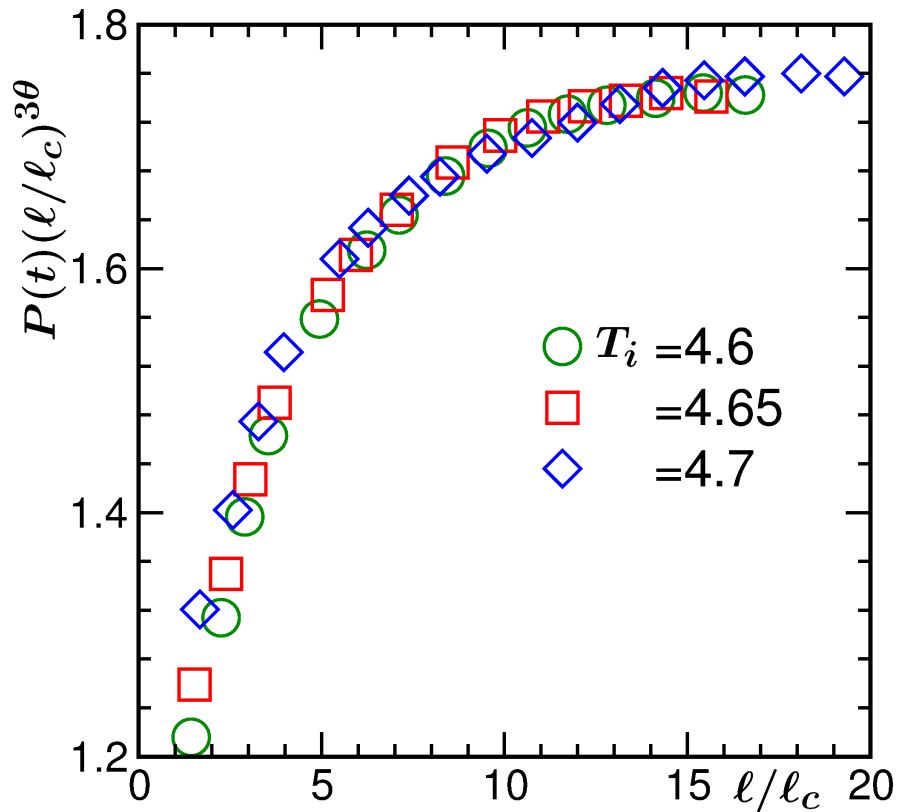


Figure 2.23: $P(t)(\ell/\ell_c)^{3\theta}$, with $\theta = 0.18$, are plotted vs ℓ/ℓ_c , for quenches from three values of T_i to $T_f = 0$, in $d = 3$, using linear scale.

confirmed. In the present case, the value of ξ at T_f is zero. It remains to be seen how $\xi(T_f)$, for $T_f \neq 0$, interferes with the crossover. Even though we have studied cases where both $\xi(T_i)$ and $\xi(T_f)$ are nonzero, this particular aspect requires more careful study.

2.4 Conclusions

In conclusion, we have studied phase ordering dynamics in Ising ferromagnets for various combinations of initial (T_i) and final (T_f) temperatures in $d = 2$ and 3 . In this work, the primary focus has been on the persistence

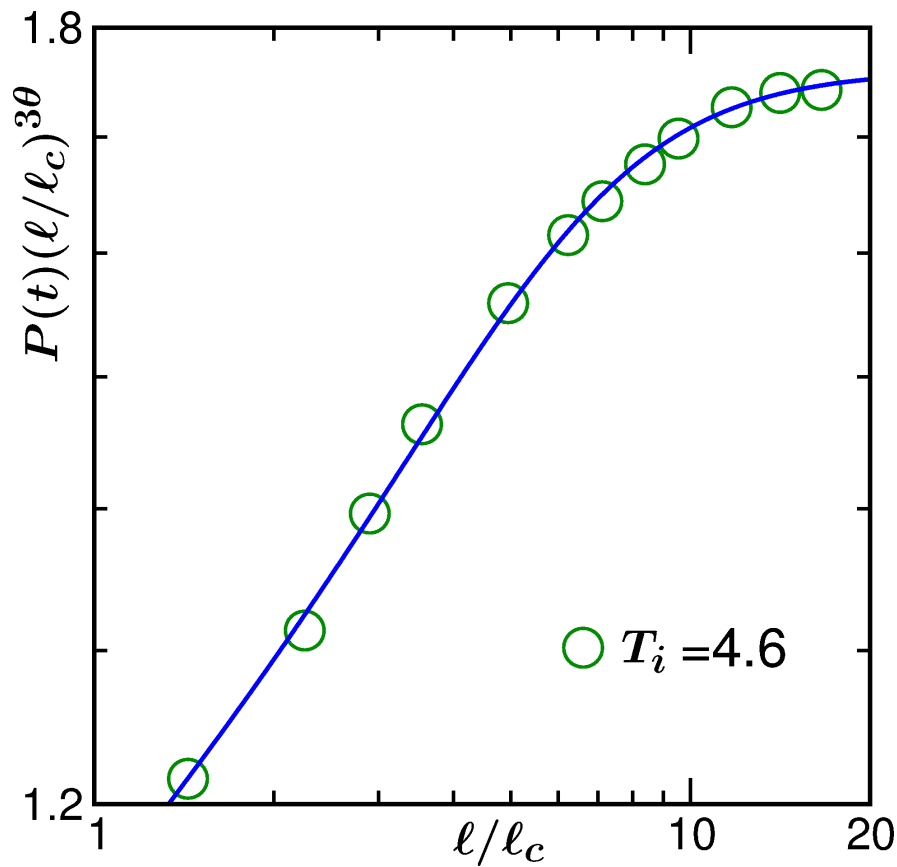


Figure 2.24: Log-log plot of $P(t)(\ell/\ell_c)^{3\theta}$ vs ℓ/ℓ_c for $T_i = 4.6$. The continuous line is a fit to the function in Eq. (2.13). Further details are provided in the text.

probability, P , and its connection with the growth of average domain size, ℓ , as well as with the equilibrium initial correlation length ξ .

Our general observation has been that, irrespective of the value of T_i , the decay of P becomes faster with the increase of T_f , after a certain critical number for the latter. This is understood to be due to spins affected by thermal fluctuations. When this effect is taken care of [19], the long time decay appears to be power law with exponent [20,21] consistent with the one for quench to $T_f = 0$.

As T_i approaches T_c , two-step power-law decay becomes prominent, the second part having exponent $\theta \simeq 0.225$ in $d = 2$ and $\simeq 0.18$ in $d = 3$, same as $T_i = \infty$ and $T_f = 0$ case. For $T_i = T_c$, thought to provide a new universality class, the first part of the two-step process lives for ever. The corresponding values of the exponent have been identified to be $\theta_c \simeq 0.035$ in $d = 2$ and $\theta_c \simeq 0.105$ in $d = 3$. Thus the decay of persistence probability is strongly connected with the initial correlation length. It has been shown that the crossover length to the second step of decay diverges as the equilibrium correlation length in both the dimensions. This leads to the question of difference in the fractal dimensions in the pre- and post-crossover regimes. Our preliminary study in this respect confirms the expectation that, for finite T_i , in the post-crossover regime only the fractal dimension is same as the $T_i = \infty$ case. We have also estimated the crossover function between the two steps. It appears, a convergence to the asymptotic decay occurs in a power-law manner, as a function of ℓ/ξ .

We have not observed any initial configuration dependence of the growth of the average domain size. This is consistent with a previous study [36] but more explicitly demonstrated here. Essentially, even the transients are only weakly affected due to change in initial temperature. However, stronger finite-size effects are detected for lower values of T_i . For domain growth, a striking observation is that the early time exponent is much higher than the asymptotic value, despite T_f being zero. This is at variance with the conserved order parameter dynamics. These are all interesting new results, requiring appropriate theoretical attention.

In future we will focus on persistence for the conserved order parameter

dynamics. For the conserved dynamics, initial temperature dependence of aging and domain growth are also important open problems.

The materials of the chapter are taken from the following article, with kind permission of The European Physical Journal (EPJ): **Saikat Chakraborty** and Subir K. Das, “Role of Initial Correlation in Coarsening of a Ferromagnet”, *Eur. Phys. J. B* **88**, 160 (2015).

Bibliography

- [1] A. Onuki, *Phase Transition Dynamics* (Cambridge University Press, Cambridge, 2002).
- [2] S. Puri and V. Wadhawan, *Kinetics of Phase Transitions* (Boca Raton, CRC Press, 2009).
- [3] A.J. Bray, *Adv. Phys.* **51**, 481 (2002).
- [4] K. Binder, in *Phase transformation of materials*, edited by R.W. Cahn, P. Haasen, E.J. Kramer, *Mater. Sci. Technol. Vol. 5* (VCH, Weinheim, 1991), p. 405.
- [5] M.C. Cross and P.C. Hohenberg, *Rev. Mod. Phys.* **65**, 851 (1993).
- [6] T. Ohta, D. Jasnow and K. Kawasaki, *Phys. Rev. Lett.* **49**, 1223 (1982).
- [7] A.J. Bray and S. Puri, *Phys. Rev. Lett.* **67**, 2670 (1991).
- [8] H. Toyoki, *Phys. Rev. B* **45**, 1965 (1992).
- [9] S.K. Das, S. Puri and M.C. Cross, *Phys. Rev. E* **64**, 46206 (2001).
- [10] I.M. Lifshitz and V.V. Slyozov, *J. Phys. Chem. Solids* **19**, 35 (1961).

-
- [11] K. Binder and D. Stauffer, Phys. Rev. Lett. **33**, 1006 (1974).
- [12] S.M. Allen and J.W. Cahn, Acta Metall. **27**, 1085 (1979).
- [13] E.D. Siggia, Phys. Rev. A **20**, 595 (1979).
- [14] D.A. Huse, Phys. Rev. B **34**, 7845 (1986).
- [15] S. Majumder and S.K. Das, Phys. Rev. E **81**, 050102 (2010).
- [16] S.N. Majumdar, C. Sire, A.J. Bray and S.J. Cornell, Phys. Rev. Lett. **77**, 2867 (1996).
- [17] S.N. Majumdar, A.J. Bray, S.J. Cornell and C. Sire, Phys. Rev. Lett. **77**, 3704 (1996).
- [18] B. Derrida, V. Hakim and R. Zeitak, Phys. Rev. Lett. **77**, 2871 (1996).
- [19] B. Derrida, Phys. Rev. E **55**, 3705 (1997).
- [20] D. Stauffer, Int. J. Mod. Phys. C **8**, 361 (1997).
- [21] G. Manoj and P. Ray, Phys. Rev. E **62**, 7755 (2000).
- [22] D. Chakraborty and J.K. Bhattacharjee, Phys. Rev. E **76**, 031117 (2007).
- [23] M. Saharay and P. Sen, Physica A **318**, 243 (2003).
- [24] R. Paul, A. Gambassi and G. Schehr, Europhys. Lett. **78**, 10007 (2007).
- [25] A.J. Bray, S.N. Majumdar and G. Schehr, Adv. Phys. **62**, 225 (2013).
- [26] D.S. Fisher and D.A. Huse, Phys. Rev. B **38**, 373 (1988).

-
- [27] F. Liu and G.F. Mazenko, Phys. Rev. B **44**, 9185 (1991).
- [28] F. Corberi, E. Lippiello, M. Zannetti, Phys. Rev. E **74**, 041106 (2006).
- [29] S. Ahmad, F. Corberi, S.K. Das, E. Lippiello, S. Puri and M. Zannetti, Phys. Rev. E **86**, 061129 (2012).
- [30] S. Majumder and S.K. Das, Phys. Rev. Lett. **111**, 055503 (2013).
- [31] J. Midya, S. Majumder and S.K. Das, J. Phys. : Condens. Matter. **26**, 452202 (2014).
- [32] C. Dasgupta and R. Pandit, Phys. Rev. B **33**, 4752 (1986).
- [33] K. Humayun and A.J. Bray, J. Phys. A : Math. Gen. **24**, 1915 (1991).
- [34] A.J. Bray, K. Humayun and T.J. Newman, Phys. Rev. B **43**, 3699 (1991).
- [35] T. Blanchard, L.F. Cugliandolo and M. Picco, J. Stat. Mech: Theory and experiment P12021 (2014). The value $\theta = 0.035$ obtained by us is extremely close to the conclusion from this study (reference [35]) for triangular lattice. This implies, the lattice structure plays insignificant role.
- [36] A. Sicilia, J.A. Arenzon, A.J. Bray and L.F. Cugliandolo, Phys. Rev. E **76**, 061116 (2007).
- [37] D.P. Landau and K. Binder, *A Guide to Monte Carlo Simulations in Statistical Physics* (Cambridge University Press, Cambridge, 2009).
- [38] R.J. Glauber, J. Math. Phys. **4**, 294 (1963).

-
- [39] M.E. Fisher, in *Critical Phenomena*, edited by M.S. Green (Academic Press, London, 1971).
- [40] S. Majumder and S.K. Das, *Phys. Chem. Chem. Phys.* **15**, 13209 (2013).
- [41] V. Privman (ed.), *Finite Size Scaling and Numerical Simulation of Statistical Systems*, (World Scientific, 1990).
- [42] S.K. Das, M.E. Fisher, J.V. Sengers, J. Horbach and K. Binder, *Phys. Rev. Lett.* **97**, 25702 (2006).
- [43] S. Cueille and C. Sire, *J. Phys. A: Math. Gen.* **30**, L791 (1997).
- [44] U. Wolff, *Phys. Rev. Lett.* **62**, 361 (1989).

Chapter 3

Fractality in Persistence Decay and Domain Growth during Ferromagnetic Ordering: Dependence upon Initial Correlation

3.1 Introduction

Kinetics of phase transitions [1–4] remains an active area of research for several decades. In this area, typically one is interested in the nonequilibrium dynamics related to the evolution of a system to a new equilibrium state, having been quenched from a configuration prepared outside the coexistence curve to inside it, via the variation of temperature (T), pressure, etc.

In this work, our focus is on the paramagnetic to ferromagnetic transition [5]. When a system is quenched, via variation of T , from the paramagnetic phase to ferromagnetic one, domains rich in like spins form and grow with time [2]. Aspects that drew attention of researchers, in this problem, are understanding of domain patterns [2], growth of domains [2], aging properties of the evolution [6–8], as well as the pattern (and corresponding dynamics) exhibited by atomic magnets (or spins) that did not change orientation till time t , referred to as persistent spins [4, 9–25]. This work deals with issues related to domain growth and persistence.

During the process of ferromagnetic ordering (where the order parameter is a nonconserved quantity), the average domain size, ℓ , increases as [2]

$$\ell \sim t^\alpha, \quad (3.1)$$

where α , the growth exponent, may have dependence upon system dimensionality (d) based on the order-parameter symmetry. This growth occurs via motion and annihilation of defects, facilitated by change in orientation of the spins, S_i , the subscript i being an index related to an atom or spin, typically considered to be located on a regular lattice. In this work we study the spin-1/2 Ising model, to be defined later, for which defects are the domain boundaries. In this case, S_i is a scalar quantity which gets affected only via (complete) flipping or change in sign. For this model, the theoretical expectation for α is same in both $d = 2$ and 3.

The persistence probability, P , defined as the fraction of unaffected spins,

typically decays as [4]

$$P \sim t^{-\theta}, \quad (3.2)$$

where θ is expected to have dependence upon d . The persistent spins exhibit interesting fractal pattern with dimensionality [17] d_f whose dependence upon θ will be introduced later. Unless mentioned otherwise, all our results on this issue correspond to local persistence, probability for which, as already mentioned, is calculated by counting unaffected “microscopic” spins. There has also been interest in the calculation of such probability by dividing the system into blocks of linear dimension ℓ_b and counting the persistence of coarse-grained or block spin variables [14, 15]. In the limit $\ell_b \rightarrow a$, the microscopic lattice constant, such block persistence probability, P_b , will correspond to P , the “local or site persistence” probability. On the other hand, for $\ell_b \rightarrow \infty$, one obtains “global persistence” probability, further discussion and results for which will be presented later.

For Ising model, values [2, 17, 19] of α , θ and d_f are accurately estimated via Monte Carlo (MC) simulations, in $d = 2$, for quenches from initial temperature $T_i = \infty$ to the final value $T_f = 0$. It is reasonably well established [2, 4, 11–19, 24] that, in this case, the values of α , θ and d_f are $1/2$, 0.225 , and 1.58 . However, the conclusions, if exists, on the corresponding numbers for $d = 3$ are questionable [26–28]. Recent focus, on the other hand, for persistence as well as for other aspects of coarsening, has been on [23–25, 29–31] quenches from temperatures providing large equilibrium correlation length ξ . In this context, in a recent work [24], we have explored the initial correlation dependence of α and θ . Our observation was, while α is insensitive to the

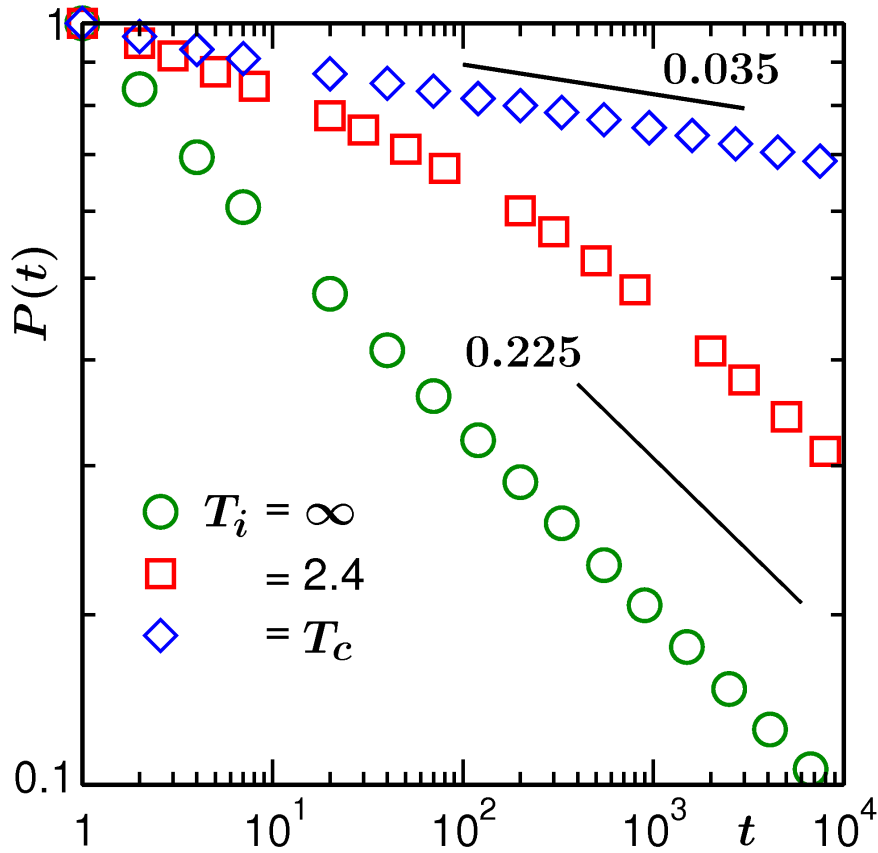


Figure 3.1: Log-log plots of local persistence probability, $P(t)$, vs t , for quenches (of the Glauber Ising model) from different values of initial temperature T_i ($\geq T_c$, the critical temperature), to the final value $T_f = 0$. All results correspond to space dimension $d = 2$ and square lattice, with linear dimension of the square box being $L = 2048$, in units of the lattice constant a . The lines represent various power-law decays, values of the exponents being mentioned in appropriate places.

variation of T_i (at least in $d = 2$), P (and thus θ) is strongly influenced by the choice of the latter, viz., we obtained for $d = 2$ and 3, $\theta = \theta_c \simeq 0.035$ and $\simeq 0.105$ for $T_i = T_c$, the critical temperature (see Fig. 3.1 for $d = 2$). The numbers quoted above are significantly different from those for $T_i = \infty$. For intermediate temperatures, as seen in Fig. 3.1, two step decays can be

noticed. A slower decay was observed for $\ell < \xi$. The corresponding exponent θ_I approaches θ_c as $\xi \rightarrow \infty$, i.e, when $T_i \rightarrow T_c$. For $\ell \gg \xi$, behavior consistent with $T_i = \infty$ was obtained. This implies, dynamics of the spins is strongly influenced by the relative values of nonequilibrium domain length ℓ and the equilibrium correlation length ξ in the initial configuration. The overall time decay of P , for all T_i , was empirically constructed to be [24]

$$P(t)x^{2\theta} = A \left(\frac{x}{g(x) + x} \right)^\phi; \quad x = \ell/\xi, \quad (3.3)$$

with

$$g(x) = \frac{C_0}{1 + C_1 x^\psi}, \quad (3.4)$$

where A is the amplitude of the long time decay, $\phi = (\theta - \theta_I)/\alpha$, $\psi \simeq 2$, whereas C_0 and C_1 are dimension dependent constants.

An extension of a study [17] (via a different model in $d = 1$) predicts

$$d_f = d - z\theta, \quad (3.5)$$

where z , to be more formally defined later, is a dynamical exponent related to the growth of the persistence pattern. From previous studies [24,31], even though it has been reported that the decay of P is disconnected with the growth of ℓ , z and α may be related. Nevertheless, since such a connection is unclear, to gain knowledge about the variation of d_f , as a function of T_i , estimation of z is needed. Even if such a connection exists, as mentioned, the value of α in $d = 3$ is not unambiguous. In this dimension, the theoretically [2] expected value of α ($= 1/2$) disagrees with some computer simulations [14]

which report numbers close to $1/3$. This difference can possibly [26] be due to long transient period. Thus, lengthy simulation runs with large systems are needed. It will be interesting to see if such long simulation, luck favoring, can provide the theoretically expected value. If yes, in that time regime, do we see change in other quantities as well?

In this work, our objective thus, is to estimate d_f , z , α and θ , for $T_i = \infty$ and $T_i = T_c$, in space dimensions 2 and 3, for quenches to $T_f = 0$. For the ease of reading, in Table 3.1 we provide a list of values of these quantities, obtained from computer simulations. While the ones with asterisks, to the best of our knowledge, will be calculated (or the simulation results will be shown to be consistent with corresponding theoretical expectations) for the first time, the numbers appearing inside the parentheses are improvements over the existing ones that appear outside. We will start presenting results with the objective of calculating d_f . Other quantities will be needed for this purpose and will be estimated in due course.

Table 3.1: List of some nonequilibrium exponents for Ising model.

Case	α	z	θ	d_f
$d = 2, T_i = \infty$	$1/2$	2	0.225	1.58 (1.53)
$d = 2, T_i = T_c$	$1/2$	2*	0.035	1.92*
$d = 3, T_i = \infty$	$1/3$ ($1/2$)	2*	0.18 (0.15)	2.65*
$d = 3, T_i = T_c$	$1/2$	2*	0.105	2.77*

In Fig. 3.2 we show persistence snapshots for $T_i = \infty$ and T_c , both from $t = 10^4$ Monte Carlo steps (MCS), this time unit to be defined soon, for $d = 2$ Ising model. It is clear that the patterns are different and so, different values of d_f are expected. In Fig. 3.3, snapshots from an intermediate

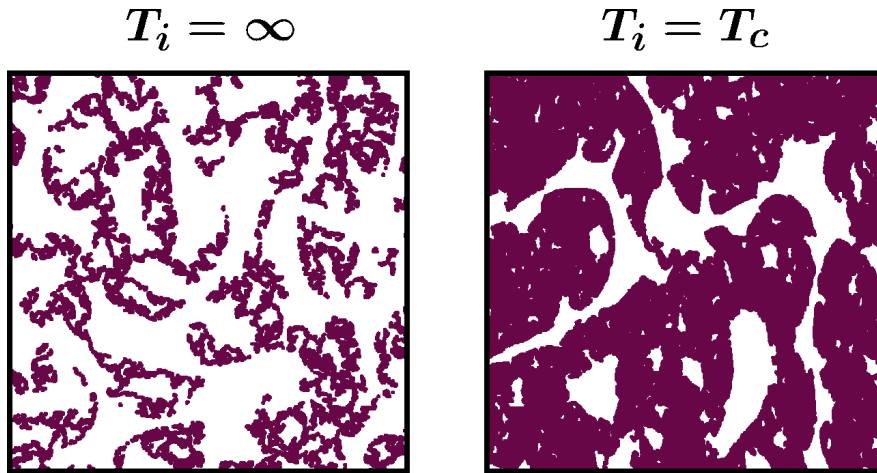


Figure 3.2: Snapshots of the persistent spins are shown for quenches from $T_i = \infty$ and T_c , to $T_f = 0$. The results correspond to $d = 2$, $L = 2048$ and $t = 10^4$ MCS. In both the cases only parts of the boxes are shown. The persistent spins are marked in dots.

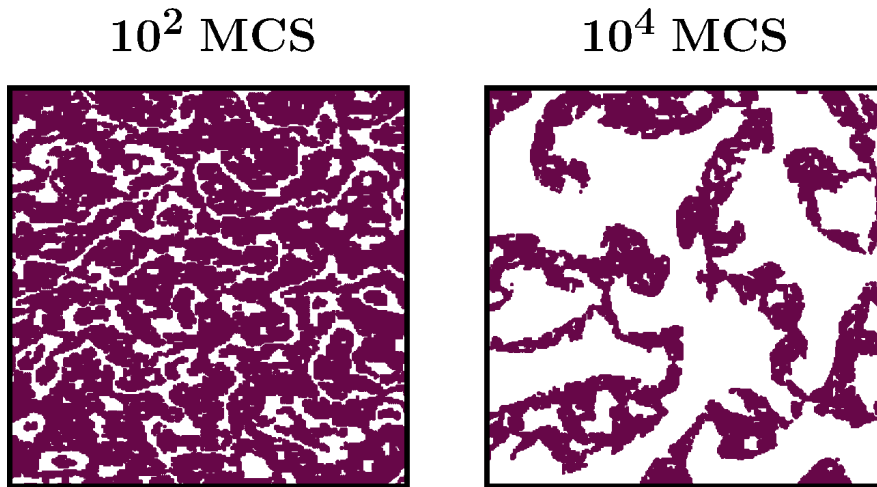


Figure 3.3: Snapshots of the persistent spins from different times, mentioned on the figure, are shown for $T_i = 2.4$ and $T_f = 0$. Other details are same as Fig. 3.2.

temperature $T_i = 2.4$ ($> T_c$), for $d = 2$, are presented. The first frame corresponds to a time falling in the slower decay regime of Fig. 3.1 (for the corresponding temperature), whereas the second one is from the faster decay

regime, implying $\ell \gg \xi$. The earlier time snapshot resembles the $T_i = T_c$ picture of Fig. 3.2 and the second one has similarity with $T_i = \infty$ pattern. This justifies our focus only on these two limiting initial temperatures with $\xi = 0$ and ∞ , rather than exploring a wide temperature range, to accurately quantify d_f and z .

The rest of the chapter is organized as follows. In the next section we describe the model and method. Section 3.3 provides a brief overview of an earlier work. Results are presented in section 3.4. Finally, section 3.5 concludes the chapter with a brief summary and outlook.

3.2 Model and Method

As already mentioned, we study the Ising model [5], on square or simple cubic lattice systems, depending upon the dimensionality, with nearest neighbor interactions. The Hamiltonian for the model is given by

$$H = -J \sum_{\langle ij \rangle} S_i S_j; S_i = \pm 1, \quad (3.6)$$

where J is the interaction strength (> 0) and $\langle ij \rangle$ implies interaction among nearest neighbors. The values of T_c for this model in $d = 2$ and 3 are respectively [32] $\simeq 2.27J/k_B$ and $\simeq 4.51J/k_B$, k_B being the Boltzmann constant.

Kinetics in this model was introduced via Glauber spin-flip mechanism [32, 33]. In this MC approach, a trial move consists of changing the sign of a randomly chosen spin. Since our quenches were done to $T_f = 0$, a

move was accepted only if it had reduced the energy. Needless to say, initial configurations were prepared at nonzero T values. In that case, the Metropolis criterion for the acceptance of a move was implemented via appropriate calculation of the Boltzmann factor [32] and its comparison with a random number, ranging between 0 and 1, whenever the move brought an increment in the energy. For preparation of initial configurations at temperatures very close to T_c , in addition to the Glauber spin-flip moves, we have applied Wolff algorithm [34] as well, which facilitates faster equilibration. Time, in our simulations are measured in units of MCS, each MCS consisting of L^d steps, L being the linear dimension of a square or cubic box. Periodic boundary conditions were applied in all directions. Final results are presented after averaging over multiple initial realizations, the number ranging from 20 to 70. In $d = 2$ all results are for $L = 2048$. In $d = 3$, the results for $T_i = \infty$ are for $L = 512$ and for $T_i = T_c$, we presented results from $L = 400$ and 256.

3.3 An Overview of the Background On fractality of persistence pattern

In this section we provide a discussion on the theoretical background for fractality of the structures formed by persistent spins, following the work by Manoj and Ray [17].

From a density correlation function, $D(r, t)$, isotropic in an unbiased system, total mass or number of particles in a circular or spherical (depending

upon dimensionality) region of radius R can be obtained as

$$M(R, t) \sim \int_0^R D(r, t) r^{d-1} dr, \quad (3.7)$$

r ($= |\vec{r}|$) being the scalar distance of a point in that region from the central one. An appropriate correlation function in the present context is

$$D(r, t) = \frac{\langle \rho(\vec{r}_0, t) \rho(\vec{r}_0 + \vec{r}, t) \rangle}{\langle \rho(\vec{r}_0, t) \rangle}, \quad (3.8)$$

with ρ being unity at a space point if the spin there did not flip till time t and zero otherwise. The average order parameter for the persistent pattern is

$$\langle \rho(\vec{r}, t) \rangle = \frac{\int d\vec{r} \rho(\vec{r}, t)}{\int d\vec{r}} = P(t). \quad (3.9)$$

This being a nonconserved (time dependent) quantity and, since, in the definition of $D(r, t)$, the average value is not subtracted from ρ , decorrelation here means, decay of $D(r, t)$ to a “non-zero” value ($=P(t)$), for $t < \infty$. The distance, $\ell_p(t)$, at which $D(r, t)$ reaches this plateau is the characteristic length scale of the pattern. In that case, there may exist scaling of the form

$$\frac{D(r, t)}{P(t)} \equiv f(r/l_p). \quad (3.10)$$

For x ($\equiv r/l_p$) > 1 , f should be unity. On the other hand, for fractal dimension d_f and $x < 1$, one should have

$$f(x) \sim x^{d_f-d}, \quad (3.11)$$

since

$$M \sim x^{d_f}. \quad (3.12)$$

Considering that $P(t)$, the plateau value, decays in a power-law fashion, a power-law behavior of $f(x)$ is indeed expected, once scaling is achieved. A continuity, at $r = \ell_p$, in such a situation demands

$$t^{(d_f-d)/z} = t^{-\theta}, \quad (3.13)$$

providing Eq. (3.5), where z is the dynamic exponent characterizing the growth of the persistence pattern, mentioned before, as

$$\ell_p \sim t^{1/z}. \quad (3.14)$$

For this model, as mentioned, value of α has been estimated [24] for various T_i values in $d = 2$. However, a priori it is unclear whether there is a general validity of the relation

$$z\alpha = 1. \quad (3.15)$$

Then it is necessary to calculate both z and θ , for correlated and uncorrelated initial configurations, to validate Eq. (3.5). On the other hand, as already mentioned, the value of α is ambiguous in $d = 3$.

3.4 Results

In Fig. 3.4 we show $D(r, t)$ as a function of r for $T_i = 2.4$, from two different times, mentioned on the figure, for $d = 2$. As expected, the correlation

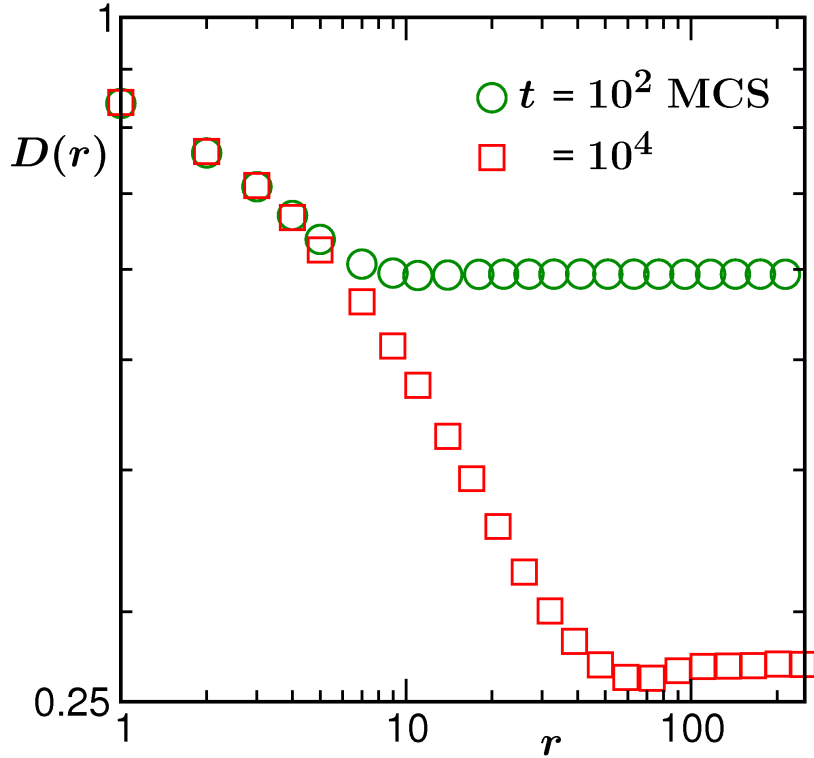


Figure 3.4: Density correlation functions, $D(r, t)$, related to the persistent spins, are plotted vs r . Results are presented from two different times, for $T_i = 2.4$ and $T_f = 0$. The system dimensionality is $d = 2$ and value of L is 2048.

function decays to different constant value, $P(t)$, at different length ℓ_p , for different times. Before decaying to the plateau, the early time data appear to obey a power-law. The later time data, for smaller r , follows the same power-law before crossing over to another, faster, power-law decay. This implies, there exist two length scales in the problem, below and beyond the equilibrium scale ξ . Inside the larger structure, the small length scale structure remains hidden, which will become irrelevant in the long time limit. For $\xi = \infty$, i.e., $T_i = T_c$, however, the latter will be the only structure and remain for ever. The exponent for large r , for $T_c < T_i < \infty$ and $t \gg 0$,

should be related to the d_f value for $T_i = \infty$ case whereas, in case of small r , the exponent should be connected to d_f for $T_i = T_c$ case. Below we focus on these two cases, i.e., $T_i = \infty$ and $T_i = T_c$, separately, first for $d = 2$, followed by $d = 3$. As need occurs, we will present results related to α , θ and z .

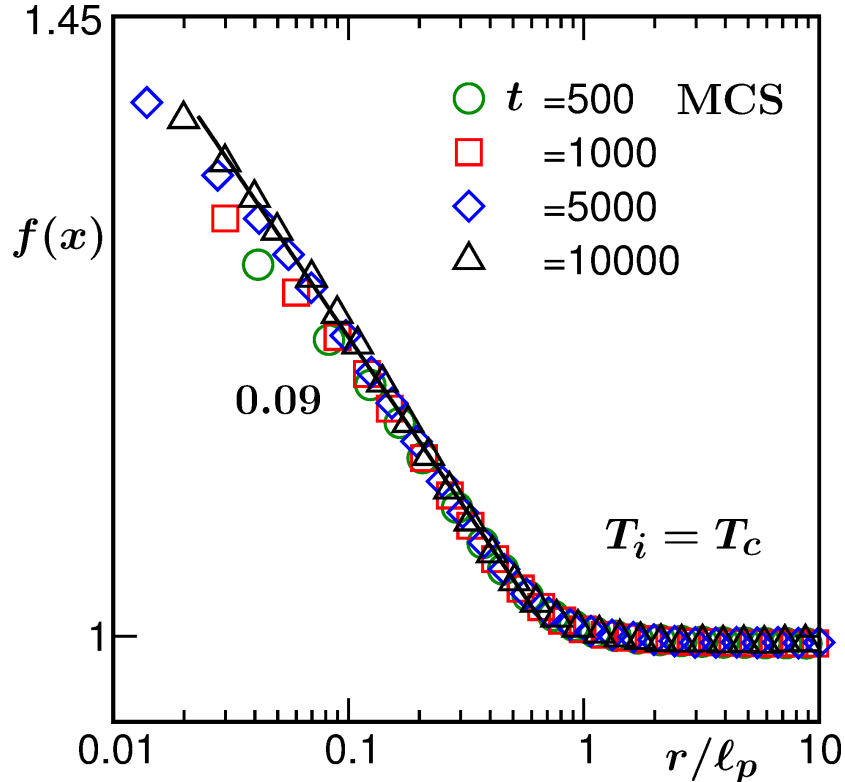


Figure 3.5: Scaling analysis of $D(r, t)$ for the $d = 2$ Ising model, with $T_i = T_c$ and $T_f = 0$, where $f(x)$ is plotted vs $x = r/\ell_p$, using data from different times after the quench, on log-log scale. The solid line corresponds to a power-law decay with an exponent 0.09. The value of L is 2048 for all the results.

In Fig. 3.5 we present a scaling exercise [17, 19] for $D(r)$ where we have plotted $f(x)$ as a function of x , using data from different times after quench, for $T_i = T_c$ and $d = 2$. Scaling appears good and gets better with the progress of time. On this log-log plot, look of the data appear, before decaying to unity, linear, implying a power-law decay. The exponent appears to be \simeq

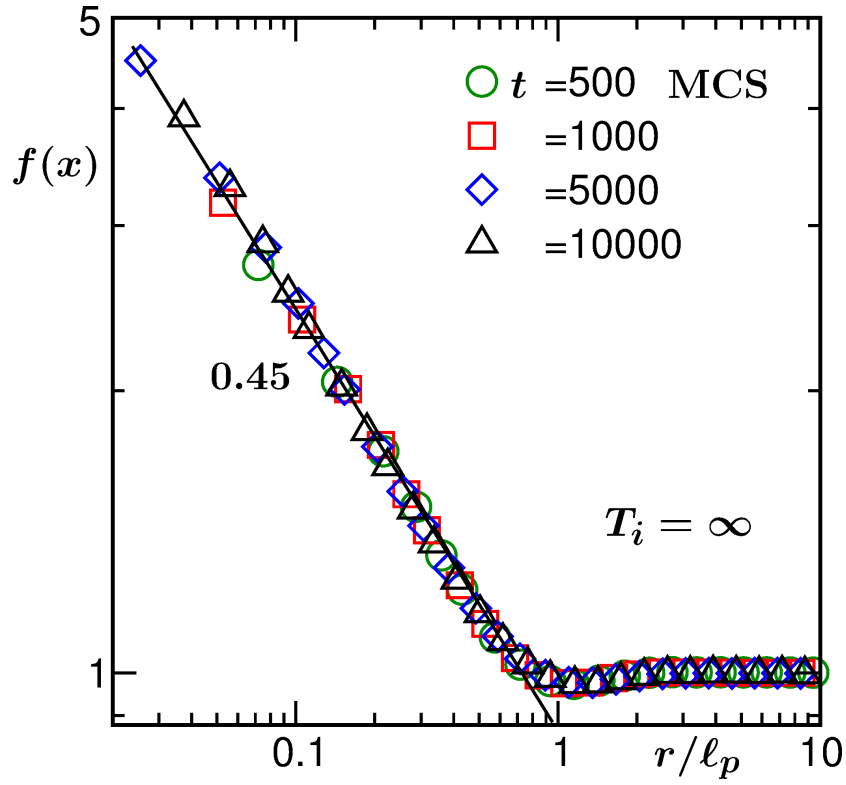


Figure 3.6: Same as Fig. 3.5 but for $T_i = \infty$. The solid line here has the power-law decay exponent 0.45.

0.09. In Fig. 3.6, we show analogous exercise for $T_i = \infty$. Even though this case in this dimension was studied by Jain and Flynn [19], for the sake of comparison and completeness, we present it here from our own simulations. In this case, the exponent for the power-law decay appears consistent with 0.45. Then, in $d = 2$, for $T_i = \infty$, the fractal dimensionality is 1.55 and for $T_i = T_c$, the number is 1.91, if Eq. (3.11) is valid.

We show the plots of ℓ_p vs t in $d = 2$, for $T_i = \infty$ (Fig. 3.7) and $T_i = T_c$ (Fig. 3.8), on log-log scales. In both the cases the data appear consistent with $z = 2$, validating Eq. (3.15) (note that α is established to be $1/2$ in $d = 2$). Nevertheless, we intend to make more accurate quantification.

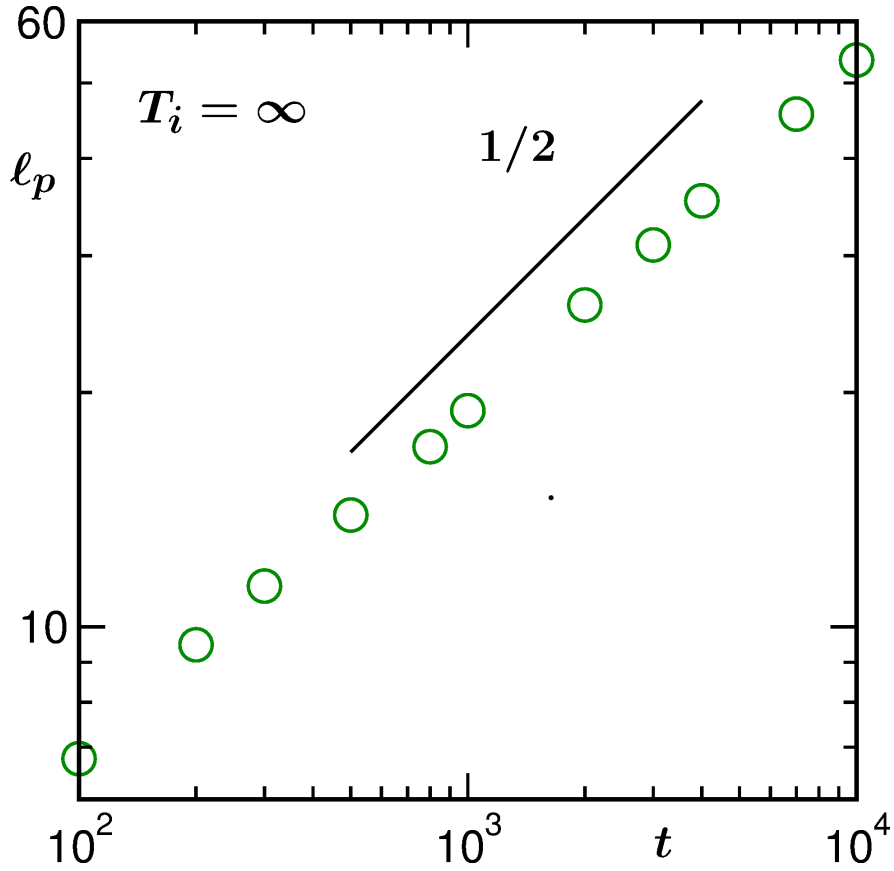


Figure 3.7: Log-log plot of persistence length scale, ℓ_p , as a function of t , for $d = 2$ Ising model, following quench from $T_i = \infty$ to $T_f = 0$, with $L = 2048$. The solid line represents a power-law growth with the exponent $1/2$.

For this purpose, in Fig. 3.9 and Fig. 3.10 we have shown instantaneous exponents (dash-dotted lines), z_i , calculated as [35]

$$\frac{1}{z_i} = \frac{d \ln \ell_p}{d \ln t}, \quad (3.16)$$

vs $1/\ell_p$. In both the cases we obtain the value of z via linear extrapolation (see the consistency of the simulation data with the solid line) to $\ell_p = \infty$. For $T_i = \infty$, from this exercise, we quantify $z = 2.15$ and for $T_i = T_c$,

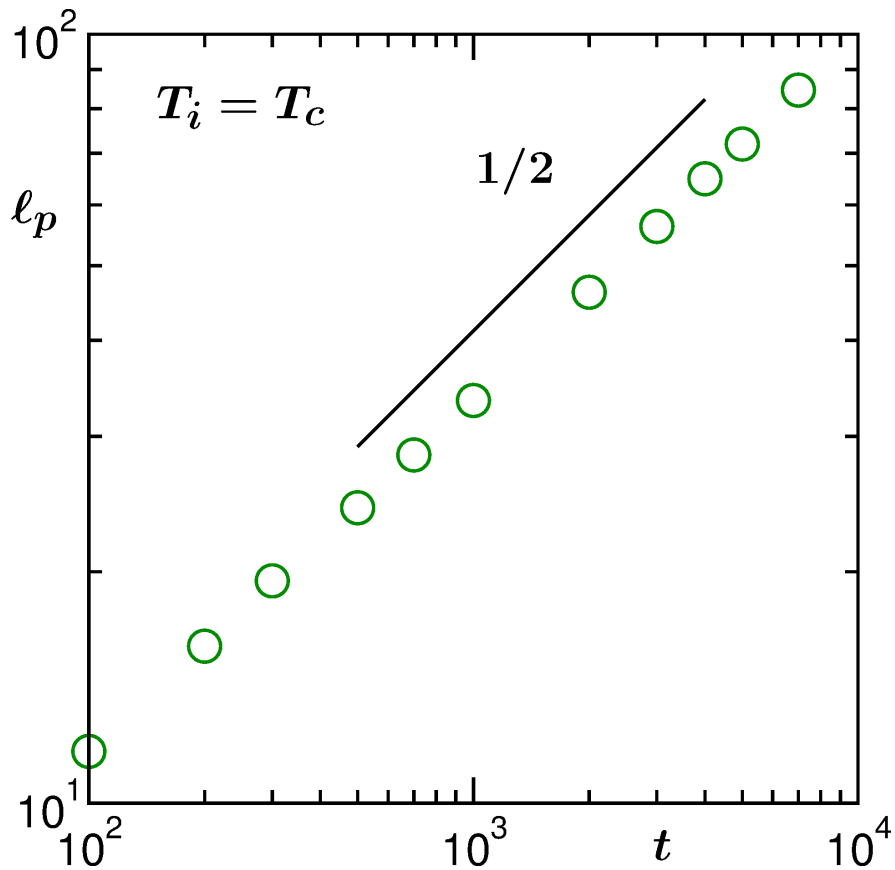


Figure 3.8: Same as Fig. 3.7, but here $T_i = T_c$. The solid line corresponds to power-law growth with exponent $1/2$.

we obtain the number $z = 2.02$ (see the dashed horizontal lines). These numbers, in addition to verifying Eq. (3.15), are also consistent with the numbers obtained via least square fitting of the ℓ_p vs t data to the form

$$\ell_p = \ell_z^0 + A_z t^{1/z}, \quad (3.17)$$

where ℓ_z^0 and A_z are positive constants. This consistency may imply, early time corrections to the exponents are insignificant. Note here that, in absence

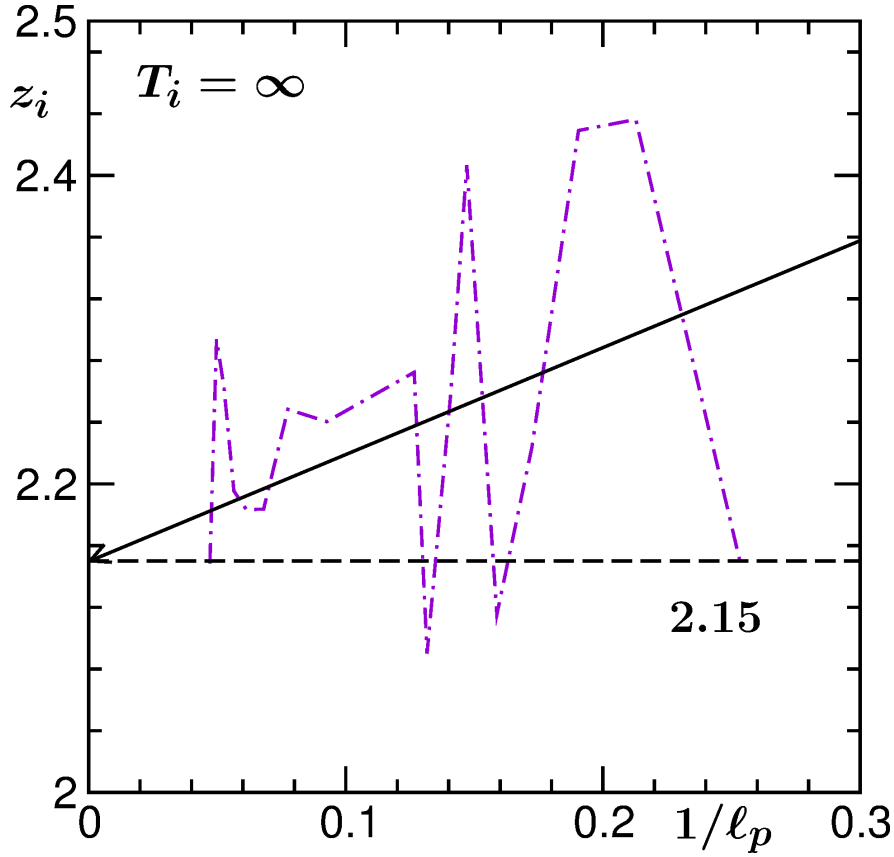


Figure 3.9: Instantaneous exponent, z_i , obtained using the data in Fig. 3.7. The horizontal dashed line correspond to our estimate for z , whereas solid line is guide to the eyes.

of any correction, one expects [36, 37]

$$\frac{1}{z_i} = \frac{1}{z} \left[1 - \frac{\ell_z^0}{\ell_p} \right], \quad (3.18)$$

a linear behavior of $1/z_i$, when plotted vs $1/\ell_p$, with slope $-\ell_z^0/z$. A positive slope in both is due to the fact that we have presented inverse of the quantity discussed in Eq. (3.18). Using these values of z , and numbers for θ , mentioned earlier, in Eq. (3.5), we obtain $d_f = 1.93$ for $T_i = T_c$ and $d_f = 1.51$

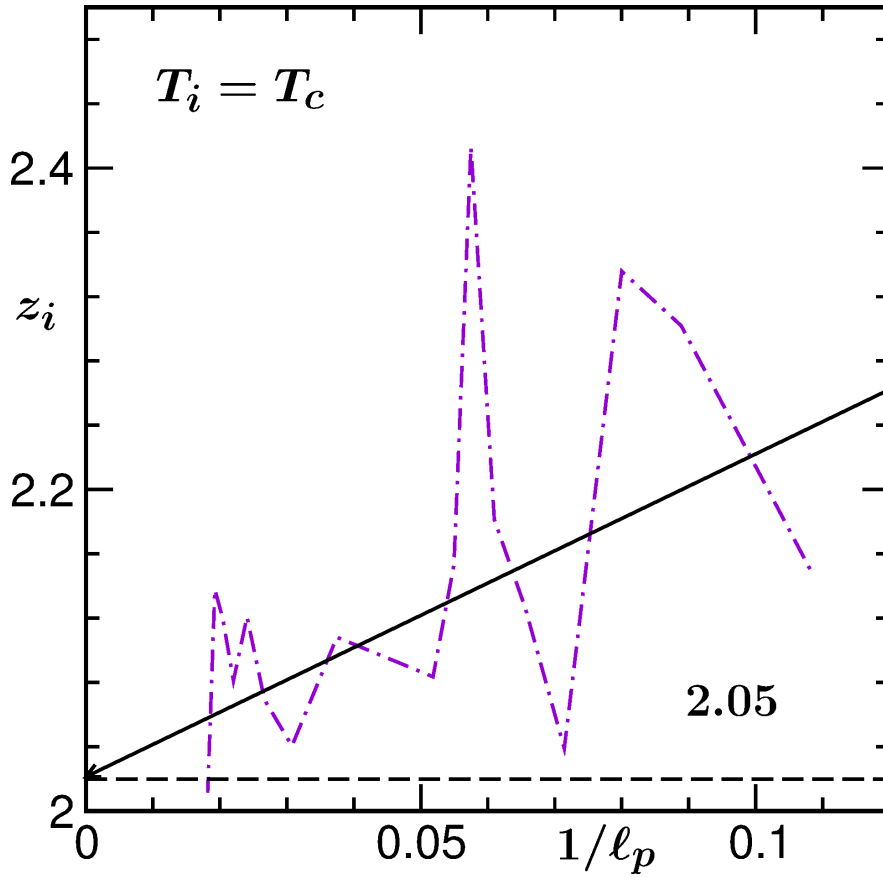


Figure 3.10: Same as Fig. 3.9, but here $T_i = T_c$. The dashed and the solid lines have the same meaning as in Fig. 3.9.

for $T_i = \infty$. These values, within computational errors, are consistent with the conclusions from Fig. 3.5 and 3.6. Next we present results from $d = 3$.

In $d = 3$, we start by presenting results for the growth of ℓ , considering the controversy [14,24,26] on the value of α discussed above. In $d = 2$, we avoided presenting results on this aspect with the understanding that the issue there is well settled. Nevertheless, in the context of global persistent decay, we will make indirect conclusion about it. Here note that the estimation of ℓ was

done from the first moment of domain size distribution, $p(\ell_d, t)$, as

$$\ell(t) = \int \ell_d p(\ell_d, t) d\ell_d, \quad (3.19)$$

where ℓ_d is the distance between two domain boundaries in a particular direction. Fig. 3.11 shows a plot of ℓ vs t , on log-log scale, for quenches of

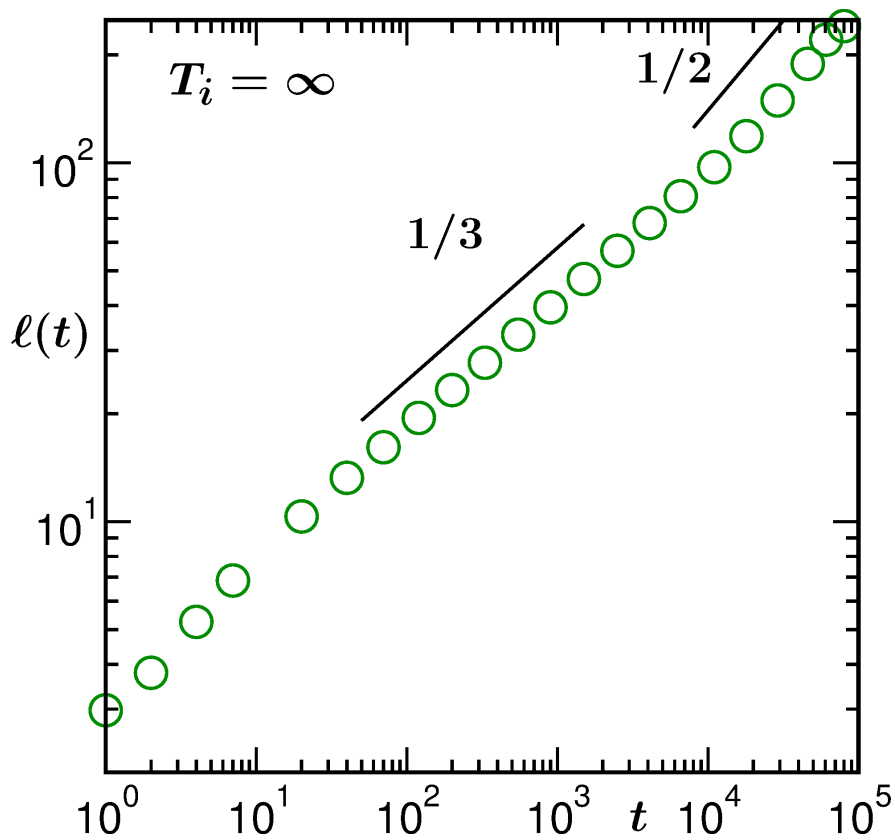


Figure 3.11: Log-log plot of ℓ vs t , in $d = 3$, for $T_i = \infty$. The solid lines correspond to different power laws, exponents for which are mentioned.

the $d = 3$ Ising system from $T_i = \infty$ to $T_f = 0$. There exists an intermediate time regime, extending over more than two decades, during which the simulation data show consistency with an exponent $\alpha = 1/3$, in agreement with previous results [14]. However, as discussed and a trend demonstrated

in Ref. [26], the discrepancy in the earlier reports from the theoretical number $1/2$ can be due to long transient. Thus, long simulation runs with large systems are necessary. We have simulated a system with $L = 512$ for time longer than any of the previous works, to the best of our knowledge. Indeed, it appears that the long time behavior, over the latest time decade in the presented time range, is consistent with $\alpha = 1/2$. In Fig. 3.12 we show the

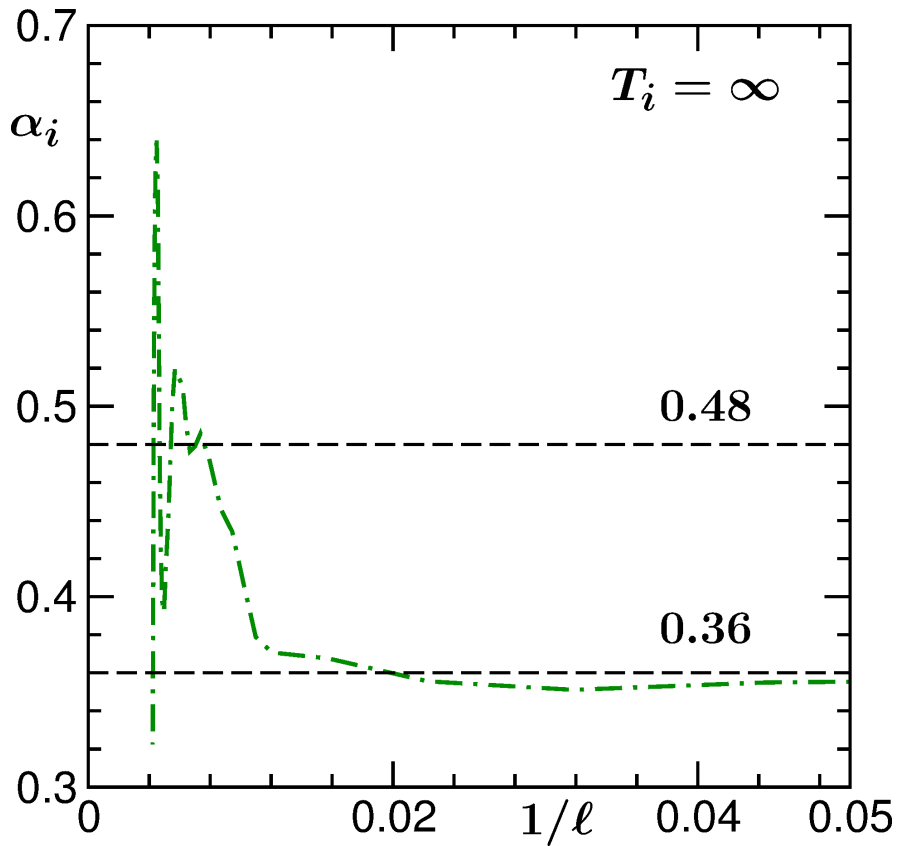


Figure 3.12: Plot of instantaneous exponent α_i , as a function of $1/\ell$. The dashed horizontal lines represent exponent values 0.36 and 0.48. The results are for $T_i = \infty$ and $d = 3$.

instantaneous exponent

$$\alpha_i = \frac{d \ln \ell}{d \ln t}, \quad (3.20)$$

as a function of $1/\ell$. This provides an accurate picture, the long time exponent being within 5% of the theoretical value. One may then ask, is the value of θ going to change, beyond this crossover time? Even if θ has no dependence on the value of α , such a change may still occur. Note that conclusion on the value of θ , in earlier works [16, 24], were drawn from runs shorter than this. Indeed, a jump in θ_i , calculated from

$$\theta_i = -\frac{d \ln P}{d \ln t}, \quad (3.21)$$

occurs (see Fig. 3.13 and Fig. 3.14) from an early time value of $\simeq 0.18$ to

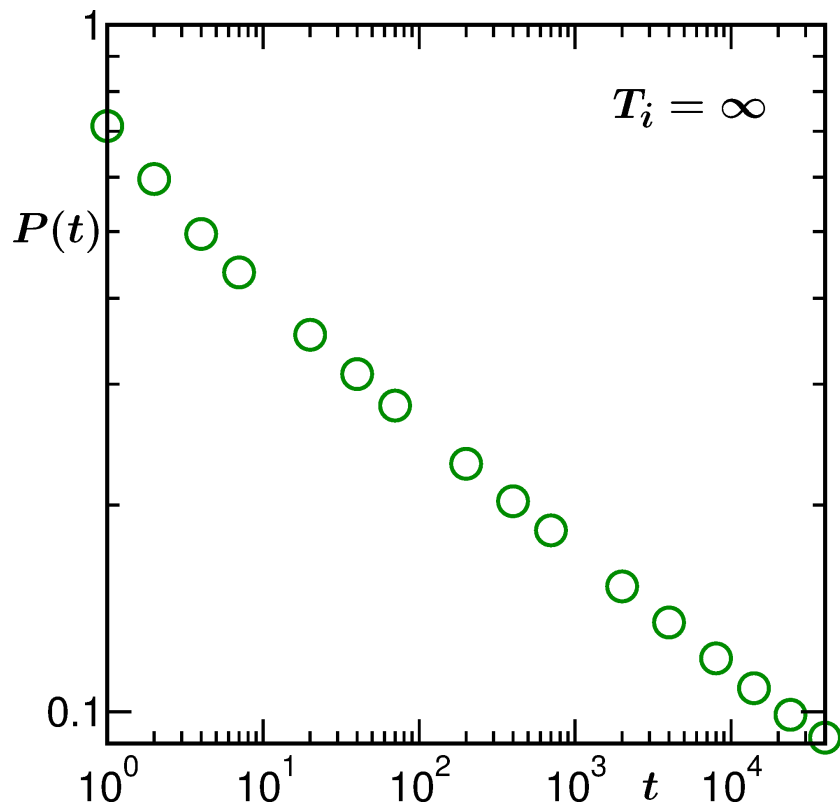


Figure 3.13: Log-log plot of $P(t)$ vs t , for $d = 3$ and $T_i = \infty$.

$\simeq 0.15$. This may, of course, be due to statistical or other reasons. However,

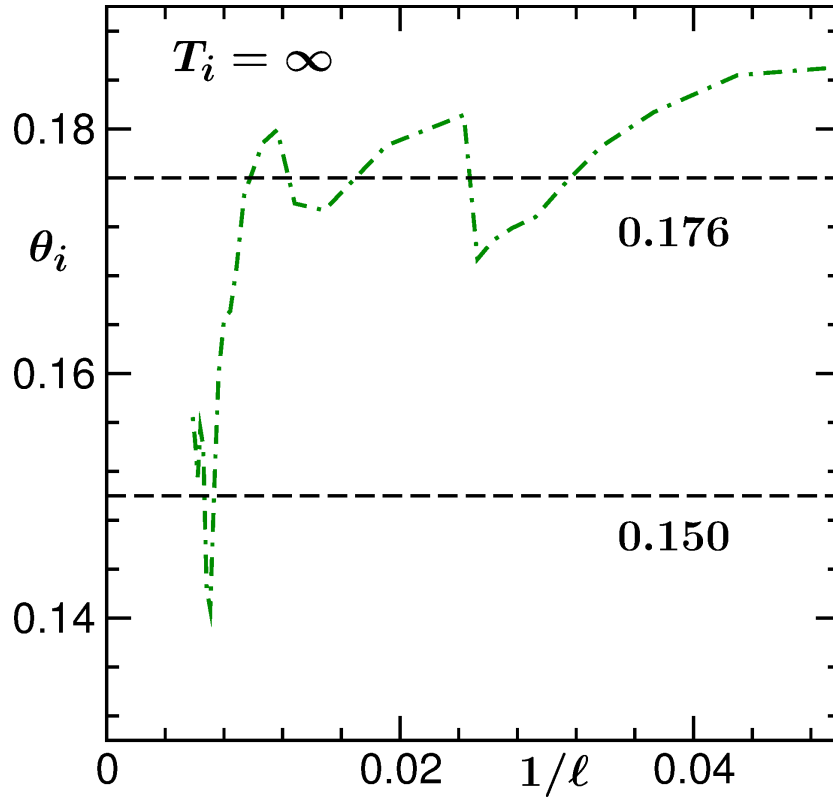


Figure 3.14: Instantaneous exponent θ_i is plotted as a function of $1/\ell$. Horizontal dashed lines are for $\theta = 0.176$ and 0.15 . The results correspond to $T_i = \infty$ and $d = 3$.

since the jump in α_i occurs around the same time as the one for θ_i and fluctuation is seen around stable mean values, in both α_i and θ_i , we accept this as the correct number for θ in the asymptotic time limit.

Whether due to lattice anisotropy [14] or anything else, the solution to overcome such long transient is certainly related to being able to access large length scales. For T_i close to T_c , since this is automatically the case, due to large initial correlation, we expect an enhanced value of α from early time. Corresponding ℓ vs t data are presented in Fig. 3.15. On the log-log scale, this data set shows consistency with $\alpha = 0.45$. Here we mention that study

for $T_i = T_c$ has additional problems related to longer equilibration time at the initial temperature and stronger finite-size effects during the nonequilibrium evolution [24]. The latter remark can be appreciated from the plot in Fig.

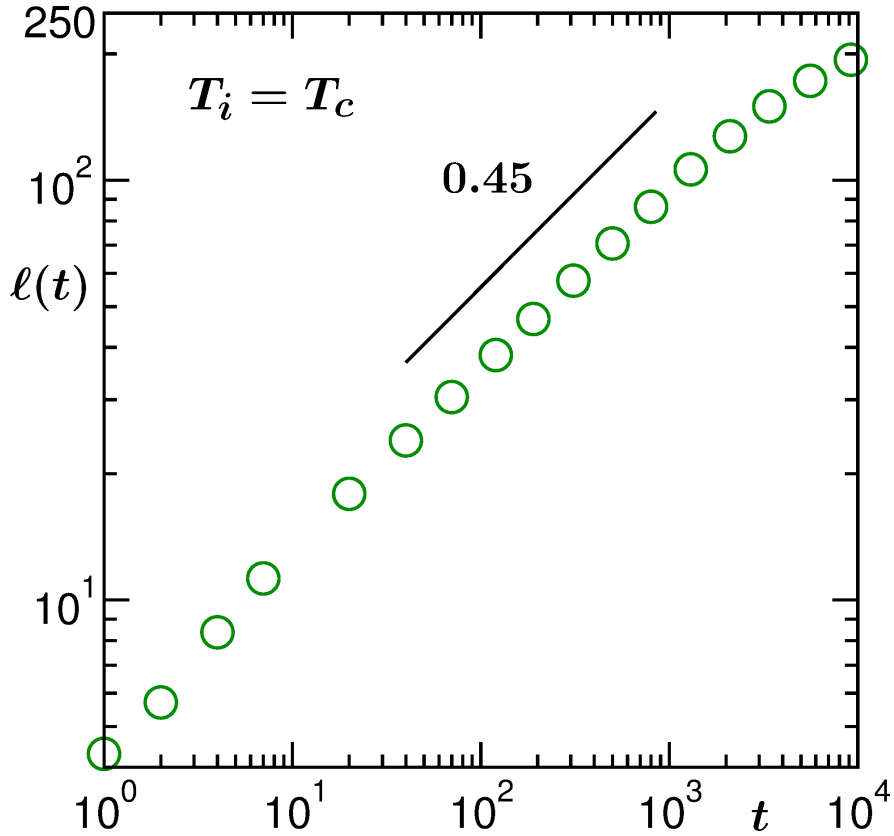


Figure 3.15: Log-log plot of ℓ vs t , for $d = 3$, $L = 400$ and $T_i = T_c$. The solid line corresponds to a power-law growth with exponent 0.45.

3.15 where a bending of the data set (from the power-law behavior) is visible from $t = 10^3$. This should be compared with the corresponding data in Fig. 3.11 for $T_i = \infty$. Thus, accessing very large length scales, without finite-size effects, in this case is extremely difficult. The P vs t data, shown in Fig. 3.16, exhibit consistency [24] with $\theta_c \simeq 0.105$. Since, α is very close to $1/2$ already, we do not expect much change in θ_c even in true asymptotic length

or time limit. The calculations of α_i and θ_i in this case provide numbers consistent with the ones quoted above.

Next, we come back to the issue of fractality. For $d = 3$ Ising model, our results in this context are entirely new irrespective of the value of T_i .

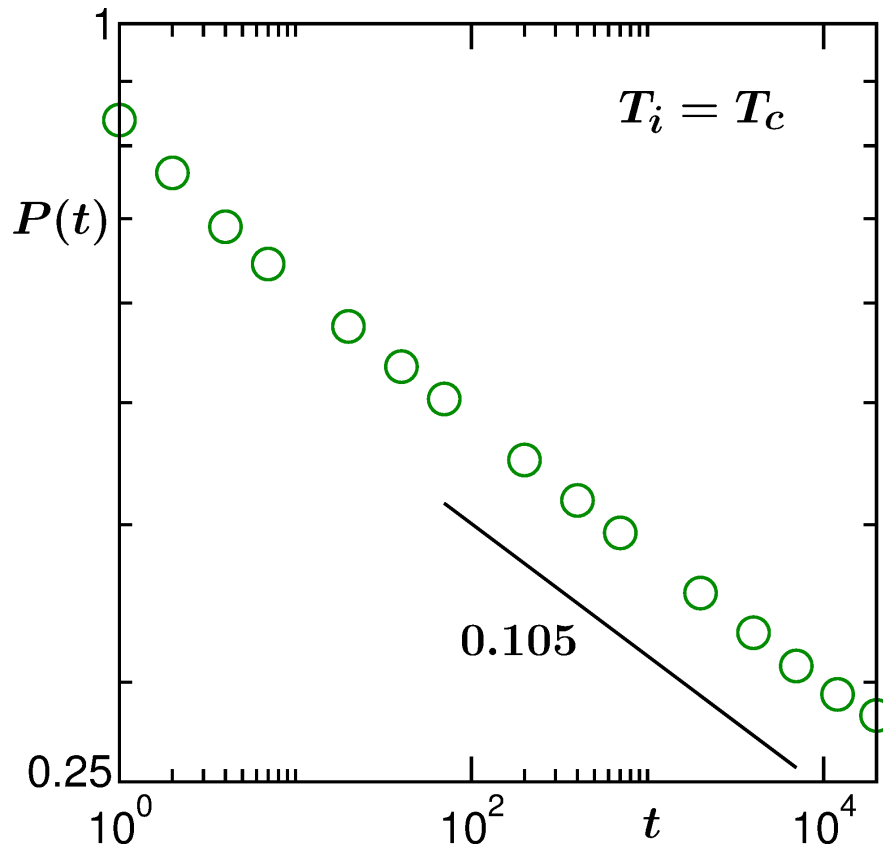


Figure 3.16: Plot of P vs t , for $d = 3$, $T_i = T_c$ and $T_f = 0$, on log-log scale. The solid line there represents a power-law decay with exponent 0.105.

Fig. 3.17 is analogous to Fig. 3.6 ($T_i = \infty$ results for $f(x)$) but here it is for $d = 3$. The corresponding $f(x)$ vs x scaling plot for $T_i = T_c$ in $d = 3$ is presented in Fig. 3.18. Again, for both $T_i = \infty$ and $T_i = T_c$, good data collapse are obtained for results from different times, in these scaling plots. For both values of T_i , we have used data sets lying in the time ranges

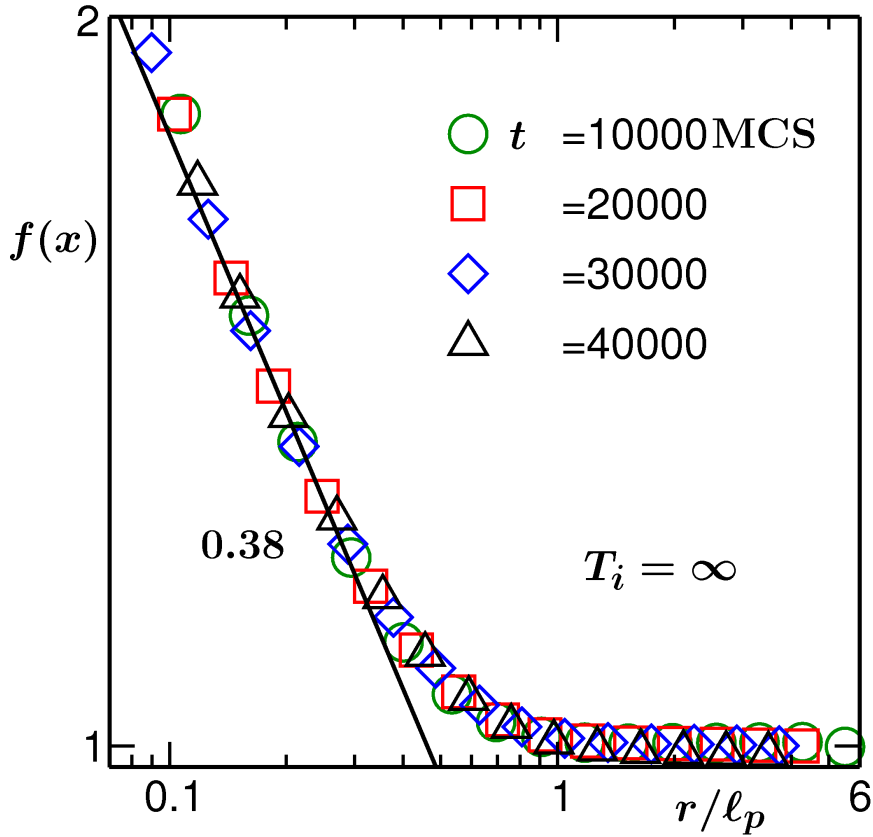


Figure 3.17: Scaling function $f(x)$ is plotted vs x , for $d = 3$, $T_i = \infty$ and $T_f = 0$, using data from few different times. The solid line has a power-law decay with exponent 0.38. The results were obtained for simple cubic lattice with $L = 256$.

that provide consistency with the expected theoretical number for α . In the relevant region, the $T_i = T_c$ results have power-law decay with exponent 0.24. In case of $T_i = \infty$, the value of this exponent is approximately 0.38. These numbers imply $d_f = 2.76$ and 2.62 for $T_i = T_c$ and $T_i = \infty$, respectively.

We show ℓ_p vs t plots from $d = 3$ for $T_i = \infty$ and $T_i = T_c$ in Fig. 3.19 and Fig. 3.20 respectively. In the long time limit, the results, in both of them, appear consistent with growth having $z = 2$. This is in agreement with Eq. (3.15). From the log-log plot for $T_i = \infty$, like ℓ vs t , a long time transient is

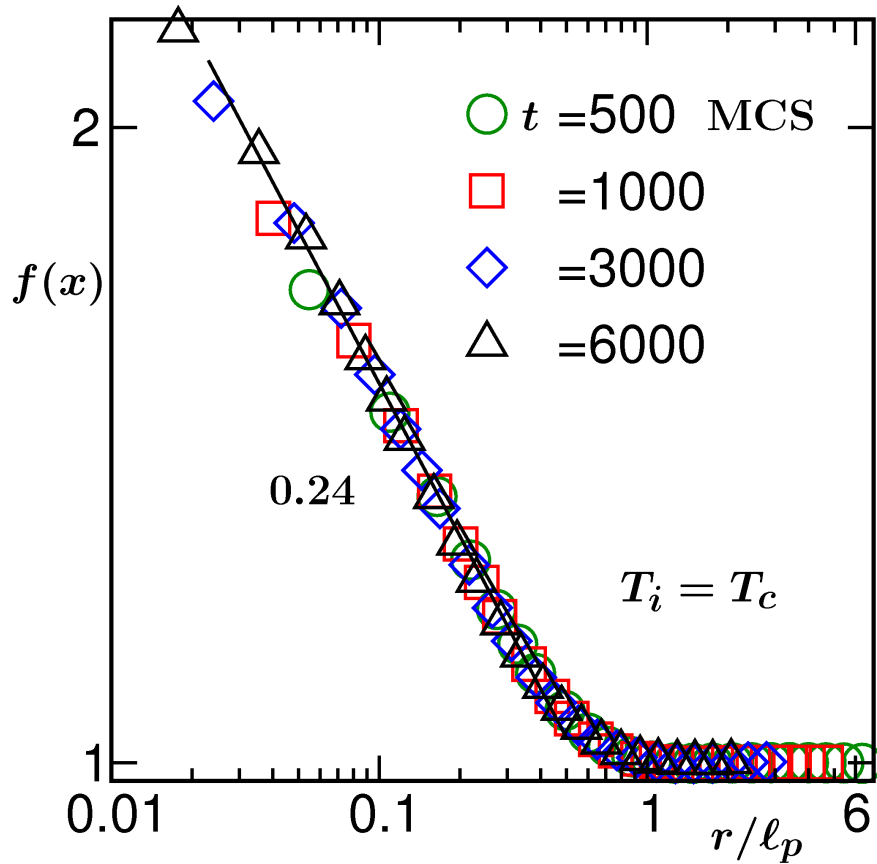


Figure 3.18: Same as Fig. 3.17 but for $T_i = T_c$. Here the solid line has a power-law decay exponent 0.24.

clearly visible. To quantify z more accurately (in the $t \rightarrow \infty$ limit), for both $T_i = \infty$ (Fig. 3.21) and $T_i = T_c$, (Fig. 3.22) we have shown the instantaneous exponents, vs $1/\ell_p$. From there, we extract $z = 2.1$ for $T_i = \infty$ and 2.15 for $T_i = T_c$. Along with the above mentioned numbers for z , using the values of θ for quenches from $T_i = T_c$ and $T_i = \infty$, we obtain $d_f \simeq 2.78$ and 2.68. These numbers are consistent with those obtained from the scaling plots in Fig. 3.17 and 3.18, providing higher confidence on our estimation of θ from long time limit, for $T_i = \infty$. An interesting exercise here would have been to

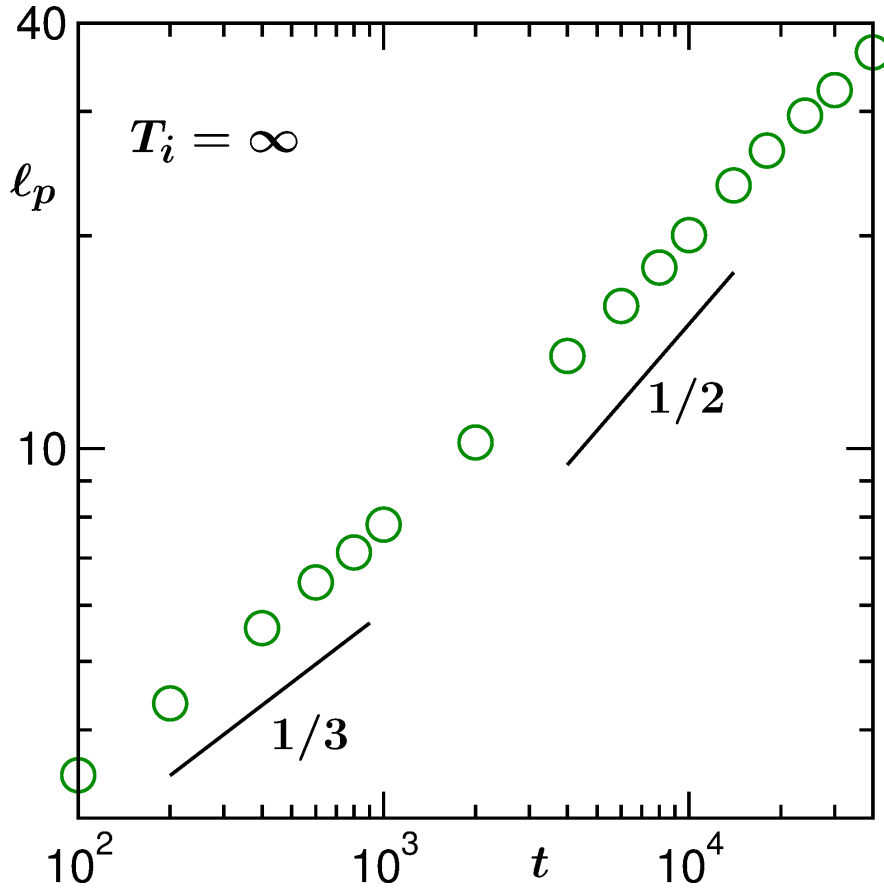


Figure 3.19: Log-log plot of persistence length scale, ℓ_p , as a function of t , for $d = 3$ Ising model, following quench from $T_i = \infty$ to $T_f = 0$, with $L = 512$. The solid lines correspond to power-law growths with exponents mentioned there.

plot $z_i \alpha_i$ vs t . However, a constant value of unity cannot be obtained because of the fact that ℓ and ℓ_p have different initial off-sets. This is evident from Fig. 3.12 and Fig. 3.21. While for the time dependence of ℓ , a long transient with $\alpha \simeq 1/3$ is visible, this is not so for the time dependence of ℓ_p . Thus, because of the off-set related reason mentioned above, $z_i \alpha_i = 1$ is expected to be valid only in the $t \rightarrow \infty$ limit.

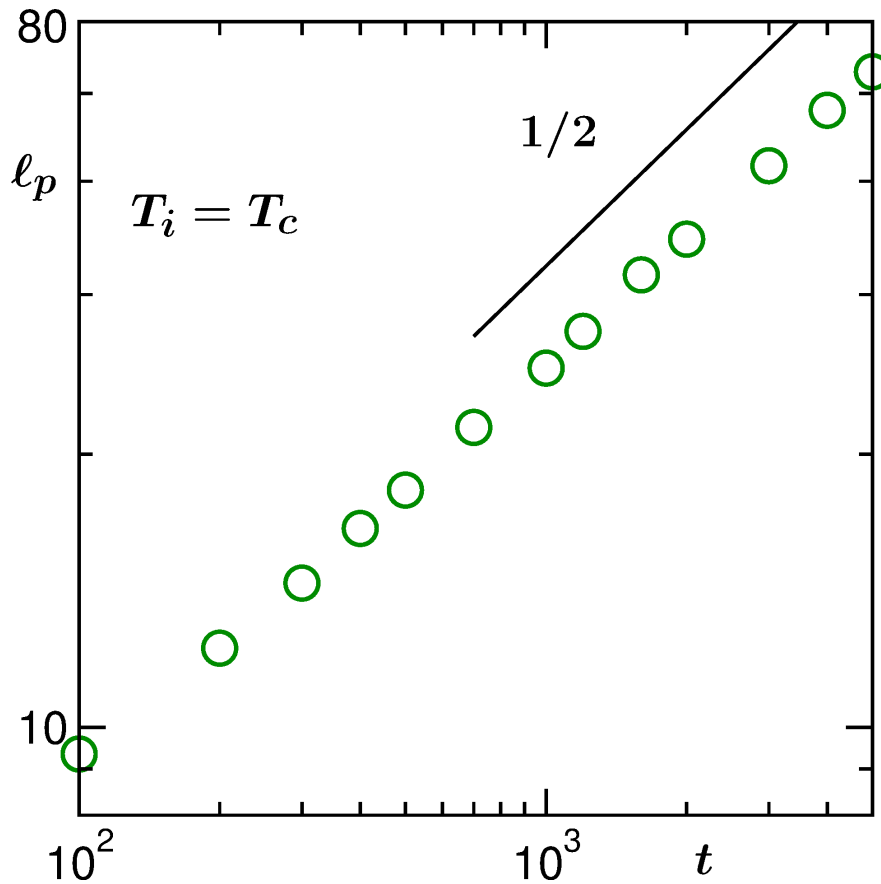


Figure 3.20: Same as Fig. 3.19, but here $T_i = T_c$ and $L = 256$.

Finally, we turn our attention to the block persistence which was introduced by Cueille and Sire [14]. The corresponding probability P_b , as already mentioned, is related to the change in the order-parameter variable obtained by coarse-graining the site or microscopic spin variables over a block of linear size ℓ_b . It is expected that the decay of this probability will be significantly slower than the site or local persistence probability, to which the former should cross over only for $\ell > \ell_b$. This two time-scale behavior is desirable by considering that, in the early time regime, a slower decay is forced by the fact that a sign change in block spin variable happens only when ℓ becomes

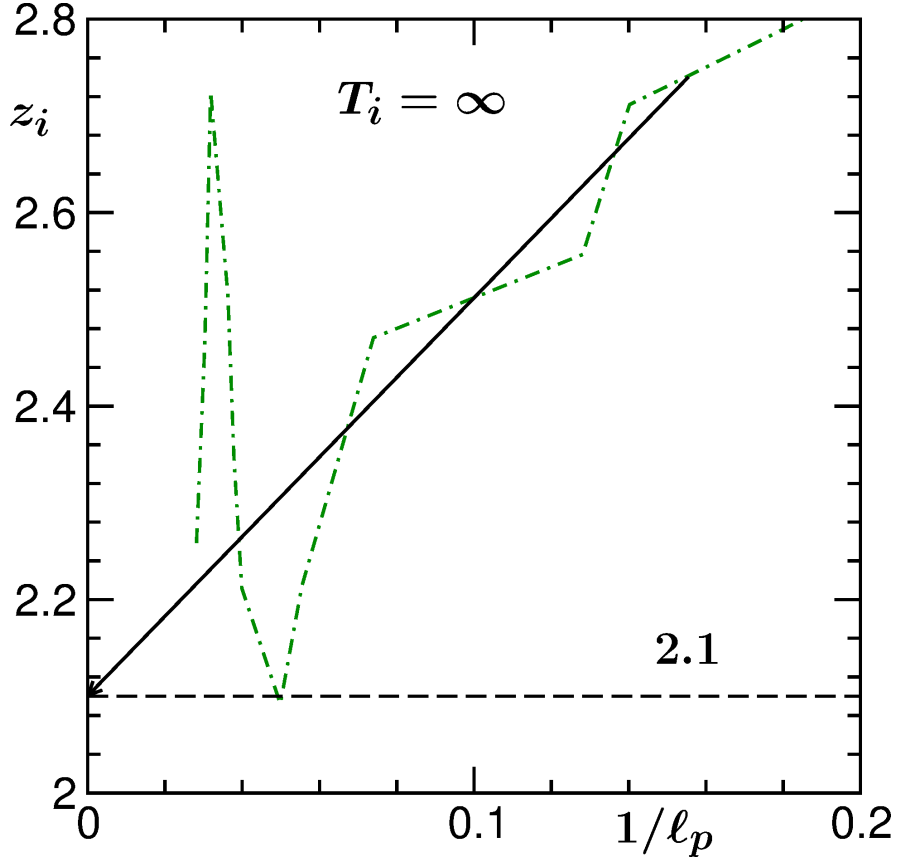


Figure 3.21: Instantaneous exponent, z_i , obtained using the data in Fig. 3.19, is plotted vs. $1/\ell_p$. The horizontal dashed line correspond to our estimates for z and the solid line there is guide to the eyes.

comparable to ℓ_b and in the large ℓ limit, the blocks effectively appear as sites. It is expected then that a scaling should be obtained as [14]

$$P_b \ell_b^{\theta_0/\alpha} \equiv h(t/\ell_b^{1/\alpha}), \quad (3.22)$$

where θ_0 is the exponent of the early part of the decay or global persistence exponent in the sense that when $\ell_b \rightarrow \infty$, this is the only exponent. In $d = 2$, we will see that the best scalings, in accordance with Eq. (3.22), are obtained

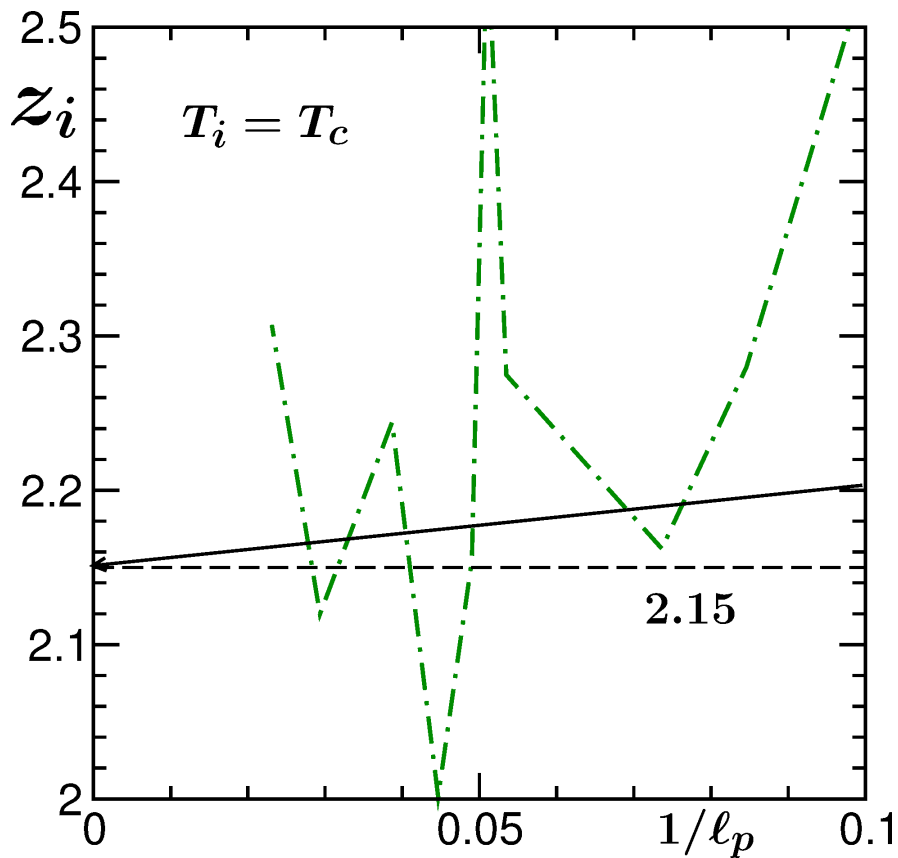


Figure 3.22: Same as 3.21, with $T_i = T_c$ and $L = 256$.

for $\alpha = 1/2$, irrespective of the value of T_i . In $d = 3$, on the other hand, due to long transient in the dynamics, we avoid presenting these results.

In addition to the above mentioned understandings, calculation of persistence probability via such blocking may have advantage for quenches to nonzero temperature. Note that for $T_f \neq 0$, thermal fluctuation from bulk of the domains affects the calculation when done via standard method. Considering that domain growth occurs essentially due to spin flips along the domain boundaries, in the calculation of P , dynamics inside the domains needs to be discarded. In a method, prescribed by Derrida [12], this is done

by simulating an ordered system, alongside the coarsening one, and subtracting the common flipped spins, identifiable as the bulk flips, between the two systems, from the total, thus sticking to the effects of only the boundary motion. In the block spin method, if ℓ_b is significantly larger than ξ at T_f , thermal fluctuations will not alter the sign of block spins and in the large ℓ ($> \ell_b$) limit, as previously stated, one expects the decay to be consistent with local persistence. This saves computational time for simulating the additional systems with ordered configurations.

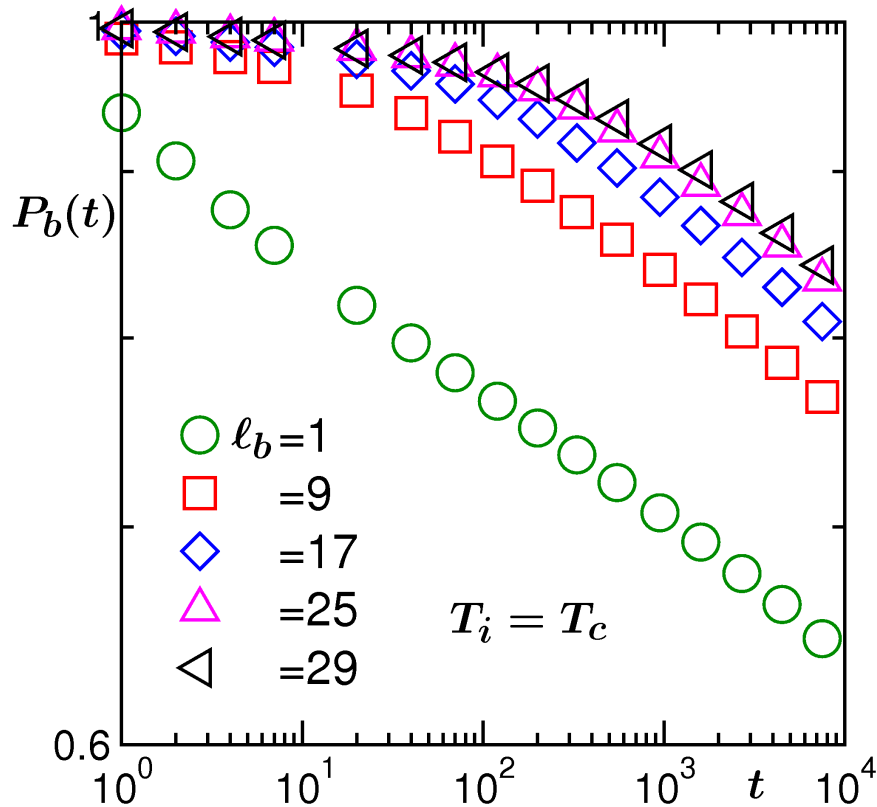


Figure 3.23: Plots of block persistence probabilities, $P_b(t)$, vs t , from different values of ℓ_b , for $T_i = T_c$, in $d = 2$. We have used $L = 2048$.

In Fig. 3.23 we show P_b vs t plots from $d = 2$, for a few different values

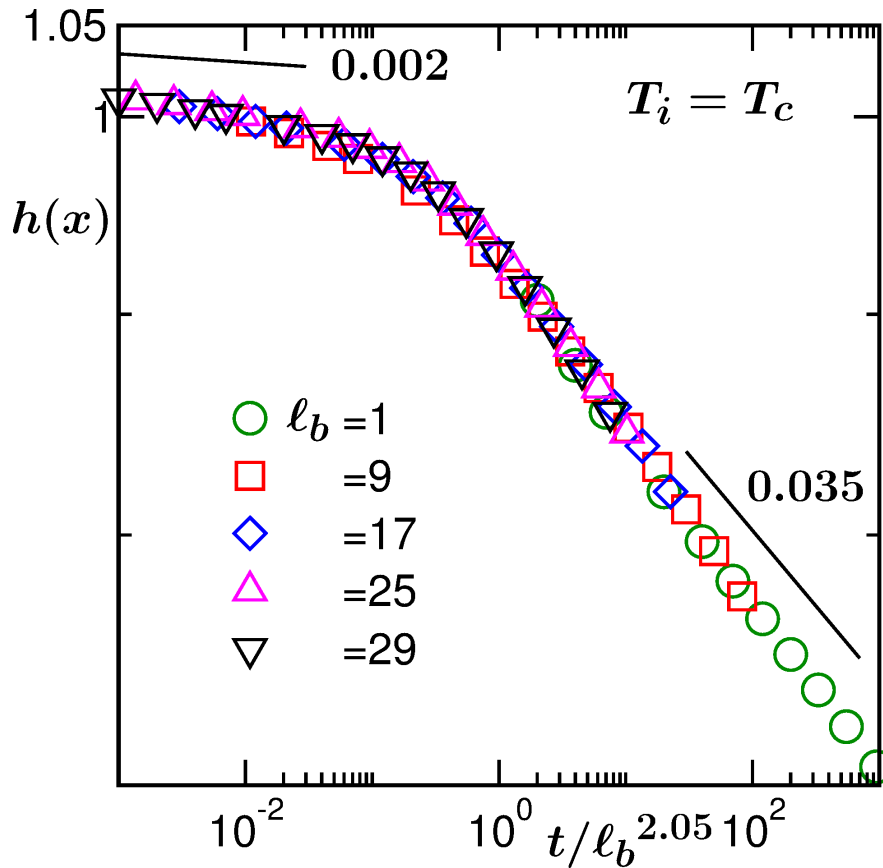


Figure 3.24: Scaling plots of the persistence probabilities in Fig. 3.23. The scaling function $h(x)$ is plotted, on a log-log scale, vs $x = t/\ell_b^{1/\alpha}$. Various power-law decays are shown by solid lines with the exponent values being mentioned next to appropriate lines.

of ℓ_b and $T_i = T_c$. It appears, as discussed, there exist two step decays and crossover to the faster (consistent with the local persistent decay) one is delayed with increasing ℓ_b .

In Fig. 3.24 we show a scaling exercise using the data of Fig. 3.23 where we have plotted $h(x)$ vs $t/\ell_b^{1/\alpha}$. For obtaining collapse of data, we have adjusted θ_0 and α . The value of α used here is 0.49, that provides

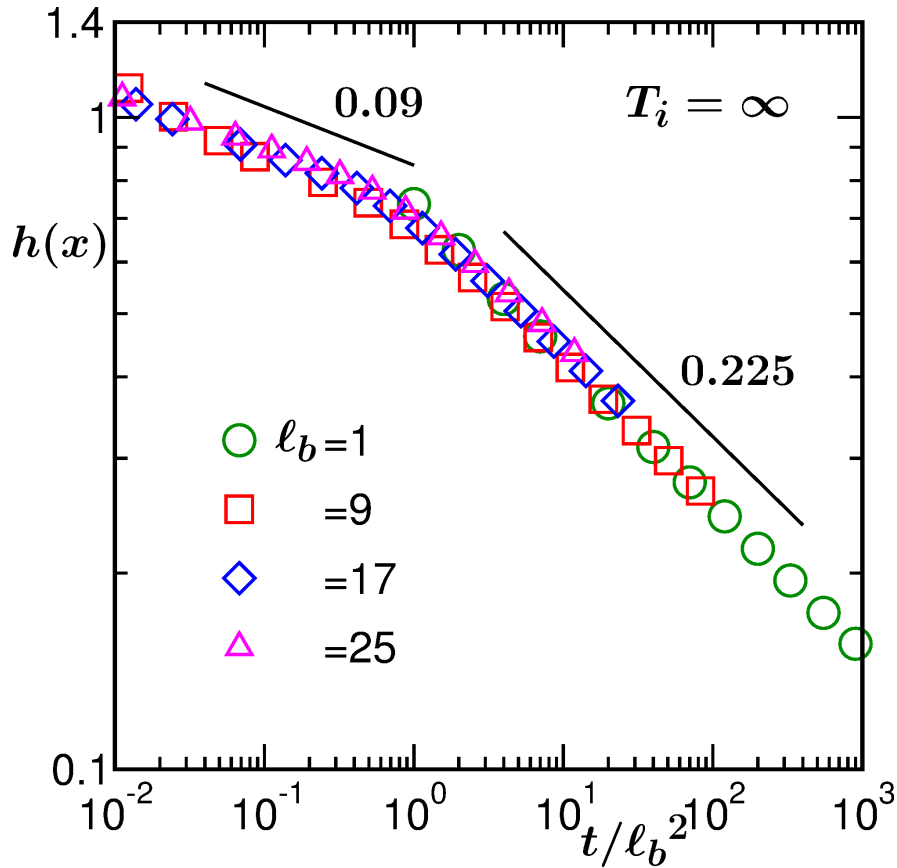


Figure 3.25: Scaling plot similar to Fig. 3.24 is presented for $T_i = \infty$ with $d = 2$ and $L = 2048$. Solid lines in the figure represent various power-laws with exponents mentioned there.

the best collapse. This number is certainly consistent with $1/2$, within numerical error. Early time behavior corresponds to global persistence with $\theta_0 = 0.002$ and the late time behavior is consistent with our previous estimation of $\theta_c \simeq 0.035$, for the site persistence probability. In Fig. 3.25 we have shown corresponding scaling results for $T_i = \infty$, for which θ_0 and θ values (mentioned on the figure) are consistent with previous findings [14]. The value of α that provides the best collapse here is 0.5 . Note that in our earlier work such independence of α from T_i was directly (from the analysis

of ℓ vs t data) checked for this dimension.

3.5 Conclusion

We have presented results for coarsening dynamics in Ising model, with nonconserved order parameter, from space dimensions $d = 2$ and 3 . The results include domain growth law and persistence, for quenches with initial configurations of varying correlation length ξ . While presented results for persistence are mostly related to local order parameter [9–13], for the global case [14, 15] we have obtained new exponent for quench from initial temperature $T_i = T_c$, in $d = 2$. For local persistence, our results are summarized in the next paragraph.

A central objective of this chapter has been to identify the differences in the patterns formed by persistent spins when systems are quenched from $T_i = \infty$ and $T_i = T_c$, to the final temperature $T_f = 0$. For both the cases, corresponding fractal dimensionalities d_f , as well as the exponent z , related to the growth of the persistent pattern, have been obtained in various dimensions. A scaling law connecting d_f , d , z and θ , predicted by Manoj and Ray [17], has been observed to be valid, irrespective of the values of d and T_i . Combining various methods, we quote, for $T_i = \infty$,

$$\begin{aligned} d_f &= 1.53 \pm 0.02, \quad d = 2, \\ d_f &= 2.65 \pm 0.03, \quad d = 3, \end{aligned} \tag{3.23}$$

and for $T_i = T_c$,

$$\begin{aligned}d_f &= 1.92 \pm 0.02, \quad d = 2, \\d_f &= 2.77 \pm 0.02, \quad d = 3.\end{aligned}\tag{3.24}$$

On the standard domain growth problem, it is shown that the values of α in both dimensions for all initial temperatures are consistent with the theoretical expectation $\alpha = 1/2$. This number describes the growth of the persistent pattern as well, validating Eq. (3.15) and confirming that domain growth occurs essentially due to dynamics of spins along the domain boundaries. This resolves a controversy in $d = 3$ for which some previous computer simulations reported $\alpha = 1/3$. As mentioned in Ref. [26], this discrepancy must have been due to lack of data for extended period of time. Long simulations in our work, in addition to resolving this controversy, corrects the value of θ as well in this dimension.

In future we will address similar issues for conserved order parameter dynamics, including aging phenomena. For both conserved and nonconserved dynamics, scaling properties and form of the two-point correlation function will be an important problem for the case of correlated initial configurations.

The materials of the chapter are taken from the following article, with kind permission of American Physical Society (APS): **Saikat Chakraborty** and Subir K. Das, “Fractality in Persistence Decay and Domain Growth

during Ferromagnetic Ordering: Dependence upon initial correlation”, Phys. Rev. E **93**, 032139 (2016).

Bibliography

- [1] A. Onuki, *Phase Transition Dynamics*, Cambridge University Press, Cambridge, UK (2002).
- [2] A. J. Bray, *Adv. Phys.* **51**, 481 (2002).
- [3] R. A. L. Jones, *Soft condensed matter*, Oxford University Press, Oxford, Oxford (2008).
- [4] A. J. Bray, S. N. Majumdar and G. Schehr, *Adv. Phys.* **62**, 225 (2013).
- [5] N. Goldenfeld, *Lecture Notes on Phase Transitions and the Renormalization Group*, Addison-Wesley, Reading, MA (1992).
- [6] D. S. Fisher and D. A. Huse, *Phys. Rev. B* **38**, 373 (1988).
- [7] F. Corberi, E. Lippiello and M. Zannetti, *Phys. Rev. E* **74**, 041106 (2006).
- [8] J. Midya, S. Majumder and S. K. das, *J. Phys. : Condens. Matter* **26**, 452202 (2014).
- [9] S. N. Majumdar, C. Sire, A. J. Bray and S. J. Cornell, *Phys. Rev. Lett.* **77**, 2867 (1996).

-
- [10] S. N. Majumdar, A. J. Bray, S. J. Cornell and C. Sire, Phys. Rev. Lett. **77**, 3704 (1996).
- [11] B. Derrida, V. Hakim and R. Zeitak, Phys. Rev. Lett. **77**, 2871 (1996).
- [12] B. Derrida, Phys. Rev. E **55**, 3705 (1997).
- [13] D. Stauffer, Int. J. Mod. Phys. C **8**, 361 (1997).
- [14] S. Cueille and C. Sire, J. Phys. A: Math and Gen. **30**, L791 (1997).
- [15] S. Cueille and C. sire, European Phys. J. B **7**, 111 (1999).
- [16] G. Manoj and P. ray, Phys. Rev. E **62**, 7755 (2000).
- [17] G. Manoj and P. ray, J. Phys. A: Math and General **33**, 5489 (2000).
- [18] G. Manoj and P. ray, J. Phys. A: Math and General **33**, L109 (2000).
- [19] S. Jain and H. Flynn, J. Phys. A: Math and General **33**, 8383 (2000).
- [20] M. Saharay and P. Sen, Physica A **318**, 243 (2003).
- [21] D. Chakraborty and J. K. Bhattacharjee, Phys. Rev. E **76**, 031117 (2007).
- [22] R. Paul, A. Gambassi and G. Schehr, Europhys. Lett. **78**, 10007 (2007).
- [23] T. Blanchard, L. F. Cugliandolo and M. Picco, J. Stat. Mech. P12021 (2014).
- [24] S. Chakraborty and S. K. Das, European Phys. J. B **88**, 160 (2015).
- [25] A. Gambassi, R. Paul, G. Schehr, J. Stat. Mech P12029 (2010).

-
- [26] F. Corberi, E. Lippiello and M. Zannetti, Phys. Rev. E **78**, 011109 (2008).
- [27] J. G. Amar and F. Family, Bull. Am. Phys. Soc. **34**, 491 (1989).
- [28] J. D. Shore, M. Holzer, and J. P. Sethna, Phys. Rev. B **46**, 11376 (1992).
- [29] C. Dasgupta and R. Pandit, Phys. Rev. B **33**, 4752 (1986).
- [30] K. Humayun and A. J. Bray, J. Phys. A: Math and Gen. **24**, 1915 (1991).
- [31] A. Sicilia, J. A. Arenzon, A. J. Bray and L. F. Cugliandolo, Phys. Rev. E **76**, 061116 (2007).
- [32] D. P. Landau and K. Binder, *A Guide to Monte Carlo Simulations in Statistical Physics*, Cambridge University Press, Cambridge (2009).
- [33] R. J. Glauber, J. Math. Phys. **4**, 294 (1963).
- [34] U. Wolff, Phys. Rev. Lett. **62**, 361 (1989).
- [35] D. A. Huse, Phys. Rev. B **34**, 7845 (1986).
- [36] J. G. Amar, F. E. Sullivan and R. D. Mountain, Phys. Rev. B **37**, 196 (1988).
- [37] S. Majumder and S. K. Das, Phys. Rev. E **81**, 050102 (2010).

Chapter 4

Kinetics of Ferromagnetic Ordering in 3D Ising Model for Zero Temperature Quench

4.1 Introduction

When a paramagnetic system is quenched inside the ferromagnetic region, by a change of the temperature from T_i ($> T_c$) to T_f ($< T_c$), T_c being the critical temperature, it becomes unstable to fluctuations [1–5]. Such an out-of-equilibrium system moves towards the new equilibrium via the formation and growth of domains [1–3]. These domains are rich in atomic magnets aligned in the same direction and grow with time (t) via the curvature driven motion of the interfaces [2, 3, 6]. The interface velocity scales with ℓ , the average domain size, as [2, 6]

$$\frac{d\ell}{dt} \sim \frac{1}{\ell}. \quad (4.1)$$

This provides a power-law growth [2, 6]

$$\ell \sim t^\alpha, \quad (4.2)$$

with $\alpha = 1/2$. Depending upon the order-parameter symmetry and system dimensionality (d), there may exist corrections to this growth law [2].

Apart from the above mentioned change in the characteristic length scale, the domain patterns at different times, during the growth process, are statistically self-similar [2, 3]. This is reflected in the scaling property [2],

$$C(r, t) \equiv \tilde{C}(r/\ell), \quad (4.3)$$

of the two-point equal-time correlation function C , where r ($= |\vec{r}_1 - \vec{r}_2|$) is the scalar distance between two space points and \tilde{C} is a master function, independent of time. A more general correlation function involves two space points and two times, and is defined as [3]

$$C(\vec{r}_1, t_w; \vec{r}_2, t) = \langle \psi(\vec{r}_1, t_w) \psi(\vec{r}_2, t) \rangle - \langle \psi(\vec{r}_1, t_w) \rangle \langle \psi(\vec{r}_2, t) \rangle, \quad (4.4)$$

where ψ is a space and time dependent order parameter. The total value of the order parameter, obtained by integrating ψ over the whole system, is not time invariant for a ferromagnetic ordering [2]. Thus, the coarsening in this case belongs to the category of “nonconserved” order parameter dynamics

[2]. For $\vec{r}_1 = \vec{r}_2$, the definition in Eq. (4.4) corresponds to the two-time autocorrelation function, frequently used for the study of aging properties [3, 7, 8] of an out-of-equilibrium system, $t_w (\leq t)$ being referred to as the waiting time or the age of the system. For the two point equal-time case, on the other hand, $t_w = t$. The autocorrelation will henceforth be denoted as $C_{\text{ag}}(t, t_w)$. This quantity usually scales as [3, 7–12]

$$C_{\text{ag}}(t, t_w) = \tilde{C}_{\text{ag}}(\ell/\ell_w), \quad (4.5)$$

where \tilde{C}_{ag} is another master function, independent of t_w , and ℓ_w is the value of ℓ at t_w . Another interesting quantity, in the context of phase ordering dynamics, is the persistence probability P [13–20]. This is defined as the fraction of unaffected atomic magnets (or spins) and decays in a power-law fashion with time as [13]

$$P \sim t^{-\theta}. \quad (4.6)$$

In the area of nonequilibrium statistical physics, there has been immense interest in estimating the exponents α and θ , as well as in obtaining the functional forms of \tilde{C} and \tilde{C}_{ag} , via analytical theories and computer simulations [2, 3, 13].

In this work, we study all these properties for the nonconserved coarsening dynamics in the Ising model [21],

$$H = -J \sum_{\langle ij \rangle} S_i S_j, \quad J > 0, \quad S_i = \pm 1, \quad (4.7)$$

via Monte Carlo (MC) simulations [21]. We focus on $d = 3$ and study ordering

at $T_f = 0$, for rapid quenches from $T_i = \infty$. This dimension, particularly for $T_f = 0$, received less attention compared to the $d = 2$ case. In $d = 2$, the MC results for $C(r, t)$ are found to be in nice agreement with the Ohta-Jasnow-Kawasaki (OJK) function [2, 3, 22] (D being a diffusion constant)

$$C(r, t) = \frac{2}{\pi} \sin^{-1} \left[\exp \left(-\frac{r^2}{8Dt} \right) \right]. \quad (4.8)$$

This expression also implies $\alpha = 1/2$, validity of which has been separately checked [2, 3]. For the latter dimension ($d = 2$), in the long time limit, the autocorrelation is understood to scale with x ($= \ell/\ell_w$) as [7, 9, 12, 23]

$$C_{\text{ag}}(t, t_w) \sim x^{-\lambda}, \quad (4.9)$$

with λ following a lower bound,

$$\lambda \geq \frac{d}{2}, \quad (4.10)$$

predicted by Fisher and Huse (FH) [7]. In this case, also the persistence exponent θ has been estimated [17, 18, 24, 25] for quenches to $T_f = 0$. Furthermore, a few of these aspects, viz., the equal-time correlation function (for large r) and domain growth, are understood to be independent of the value of T_f .

While the above aspects were studied in $d = 3$ as well, our interest in the zero temperature quench in this dimension was drawn by works [26–29] that reported much slower domain growth than the theoretical expectation.

Here we mention that below and above the roughening transition temperature (T_R), value of which is nonzero [29] ($\simeq 0.57T_c$) in $d = 3$, there exist differences in structural properties [27]. Above T_R interfaces are rounded and the corresponding width (in equilibrium) logarithmically diverges with the system size. Below T_R , on the other hand, the interfaces are flat and the width has no such system-size dependence. Thus, it may be natural to expect that the dynamics will also be different for $T_f < T_R$ and $T_f > T_R$. As stated above, in this work we study structure and dynamics of coarsening for $T_f = 0$ and compare some of these results with those for $T_f = 0.6T_c$ that lies above T_R . Here note that the coarsening dynamics for $T_f > T_R$ is well understood [5].

The ordering dynamics of $d = 3$ Ising model at $T_f = 0$ were studied by other authors as well [30–32]. For $T_f = 0$ sponge-like structure was reported [31, 32] in $d = 3$ and late time behavior, from simulations of small system sizes, of the domain growth was shown [31, 32] to be extraordinarily slow. Our focus here, thus, will be to probe the dynamics over long time without being affected by finite size of the systems. Here we also mention that the zero-temperature late time dynamics of the time dependent Ginzburg-Landau (TDGL) model in this dimension was shown [33] to be consistent with theoretical expectation. Thus, it is important to establish that Ising model is not different. For experimental results in this context, see Ref. [5].

While addressing this issue, via simulations with large system sizes over long period, we made further interesting observations in other quantities. In this chapter, we present these results on pattern, growth, aging and persistence. While our studies for pattern and aging are new, the results for growth

and persistence are presented in forms different from a previous work [34], to bring completeness to the discussion. It appears, previous conclusions on the value of α was led by the presence of an exceptionally long transient period, which was later hinted in Ref. [29]. In the “true” long time limit, the growth exponent is indeed $1/2$. Such a trend we observe in the decay of the persistence probability as well. On the other hand, the pattern and aging properties do not seem to exhibit any crossover. These results are very much different from those obtained for quenches to a temperature above the roughening temperature. Such temperature dependence does not exist in the $d = 2$ case. Wherever necessary we presented results from the latter dimension as well.

The rest of the chapter is organized as follows. In section 4.2 we describe the methods. Results are presented in section 4.3. Finally, we conclude the chapter in section 4.4 by presenting a summary.

4.2 Methods

All our results were obtained via MC simulations of the Ising model using Glauber spin-flip moves [21, 35], where, in each trial move the sign of a randomly chosen spin was changed. Here we use the name Glauber only to emphasize that the trial moves are related to flipping of single spins, to distinguish it from the exchange moves of Kawasaki, involving pairs of spins, that provide conserved order-parameter dynamics [21]. Algorithm for accepting these moves are described below. For $T_f = 0$, a move was accepted if it brought a negative change in the energy. Here note that in the zero

temperature case moves that bring no change in energy are accepted with different probabilities [31, 32], viz., 0, 1/2 and 1, results from which are consistent with each other. In this work we accept such moves with probability 1. On the other hand, for $T_f > 0$, whenever a trial move brought a higher energy contribution, the acceptance was decided by comparing the corresponding Boltzmann factor with a random number (drawn from an uniform distribution), a standard practice followed in the Metropolis algorithm [21]. As stated in Ref. [21], the conclusions should remain same if one uses the Glauber acceptance algorithm instead.

In $d = 2$ we have used square lattice and for $d = 3$ the results are from simple cubic lattice. All simulations were performed in periodic boxes of volume $V = L^d$, L being the linear dimension of a box, in units of the lattice constant. For this model, the d -dependent critical temperatures [21] are $T_c \simeq 2.269J/k_B$ ($d = 2$) and $T_c \simeq 4.51J/k_B$ ($d = 3$), k_B being the Boltzmann constant. Time in our simulations was measured in units of MC step (MCS), each MCS consisting of L^d trial moves [21]. Unless otherwise mentioned, all results are presented after averaging over at least 10 independent initial configurations, with $L = 512$. For the rest of the chapter we set k_B , the lattice constant and the interaction strength (J) to unity.

The average domain size was calculated in two different ways: (i) from the first moment of the domain size distribution $P_d(\ell_d, t)$ as [36]

$$\ell = \int \ell_d P_d(\ell_d, t) d\ell_d, \quad (4.11)$$

ℓ_d being the distance between two successive interfaces along any direction,

and (ii) using the scaling property of the correlation function as [2]

$$C(\ell, t) = 0.1. \quad (4.12)$$

The average domain size can also be calculated from the first moment of the structure factor (to be introduced later) as well as from the excess energy above the ground state [37]. The results from all these methods should be proportional to each other in the dynamical scaling regime. This fact we have checked by working with a number of methods in other works. Unless otherwise mentioned, presented results in this work are from Eq. (4.11). For this purpose, we have eliminated the noise in the configurations at nonzero temperatures, by applying a majority spin rule [36]. Note that the order-parameter ψ here is equivalent to the Ising spin variable S_i . Thus, further discussions on the calculation of the other quantities are not needed since those are clearly understandable from the definitions.

4.3 Results

We start by showing the plots of ℓ vs t , for $d = 2$ and 3, at $T_f = 0$, on a log-log scale, in Fig. 4.1. The system size considered here is comparable to the early studies [26, 27] in $d = 3$. The data for $d = 2$ is clearly consistent with the exponent $\alpha = 1/2$, for the whole time range [2, 3]. On the other hand, after $t = 10$ the $d = 3$ data appear parallel to $\alpha = 1/3$. For accurate estimation of the exponent for a power-law behavior it is useful to calculate

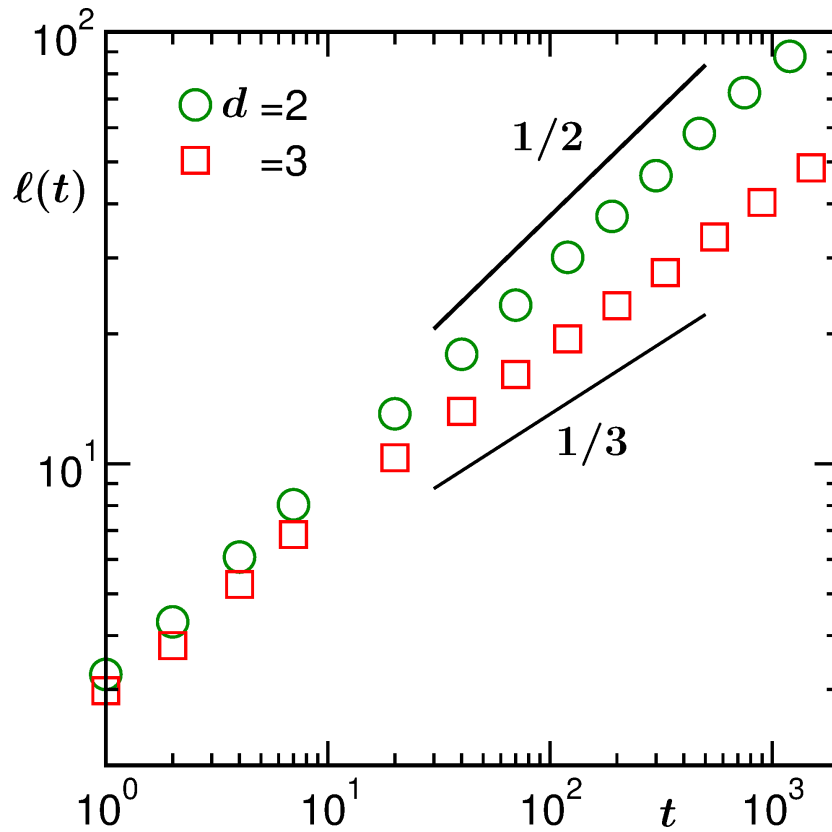


Figure 4.1: Log-log plots of the average domain length, $\ell(t)$, vs time, for $T_f = 0$. Results from both $d = 2$ and 3 are presented. In both the cases linear dimension of the system is $L = 200$. The solid lines correspond to two different power-law growths, exponents being mentioned in the figure.

the instantaneous exponent [38]

$$\alpha_i = \frac{d \ln \ell}{d \ln t}, \quad (4.13)$$

as well as perform finite size scaling (FSS) analysis [21, 39]. In Fig. 4.2 we plot α_i as a function of $1/\ell$. Clearly, for $d = 3$, the convergence of the data set, in the limit $\ell = \infty$, is consistent with $\alpha = 1/3$, while the $d = 2$ data converge to $\alpha = 1/2$. Since the data for large ℓ in this figure are noisy, to

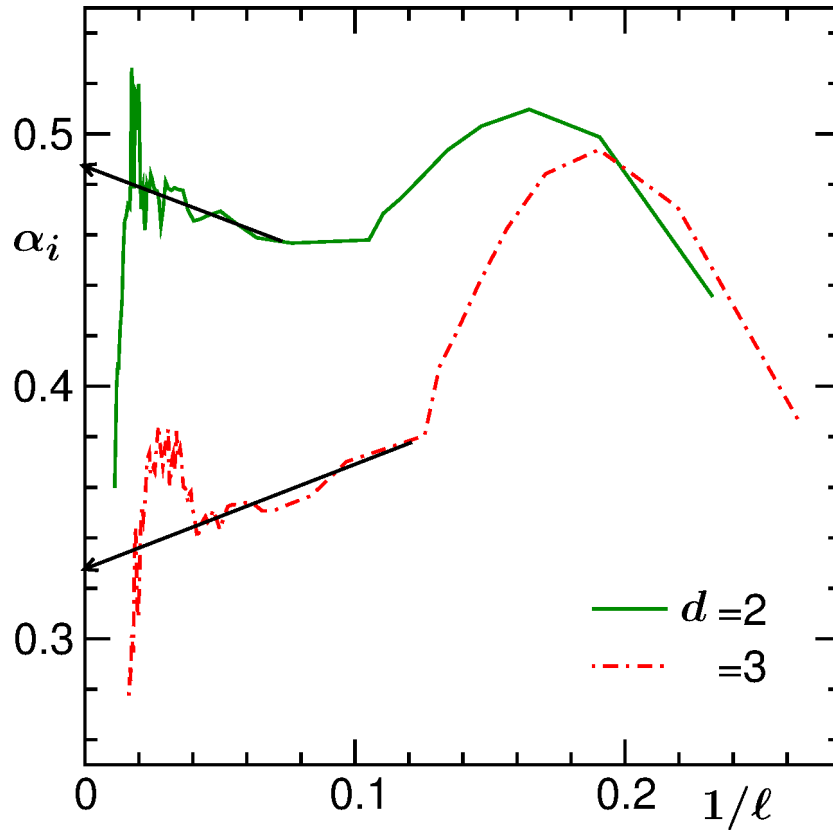


Figure 4.2: Plots of the instantaneous exponent, α_i , vs $1/\ell$, obtained from the data in Fig. 4.1.

understand the stability of the $d = 3$ exponent over long period, we perform the FSS analysis (see Fig. 4.3). We do not perform this exercise for $d = 2$, since, in this case we have already seen that the data are consistent with the theoretical expectation, as established previously [2, 3]. In fact, from here on, unless otherwise mentioned, all results are from $d = 3$ and $T_f = 0$.

In analogy with the critical phenomena [39], a finite-size scaling method in the domain growth problems can be constructed as [36, 40, 41]

$$\ell(t) = LY(y), \quad (4.14)$$

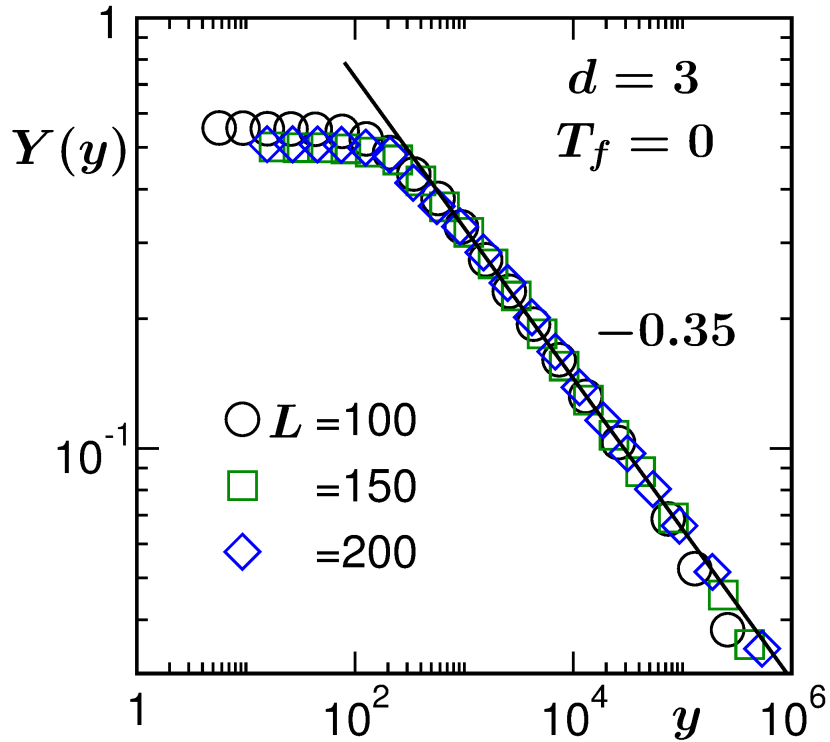


Figure 4.3: Finite-size scaling exercise for the $d = 3$ results for $\ell(t)$. Here we have shown the scaling function Y with the variation of the dimensionless quantity y . Y was obtained from the best collapse of data from three different system sizes (mentioned in the figure). The solid line corresponds to a power law decay with exponent 0.35. These results are from $T_f = 0$.

where the finite-size scaling function Y is independent of the system size but depends upon y ($= L^{1/\alpha}/t$), a dimensionless scaling variable. In the long time limit ($y \rightarrow 0$), when $\ell \simeq L$, Y should be a constant. At early time ($y \gg 0$), on the other hand, the behavior of Y should be such that Eq. (4.2) is recovered (since the finite-size effects in this limit are non-existent). Thus

$$Y(y \gg 0) \sim y^{-\alpha}. \quad (4.15)$$

In the FSS analysis, α is treated as an adjustable parameter. For appropriate

choice of α , in addition to observing the behavior in Eq. (4.15), data from all different values of L should collapse onto a single master curve. In Fig. 4.3 we have used $\alpha = 0.35$. The quality of collapse and the consistency of the power-law decay of the scaling function with the above quoted exponent, over several decades in y , confirm the stability of the value. Thus, it was not inappropriate for the previous studies [26, 27] to conclude that the growth is much slower. Nevertheless, given the increase of computational resources over last two decades, it is instructive to simulate larger systems over longer periods [29], to check if a crossover to the theoretically expected exponent occurs at very late time.

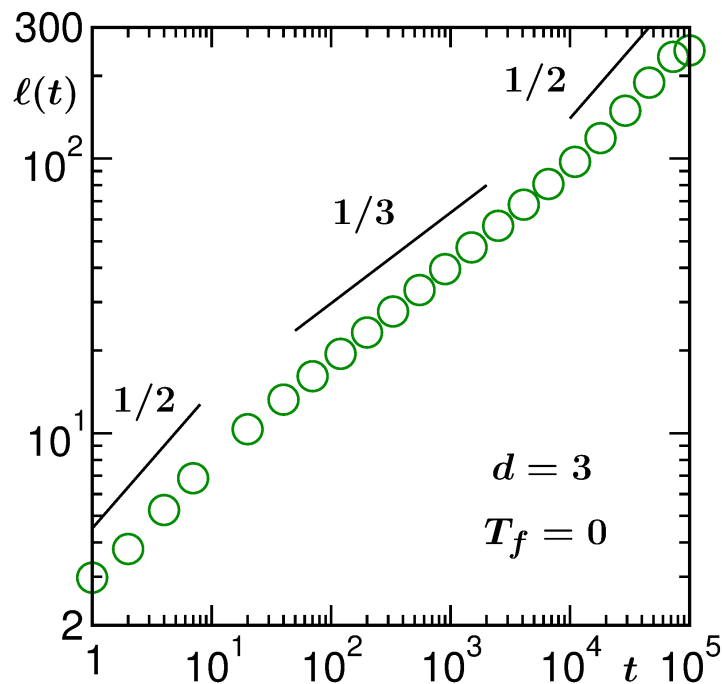


Figure 4.4: Log-log plot of $\ell(t)$ vs t , for $d = 3$ and $T_f = 0$, with $L = 512$. The rest of the results are presented for this particular system size. The solid lines indicate different power-law growths, the exponents being mentioned.

In Fig. 4.4 we present the ℓ vs t data, on a log-log scale, from a much

larger system size [34] than the ones considered in Fig. 4.1 to Fig. 4.3. Interestingly, three different regimes are clearly visible. A very early time regime shows consistency with $\alpha = 1/2$. This is followed by an exponent $1/3$, that stays for about three decades in time. Finally, the expected $\alpha = 1/2$ behavior is visible, for nearly a decade, before the finite size effects appear. In this case, an appropriate FSS analysis, to confirm the later time exponent, requires even bigger systems with runs over much longer times, which, given the resources available to us, was not possible. Thus, for an accurate quantification of the asymptotic value of α , we restrict ourselves to the analysis via the instantaneous exponent [38]. In Fig. 4.5, we have

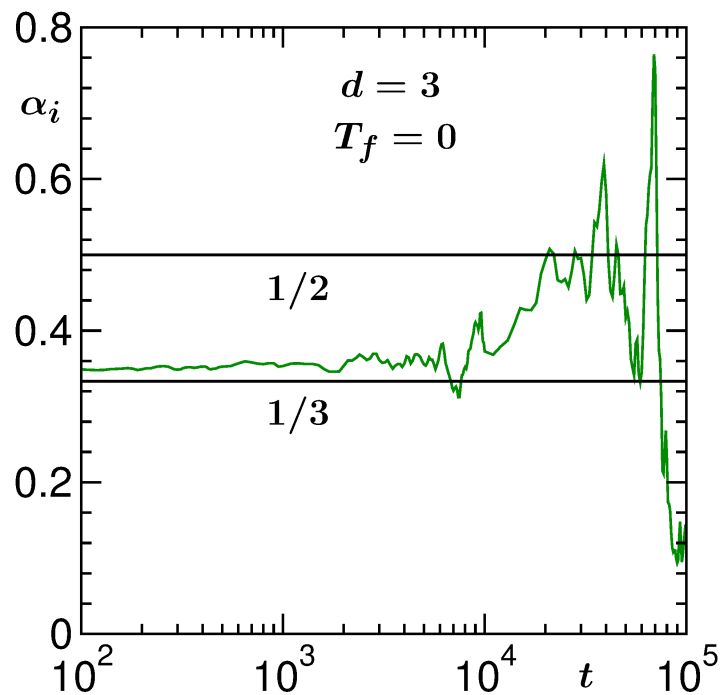


Figure 4.5: Plot of instantaneous exponent α_i as a function of t , the x -axis being in log scale, for the data presented in Fig. 4.4. The horizontal solid lines there correspond to $\alpha = 1/3$ and $1/2$.

plotted α_i as a function of t . The quantity shows a nice late time oscillation around the value $1/2$. This is at variance with the data at high temperature. See the ℓ vs t data, on a log-log scale, from $T_f = 0.6T_c$, in Fig. 4.6. Here we observe $\alpha \simeq 1/2$ for the whole time range. For this data set as well we avoid presenting results from further analyses. We have not been able to understand the multiple scaling regimes in the $T_f = 0$ data. As mentioned above, for $T_f = 0$, similar results [33] with different regimes were observed in the TDGL model as well.

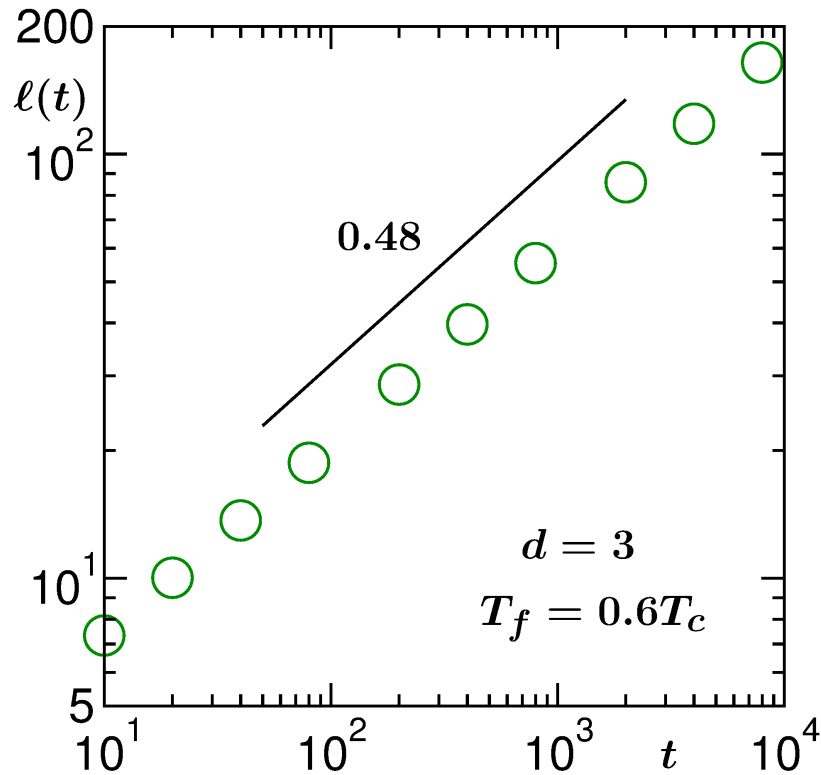


Figure 4.6: Same as Fig. 4.4 but for $T_f = 0.6T_c$. The continuous line there corresponds to a power-law growth with exponent 0.48.

For $T_f = 0$, the crossover that occurs in the time dependence of ℓ , may be present in other properties as well [34]. These we check next. For the

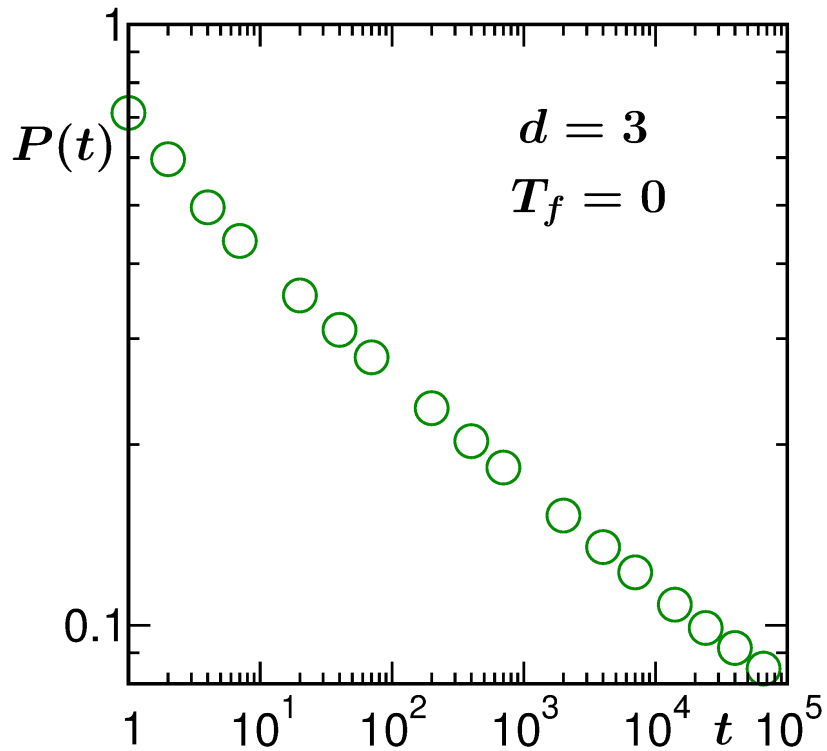


Figure 4.7: Log-log plot of the persistence probability, $P(t)$, as a function of t , for $d = 3$, $T_f = 0$ and $L = 512$.

persistence probability, the value of θ was previously estimated [18], also from smaller system sizes, to be $\simeq 0.17$. In Fig. 4.7 we show a log-log plot of P vs t and the corresponding instantaneous exponent θ_i (see Fig. 4.8), calculated as [38]

$$\theta_i = -\frac{d \ln P}{d \ln t}, \quad (4.16)$$

vs t , for the same (large) system as in Fig. 4.4. The early time data is consistent with the previous estimate. At late time there is a crossover [34] to a smaller value $\simeq 0.15$, the crossover time being the same as that for the average domain size. Here note that, despite improvements [16, 28, 34], the

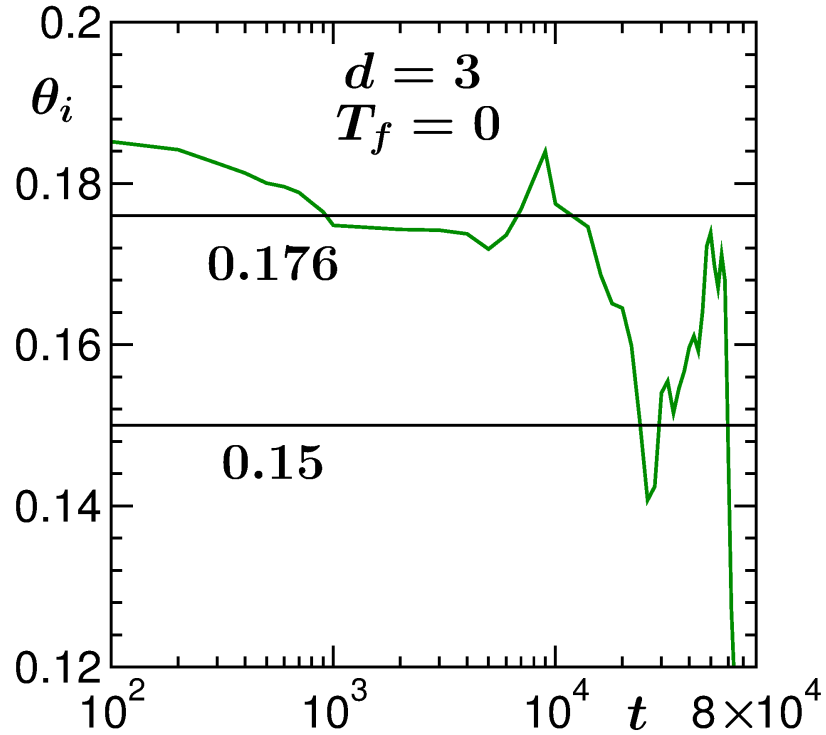


Figure 4.8: Instantaneous exponent, θ_i , vs t , x -axis being in a log scale. The horizontal solid lines there correspond to the ordinate values 0.176 and 0.15.

situation with respect to the calculation of persistence at non-zero temperature may not be problem free, for the reason stated below. Curvature driven coarsening essentially occurs due to flipping of spins in the domain-boundary regions. However, for $T_f > 0$, spins inside the domains also flip. Even though the growth mechanism is same, such microscopic dynamics for $T_f > 0$, due to thermal fluctuation, affects the calculation of P . To overcome the problem, Derrida [16] proposed simulations of ordered systems as references so that the bulk spin-flips can be appropriately discounted. While we have checked that this method works reasonably well for T_f close to 0, at very high temperature calculations may still suffer from errors because of interface broadening

effect. Thus, for this quantity we avoid presenting results from $T_f = 0.6T_c$.

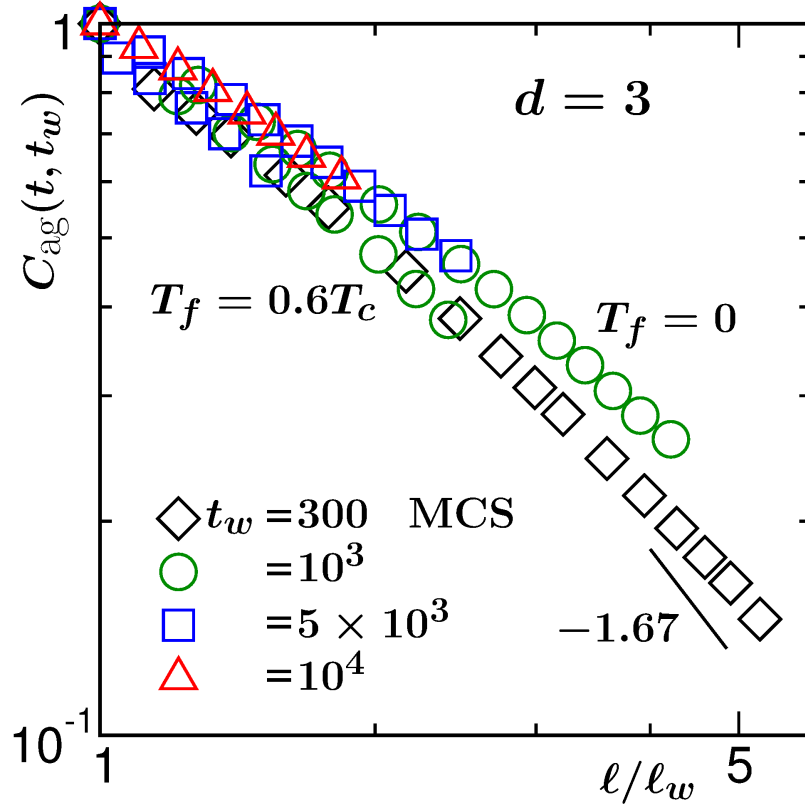


Figure 4.9: Log-log plots of the autocorrelation function, $C_{\text{ag}}(t, t_w)$, vs ℓ/ℓ_w , for $T_f = 0$ and $0.6T_c$. For each value of T_f , results from multiple ages are presented. The solid line corresponds to a power-law decay, exponent for which is mentioned on the figure.

In Fig. 4.9 we show the plots of $C_{\text{ag}}(t, t_w)$, vs ℓ/ℓ_w , from $T_f = 0$ and $0.6T_c$, on a log-log scale, for different values of t_w . Good collapse of data, for both the values of T_f , are visible over the whole range of the abscissa variable. This, in addition to establishing the scaling property of Eq. (4.5), implies the absence of the finite-size effects [23,42]. On the issue of the finite size effects for the nonconserved Ising model, a previous study [23] showed that such effects become important only for $\ell > 0.4L$. The length of our

simulations were set in such a way that we are on the edge of this limit. For $T_f = 0$, this can be appreciated from the ℓ vs t data in Fig. 4.4. Here note that for conserved Ising model the finite-size effects start appearing when ℓ is approximately 3/4th of the equilibrium domain size limit [36]. Thus, the effects are rather strong here and this fact is consistent with the late time dynamics reported elsewhere [31, 32].

From a Gaussian auxiliary field ansatz, in the context of the time dependent Ginzburg-Landau model [2], Liu and Mazenko (LM) [9] constructed a dynamical equation for $C(\vec{r}_1, t_w; \vec{r}_2, t)$. For $t \gg t_w$, from the solution of this equation, they obtained (see Eq. (4.9)) $\lambda \simeq 1.67$ in $d = 3$. The solid line in Fig. 4.9 represents a power-law decay with the above mentioned value of the exponent. The simulation data, for both values of T_f , appear inconsistent with this exponent. Rather, the simulation results on the log-log scale exhibit continuous bending. Such bending may be due to the presence of correction to the power law decay at small values of x . Thus, more appropriate analysis is needed to understand these results.

In Fig. 4.10 we plot the instantaneous exponent [9, 23, 38]

$$\lambda_i = -\frac{d \ln C_{\text{ag}}}{d \ln x}, \quad x = \frac{\ell}{\ell_w}, \quad (4.17)$$

as a function of $1/x$, for $T_f = 0.6T_c$. A linear behavior is visible, extrapolation of which, to $x = \infty$, leads to $\lambda \simeq 1.63$. The latter number follows the FH bound [7] (see Eq. 4.10)) and is in good agreement with the theoretical prediction of LM [9]. Inserting the linear trend of λ_i in its definition (Eq.

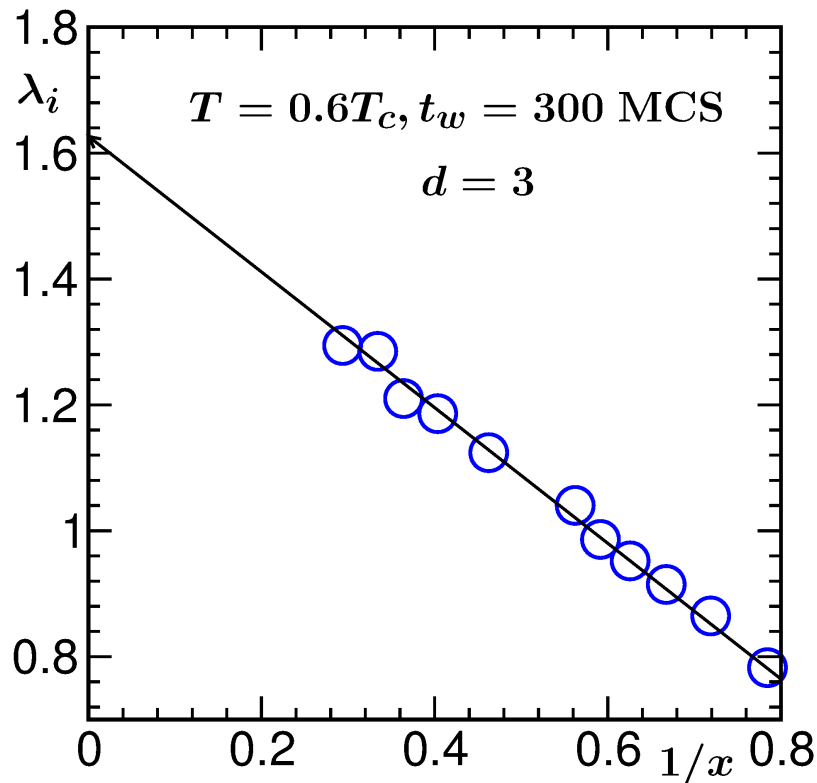


Figure 4.10: Plot of the instantaneous exponent, λ_i , vs $1/x$, for $T_f = 0.6T_c$, with $t_w = 300 \text{ MCS}$. The solid line is a guide to the eyes.

(4.17)), one obtains a full form for the autocorrelation function to be [23]

$$C_{\text{ag}} = C_0 \exp\left(-\frac{B}{x}\right) x^{-\lambda}, \quad (4.18)$$

where C_0 and B are constants. This empirical form was obtained by keeping in mind its usefulness in estimation of an accurate value for λ via finite-size scaling analysis. In fact, such an analysis [23] provided a value 1.66 ± 0.03 which, though closer to the LM one, is slightly higher than a previous estimate [43]. Here note that there already exists [12] a full form, derived from the local scale invariance, for the decay of C_{ag} during coarsening in

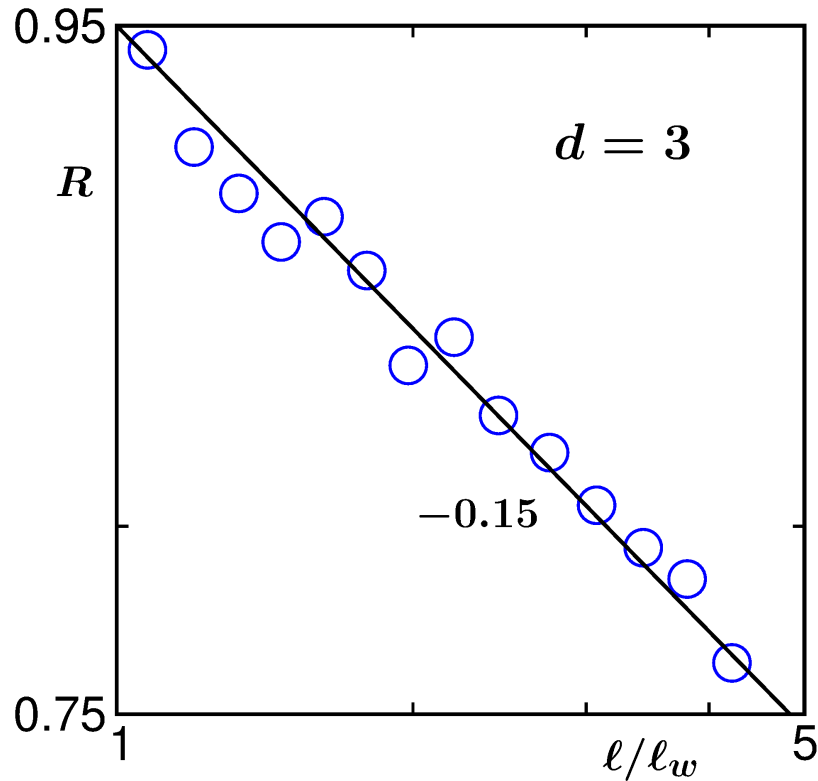


Figure 4.11: Log-log plot of the ratio, R , between the master curves for the autocorrelations at $T_f = 0.6T_c$ and 0, as a function of x .

the ferromagnetic Ising model. Validity of this has been demonstrated in studies [44] of q (> 2)-state Potts model. The accuracy of our expression can be justified by comparing it with the latter. However, even though derived from a rigorous theoretical method, this expression contains a large number of unknowns which are not easy to estimate via fitting of the simulation data. In $d = 2$, for which the values of the unknowns were provided by the authors, we have checked that our equation is a reasonable approximation to this.

The decay of C_{ag} , as seen in Fig. 4.9, for $T_f = 0$ appears slower than that for $T_f = 0.6T_c$. To confirm that, in Fig. 4.11 we plot the ratio R , between C_{ag} for $T_f = 0.6T_c$ and $T_f = 0$, on a log-log scale, vs x . Over the whole range

of x , that covers pre- as well as post-crossover regimes for domain growth, the data exhibit power-law behavior that can be captured by a single exponent $\simeq 0.15$. This implies an absence of crossover in the decay of this quantity and $\lambda \simeq 1.5$, a number significantly smaller than that for $T_f = 0.6T_c$. Irrespective of whether the FH lower bound has actually been violated or not, such small value of λ , compared to the $T_f = 0.6T_c$ case, is an interesting observation which calls for further discussion and calculation of the structural properties. Yeung, Rao and Desai (YRD) made a more general prediction of the lower bound [11], viz.,

$$\lambda \geq \frac{d + \beta}{2}, \quad (4.19)$$

where β is the exponent [45, 46] for the small wave-number (k) power-law enhancement of the structure factor (the Fourier transform of $C(r, t)$):

$$S(k) \sim k^\beta. \quad (4.20)$$

Here note that $S(k, t)$ has the scaling form (for a self-similar pattern) [2]

$$S(k, t) \equiv \ell^d \tilde{S}(k\ell), \quad (4.21)$$

where \tilde{S} is a time independent master function. We call Eq. (4.19) a more general lower bound because of the fact that this was derived by keeping both conserved and nonconserved order-parameter dynamics in mind. For nonconserved order parameter [11], as in the present case, $\beta = 0$. Thus the YRD lower bound in this case is same as the FH lower bound. Also note here that originally the FH bound was predicted from the studies of spin-glass

systems which later was found to be relevant in coarsening systems like the one considered here, as also was hinted by these authors. The YRD result, on the other hand, was derived by focusing on coarsening in ferromagnets and multicomponent mixtures. The FH bound can as well be appreciated

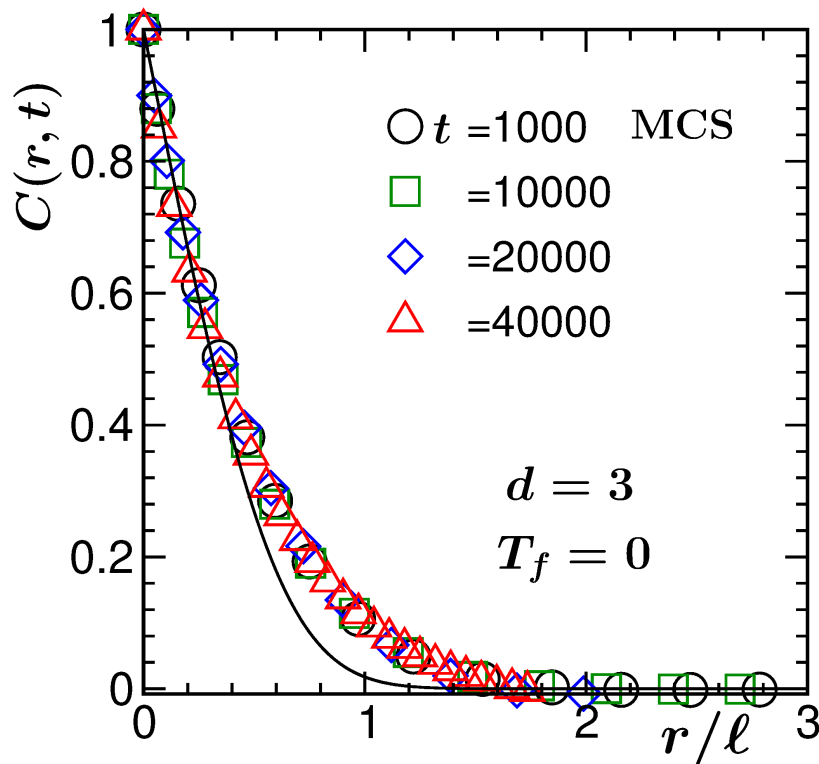


Figure 4.12: Scaling plot of the two-point equal time correlation functions from $T_f = 0$ and $d = 3$. The distance along the abscissa has been scaled by the average domain sizes at different times from which data are presented. The solid curve corresponds to the OJK form (see Eq. (4.8)).

from the OJK expression for the general correlation function [3, 22] of Eq. (4.4). This has the form

$$C(r; t, t_w) = \frac{2}{\pi} \sin^{-1} \gamma, \quad (4.22)$$

with

$$\gamma = \left(\frac{2\sqrt{tt_w}}{t+t_w} \right)^{d/2} \exp \left[- \frac{r^2}{4D(t+t_w)} \right]. \quad (4.23)$$

For $t = t_w$, this leads to Eq. (4.8). For $r = 0$ and $t \gg t_w$, Eq. (4.23) provides

$$C_{\text{ag}}(t, t_w) \sim \left(\frac{t}{t_w} \right)^{-d/4}. \quad (4.24)$$

For $\alpha = 1/2$, the exponent in Eq. (4.24) provides $\lambda = d/2$, which coincides with the FH lower bound. Since the latter bound is embedded in Eq. (4.22)

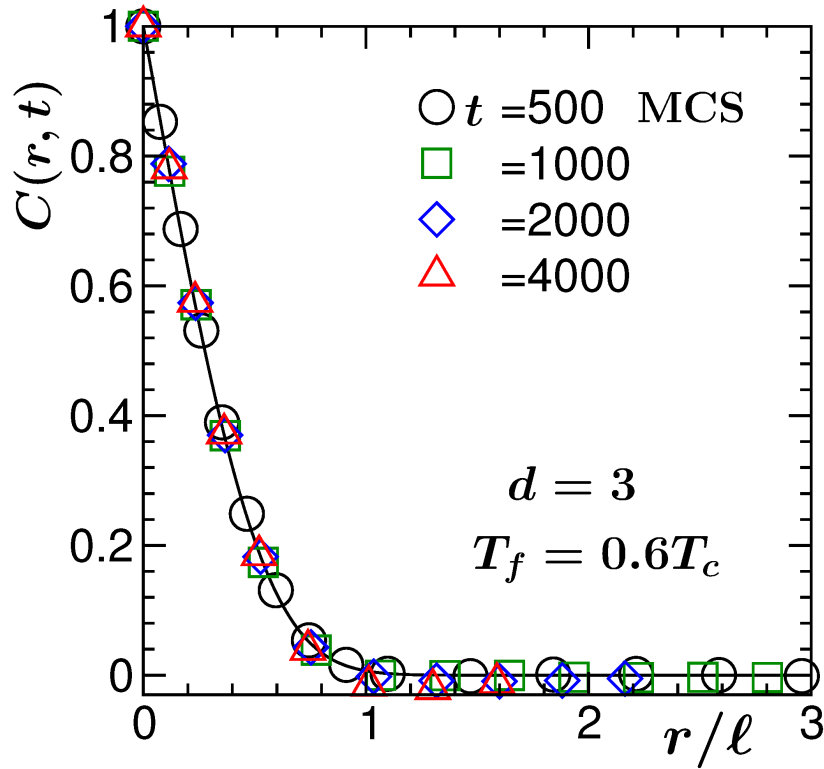


Figure 4.13: Same as Fig. 4.12, but for $T_f = 0.6T_c$. The solid curve there represents the OJK form (see Eq. (4.8)).

and the violation of it for $T_f = 0$ is a possibility, it is instructive to calculate the structural quantities, viz., $C(r, t)$ and $S(k, t)$, given that Eq. (4.22)

contains expressions for the latter quantities as well.

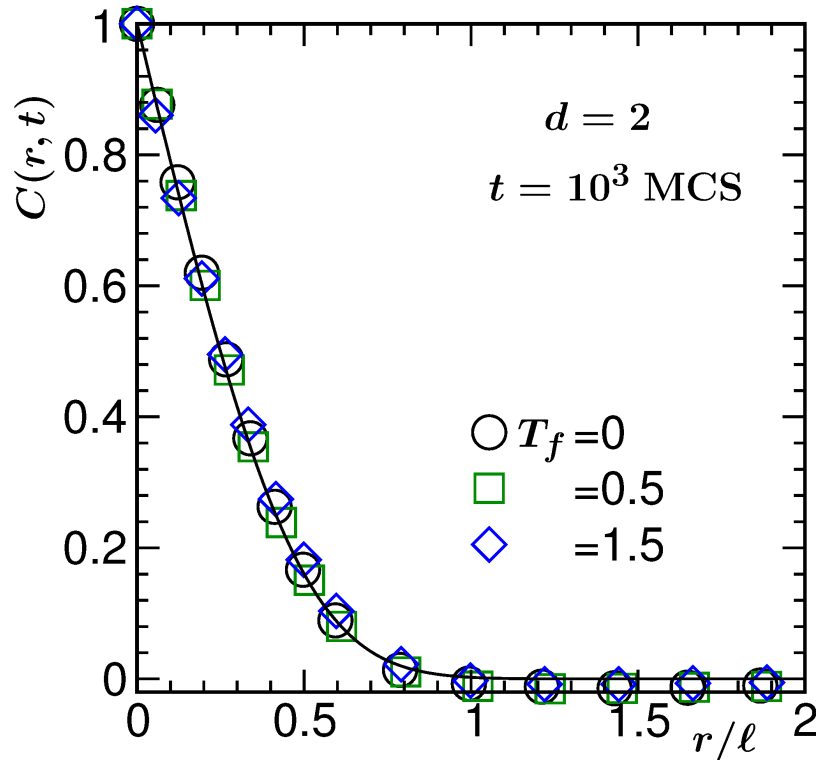


Figure 4.14: Scaled correlation functions from different T_f in $d = 2$. The continuous curve is the the OJK function of Eq. (4.8).

In Fig. 4.12 we show a scaling plot of $C(r, t)$, vs r/ℓ , for $T_f = 0$, ℓ being extracted from Eq. (4.12). Nice collapse is visible for data from wide time range. Given that no crossover in $C(r, t)$ is observed and aging property is strongly related to the structure, it is understandable why a crossover in the autocorrelation is nonexistent. The continuous line in this figure is the OJK function [2, 3, 22] of Eq. (4.8). There exists significant discrepancy between the analytical function and the simulation results. This is expected, given the sponge-like structure [31, 32] observed for $T_f = 0$. In Fig. 4.13 of this figure we plot the corresponding results for $T = 0.6T_c$ which, on the other

hand, shows nice agreement with Eq. (4.8). Here note that in $d = 2$ such temperature dependence does not exist [3]. For the sake of completeness, this we have demonstrated in Fig. 4.14. Data from all the temperatures in this case are nicely described by the OJK function.

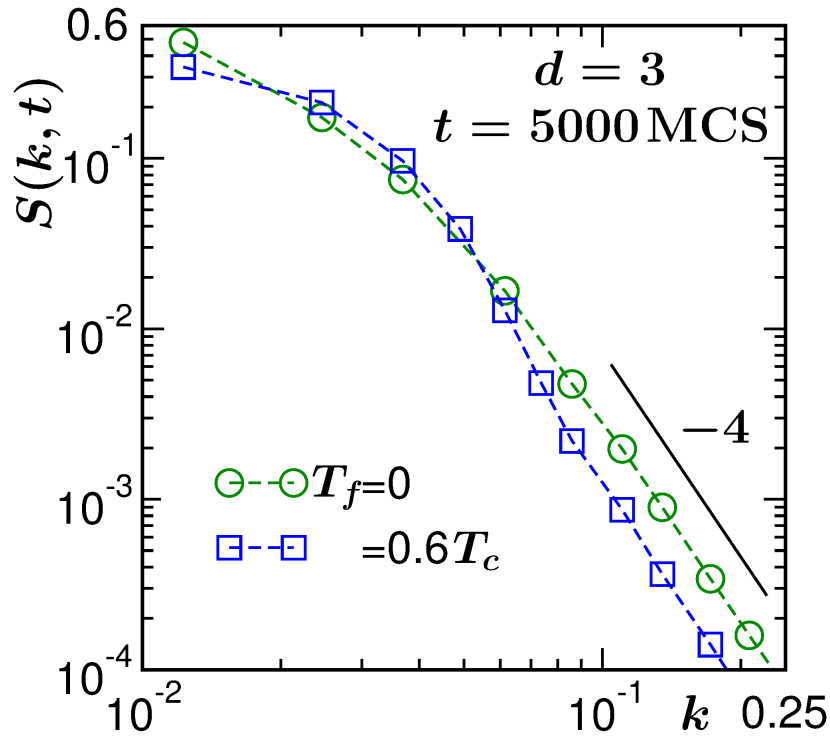


Figure 4.15: Plots of the structure factors, from $T_f = 0$ and $0.6T_c$, vs k . The solid line represents the Porod law. For both the temperatures, we have presented results from $t = 5000$. These results are from $d = 3$.

In Fig. 4.15 we show a comparison between the structure factors from $T_f = 0$ and $T_f = 0.6T_c$, in $d = 3$. The k^{-4} line in this figure corresponds to the Porod law [2, 3, 47] for the long wave-number decay of $S(k, t)$, a consequence of scattering at sharp interfaces like facets at $T_f = 0$. Data from both the temperatures show reasonable consistency with this decay, even in intermediate range of k . For the sake of bringing clarity in the small k region,

we did not present the results for the whole range of k . In the smaller wave-number region, disagreement between the slopes in the two cases is visible. This may provide explanation for the small value of λ for $T_f = 0$. For this purpose, below we provide a discussion on the derivation of YRD. Starting from the equal-time structure factors at t_w and t , YRD arrived at [11]

$$C_{\text{ag}}(t, t_w) \leq \ell^{d/2} \int_0^{2\pi/\ell} dk k^{d-1} [S(k, t_w) \tilde{S}(k\ell)]^{1/2}. \quad (4.25)$$

To obtain the lower bound, they used the small k form for $S(k, t_w)$, as quoted in Eq. (4.20). In Fig. 4.15 we see that, compared to $T_f = 0.6T_c$, the structure factor for $T_f = 0$ starts decaying at a smaller value of k , providing an effective negative value for β . The statement on the negative value of β can be further appreciated from the fact that the upper limit of integration in Eq. (4.25) is higher for $T_f = 0$ given that average domain size in this case is smaller. This is the reason for such a small value of λ . In future, we intend to calculate λ more accurately for $T_f = 0$.

Given that $T_f = 0.6T_c$ lies above the roughening transition temperature, possibility exists [29] that the observed differences between kinetics at the two different values of T_f may be related to this transition [48]. Here note that the results for $T_f = 0.6T_c$ are in agreement with our preliminary results for even higher values of T_f . Systematic studies, however, are needed below T_R to rule out that these are not zero-temperature properties, thereby confirming the above mentioned possibility. We mention here, most of the previous studies with nonconserved Ising model focused on $d = 2$, for which there is no non-zero T_R . Furthermore, question remains, why the crossovers, exhibited by the

growth of domains and the decay of persistence, are missing in the structure and aging? This fact, e.g. for aging, may have similarity with outcomes from some studies in upper critical dimension. If t and t_w are chosen to be very large, it will be difficult to identify any correction that appears only additively to the leading order scaling form [49, 50].

Even though the focus of the chapter is on the coarsening dynamics at $T_f = 0$, we would like to further discuss the results for $T_f > 0$. We restate the fact that for nonzero temperature $C(r, t)$ and $\ell(t)$ were calculated after eliminating the thermal noise from the original configurations via a majority spin rule. This exercise essentially makes the interfaces sharp and provides “pure” domain structure in the bulk, facilitating appropriate identification of the domain length by washing out fluctuations at the scale of equilibrium correlation length. Almost perfect match of the OJK function of Eq. (4.8) with the simulation data is because of this reason. If the noise is not eliminated, there will be discrepancy in the small r region, reason for deviation from the Porod law in large k limit. This was pointed out by Oono and Puri [51]. The corresponding modified form [4, 5, 51] of $C(r, t)$ contains a factor $(1 + a\omega^2/t)^{-1}$, appearing in front of the exponential in Eq. (4.8), where a is a constant and ω is the interface width. Given that there now exist multiple unknowns, extraction of $\ell(t)$, as well as ω , via fitting of the simulation data (obtained from original configurations) to this modified form, is less reliable. Our noise elimination exercise is performed by keeping such problem in mind. However, the values of $\ell(t)$, obtained from such noise-free configurations, contain ω as well. One important question can now be asked: whether the true domain size should include ω or not. If the answer is in

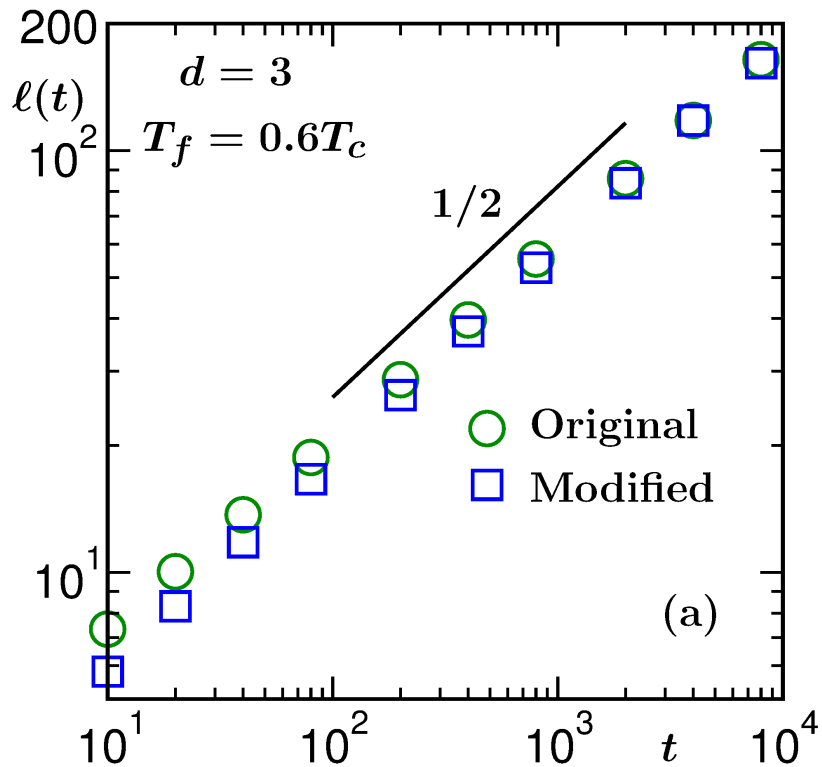


Figure 4.16: Log-log plots of ℓ vs t , with (modified) and without (original) subtracting the interface width ($\omega(t)$) from $\ell(t)$. The solid line represents a power-law with $\alpha = 1/2$.

affirmative, all our analyses and conclusions are correct. Otherwise, ω should be appropriately subtracted. Abraham and Upton [52] pointed out that in $d = 3$, above the roughening transition, $\omega \sim (\ln t)^{1/2}$. Further analyses for $T_f = 0.6T_c$ (in $d = 3$) have been performed by subtracting such logarithmic time dependence of ω from $\ell(t)$. This way, compared to Fig. 4.6, the early time log-log data for ℓ vs t appear more consistent with the exponent $\alpha = 1/2$. Such an exercise, however, does not alter our conclusion on the late time behavior. This is expected, since the (weak) correction is additive. Similar fact we observe in the aging exponent λ . These results are presented

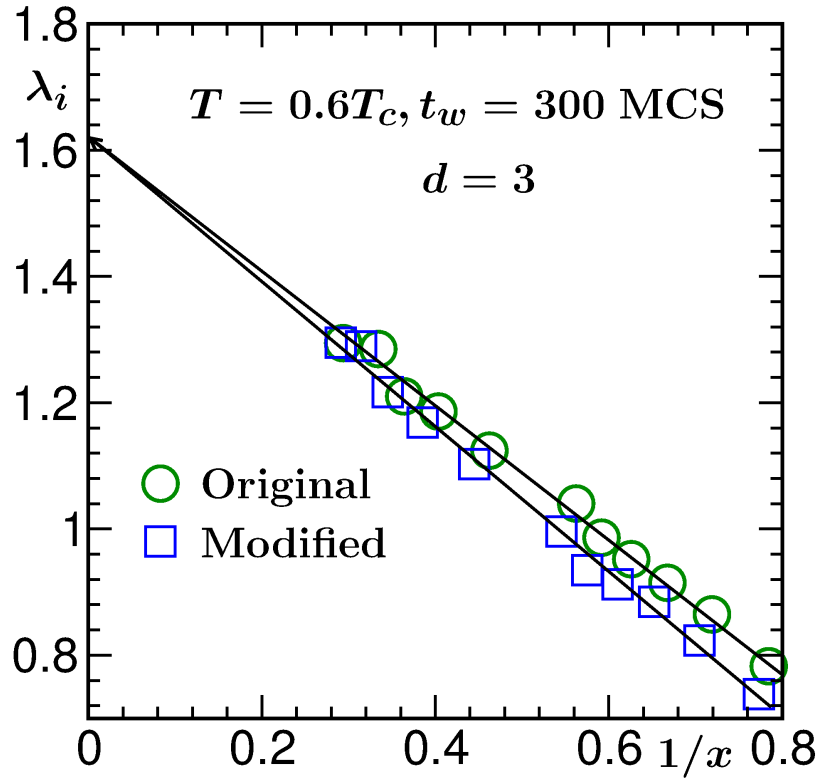


Figure 4.17: Plots of λ_i vs $1/x$ ($x = \ell/\ell_w$) with and without subtracting $\omega(t)$ from ℓ and ℓ_w . The solid lines are guides to the eye. All results correspond to $d = 3$ and $T_f = 0.6T_c$.

in Fig. 4.16 and Fig. 4.17 where the first figure contains the data for domain growth and results for λ_i are shown in the latter. In both the cases we have shown comparative pictures between the original and modified analyses. Of course, $T_f = 0$ results do not require any such exercise.

4.4 Conclusion

We have studied kinetics of phase transition in $3D$ non-conserved Ising model via the Monte Carlo simulations [21], following quench from $T_i = \infty$

to $T_f = 0$. Results are presented for domain growth, persistence probability, aging and pattern, all of which exhibit new features, compared to studies in $d = 2$ and quenches to higher temperature for $d = 3$. The time dependence of the average domain size shows consistency with the expected theoretical behavior only after an exceptionally long transient period [29, 34]. This is reflected in the persistence probability [34]. However, no such transient was observed for quenches to a temperature above the roughening transition.

The two-point equal time correlation function does not follow the Ohta-Jasnow-Kawasaki form [22], derived for the nonconserved order-parameter dynamics with scalar order parameter. The latter form, however, is found to be consistent with the simulation data above the roughening transition temperature. Unlike the domain growth and persistence, we did not observe any time dependence (crossover) for this observable. This is reflected in the decay of the autocorrelation function. The latter quantity, at $T_f = 0$, appears to have a power-law decay exponent marginally satisfying the Fisher-Huse lower bound. These results are at deviation with those from $d = 2$ for which there is no non-zero roughening transition.

It will be important to understand the temperature dependence in all these quantities via more systematic studies. This may as well provide improvements in the inputs for the derivation of the OJK function. Furthermore, the reason for long transient in domain growth and persistence deserves attention. These we aim to address in future works.

The materials of the chapter are taken from the following article, to be published in *Eur. Phys. J. Spec. Top.*, with kind permission of The European Physical Journal (EPJ): Subir K. Das and **Saikat Chakraborty**, “Kinetics of Ferromagnetic Ordering in 3D Ising Model: How far do we understand the case of zero temperature quench?”

Bibliography

- [1] A. Onuki, *Phase Transition Dynamics*, Cambridge University Press, Cambridge, UK (2002).
- [2] A.J. Bray, *Adv. Phys.* **51**, 481 (2002).
- [3] S. Puri and V. Wadhawan (ed.), *Kinetics of Phase Transitions* (Boca Raton: CRC Press, 2009).
- [4] S. Dattagupta and S. Puri, *Dissipative Phenomena in Condensed Matter: Some Applications* (Springer-Verlag, Heidelberg, 2004).
- [5] M. Henkel and M. Pleimling, *Non-equilibrium Phase Transitions*, Vol. 2 (Springer, Netherlands, 2010).
- [6] S.M. Allen and J.W. Cahn, *Acta Metall.* **27**, 1085 (1979).
- [7] D.S. Fisher and D.A. Huse, *Phys. Rev. B* **38**, 373 (1988).
- [8] F. Corberi, E. Lippiello and M. Zannetti, *Phys. Rev. E* **74**, 041106 (2006).
- [9] F. Liu and G.F. Mazenko, *Phys. Rev. B* **44**, 9185 (1991).
- [10] S.N. Majumdar and D.A. Huse, *Phys. Rev. E* **52**, 270 (1995).

-
- [11] C. Yeung, M. Rao and R.C. Desai, Phys. Rev. E **53**, 3073 (1996).
- [12] M. Henkel, A. Picone and M. Pleimling, Europhys. Lett. **68**,191 (2004).
- [13] A.J. Bray, S.N. Majumdar and G. Schehr, Adv. Phys. **62**, 225 (2013).
- [14] S.N. Majumdar, C. Sire, A.J. Bray and S.J. Cornell, Phys. Rev. Lett. **77**, 2867 (1996).
- [15] S.N. Majumdar, A.J. Bray, S.J. Cornell and C. Sire, Phys. Rev. Lett. **77**, 3704 (1996).
- [16] B. Derrida, Phys. Rev. E **55**, 3705 (1997).
- [17] D. Stauffer, Int. J. Mod. Phys. C **8**, 361 (1997).
- [18] G. Manoj and P. Ray, Phys. Rev. E **62**, 7755 (2000).
- [19] B. Derrida, A.J. Bray and C. Godrèche, J. Phys. A **27**, L357 (1994).
- [20] D. Stauffer, J. Phys. A **27**, 5029 (1994).
- [21] D.P. Landau and K. Binder, *A Guide to Monte Carlo Simulations in Statistical Physics*, Cambridge University Press, Cambridge (2009).
- [22] T. Ohta, D. Jasnow and K. Kawasaki, Phys. Rev. Lett. **49**, 1223 (1982).
- [23] J. Midya, S. Majumder and S.K. Das, J. Phys. : Condens. Matter **26**, 452202 (2014).
- [24] T. Blanchard, L.F. Cugliandolo and M. Picco, J. Stat. Mech. P12021 (2014).

-
- [25] S. Chakraborty and S.K. Das, European Phys. J. B **88**, 160 (2015).
- [26] J.G. Amar and F. Family, Bull. Am. Phys. Soc. **34**, 491 (1989).
- [27] J.D. Shore, M. Holzer, and J.P. Sethna, Phys. Rev. B **46**, 11376 (1992).
- [28] S. Cueille and C. Sire, J. Phys. A **30**, L791 (1997).
- [29] F. Corberi, E. Lippiello and M. Zannetti, Phys. Rev. E **78**, 011109 (2008).
- [30] V. Spirin, P. L. Krapivsky, and S. Redner, Phys. Rev. E **63**, 036118 (2001); **65**, 016119 (2001).
- [31] J. Olejarz, P. L. Krapivsky, and S. Redner, Phys. Rev. E **83**, 051104 (2011).
- [32] J. Olejarz, P. L. Krapivsky, and S. Redner, Phys. Rev. E **83**, 030104(R) (2011).
- [33] G. Brown and P.A. Rikvold, Phys. Rev. E **65**, 036137 (2002).
- [34] S. Chakraborty and S.K. Das, Phys. Rev. E **93**, 032139 (2016).
- [35] R.J. Glauber, J. Math. Phys. **4**, 294 (1963).
- [36] S. Majumder and S.K. Das, Phys. Rev. E **81**, 050102 (2010).
- [37] F. Corberi, M. Zannetti, E. Lippiello and A. Vezzani, arXiv:1506.01199 (2015).
- [38] D.A. Huse, Phys. Rev. B, **34**, 7845 (1986).

-
- [39] M.E. Fisher, in *Critical Phenomena*, edited by M.S. Green (Academic, London, 1971).
- [40] D.W. Heermann, L. Yixue and K. Binder, *Physica A* **230**, 132 (1996).
- [41] S.K. Das, S. Roy, S. Majumder and S. Ahmad, *EPL* **97**, 66006 (2012).
- [42] J. Midya, S. Majumder and S.K. das, *Phys. Rev. E* **92**, 022124 (2015).
- [43] M. Henkel and M. Pleimling, *Phys. Rev. E* **68**, 065101 (R) (2003).
- [44] E. Lorenz and W. Janke, *EPL* **77**, 10003 (2007).
- [45] C. Yeung, *Phys. Rev. Lett.* **61**, 1135 (1988).
- [46] S.N. Majumdar, D.A. Huse and B.D. Lubachevsky, *Phys. Rev. Lett.* **73**, 182 (1994).
- [47] G. Porod, in *Small-Angle X-ray scattering*, edited by O. Glatter and O. Kratky, Academic press, New York, 42 (1982).
- [48] H. van Beijeren and I. Nolden, in *Structures and Dynamics of Surfaces II: Phenomena, Models and Methods, Topics in Current Physics vol. 43*, edited by W. Schommers and P. von Blanckenhagen (Berlin: Springer, 1987).
- [49] M.O. Hase and S.R. Salinas, *J. Phys.: Math. Gen.* **39**, 4875 (2006).
- [50] M. Ebbinghaus, H. Grandclaude and M. Henkel, *European Phys. J. B* **63**, 85 (2008).
- [51] Y. Oono and S. Puri, *Mod. Phys. Lett. B* **2**, 861 (1988).

- [52] D.B. Abraham and P.J. Upton, Phys. Rev. B **39**, 736 (1989).

Chapter 5

Aging during Coarsening in Ferromagnetic Ising Model for Zero Temperature Quench

5.1 Introduction

Following quench from a homogeneous configuration to a state inside the coexistence curve, as a system evolves towards the new equilibrium, various correlation functions exhibit interesting scaling properties [1–10]. A rather general correlation function involves two space points (\vec{r}_1, \vec{r}_2) and two times (t, t_w) , and has the definition [2]

$$C_{22}(\vec{r}_1, \vec{r}_2; t, t_w) = \langle \psi(\vec{r}_1, t) \psi(\vec{r}_2, t_w) \rangle - \langle \psi(\vec{r}_1, t) \rangle \langle \psi(\vec{r}_2, t_w) \rangle. \quad (5.1)$$

Here ψ is a space and time dependent order-parameter field. For isotropic structures, which we assume to be true for the cases addressed in this chapter, the space dependence in C_{22} comes through $r = |\vec{r}_1 - \vec{r}_2|$, the scalar distance between \vec{r}_1 and \vec{r}_2 . For $t = t_w$, C_{22} is referred to as the two point equal time correlation function [1, 2], to be denoted by $C(r, t)$. On the other hand, for $\vec{r}_1 = \vec{r}_2$, C_{22} is referred to as the two-time autocorrelation function [2]. The latter quantity, to be represented by $C_{\text{ag}}(t, t_w)$, is often used for studying aging in nonequilibrium systems [2, 3], where t_w ($< t$) is referred to as the age of the system.

The two point equal time correlation function follows the scaling behavior [1, 2, 9]

$$C(r, t) \equiv \tilde{C}(r/\ell(t)), \quad (5.2)$$

where \tilde{C} is a time independent master function [1] and ℓ is the average length of domains, rich or poor in particles or spins of particular type. Typically, ℓ grows as a power-law [1] with exponent α ($\ell \sim t^\alpha$). The scaling property in Eq. (5.2) implies that the structures at two different times differ from each other only by a change in length scale [1]. On the other hand, $C_{\text{ag}}(t, t_w)$, in many situations, exhibits the scaling form [2–4, 6–8, 10–12]

$$C_{\text{ag}}(t, t_w) \equiv \tilde{C}_{\text{ag}}(x); \quad x = \ell/\ell_w, \quad (5.3)$$

where ℓ_w is the characteristic length scale of the system at time t_w .

There has been serious interest in understanding the forms of these correlation functions for coarsening dynamics with and without conservation [1,2] of the total value of the order parameter ($= \int_V d^3\vec{r}\psi(\vec{r}, t)$, V being the system volume). Remarkable progress has been made with respect to the nonconserved order-parameter case [1, 2]. Most of these studies are related to the coarsening in ferromagnetic Ising model [1, 2] ($\langle ij \rangle$ stands for nearest neighbors)

$$H = -J \sum_{\langle ij \rangle} S_i S_j, \quad S_i = \pm 1, \quad J > 0, \quad (5.4)$$

or the time dependent Ginzburg-Landau (TDGL) model [1, 2], a coarse grained version of the kinetic Ising model.

Ohta, Jasnow and Kawasaki (OJK) [9], via a Gaussian approximation of an auxiliary field [1, 2, 9], obtained an expression for C_{22} that reads

$$C_{22}(r; t, t_w) = \frac{2}{\pi} \sin^{-1} \gamma, \quad (5.5)$$

where

$$\gamma = \left(\frac{2\sqrt{tt_w}}{t + t_w} \right)^{d/2} \exp \left[\frac{-r^2}{4D(t + t_w)} \right], \quad (5.6)$$

d being the system dimension and D a diffusion constant. For $t = t_w$, from Eqs. (5.5) and (5.6) one obtains

$$C(r, t) = \frac{2}{\pi} \sin^{-1} \left[\exp \left(\frac{-r^2}{8Dt} \right) \right]. \quad (5.7)$$

On the other hand, for $r = 0$ and $t \gg t_w$, we have

$$C_{\text{ag}}(t, t_w) \sim \left(\frac{t}{t_w} \right)^{-d/4}. \quad (5.8)$$

Given that [1, 2, 13] the value of α is $1/2$ for the nonconserved Ising model, Eq. (5.8) implies

$$C_{\text{ag}}(t, t_w) \sim \left(\frac{\ell}{\ell_w} \right)^{-\lambda}; \quad \lambda = \frac{d}{2}. \quad (5.9)$$

Liu and Mazenko (LM) [4], via similar Gaussian approximation of the auxiliary field of the order parameter in the TDGL equation, obtained different values for λ . Exact solution of the dynamical equation for C_{22} , that LM constructed, provides the result same as the OJK one in $d = 1$. Approximate solutions in $d = 2$ and 3 provide [4] $\lambda \simeq 1.29$ and $\simeq 1.67$, respectively.

For the exponent λ , Fisher and Huse (FH) [3] provided the bounds

$$\frac{d}{2} \leq \lambda \leq d, \quad (5.10)$$

that apply to nonconserved order parameter dynamics. Later, Yeung, Rao and Desai (YRD) [6], by incorporating the structural differences between conserved and nonconserved dynamics, obtained more general lower bounds as

$$\lambda \geq \frac{d + \beta}{2}, \quad (5.11)$$

where β is a power-law exponent related to the small wave-number (k) enhancement of the structure factor [14, 15]:

$$S(k, t) \sim k^\beta. \quad (5.12)$$

It has been shown that $\beta = 0$ for nonconserved dynamics. This leads to the FH lower bounds. Here note that $S(k, t)$ is the Fourier transform of $C(r, t)$ and has the scaling form [1, 2]

$$S(k, t) \equiv \ell^d \tilde{S}(k\ell), \quad (5.13)$$

where $\tilde{S}(k\ell)$ is a time independent master function.

Predictions of both OJK and LM follow the FH bounds. Simulations of the nonconserved Ising model in $d = 2$ showed consistency [2, 16] with the OJK function in Eq. (5.7) and the LM value [11] for λ . The latter fact appeared true [11, 16] in $d = 3$ as well for quenches to a nonzero temperature (T_f) from an initial temperature (T_i) far above the critical value (T_c). However, the $d = 3$ Ising model appears to be different and difficult [17–23] for $T_f = 0$. There exists difference (with respect to the theoretical expectation [13]) in the time dependence of ℓ . In a recent work [23], we showed, via simulations of very large systems, that the expected power-law with exponent $\alpha = 1/2$ becomes visible only at very late time. Studies with smaller systems revealed interesting behavior with respect to achieving the expected ground state [21, 22]. Interesting structural aspects were also reported. In the structural context, we showed that \tilde{C} , unlike the $d = 2$ case, differs from that at high temperatures [16]. Given the connection between structural and aging properties discussed above, it is then a natural question to ask, does there exist difference in the values of λ for $T_f = 0$ and $T_f > 0$? Our previous study [16], in fact, suggested the possibility of violation of the FH lower bound for $T_f = 0$ in $d = 3$. To confirm that, better analysis of data are

needed.

In this chapter, for the nonconserved Ising model we present results for the decay of $C_{\text{ag}}(t, t_w)$, for $T_f = 0$, in $d = 2$ and 3 . Via state-of-the-art finite-size scaling [11, 12, 24, 25] analysis of the Monte Carlo (MC) simulation [25] results, we arrive at the following conclusions. As previously observed, we do not notice any temperature dependence in the case of $d = 2$. For $d = 3$, the estimated value of the exponent, obtained from significantly long period of simulations, indeed violates the FH lower bound. This however can be explained via the structural consideration of YRD.

The rest of the chapter is organized as follows. In Section 5.2, we discuss the methods. Results are presented in Section 5.3. Finally we summarize our results in Section 5.4.

5.2 Methods

Coarsening in the nearest neighbor Ising model is studied via MC simulations [25] in periodic square ($d = 2$) or cubic ($d = 3$) boxes. We have used square lattice in $d = 2$ and simple cubic lattice in $d = 3$. The values of T_c for this model [25] in $d = 2$ and 3 are respectively $\simeq 2.269J/k_B$ and $\simeq 4.51J/k_B$, k_B being the Boltzmann constant. We have used the Glauber spin-flip moves [26], a standard method to introduce kinetics for nonconserved case. Essentially, for a trial move, the sign of a randomly chosen spin is changed. The move is accepted if such a change lowers the energy of the system. For no energy change, one can use different probabilities for accepting the moves [21, 22]. In this work all such moves were accepted. Time

in our simulations was measured in units of MC steps (MCS) [25], one step consisting of L^d trial moves, L being the linear dimension of a system (in units of the lattice constant). For the sake of convenience, in the rest of the chapter we set k_B , J and the lattice constant to unity.

For the calculation of length [16], we have identified the size, ℓ_d , of various domains by scanning the systems in all possible directions. Two successive changes in sign in any direction identified a domain and the distance between the locations of sign changes provided the the corresponding length. The average value, ℓ , was obtained from the first moment of the time dependent distributions thus obtained. Here note that ℓ can be obtained from the scaling properties [1, 2] of $C(r, t)$ and $S(k, t)$ as well. The measures from different functions are expected to be same, apart from constants of proportionality.

Note that the spin variable S_i is similar to the order parameter field ψ . Thus, the calculations of various correlation functions do not require any further discussion.

All our results are presented after averaging over a minimum of 10 independent initial configurations. Other than the finite-size scaling analysis, all presented data are for $L = 512$.

5.3 Results

For the sake of completeness, we start by showing the results for domain growth in Fig. 5.1. There we have presented ℓ vs t data for both $d = 2$ and 3, on a log-log scale. The solid lines represent power-laws with the exponent values mentioned next to them. Clearly, for $d = 2$, the data set

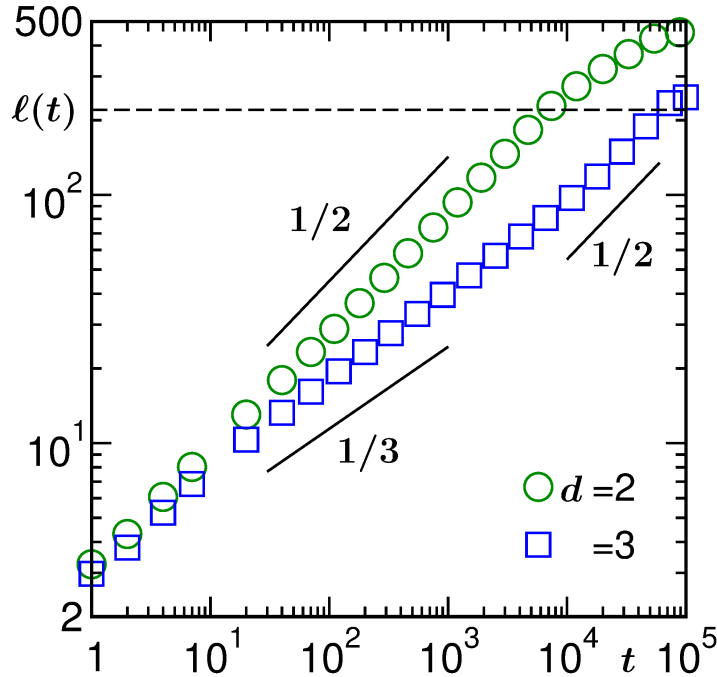


Figure 5.1: Plots of the average domain size, ℓ , vs time, on a log-log scale. Results from both $d = 2$ and 3 are included. The solid lines represent power-laws, exponents for which have been mentioned. The horizontal dashed line marks the location of the appearance of finite-size effects.

for the whole presented time range show consistency with $\alpha = 1/2$. The deviation at the end is related to the finite-size effects which appear when [11] $\ell \simeq 0.4L$. The data from $d = 3$, on the other hand, show different trend. After a very brief initial period, the result is consistent with $\alpha = 1/3$ over a few decades [23]. Towards the end, there, of course, exists consistency with [23] $\alpha = 1/2$. Appearance of the finite-size effects again is consistent with the number mentioned above. The behavior in the finite-size affected regime is rather complex, leading to difficulty in arriving at the final ground state [21, 22].

Next, in Fig. 5.2 and Fig. 5.3 we demonstrate the scaling property of

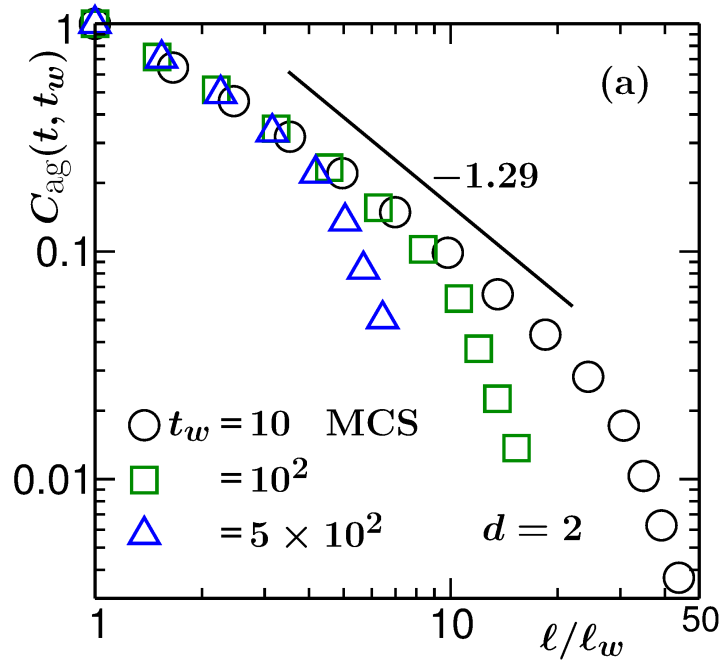


Figure 5.2: Log-log plots of the correlation function $C_{\text{ag}}(t, t_w)$, vs l/l_w , for $d = 2$. Results from a few different values of t_w are shown. The solid line corresponds to a power-law decay with exponent $\lambda = 1.29$.

the autocorrelation function [16]. Here $C_{\text{ag}}(t, t_w)$ is plotted as a function of l/l_w , for different values of t_w . Results in Fig. 5.2 are from $d = 2$, whereas the $d = 3$ data are presented in Fig. 5.3. Very nice collapse of data can be appreciated for both the dimensions. Deviations from the scaling, in the case of $d = 2$, is related to finite-size effects [11, 12]. This appears at a smaller value of x for a larger value of t_w , as expected. For $d = 3$, the presented data are from the finite-size unaffected region. The solid lines in these figures are power-laws with LM values of λ . Clearly, there exist discrepancies between the LM exponents and the simulation results. We observe continuous bending [11] in the scaling functions obtained from the simulations. This is possible when there exist corrections [11]. In such a

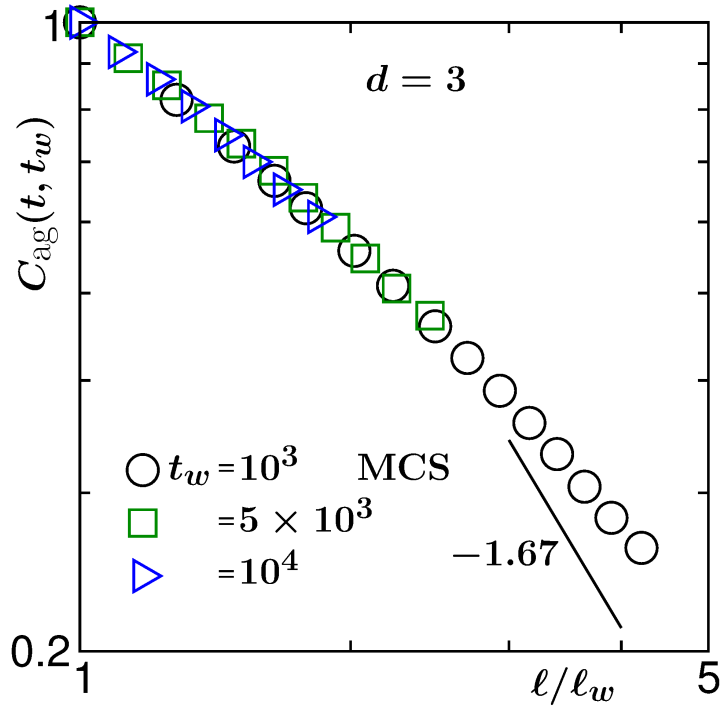


Figure 5.3: Same as Fig. 5.2, but here it is for $d = 3$. The solid line here has the power-law exponent 1.67.

situation, calculation of the instantaneous exponent [4, 11, 12, 27]

$$\lambda_i = -\frac{dC_{\text{ag}}}{dx}, \quad (5.14)$$

can provide useful information. In Fig. 5.4 we show λ_i , as a function of $1/x$, for the $d = 2$ case. Results for two different values of t_w are included. Data for the larger value of t_w deviates from a small x linear behavior, as x increases. This is due to finite-size effects and can be appreciated from the continued linear trend exhibited by the data from the smaller value of t_w . A linear extrapolation to $x = \infty$ provides a value $\lambda \simeq 1.3$. Invoking the linear behavior in the definition in Eq. (5.14) one obtains an exponential correction

factor [11, 12], i.e.,

$$C_{\text{ag}}(t, t_w) = Ae^{-\frac{B}{x}} x^{-\lambda}, \quad (5.15)$$

A and B being constants. Thus, one obtains a power law only in the $t \gg t_w$

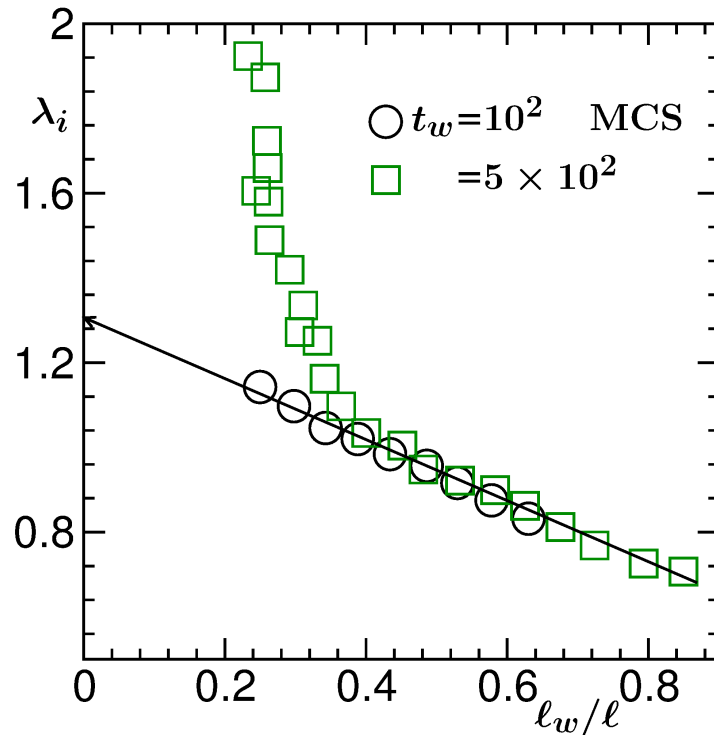


Figure 5.4: Instantaneous exponent, λ_i , for the $d = 2$ Ising model, is plotted as a function of ℓ_w/ℓ . The values of t_w are mentioned on the figure. The solid line is a guide to the eye.

limit. Similar behavior is observable in Fig. 5.5 where we have presented data for $d = 3$. Here the strong oscillation of the larger t_w data is related to the statistical fluctuation. In this case the data exhibit convergence to a value $\lambda \simeq 1.2$. While for $d = 2$ the convergence is consistent with that for higher temperature, there exists serious departure in the case of $d = 3$ from the LM prediction. Note that the LM prediction in $d = 3$ matches well with the

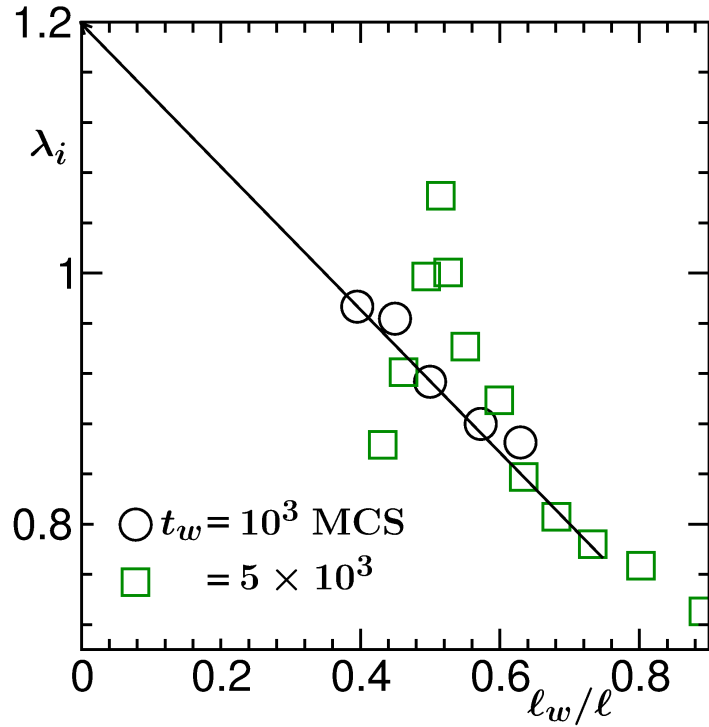


Figure 5.5: Same as Fig. 5.4, but here it is for $d = 3$.

the conclusions from the simulation studies at higher temperature [11]. In fact $\lambda = 1.2$ is far below the lower bound of FH. Even though reasonably accurate estimate is possible from such extrapolations, one can do better by performing finite-size scaling analysis [11, 12], given that the data at large x may suffer from statistical error and finite-size effects. A finite-size data collapse exercise (using different system sizes) will also be useful for bringing confidence in the form of Eq. (5.15), which essentially is an empirical form.

In Fig. 5.6 and Fig. 5.7 we present C_{ag} vs ℓ/ℓ_w results from different system sizes, by fixing the value of t_w , in $d = 2$ and $d = 3$, respectively. Results from smaller systems deviate from the master curves for large value of x . In a finite-size scaling method one looks for collapse of data from

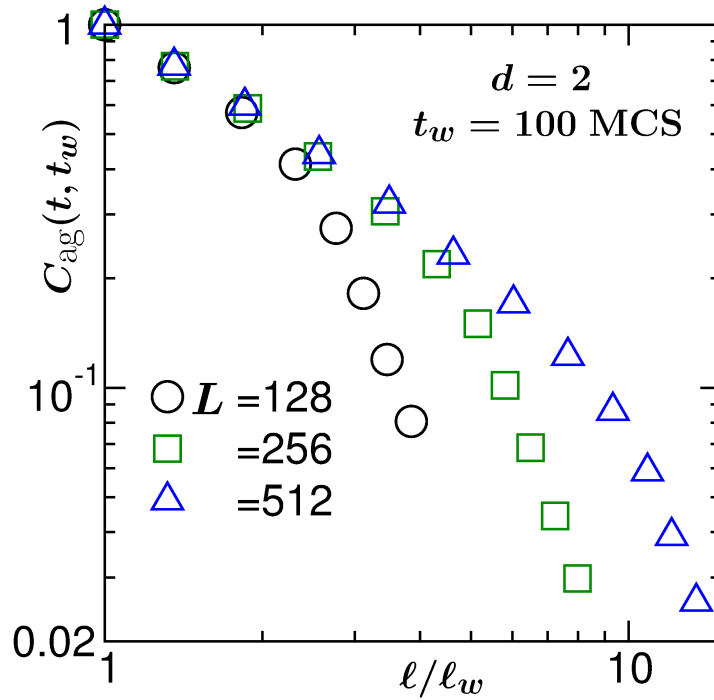


Figure 5.6: Same as Fig. 5.2, but here we have fixed the value of t_w and presented data from different L in $d = 2$. The value of t_w is mentioned.

various system sizes [24, 25]. Such a method for the analysis of the data for autocorrelation function was recently constructed [11, 12]. Like in the critical phenomena [24, 25], here also one introduces a scaling function Y , independent of system size, as

$$C_{\text{ag}}(t, t_w) = A e^{-\frac{B}{x}} x^{-\lambda} Y(y), \quad (5.16)$$

where y is a dimensionless scaling variable. In the present case this should be the ratio between x' ($= L/l_w$) and x . The choice of x' is driven by the dimension of x and the fraction of the total system size available to explore, given that the measurement starts at t_w . Thus, $y = L/l$.

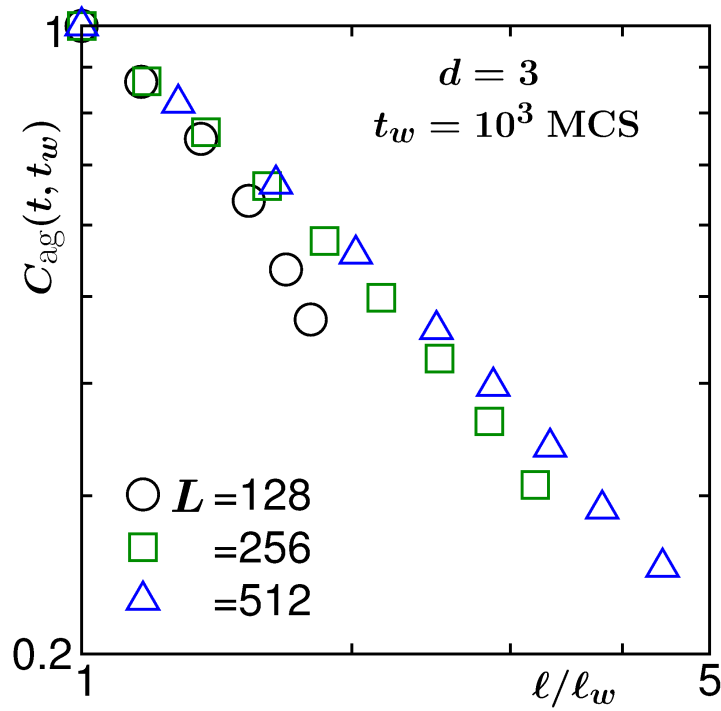


Figure 5.7: Same as Fig. 5.6, but here it is for $d = 3$ and t_w value is different.

The behavior of Y , to be obtained from collapse of data from different values of L (as mentioned above), can be described as follows. For large y , i.e., $\ell \ll L$, we do not expect finite-size effects. In that case, inspection of Eq. (5.16) states that Y should be a constant. For small y , i.e., as $\ell \rightarrow L$, from the behavior of C_{ag} (in Fig. 5.6 and Fig. 5.7), it is clear that Y should decrease. Such characteristic features, as well as a collapse of data from various different system sizes can be realized if λ is chosen appropriately, alongside the constant B . In our data collapse exercise we will treat these two quantities as adjustable parameters.

Given that the autocorrelations are normalized to unity for $x = 1$, the value of A should be 1. At nonzero temperatures, there exists coupling between equilibration of domain magnetization and that of the whole system

[2]. For low value of T_f , the relaxation related to the domain magnetization occurs very fast to a value almost unity. Thus scaling of C_{ag} , with respect to

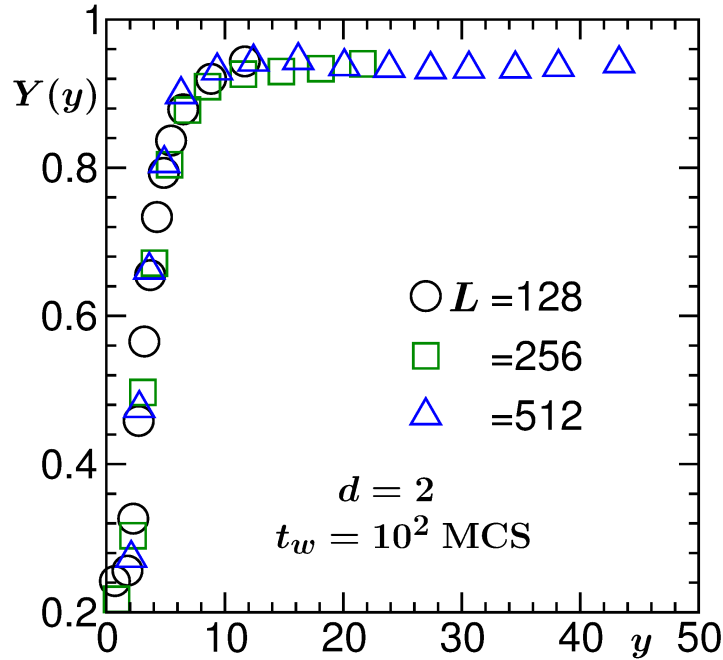


Figure 5.8: Finite-size scaling analysis of the autocorrelation function in $d = 2$. Here we have obtained the scaling function Y from the collapse of data from different system sizes, for a fixed value of t_w , mentioned on the figure.

ℓ/ℓ_w , is expected to be observed from rather small values of t_w . Nevertheless, minor mismatch at early time is observed even in the $T_f = 0$ case for different system sizes. This may have to do with sponge like structure formation [21, 22], particularly in $d = 3$. Thus, we will avoid very small x limit data and normalize the rest of the data sets in such away that there is matching in the value of A for data coming from all system sizes, before performing the finite-size scaling analysis. Even though in an earlier study [11], we have obtained good data collapse by using finite-size ℓ in the scaling variable y ,

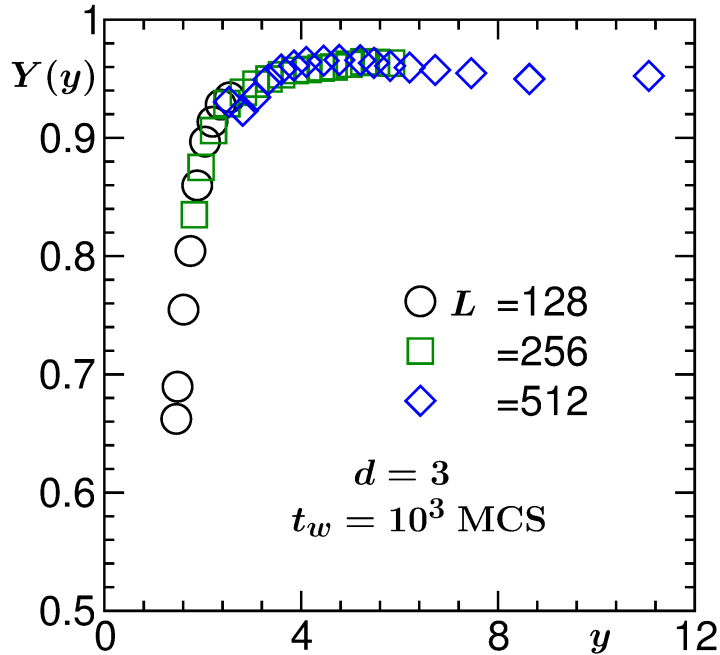


Figure 5.9: Same as Fig. 5.8, but here we do the exercise for $d = 3$.

ideally one should use the thermodynamic limit value. For $d = 2$, we will use $\ell \sim t^{1/2}$, since this behavior is observed from very early time. On the other hand, the $d = 3$ case is rather complex. In this case, we will use the ℓ values from $\ell = 512$ since this data set does not suffer from finite-size effects in the time period over which C_{ag} has been calculated.

Results from the finite-size scaling analysis are presented for $d = 2$ in Fig. 5.8, whereas same results for $d = 3$ are presented in Fig. 5.9. In the case of $d = 2$, very good collapse of data is obtained for $\lambda = 1.32$ and $B = 0.80$. This value of λ , within statistical error, is in agreement with a previous study [11] for $T_f = 0.6T_c$ and consistent with the prediction of LM. For $d = 3$, on the other hand, the number ($\lambda = 1.1$) is very different from that at higher temperature [11]. Here note that the high temperature result is in good

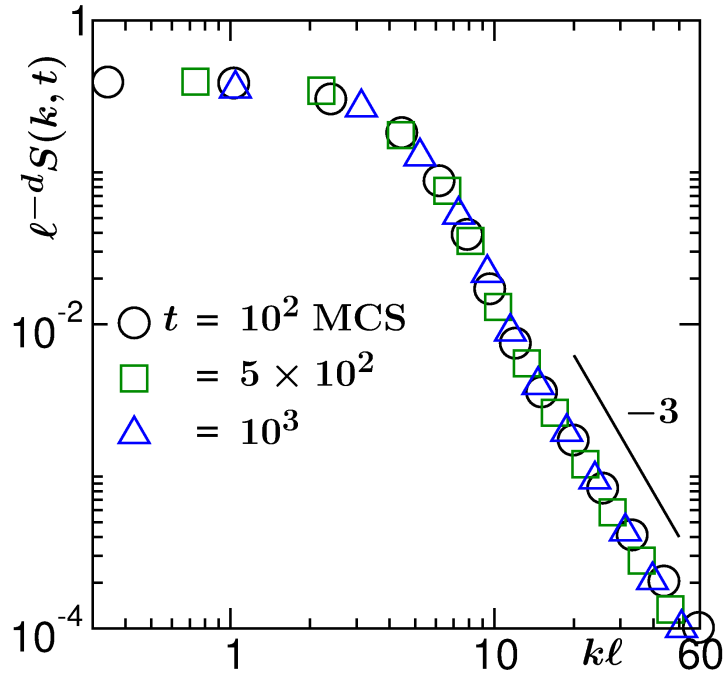


Figure 5.10: Scaling plot of the structure factor in $d = 2$. The solid line represents a power-law, exponent for which is mentioned in the figure.

agreement with the LM value. Furthermore, the value of λ at $T_f = 0$ is far below the lower bound of FH, the conclusion being consistent with that from the analysis of the instantaneous exponent. The question then comes, is it a true violation of the bound? This can be understood from the derivation of YRD.

In Fig. 5.10 and Fig. 5.11 we show the plots of $S(k, t)$ from $d = 2$ and 3 respectively. Our focus here is to obtain the scaling behavior of Eq. (5.13). Nice collapse of data, in both the dimensions, signify that the chosen values of t_w for the finite-size scaling analyses are well inside the scaling regime. The power-laws with exponent -3 and -4 represent the Porod laws [28]. Starting from the equal time structure factors at t_w and t , YRD, for the derivation of

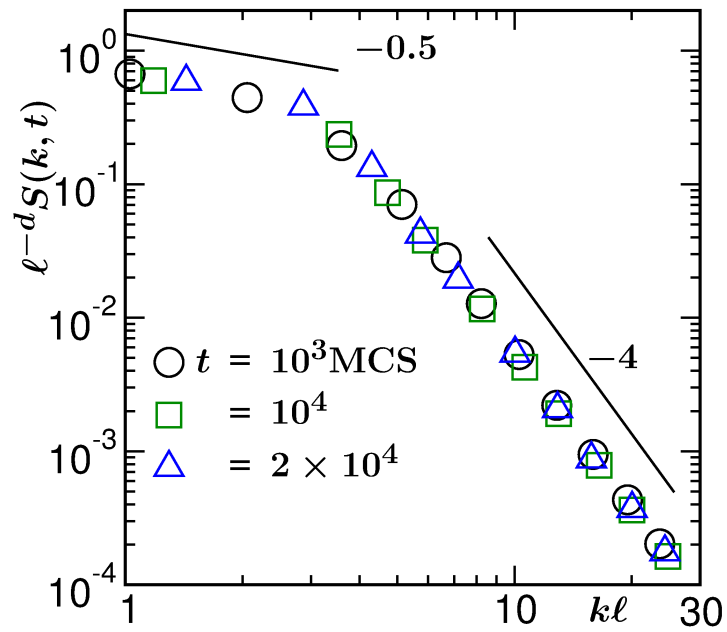


Figure 5.11: Same as Fig. 5.10, but here it is in $d = 3$.

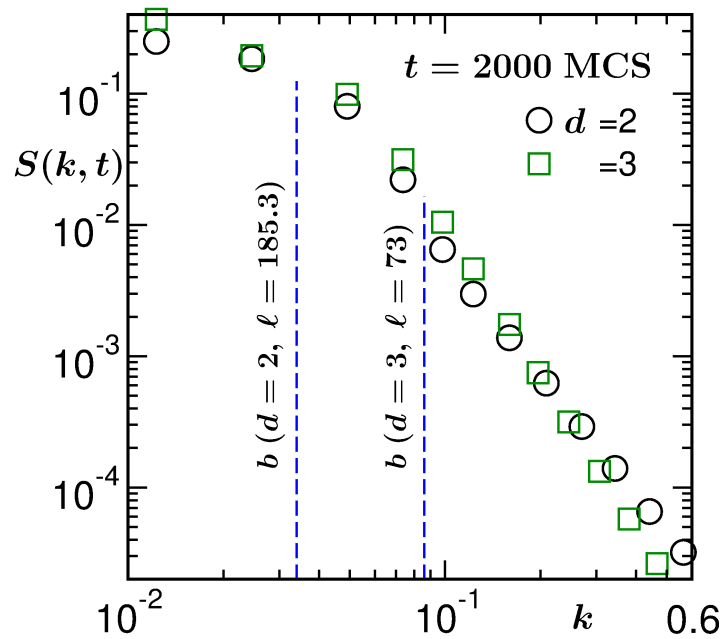


Figure 5.12: Plots of the structure factor, vs k , on a double log scale, for $d = 2$ and $d = 3$.

the lower bound, used the small k behavior of $S(k, t_w)$ [cf. Eq. (5.12)] in

$$C_{\text{ag}} \leq \ell^{d/2} \int_0^b dk k^{d-1} [S(k, t_w) \tilde{S}(kl)]^{1/2}, \quad (5.17)$$

where b , the upper limit of the integration, equals $2\pi/\ell$. In Fig. 5.12 we present $S(k, t)$ vs k plots on a log-log scale. For both $d = 2$ and 3 , we have chosen $t = 2000$ MCS. The vertical dashed lines there correspond to the upper limit b for different dimensions, corresponding to a time (10^4 MCS) reasonably larger than 2000 MCS. It appears, the upper limit of integration for $d = 3$ covers a significant range of k over which $S(k, t)$ decreases, providing a negative value of β . Given that the growth of ℓ is much slower in $d = 3$ than in $d = 2$ over a long intermediate period, one needs to go to very large ℓ to access $\beta = 0$ behavior. Thus, even if a crossover occurs to the value predicted by LM, simulations with much larger systems with orders of magnitude longer period of time will be needed to observe that.

5.4 Conclusion

We have studied the aging property of the nearest neighbor ferromagnetic Ising model via Monte Carlo simulations [25] using Glauber spin flip [25, 26] moves. Our focus was on zero temperature quench for $d = 2$ and 3 . Quantitative information on the decay of the two time autocorrelation function was obtained via finite-size scaling [11, 12] and other methods of analysis. These were discussed with reference to the corresponding results for quenches to nonzero temperatures [11].

The autocorrelations exhibit nice scaling with respect to $x (= \ell/\ell_w)$. The late time behavior is described by power-laws, $C_{\text{ag}}(t, t_w) \sim x^{-\lambda}$. At early time there exists exponential correction factor. These features are very much similar to those for high temperature quenches [11].

In $d = 2$, the value of λ is in agreement with the LM value. However, the $d = 3$ result differs significantly from the nonzero temperature result [11], the latter being consistent with the LM value. The estimated value not only differs from the LM prediction, it appears to be far below the lower-bound of FH. We argue, via analysis of the structure factor, in line with the derivation of YRD, that this is not a true violation if the small k behavior of $S(k, t)$ is appropriately accounted for.

Bibliography

- [1] A.J. Bray, *Adv. Phys.* **51**, 481 (2002).
- [2] S. Puri and V. Wadhawan (ed.), *Kinetics of Phase Transitions* (CRC Press, Boca Raton, 2009).
- [3] D.S. Fisher and D.A. Huse, *Phys. Rev. B* **38**, 373 (1988).
- [4] F. Liu and G.F. Mazenko, *Phys. Rev. B* **44**, 9185 (1991).
- [5] S.N. Majumdar and D.A. Huse, *Phys. Rev. E* **52**, 270 (1995).
- [6] C. Yeung, M. Rao and R. C. Desai, *Phys. Rev. E* **53**, 3073 (1996).
- [7] F. Corberi, E. Lippiello and M. Zannetti, *Phys. Rev. E* **74**, 041106 (2006).
- [8] M. Henkel, A. Picone, and M. Pleimling, *Europhys. Lett.* **68**, 191 (2004).
- [9] T. Ohta, D. Jasnow and K. Kawasaki, *Phys. Rev. Lett.* **49**, 1223 (1982).
- [10] E. Lorenz and W. Janke, *Europhys. Lett.* **77**, 10003 (2007).

-
- [11] J. Midya, S. Majumder and S.K. Das, J. Phys. : Condens. Matter **26**, 452202 (2014).
- [12] J. Midya, S. Majumder and S.K. Das, Phys. Rev. E **92**, 022124 (2015).
- [13] S.M. Allen and J.W. Cahn, Acta Metall. **27**, 1085 (1979).
- [14] C. Yeung, Phys. Rev. Lett. **61**, 1135 (1988).
- [15] S.N. Majumdar, D.A. Huse and B.D. Lubachevsky, Phys. Rev. Lett. **73**, 182 (1994).
- [16] S.K. Das and S. Chakraborty, arXiv:1609.09348 (2016).
- [17] J.G. Amar and F. Family, Bull. Am. Phys. Soc. **34**, 491 (1989).
- [18] J.D. Shore, M. Holzer, and J.P. Sethna, Phys. Rev. B **46**, 11376 (1992).
- [19] S. Cueille and C. Sire, J. Phys. A **30**, L791 (1997).
- [20] F. Corberi, E. Lippiello and M. Zannetti, Phys. Rev. E **78**, 011109 (2008).
- [21] J. Olejarz, P.L. Krapivsky and S. Redner, Phys. Rev. E **83**, 051104 (2011).
- [22] J. Olejarz, P.L. Krapivsky and S. Redner, Phys. Rev. E **83**, 030104 (2011).
- [23] S. Chakraborty and S.K. Das, Phys. Rev. E **93**, 032139 (2016).
- [24] M.E. Fisher, in *Critical Phenomena*, edited by M.S. Green (Academic, London, 1971).

-
- [25] D.P. Landau and K. Binder, *A Guide to Monte Carlo Simulations in Statistical Physics*, (Cambridge University Press, Cambridge, 2009).
- [26] R.J. Glauber, *J. Math. Phys.* **4**, 294 (1963).
- [27] D.A. Huse, *Phys. Rev. B* **34**, 7845 (1986).
- [28] G. Porod, in *Small-Angle X-ray scattering*, edited by O. Glatter and O. Kratky (Academic Press, New York, 42, 1982).

Chapter 6

Pattern Formation, Growth and Aging in a $2D$ Active Matter Model

6.1 Introduction

Collective movements [1] performed by a school of fish, flock of birds, herd of sheep, etc., give rise to fascinating phenomena. These systems are different from the “passive” systems (i.e., traditional systems composed of particles or spins), because the constituents of the former are self-propelling in nature. From this point of view, these systems are “active”. In the theoretical literature of active matters, phase behavior [2–5] and various critical exponents have been calculated for simple model systems [6–8]. With respect to the phase behavior there exist experimental works as well [9,10]. Recently,

there is a steady growth of interest in the kinetics of phase transitions in active matters [11–14], i.e., to learn, how a system, starting from a state in the disordered or homogeneous phase, moves towards the ordered or clustered phase.

In this chapter we focus on the kinetics of clustering [15, 16] in a model active matter system. Interesting recent results [17] in spatial dimension $d = 3$ motivated us to undertake this study in $d = 2$. The questions are similar to those for passive systems, viz., the formation and growth of pattern [15, 16, 18], aging [16, 19, 20], etc.

Patterns in out-of-equilibrium systems are probed via the equal time two-point correlation function $C(r, t)$, defined as [16]

$$C(r, t) = \langle \psi(\vec{r}, t) \psi(\vec{0}, t) \rangle - \langle \psi(\vec{r}, t) \rangle \langle \psi(\vec{0}, t) \rangle, \quad (6.1)$$

where ψ is a space (\vec{r}) and time (t) dependent order parameter. One of the important properties exhibited by many of the systems undergoing phase ordering is structural self-similarity. This is reflected in the dynamic scaling [15] of the above correlation function:

$$C(r, t) \equiv \tilde{C}(r/\ell), \quad (6.2)$$

where \tilde{C} is a time independent master function and ℓ is the characteristic length scale or average domain size of the system. The latter usually grows with time as [15, 16]

$$\ell \sim t^\alpha, \quad (6.3)$$

where α is the growth exponent. The value of α depends on the spatial dimensionality, conservation and symmetry of the order parameter, transport mechanism, etc. In active matter systems, self-propulsion can give rise to more directed mobility of the particles, affecting the value of α .

While $C(r, t)$ provides information on the pattern, the relaxation of a nonequilibrium system starting from different times, i.e., aging of a system, is studied via two time quantities like the autocorrelation function [16]

$$C(t, t_w) = \langle \psi(\vec{r}, t) \psi(\vec{r}, t_w) \rangle - \langle \psi(\vec{r}, t) \rangle \langle \psi(\vec{r}, t_w) \rangle, \quad (6.4)$$

where t is the observation time and t_w is the waiting time or the age of the system. In the passive cases, C_{ag} exhibits scaling [16, 19–23] as

$$C_{\text{ag}}(t, t_w) \equiv \tilde{C}_{\text{ag}}(\ell/\ell_w), \quad (6.5)$$

where ℓ and ℓ_w are the average domain lengths corresponding to the times t and t_w . In a good majority of cases, the master function \tilde{C}_{ag} has a late time power-law behavior:

$$\tilde{C}_{\text{ag}} \sim \left(\frac{\ell}{\ell_w} \right)^{-\lambda}, \quad (6.6)$$

where λ is referred to as an aging exponent. For this exponent, Yeung, Rao and Desai (YRD) provided the dimension dependent lower bounds as [21]

$$\lambda \geq \frac{d + \beta}{2}, \quad (6.7)$$

where β is a power-law exponent related to the small wave-number (k) behavior of the structure factor [16]:

$$S(k, t) \sim k^\beta. \quad (6.8)$$

The structure factor is the Fourier transform of $C(r, t)$ and has the scaling form [16]

$$S(k, t) = \ell^d \tilde{S}(k\ell), \quad (6.9)$$

where \tilde{S} is another time independent master function.

In this work, we try to examine the above mentioned scaling properties, via Molecular Dynamics (MD) simulations of a system of particles having both interparticle interaction and self-propulsion. We compare these results with those for the passive systems, wherever necessary. Unless otherwise mentioned, all results are from active systems.

The rest of the chapter is organized as follows. In section 6.2 we describe the model and methods. Results are presented in section 6.3. Finally, we conclude the chapter in section 6.4 by presenting a summary.

6.2 Model and Methods

We incorporate the two-body interparticle interaction (r is the distance between two particles) via a potential [24, 25]

$$u(r) = U(r) - U(r_c) - (r - r_c) \left(\frac{dU}{dr} \right)_{r=r_c}, \quad (6.10)$$

where $U(r)$ has the standard Lennard-Jones (LJ) form

$$U(r) = 4\epsilon \left[\left(\frac{\sigma}{r} \right)^{12} - \left(\frac{\sigma}{r} \right)^6 \right], \quad (6.11)$$

$r_c (= 2.5\sigma)$, ϵ and σ being the cut-off radius, interaction strength and particle diameter, respectively. Here note that the cut-off was introduced for faster computation. Given that the LJ potential is a short range one, introduction of r_c does not alter the critical universality class. After the cut, the potential is made continuous by shifting it to zero at $r = r_c$. However, a discontinuity in the force still remains. This is removed via the introduction of the last term [25] in Eq. (6.10). For this passive model, the critical temperature (T_c) and density (ρ_c) have the values [26] $\simeq 0.41\sigma/k_B$ and $\simeq 0.37$, respectively, in $d = 2$, where k_B is the Boltzmann constant. The (number) density is measured as N/A , N and A being respectively the number of particles and area of the system.

The self-propulsion is invoked in the model via the Vicsek model [6]. As is well known, in the Vicsek model the direction of a particle's motion is influenced by that of its neighbors. This was implemented here by applying an external force ($f_A = 1$, in dimensionless unit) to each particle, at every time step of our simulations, in a direction defined by the average velocities of all the particles contained in the radius of influence r_c . Following this exercise the magnitudes of the velocities of the particles were restored to the original values. Thus, like in the Vicsek case, this whole exercise changes only the direction of motion of the particles. Such directional feature in the Vicsek model is very much physical. Often in an assembly of active particles, the

motion of an individual is decided by its neighbors.

With this model we performed MD simulations [24, 25] in a square box of linear dimension $L\sigma$, where the temperature (T) was controlled via the Langevin thermostat [27]. At every MD step, for each particle, we have solved the Langevin equation

$$m\ddot{\vec{r}}_i = -\vec{\nabla}u_i - m\gamma\dot{\vec{r}}_i + \sqrt{6m\gamma k_B T}\vec{R}(t), \quad (6.12)$$

where m is the mass of a particle, u_i is the energy originating from interparticle potential, γ is a damping constant and $\vec{R}(t)$ is a noise having δ correlation in space and time. We have used the velocity Verlet algorithm [24] to solve Eq. (6.12), with $\Delta t = 0.002$, in units of $\sqrt{\frac{m\sigma^2}{48\epsilon}}$. For the rest of the chapter m , ϵ , σ , γ and k_B have been set to unity. It is clear that Eq. (6.12) deals with only the inter-particle potential. At the end of every MD step, the Vicsek rule was imposed.

The systems were initially thermalized at $T = 4$ and then quenched to $T = 0.25$, with density $\rho = 0.35$. All results are presented for $L = 256$ and after averaging over at least 10 initial realizations.

6.3 Results

We begin by showing the snapshots of the active system in Fig. 6.1 from four different times, during the process of evolution. The particles form clusters of elongated shape which grow with time. Even though the total order-parameter is conserved here, the structure is different from that of the

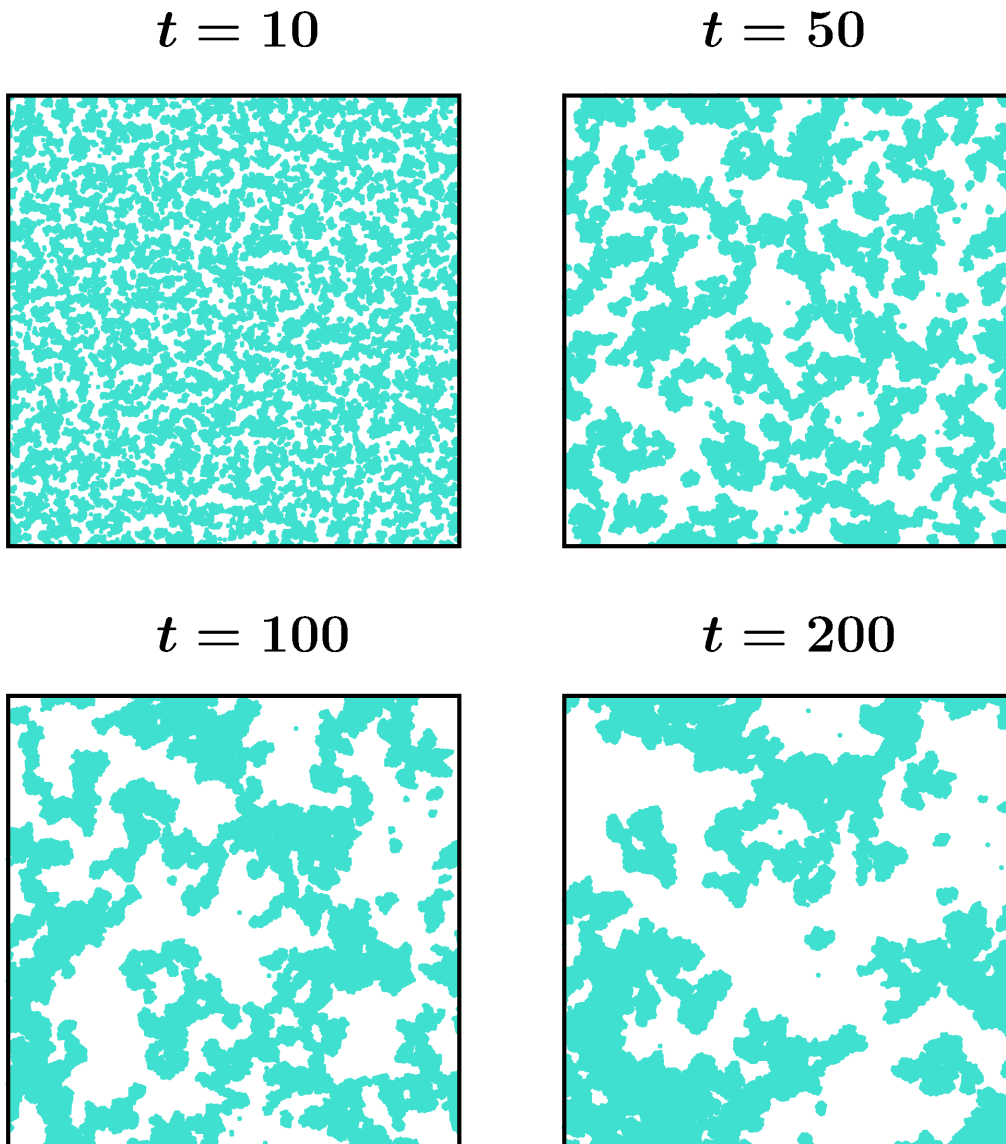


Figure 6.1: Evolution snapshots of the active system from four different times. The locations of the particles are marked by dots.

conserved passive case (see the upper frames of Fig. 6.2 where we show evolution snapshots from the conserved dynamics of the Ising model). It has more similarity with that of the nonconserved Ising model - corresponding snapshots are shown in the lower frames of Fig. 6.2. Note that the results for

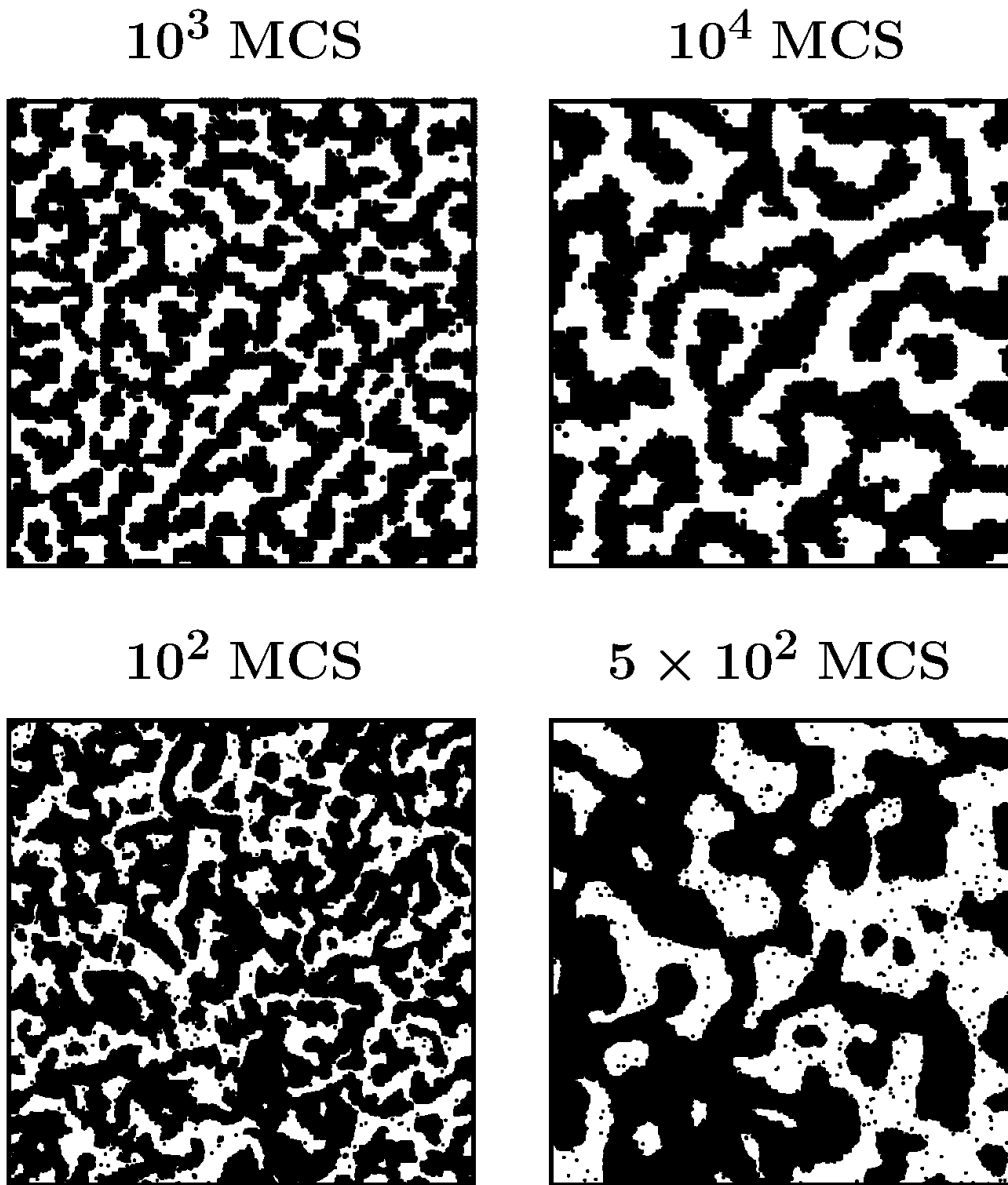


Figure 6.2: Upper frames: Evolution snapshots from the Kawasaki exchange Monte Carlo simulations of the Ising model. Lower frames: Same as above but from Glauber kinetics. The times are in units of number of Monte Carlo steps.

the conserved and nonconserved Ising models were obtained via Monte Carlo simulations [28] (at $T = 0.6T_c$) using Kawasaki exchange kinetics [28, 29]

and Glauber spin-flip mechanism [28, 30], respectively. For the quantitative understanding of the pattern and its self-similarity, we calculate $C(r, t)$. For this purpose we have mapped the continuum configurations into (square) lattice ones. To a lattice site, we have assigned the order parameter value $\psi = -1$, if it is empty, otherwise we have put $\psi = +1$.

In Fig. 6.3, we plot the scaled correlation functions. Nice collapse of data for different times is observed, as in most passive cases. This implies that the morphology of the system is statistically self-similar in nature. However, $C(r, t)$ does not show the strong oscillatory behavior [16] that is expected in the case of the passive counter part of the system. In the inset of this figure we have shown plots of correlation function for both passive conserved and passive nonconserved Ising models. The plot for the passive conserved case was obtained via Kawasaki exchange Monte Carlo simulations. For the nonconserved case, we have shown the analytical form derived by Ohta, Jasnow and Kawasaki (OJK) (via a Gaussian auxiliary field ansatz). Clearly, as stated above, the active matter $C(r, t)$ has more resemblance with the OJK function. There exists differences, of course, which we intend to understand in future.

The scaling in $C(r, t)$ is expected to be reflected in $S(k, t)$ also. This exercise has been performed in Fig. 6.4. At large k regime the Porod behavior [31],

$$S(k, t) \sim k^{-(d+1)}, \quad (6.13)$$

a consequence of scattering from sharp interfaces, can be observed. Difference in the large r regime of $C(r, t)$ between the active and (conserved) passive

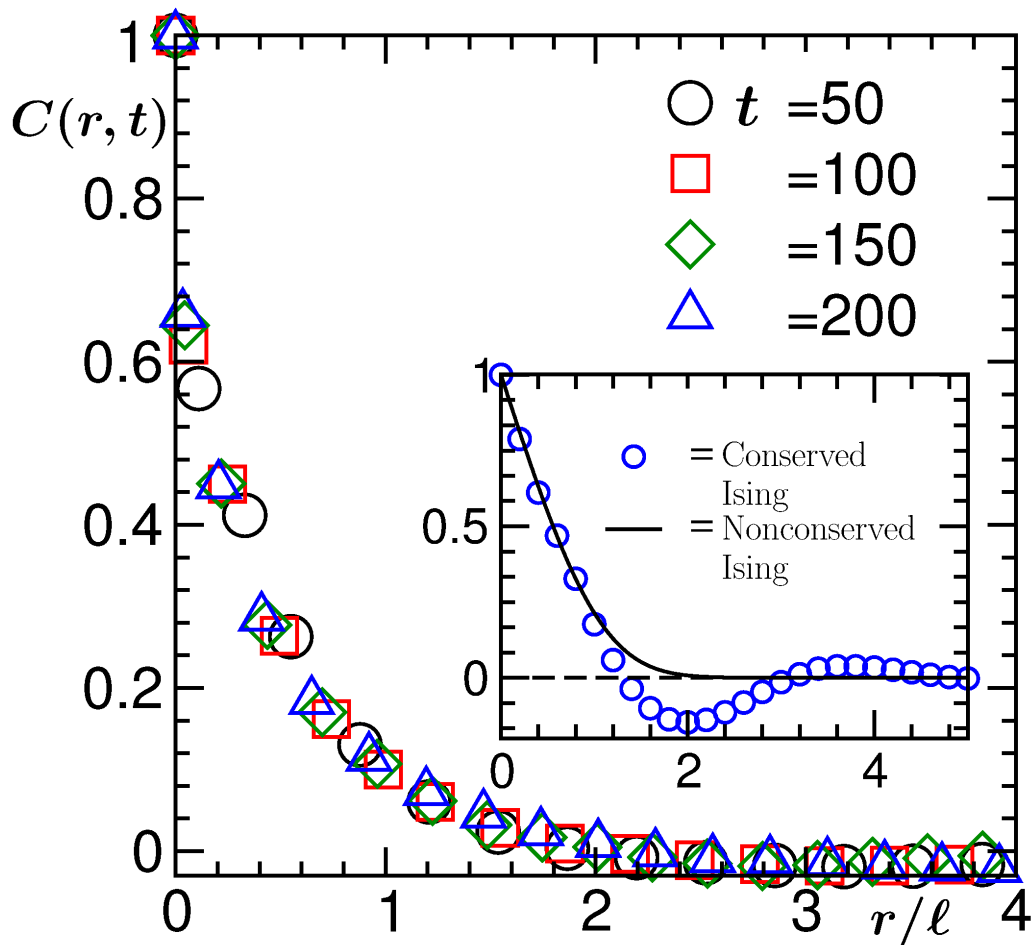


Figure 6.3: Scaling plot of the two-point equal time correlation function, for the active system. Data from four different times are presented. The symbols in the inset show $C(r, t)$ from the conserved Ising model, simulated by using the Kawasaki exchange Monte Carlo method. The solid curve there is the Ohta-Jasnow-Kawasaki (OJK) function, that matches with the correlation function for the nonconserved order-parameter dynamics of the Ising model.

system is expected to affect the small k behavior in $S(k, t)$. Indeed, we notice that in the value of the exponent β . In the case of conserved dynamics, in the scaling regime the value [21] of β for the passive system is 4, whereas for the active system we observe $\beta \simeq 1.35$. This is more close to the passive nonconserved value $\beta = 0$.

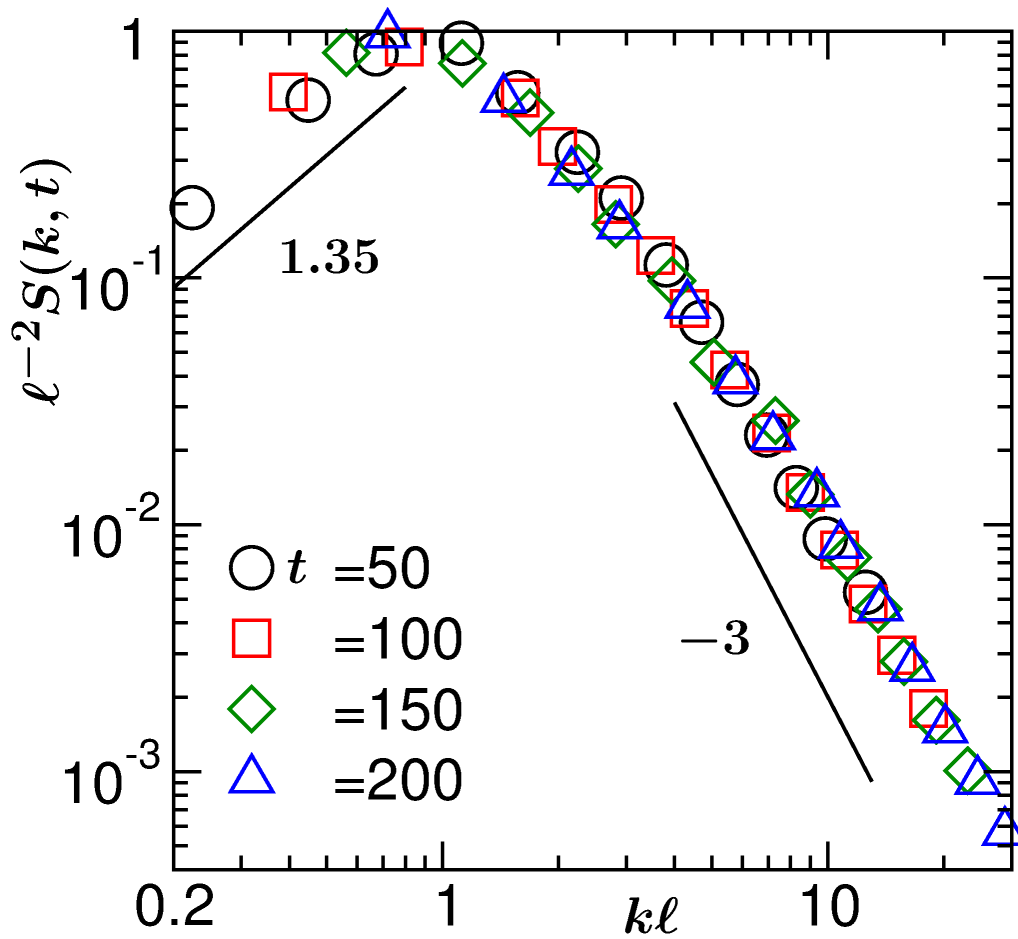


Figure 6.4: Log-log plot of the scaled structure factor. The solid lines there represent different power laws, the exponents of which are mentioned.

In Fig. 6.5, we have plotted the average domain length ℓ as a function of time. The values of ℓ were extracted from the scaling property of Eq. (6.2). Essentially, we have used

$$C(\ell, t) = 0.1. \quad (6.14)$$

After an initial slower growth (with an exponent $\alpha = 2/3$), at long time the value of α seems to be 1. The bending of the data points for very large t is due to the finite-size effects. To quantify the growth exponent α better, we

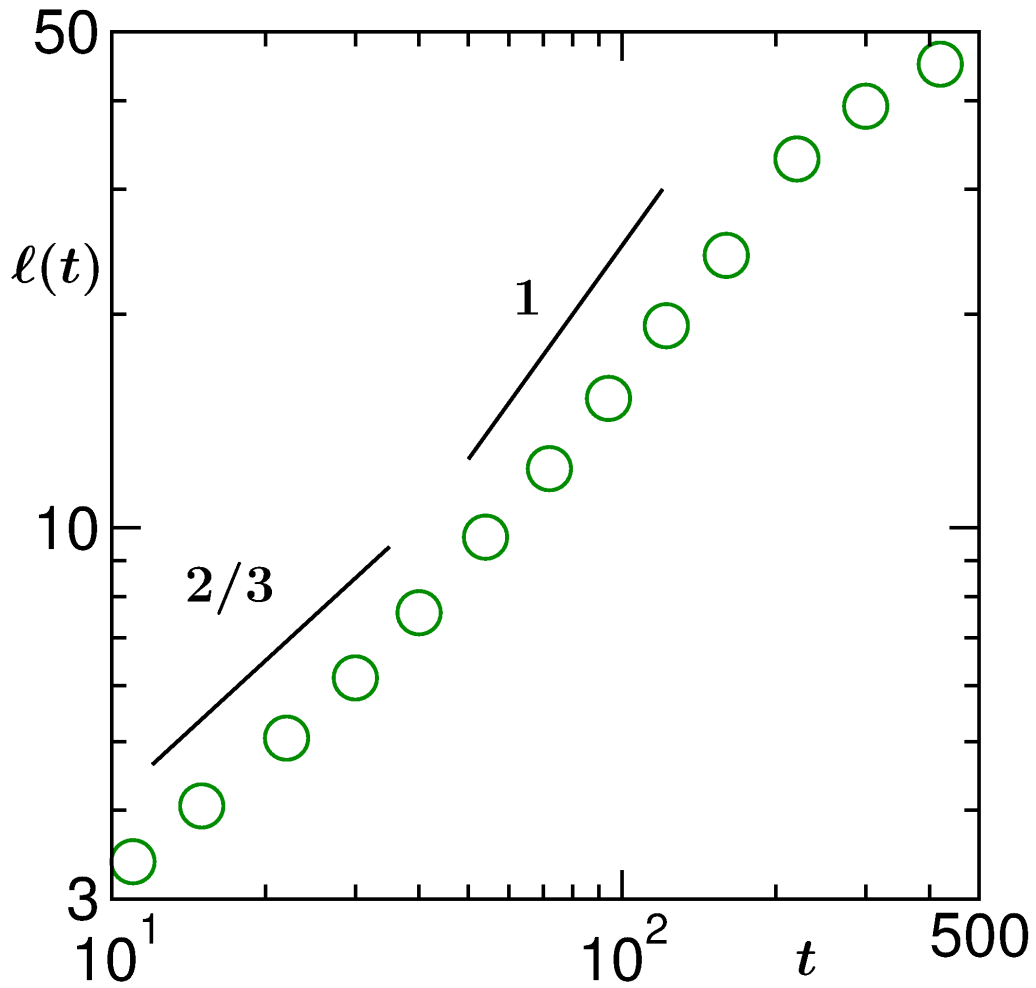


Figure 6.5: Plot of the average domain length, $\ell(t)$, vs t , in a double log scale. The solid lines represent various power-laws, exponents for which are mentioned.

calculate the instantaneous exponent α_i , defined as [32]

$$\alpha_i = \frac{d \ln \ell}{d \ln t}, \quad (6.15)$$

and plot it as a function of $1/\ell$. We show this plot in Fig. 6.6. This indeed shows that the data set, in the limit $\ell \rightarrow \infty$, converges to 1. This value is

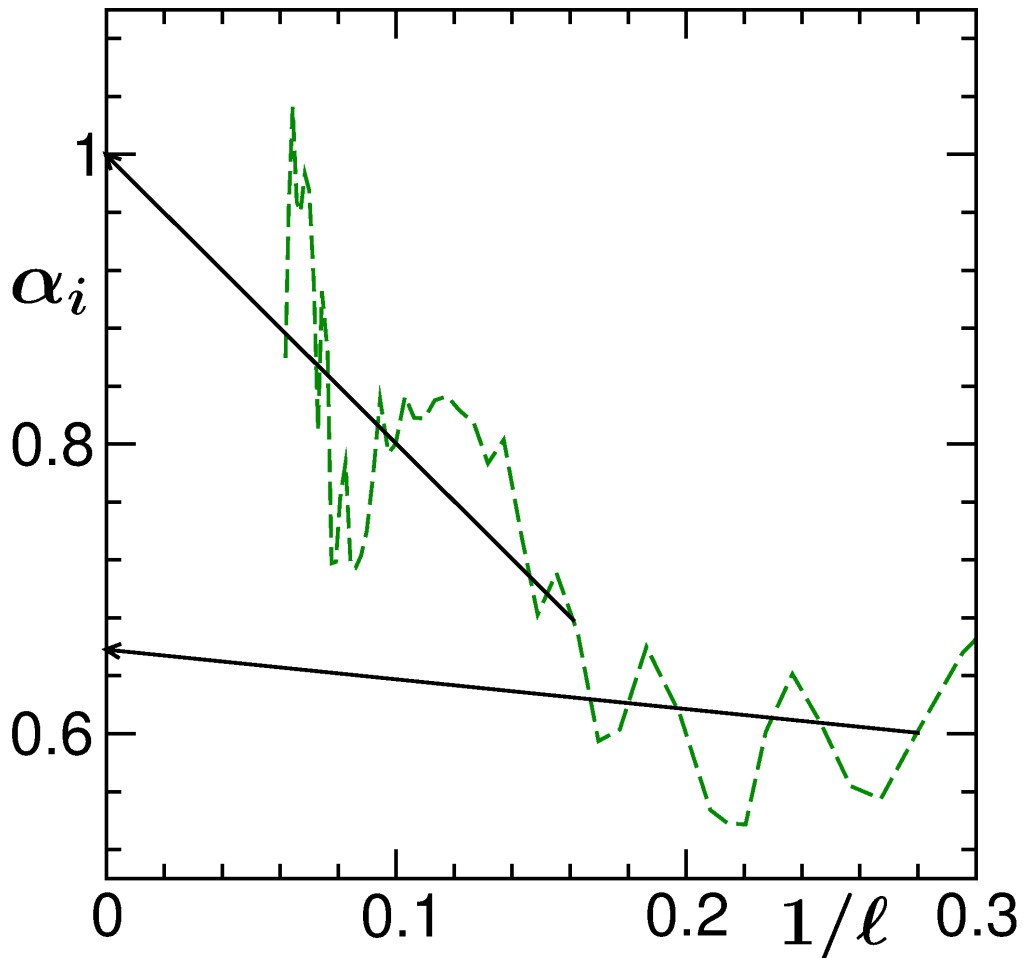


Figure 6.6: Instantaneous exponent for domain growth, α_i , is plotted as a function of $1/\ell$. Solid lines there are guides to the eye. The early time data is consistent with $2/3$. The late time data show convergence towards 1.

much larger than that in the conserved order parameter dynamics (without hydrodynamics) in passive systems. In the latter case, the growth mechanism is diffusive and the Lifshitz-Slyozov (LS) growth law [33] with $\alpha = 1/3$ is observed. Here note that our MD simulations do not use hydrodynamics preserving thermostat. The fast growth in the active system can then be attributed to coherent motion of the self-propelling particles [17] due to

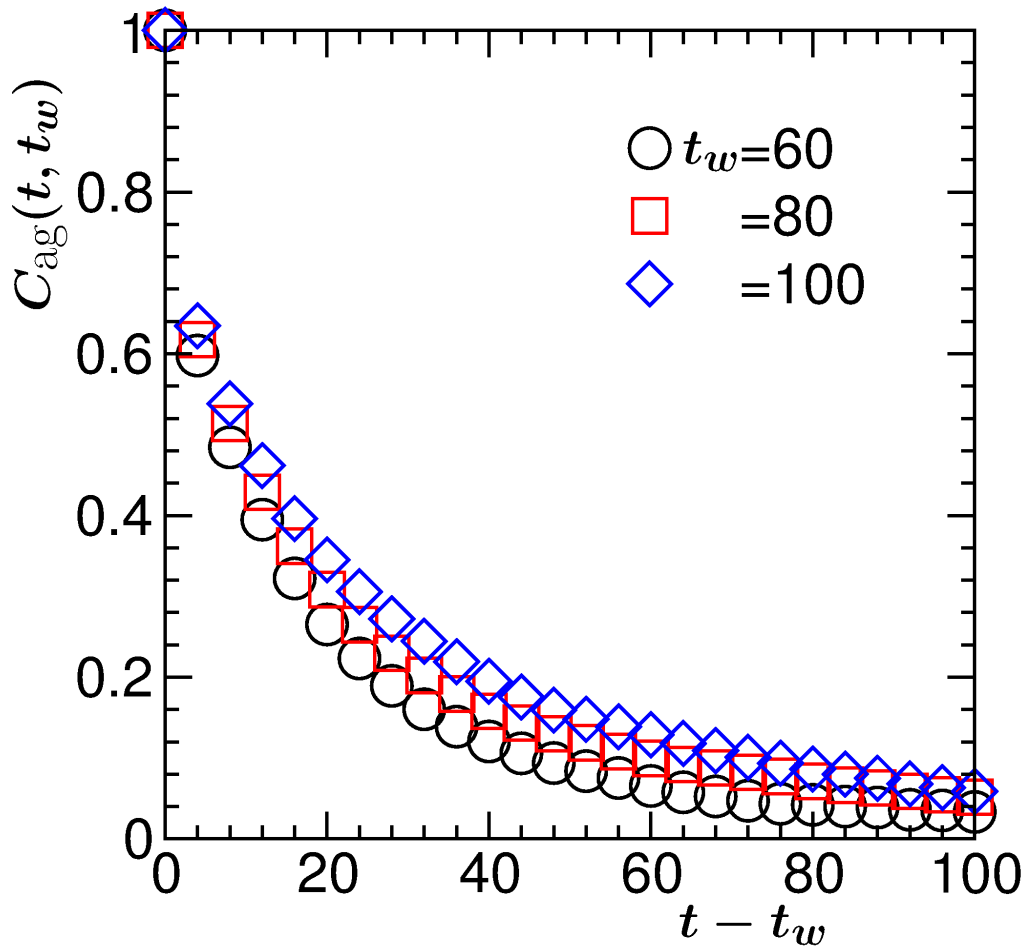


Figure 6.7: Plots of the autocorrelation function, C_{ag} , vs translated times $t - t_w$. We have presented data from three different values of t_w .

velocity parallelization coming from Vicsek activity.

In Fig. 6.7, we plot C_{ag} vs $(t - t_w)$. The nonscaling behavior of data from different t_w values implies that the time translational invariance is not obeyed during the evolution of the system, which we expect for an out-of-equilibrium system. The figure reveals that the younger system relaxes faster than older ones, the basic fact of aging. In Fig. 6.8, the plots of C_{ag} as a function of ℓ/ℓ_w are presented. Reasonably good data collapse is observed

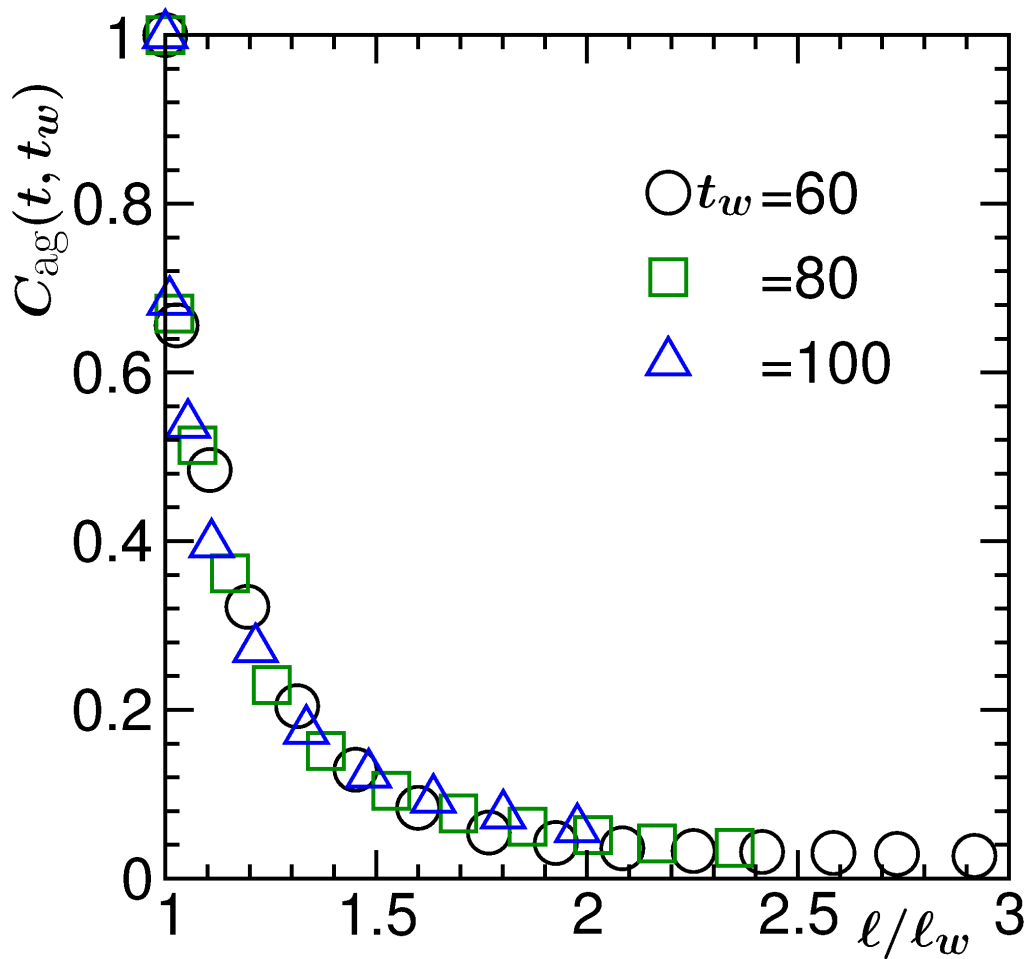


Figure 6.8: The autocorrelation function, C_{ag} , is plotted vs l/l_w . The values for t_w are mentioned on the figure.

for data sets from different times. Thus the qualitative feature in this case also is very similar to the passive cases. This is interesting by considering the fact that, in the passive case the approach of the systems is towards an equilibrium state, whereas the active matter systems move towards a steady state. To establish quantitative similarity, first one needs to see if the decay of C_{ag} is a power-law and if so, next task is to estimate the aging exponent λ . Since the system size is small the finite-size effects appear rather fast,

bringing in serious difficulties in the proper identification of such feature. In future we would like to quantify this. Given that $\beta = 1.35$ here, the YRD lower bound is 1.675. A quantitative agreement thus, between the active and passive cases is not truly expected. It is to be seen, how close the actual value of λ (if the decay is a power-law) is to this lower bound.

6.4 Conclusion

We have studied the kinetics of phase separation in a $2D$ active matter model, via Molecular Dynamics simulations (using Langevin thermostat). The focus is on quantifying morphological features, domain growth and aging property. Discussions of these results by comparing them with the existing results for the passive systems are provided.

The two-point equal time correlation function $C(r, t)$ and the structure factor $S(k, t)$ show scaling, confirming the self-similarity in the growth process. Unlike passive systems no strong oscillation is observed in $C(r, t)$ for the active case. The domain growth exponent α is found to be 1, which is much higher than the diffusive growth in passive systems. It will be interesting to find out the details of the mechanism.

The autocorrelation function exhibits quite good scaling with respect to ℓ/ℓ_w . In the small wave number (k) limit, the power-law enhancement exponent β of $S(k, t)$ is much smaller than the passive case. This reduces the lower bound of λ , compared to the passive case. Proper quantification of this exponent and other observables require much better statistics and further analyses with larger systems. These we aim to undertake in future.

Bibliography

- [1] T. Vicsek and A. Zafeiris, *Phys. Rep.* **517**, 71 (2012).
- [2] J. Schwarz-Linek, C. Valeriani, A. Cacciuto, M.E. Cates, D. Marenduzzo, A.N. Morozov, and W.C.K. Poon, *Proc. Natl. Acad. Sci. U.S.A* **109**, 4052.
- [3] J. Palacci, S. Sacanna, A.P. Steinberg, D.J. Pine, and P.M. Chaikin, *Science* **339**, 936 (2013).
- [4] S.K. Das, S.A. Egorov, B. Trefz, P. Virnau, and K. Binder, *Phys. Rev. Lett.* **112**, 198301 (2014).
- [5] B. Trefz, S.K. Das, S.A. Egorov, P. Virnau, and K. Binder, *J. Chem. Phys.* **144**, 144902 (2016).
- [6] T. Vicsek, A. Czirók, E. Ben-Jacob, I. Cohen, and O. Schochet, *Phys. Rev. Lett.* **75**, 1226 (1995).
- [7] A. Czirók and T. Vicsek, *Physica A* **281**, 17 (2000).
- [8] H. Chaté, F. Ginelli, G. Grégoire, F. Peruani, and F. Raynaud, *Eur. Phys. J. B* **64**, 451 (2008).

-
- [9] D.L. Blair, T. Neicu, and A. Kudrolli, *Phys. Rev. E* **67**, 031303 (2003).
- [10] M. Ibele, T.E. Mallouk, and A. Sen, *Angew. Chem. Int. Ed.* **48**, 3308 (2009).
- [11] G.S. Redner, M.F. Hagan, and A. Baskaran, *Phys. Rev. Lett.* **110**, 055701 (2013).
- [12] A. Wysocki, R.G. Winkler, and G. Gompper, *EPL* **105**, 48004 (2014).
- [13] F. Peruani and M. Bär, *New J. Phys.* **15**, 065009 (2013).
- [14] P. Cremer and M. Löwen, *Phys. Rev. E* **89**, 022307 (2014).
- [15] A.J. Bray, *Adv. Phys.* **51**, 481 (2002).
- [16] S. Puri and V. Wadhawan (ed.), *Kinetics of Phase Transitions* (CRC Press, Boca Raton, 2009).
- [17] S.K. Das, arXiv:1605.08155.
- [18] M.C. Cross and P.C. Hohenberg, *Rev. Mod. Phys.* **65**, 851 (1993).
- [19] D.S. Fisher and D.A. Huse, *Phys. Rev. B* **38**, 373 (1988).
- [20] F. Liu and G.F. Mazenko, *Phys. Rev. B* **44**, 9185 (1991).
- [21] C. Yeung, M. Rao, and R.C. Desai, *Phys. Rev. E* **53**, 3073 (1996).
- [22] M. Henkel, A. Picone, and M. Pleimling, *EPL* **68**, 191 (2004).
- [23] J. Midya, S. Majumder, and S.K. Das, *J. Phys.: Condens. Matter* **26**, 452202 (2014).

-
- [24] D. Frenkel and B. Smit, *Understanding Molecular Simulations: From algorithms to applications* (Academic Press, San Diego, 2002).
- [25] M.P. Allen and D.J. Tildesley, *Computer Simulations of Liquids* (Clarendon, Oxford, 1987).
- [26] J. Midya and S.K. Das, *J. Chem. Phys.* (2017).
- [27] T. Schlick, *Molecular Modeling and Simulation: An Interdisciplinary Guide*, (Springer, New York, 2010).
- [28] D.P. Landau and K. Binder, *A Guide to Monte Carlo Simulations in Statistical Physics* (Cambridge University Press, Cambridge, 2009).
- [29] K. Kawasaki, *Phys. Rev.* **145**, 224 (1966).
- [30] R.J. Glauber, *J. Math. Phys.* **4**, 294 (1963).
- [31] G. Porod, in *Small-Angle X-ray scattering*, edited by O. Glatter and O. Kratky (Academic Press, New York, 42, 1982).
- [32] D.A. Huse, *Phys. Rev. B* **34**, 7845 (1986).
- [33] I.M. Lifshitz and V.V. Slyozov, *J. Phys. Chem. Solids* **19**, 35 (1991).

Permission Requests

A) Authors of an EPJ article (= an article published in one of the journals on www.epj.org) can re-use material from their own article(s) free of charge provided that:

A.1) Full credit (journal title, volume, year of publication, page, article title, name(s) of author(s), original copyright notice) is given to the publication in which the material was originally published by adding: With kind permission of The European Physical Journal (EPJ).

A.2) If the material in question is cited from another source, authorization from and reference to that source are required.

B) More generally, authors requesting permission to re-use material from an EPJ article in form of tables and illustrations of articles can do so free of charge, provided that:

B.1) No more than three tables/figures of any given article are concerned.

B.2) The work in which this material is re-used is eventually published by one of the Scientific, Technical and Medical publishers listed on <http://www.stm-assoc.org/our-members/>.

B.3) Full credit (journal title, volume, year of publication, page, article title, name(s) of author(s), original copyright notice) is given to the publication in which the material was originally published by adding: With kind permission of The European Physical Journal (EPJ).

B.4) Permission is also obtained from the author(s) of the material to be re-used.

B.5) If the material in question is cited from another source, authorization from and reference to that source are required.

In all cases, these free permissions:

- include the use of the material in question in any electronic form,
- are limited to non-exclusive rights throughout the world,
- and do not affect any rights the EPJ publishers might have to charge for reproduction of their copyrighted material in the future.

For all cases that are not covered by A or B please consult the Rights and Permissions website <http://www.springer.com/de/rights-permissions/obtaining-permissions/882> on which an explicit step-by-step description for obtaining permissions is posted.

If your permission request is covered by A or B, we kindly ask you to make a printout this text and keep it in your files. Our experience suggests that having a printed version of this policy for reference can be handy when questions arise.

Thank you for your cooperation.

The EPJ Publishing Consortium

Copyright Transfer Statement

The European Physical Journal


A : Hadrons and Nuclei
B : Condensed Matter
and Complex Systems
C : Particles and Fields
D : Atomic, Molecular, Optical
and Plasma Physics
E : Soft Matter and Biological Physics
ST : Special Topics
H : Historical Perspectives
on Contemporary Physics
EPJ Plus

The title
"The European Physical Journal"
is a joint property of
EDP Sciences,
Società Italiana di Fisica
and Springer

edp sciences



Società Italiana
di Fisica

 Springer

The copyright to this article, including any graphic elements therein (e.g. illustrations, charts, moving images), is hereby assigned for good and valuable consideration to the publishers of The European Physical Journal (EPJ), Springer (EPJ A-H, ST and Plus), SIF (EPJ A-E and Plus) and EDP Sciences (EPJ B, D, E, H, ST) effective if and when the article is accepted for publication and to the extent assignable if assignability is restricted for by applicable law or regulations (e.g. for U.S. government or crown employees). Author warrants (i) that he/she is the sole owner or has been authorized by any additional copyright owner to assign the right, (ii) that the article does not infringe any third party rights and no license from or payments to a third party is required to publish the article and (iii) that the article has not been previously published or licensed.

The copyright assignment includes without limitation the exclusive, assignable and sublicensable right, unlimited in time and territory, to reproduce, publish, distribute, transmit, make available and store the article, including abstracts thereof, in all forms of media of expression now known or developed in the future, including pre- and reprints, translations, photographic reproductions and microform. Springer may use the article in whole or in part in electronic form, such as use in databases or data networks for display, print or download to stationary or portable devices. This includes interactive and multimedia use and the right to alter the article to the extent necessary for such use.

Authors may self-archive the Author's accepted manuscript of their articles on their own websites. Authors may also deposit this version of the article in any repository, provided it is only made publicly available 12 months after official publication or later. He/she may not use the publisher's version (the final article), which is posted on **SpringerLink** and other Springer websites, for the purpose of self-archiving or deposit. Furthermore, the Author may only post his/her version provided acknowledgement is given to the original source of publication and a link is inserted to the published article on Springer's website. The link must be provided by inserting the DOI number of the article in the following sentence : "The final publication is available at Springer via <http://dx.doi.org/10.1140/epjb/e2015-60168-4>".

Prior versions of the article published on non-commercial **pre-print servers** like arXiv.org can remain on these servers and/or can be updated with Author's accepted version. The final published version (in pdf or html/xml format) cannot be used for this purpose. Acknowledgement needs to be given to the final publication and a link must be inserted to the published article on Springer's website, by inserting the DOI number of the article in the following sentence : "The final publication is available at Springer via <http://dx.doi.org/10.1140/epjb/e2015-60168-4>". Author retains the right to use his/her article for his/her further scientific career by including the final published journal article in other publications such as dissertations and postdoctoral qualifications provided acknowledgement is given to the original source of publication.

Articles disseminated via **link.springer.com** are indexed, abstracted and referenced by many abstracting and information services, bibliographic networks, subscription agencies, library networks, and consortia.

After submission of the agreement signed by the corresponding author, changes of authorship or in the order of the authors listed will not be accepted.

The European Physical Journal B — Manuscript No. : **b150168**

Title of article : *Role of initial correlation in coarsening of a ferromagnet*

Author(s) : *Saikat Chakraborty and Subir K. Das*

Author's signature : *Subir Kumar Das*

Author's signature

30.05.2015

Date



APS JOURNALS (/)

Physical Review Letters, Physical Review X, Physical Review, and Reviews of Modern Physics

[Our Journals \(/about\)](#)

[Authors \(/authors\)](#)

[Referees \(/referees\)](#)

[Browse \(/browse\)](#)

[Search \(/search\)](#)

[Press \(/press\)](#)

[📡 \(/feeds\)](#)

APS Copyright Policies and Frequently Asked Questions

- [What is copyright?](#)
- [What does copyright protect?](#)
- [How is a copyright different from a patent or a trademark?](#)
- [What is the difference between copyright infringement and plagiarism?](#)
- [Why should I transfer copyright to APS?](#)
- [Why should I transfer copyright to APS before the article is accepted for publication by an APS journal?](#)
- [Does transferring copyright affect my patent rights?](#)
- [As the author of an APS-published article, may I post my article or a portion of my article on my own website?](#)
- [What happens if the author has posted an APS-published article on a free access e-print server or on the authors' or institutions' web pages and subsequently a fee is imposed for access to those sites?](#)
- [As the author of an APS-published article, may I post my article or a portion of my article on an e-print server?](#)
- [As the author of an APS-published article, can I post my article or a portion of my article on a web resource like wikipedia or quantiki?](#)
- [As the author \(or the author's employer\) of an APS-published article, may I use copies of part or all of my articles in the classroom?](#)
- [As the author of an APS-published article, may I use figures, tables, graphs, etc. in future publications?](#)
- [As the author of an APS-published article, may I include my article or a portion of my article in my thesis or dissertation?](#)
- [As the author of an APS-published article, may I give permission to a colleague or third party to republish all or part of the article in a print publication?](#)
- [As the author of an APS-published article, may I give permission to a colleague or third party to republish all or part of the APS-published version in an online journal, book, database compilation, etc.?](#)
- [As the author of an APS-published article, may I provide a PDF of my paper to a colleague or](#)

- As a third party (not an author), may I republish an article or portion of an article published by APS?
- As a third party, may I use articles published by APS for lecture and classroom purposes?
- How do I request permission to republish APS-copyrighted material?

What is copyright? <http://www.copyright.gov/> (<http://www.copyright.gov/>)

Copyright is a form of legal protection for original works of authorship. Copyright covers both published and unpublished works.

What does copyright protect?

Copyright, a form of intellectual property law, protects original works of authorship including literary, dramatic, musical, and artistic works, such as poetry, novels, movies, songs, computer software, and architecture. Copyright does not protect facts, ideas, systems, or methods of operation, although it may protect the way these things are expressed. See Circular 1, Copyright Basics, section "What Works Are Protected", see <http://www.copyright.gov/circs/circ01.pdf> (<http://www.copyright.gov/circs/circ01.pdf>)

How is a copyright different from a patent or a trademark?

Copyright protects original works of authorship, while a patent protects inventions or discoveries. Ideas and discoveries are not protected by the copyright law, although the way in which they are expressed may be. A trademark protects words, phrases, symbols, or designs identifying the source of the goods or services of one party and distinguishing them from those of others.

What is the difference between copyright infringement and plagiarism?

Copyright infringement occurs when an author's work is reused or republished without the permission of the copyright owner, whether or not author attribution accompanied the reuse.

Plagiarism occurs when an author's work has been reused or republished in such a manner as to make it appear as someone else's work, e.g., without quotation marks and citation of the original work.

Why should I transfer copyright to APS?

Like many other scientific publishers, the American Physical Society (APS) requires authors or their employers to provide transfer of copyright prior to publication. This permits APS to publish the article and to defend against improper use (or even theft) of the article. It also permits APS to publish the article online and to use the article in other forms or media, such as PROLA. By the APS transfer agreement, authors and their employers retain substantial rights in the work, as specified in the agreement <http://journals.aps.org/authors/transfer-of-copyright-agreement> (<http://journals.aps.org/authors/transfer-of-copyright-agreement>) and discussed in your copyright permission letter.

Why should I transfer copyright to APS before the article is accepted for publication by an APS journal?

Transferring copyright early in the process avoids the possibility of delaying publication if the transfer has to be obtained later in the process. As stated in the terms of the copyright

agreement, transfer does not take effect until the paper is accepted by an APS journal. The author retains the copyright until acceptance, and has the full freedom, for example, to withdraw the paper from consideration by an APS journal and submit it elsewhere.

Does transferring copyright affect my patent rights?

No. Copyright is separate from any patent rights, and the APS transfer agreement specifically states that patent rights are not affected. However, you should be aware that submitting a manuscript to a journal without first taking steps to protect your patent rights (e.g., filing for a patent) could endanger those rights. Consult your patent attorney.

As the author of an APS-published article, may I post my article or a portion of my article on my own website?

Yes, the author or the author's employer may use all or part of the APS published article, including the APS-prepared version (e.g., the PDF from the online journal) without revision or modification, on the author's or employer's website as long as a fee is not charged. If a fee is charged, then APS permission must be sought. In all cases, the appropriate bibliographic citation and notice of the APS copyright must be included.

What happens if the author has posted an APS-published article on a free access e-print server or on the authors' or institutions' web page and subsequently a fee is imposed for access to those sites?

When a fee is imposed, the author must either obtain permission from APS or withdraw the article from the e-print server or Institutional Repository.

As the author of an APS-published article, may I post my article or a portion of my article on an e-print server?

The author has the right to post and update the article on a free-access e-print server using files prepared and formatted by the author. Any such posting made or updated after acceptance of the article for publication by APS should include a link to the online APS journal article abstract. In all cases, the appropriate bibliographic citation and notice of the APS copyright must be included. If the author wishes to use the APS-prepared version (e.g., the PDF from the online journal) on an e-print server other than authors' or employer's website, then APS permission must be sought. Similarly, if the author wishes to post the article (any version) on an e-print server that charges a fee for use, APS permission must be sought.

As the author of an APS-published article, can I post my article or a portion of my article on a web resource like wikipedia or quantiki?

Sites like wikipedia and quantiki are strict about permissions and require that authors hold copyright to articles that they post there. In order to allow authors to comply with this requirement, APS permits authors to hold copyright to a "derived work" based on an article published in an APS journal as long as the work contains at least 10% new material not covered by APS's copyright and does not contain more than 50% of the text (including equations) of the original article. The APS will extend the author of a "derived work" the right to all papers published in APS journals.

As the author (or the author's employer) of an APS-published article, may I use copies of part or all of my article in the classroom?

Yes, the author or his/her employer may use all or part of the APS-prepared version for

educational purposes without requesting permission from the APS as long as the appropriate bibliographic citation is included.

As the author of an APS-published article, may I use figures, tables, graphs, etc. in future publications?

Yes, as the author you have the right to use figures, tables, graphs, etc. in subsequent publications using files prepared and formatted by you or the APS-prepared versions. The appropriate bibliographic citation must be included.

As the author of an APS-published article, may I include my article or a portion of my article in my thesis or dissertation?

Yes, the author has the right to use the article or a portion of the article in a thesis or dissertation without requesting permission from APS, provided the bibliographic citation and the APS copyright credit line are given on the appropriate pages.

As the author of an APS-published article, may I give permission to a colleague or third party to republish all or part of the article in a print publication?

Yes, as the author you may grant permission to third parties to republish print versions of the article provided the APS-published version (e.g., the PDF from the online journal, or a copy of the article from the print journal) is not used for this purpose. The article may not be published in another journal, and the third party may not charge a fee. The appropriate bibliographic citation and notice of the APS copyright must be included.

As the author of an APS-published article, may I give permission to a colleague or third party to republish all or part of the APS-published version in an online journal, book, database compilation, etc.?

No, an author may not grant permission in this case. To request permission to republish APS-copyrighted material, please refer to the "Reuse & Permissions" link that can be found on each APS article page.

As the author of an APS-published article, may I provide a PDF of my paper to a colleague or third party?

The author is permitted to provide, for research purposes and as long as a fee is not charged, a PDF copy of his/her article using either the APS-prepared version or the author prepared version.

As a third party (not an author), may I republish an article or portion of an article published by APS?

Yes, APS will grant permission to republish articles or portions of articles (e.g., tables, graphs, excerpts) published by APS. Depending on the reuse and medium APS has the right to grant permission subject to APS terms and conditions and a fee may be assessed.

As a third party, may I use articles published by APS for lecture and classroom purposes?

Yes, you may use photocopied articles published by APS for lecture and classroom purposes without asking permission from APS as long as you remain an Authorized User of the APS online research per your institution's site license. Also, there is no limitation on the use of APS articles

How do I request permission to republish APS-copyrighted material?

APS works with Copyright Clearance Center (CCC) for reprint and permission requests. The process is automated through the CCC RightsLink system. APS will continue to support the STM guidelines for all copyright needs. To request permission to republish APS-copyrighted material, please refer to the "Reuse & Permissions" link that can be found on each APS article page.

Once directed to CCC, the following information is required:

1. The format in which the material will be republished, e.g., print, online, CD-ROM, and/or other format
2. How much of the article you want to republish, e.g., all or portion of article; if a portion describe the specific material, e.g., figure numbers, excerpt
3. How the material will be used, e.g., in a book, journal, proceeding, thesis, etc.
4. The title of the article/thesis/chapter etc., and the name of the publication in which your work will appear
5. The name of the publisher
6. Indicate whether or not a fee will be charged for the publication

Upon submission, a letter of permission will be generated, specifying all guidelines and regulations to follow.

Blanket permissions are not granted. Please note all requests are subject to APS [terms and conditions \(/info/terms.html\)](/info/terms.html) and a fee may be assessed.

If your questions have not been addressed and you need further assistance, please email customercare@aps.org (<mailto:customercare@aps.org>).

Further information

For further information about copyright in general, please refer to the Library of Congress FAQ at <http://www.copyright.gov/help/faq/> (<http://www.copyright.gov/help/faq/>)

Journals published by the American Physical Society can be found at <http://journals.aps.org/> (<http://journals.aps.org/>).

FAQ Version: December 12, 2014

[APS \(http://www.aps.org/\)](http://www.aps.org/) | [News & Announcements \(/edannounce\)](/edannounce)

[Join APS \(http://www.aps.org/membership/join.cfm\)](http://www.aps.org/membership/join.cfm)

<http://www.twitter.com/APSphysics>

AUTHORS

5 of 6 [General Information \(/authors\)](/authors)

REFEREES

[General Information \(/referees\)](/referees) 12/27/2016 01:04 PM

[Publication Rights \(/pub_rights.html\)](/pub_rights.html)

[Update Your Information \(http://referees.aps.org/\)](http://referees.aps.org/)

[Open Access \(/open_access.html\)](/open_access.html)

[Referee FAQ \(/referees/faq.html\)](/referees/faq.html)

[Tips for Authors \(/authors/tips-authors-physical-review-physical-review-letters\)](/authors/tips-authors-physical-review-physical-review-letters)

[Outstanding Referees \(/OutstandingReferees\)](/OutstandingReferees)

[Professional Conduct \(/authors/professional-conduct-ethics\)](/authors/professional-conduct-ethics)

LIBRARIANS

[General Information \(http://librarians.aps.org/\)](http://librarians.aps.org/)

[Subscriptions \(http://librarians.aps.org/subscriptions\)](http://librarians.aps.org/subscriptions)

[Online License Agreement \(http://librarians.aps.org/sitelicense.pdf\)](http://librarians.aps.org/sitelicense.pdf)

[Usage Statistics \(http://counter.aps.org/\)](http://counter.aps.org/)

[Your Account \(https://librarians.aps.org/account\)](https://librarians.aps.org/account)

STUDENTS

[Physics \(http://physics.aps.org\)](http://physics.aps.org)

[PhysicsCentral \(http://www.physicscentral.com/\)](http://www.physicscentral.com/)

[Student Membership \(http://www.aps.org/membership/student.cfm\)](http://www.aps.org/membership/student.cfm)

APS MEMBERS

[Subscriptions \(http://www.aps.org/membership/aps-publications.cfm\)](http://www.aps.org/membership/aps-publications.cfm)

[Article Packs \(http://journals.aps.org/article-packs\)](http://journals.aps.org/article-packs)

[Membership \(http://www.aps.org/membership/index.cfm\)](http://www.aps.org/membership/index.cfm)

[FAQ \(http://www.aps.org/membership/faq.cfm\)](http://www.aps.org/membership/faq.cfm)

[APS News \(http://www.aps.org/publications/apsnews/index.cfm\)](http://www.aps.org/publications/apsnews/index.cfm)

[Meetings & Events \(http://www.aps.org/meetings/index.cfm\)](http://www.aps.org/meetings/index.cfm)

[Privacy \(http://www.aps.org/about/webpolicies.cfm#privacy\)](http://www.aps.org/about/webpolicies.cfm#privacy)

[Policies \(/policies\)](/policies)

[Contact Information \(/contact.html\)](/contact.html)

[Feedback \(mailto:feedback@aps.org\)](mailto:feedback@aps.org)

©2016 American Physical Society. (<http://www.aps.org/>) All rights reserved. *Physical Review*TM, *Physical Review Letters*TM, *Physical Review X*TM, *Reviews of Modern Physics*TM, *Physical Review A*TM, *Physical Review B*TM, *Physical Review C*TM, *Physical Review D*TM, *Physical Review E*TM, *Physical Review Applied*TM, *Physical Review Fluids*TM, *Physical Review Accelerators and Beams*TM, *Physical Review Physics Education Research*TM, *APS Physics logo*, and *Physics logo* are trademarks of the American Physical Society. Information about registration may be found [here \(/legal\)](/legal). Use of the American Physical Society websites and journals implies that the user has read and agrees to our [Terms and Conditions \(/info/terms.html\)](/info/terms.html) and any applicable [Subscription Agreement \(http://librarians.aps.org/sitelicense.pdf\)](http://librarians.aps.org/sitelicense.pdf).